Helicopter-Ship Qualification Testing

Page intentionally left blank

Helicopter-Ship Qualification Testing

The Theory and Application of a Novel Test Methodology Optimizing for Cost and Time Efficiency

Proefschrift

ter verkrijging van de graad van doctor
aan de Technische Universiteit Delft,
op gezag van Rector Magnificus prof. ir. K.C.A.M. Luyben,
voorzitter van het College voor Promoties,
in het openbaar te verdedigen
op maandag 16 maart 2015 om 15:00

door

Alrik HOENCAMP

lucht- en ruimtevaart technisch ingenieur
luitenant ter zee van de operationele dienst der Koninklijke Marine
geboren te Willemstad, Curaçao.

Dit proefschrift is goedgekeurd door de promotor:

Prof. ir. D. Stapersma

en de copromotor:

Dr. ir. M.D. Pavel

Samenstelling promotiecommissie:

Rector Magnificus,	voorzitter
Prof. ir. D. Stapersma,	Technische Universiteit Delft, promotor
Dr. ir. M.D. Pavel,	Technische Universiteit Delft, copromotor
Prof. dr. ir. Th. van Holten,	Technische Universiteit Delft
Prof. dr. ir. G. Jongbloed,	Technische Universiteit Delft
Prof. G.D. Padfield, BSc, PhD,	University of Liverpool
Prof. J.V.R. Prasad, BS, MS, PhD,	Georgia Institute of Technology
D. Lee, BSc,	Empire Test Pilots' School

Keywords: helicopter-ship qualification testing, shore-based hover trials, sea trials, predictive tool, validation, uncertainty analysis, candidate flight envelope

Cover design by B. Lint; cover photography by E. Benschop.

ISBN 978-94-6259-565-1

Ipskamp drukkers
Postbus 333
7500 AH Enschede
The Netherlands
tel: +31-(0)53-482 62 62
email: info@ipskampdrukkers.nl
website: www.ipskampdrukkers.nl

To my family
Belinda, Damian and Samuel

Page intentionally left blank

Contents

Summary

At present, the helicopter industry delivers a helicopter that has undergone elaborate in-flight test campaigns performed to demonstrate safe flight within the expected operational envelope for land-based operations. However, establishing the operational capabilities and associated limitations for safe shipboard operations is still considered a responsibility of the operator. Traditionally, each specific helicopter-ship combination is extensively evaluated at sea during varying environmental conditions like, for example, wind speeds, wind directions, sea state and time of day. While this may seem straightforward, there are some significant drawbacks to the exclusive reliance on actual flight tests conducted on board a ship, which include but are not limited to: the indispensable dependency on encountered environmental conditions and major costs associated with readiness of both helicopter and ship, usually for weeks at a time, which requires careful planning over a long period. Moreover, since one is indeed attempting to determine the limitations for a specific helicopter-ship combination, there may be safety issues involved in such experiments. In all current test methodologies, even despite any preliminary efforts before conducting the sea trials, the resulting helicopter-ship operational capabilities are still solely based on qualitatively rated test points achieved by the test pilots during dedicated sea trials. However, it occasionally happens that either due to prevailing weather conditions, ship availability or helicopter availability, the limits of the helicopter-ship combination can not be fully explored, thereby restricting the operational capability. Furthermore, the number of countries that face large cost reductions is growing, suggesting that defence organizations should be prepared for possible concessions in operational capabilities and/or lowering safety standards for evaluation of the potential boundaries for safe shipboard helicopter operations.

The goal of this research project is to develop a novel test methodology which can be used for optimizing cost and time efficiency of helicopter-ship qualification testing without reducing safety. For this purpose, the so-called "*SHOL-X*" test methodology has been established, which includes the associated predictive software tool as developed in this dissertation. The test methodology consists of three distinctive phases. In *phase I* the ship-environment in which the helicopter will operate is determined by conducting wind tunnel measurements of the airflow in the take-off and landing paths of the ship. For the helicopter a ground assessment and shore-based hover trials are carried out to verify precisely the helicopter limitations, including aspects such as pilot workload in cross-wind conditions, engine performance and control margins. Thereafter, in *phase II*, the potential operational limitations are derived by combining the behaviour of the isolated helicopter and the environmental conditions for a particular ship type. This so-called "*Candidate Flight Envelope*" is used as starting point for sea trials. Finally, in *phase III*, a (partial) flight test campaign on board the ship is conducted preferably in a range of weather conditions by day and by night. This is to determine for the particular helicopter-ship combination the effects on the pilot workload from, for example, visual references, ship motion and turbulence.

The main advantage of the new test methodology, aided by the presented predictive tool, is that the operator can perform early evaluation of safety limits for helicopters operating on ships in a wide range of in-service conditions. In this way the qualification process is less dependent on the successful outcome of solely qualitative assessed test points during dedicated sea trials. As such, the test methodology can be used to allow a well-considered assessment of the gap between the safe flight envelope, as determined by the helicopter manufacturer, and the user-defined operational flight envelope for a particular helicopter-ship combination. Additionally, the tool allows initial assessment of the impact of design changes to both helicopter and/or ship after the finally established operational limitations have been released to service with regard to flight performance and control capability. The newly developed predictive tool in this dissertation, is considered original, and can be seen as the most important novelty of this work.

The innovative test methodology, including the associated predictive tool, has already been successfully applied between 2012 and 2014 during the helicopter-ship qualification process of the NH90 NFH across the entire Dutch fleet. The academic research is mainly performed somewhere between technology readiness level 2 (i.e. technology concept and/or application formulated) and technology readiness level 4 (i.e. model and/or sub-models validation). However, the validation sea trials at full-scale enabled the high ambition of this research project to be achieved: technology readiness level 7 (i.e. model demonstration in an operational environment). This high aim might seem ambitious for an academic research; although the reader should fully understand that the aim of this research is to reduce the number of flight hours for helicopter-ship qualification testing without reducing safety.

The innovative test methodology enables the construction of operational limitations by two different options. The first and most common option is using dedicated sea trials in which the potential boundaries for the various take-off and landing procedures are validated. The second option, is the construction of the operational limitations for Hot & Heavy conditions by desk-top analysis alone, i.e., above approximately 25 °C outside air temperature (hot) with maximum weight of the helicopter (heavy). The construction of the operational limitations for Hot & Heavy conditions are based on the data gathered during shore-based hover trials and the flight test results for other referred weights (i.e. helicopter weight as a function of air density) on board the same ship type. The construction of operational limitations by desk-top analysis alone is a novel approach, and can be seen as the most important achievement of this work.

Unfortunately, the establishment of helicopter-ship operational limitations is still considered a national responsibility, and there are no internationally agreed regulations or standard procedures. Consequently, the kind of interpretation given to such limitations differs strongly between countries. Therefore, as it is assumed that each country or operator aims for maximum operational flexibility of a particular helicopter-ship combination, with minimal expenses and without any concessions in flight safety, this dissertation has the ambition to function as the starting point for international regulations or standard procedures to conduct helicopter-ship qualification testing.

Acknowledgements

This research has primarily been made possible by the support and confidence given by the Netherlands Ministry of Defence, for which I am thankful. Besides the financial contribution of the Netherlands Defence Academy (NLDA) to attend various international conferences, the most important aspect is the NH90 NFH helicopter made available by the Royal Netherlands Air Force. Of course equally important, are the various ships made available by the Royal Netherlands Navy. The availability of both the helicopter and various ship types was essential for the execution of the shore-based hover trials and full-scale sea trials.

During the past few years many people made this research project to what it finally has become. It would be impossible to mention all who have contributed. There are however some people that I would like to mention explicitly here.

On the organisatory field I would like to thank commander Hans Veken, commander Tjebbe Haringa, commander Ton Schattorie, lieutenant commander Maurice van Mourik, lieutenant commander Peter Riemens, lieutenant commander Rogier van Kralingen and major Peter Janssen, who supported the research project such that the lessons learned could be immediately implemented in the organization, and vice versa. This proved to be a valuable combination resulting in tremendous savings in time and costs of the flight test campaigns, whilst on the other hand contributing to the significance of this dissertation.

On the academic level I would like to thank professor Douwe Stapersma, who took the challenge to be promoter in a field that is not his prime expertise. Although his background as a naval engineer might have looked like a difficulty in the beginning, it proved to be a unique combination, in which he was able to challenge everything taken for granted in the helicopter community. In addition, assistant professor Marilena Pavel, as co-promoter, proved to be a good partner to discuss more in depth helicopter related aspects.

I am thankful for the input and patience of David Lee. I can only hope that our discussions of the theoretical basis will contribute in that direction. In addition, I would like to thank professor Gareth Padfield for his willingness to discuss the topic of helicopter-ship qualification testing, and to identify the novel aspects of the research, that hopefully has improved the understanding of the topic as a whole.

From an operational perspective, there was one constant force that ensured continuity in the research project as a test pilot, lieutenant commander Job Sicking. His expertise in the field of shipboard operations and high level of skills as a pilot made him an indispensable element in the project. In addition, I would like to thank lieutenant commander Bart Blok who was in the beginning of the research project a valuable instructor pilot to make the sea trials as efficient as they are now.

During the various sea trials I often witnessed the flexibility and expertise of the crew on board of the Royal Netherlands Navy ships and the maintenance personnel of the helicopter. Therefore, I would like to thank all the ship's crew and helicopter maintenance crew for their professional skills which made the trials possible.

I am thankful for the following colleagues and friends that helped proof-reading the dissertation: captain Edgar Vink and Vincent van der Kruit.

Last but not least, the moral support to complete this research project was provided by my parents, my brother, my mother-in-law, my sister-in-law, my wife Belinda and our two sons Damian and Samuel. Hopefully, both our sons have gained a lot of knowledge during this research project for their future life, whilst sitting on my lap reading along with their dad behind the computer.

Nomenclature

Roman variables

a	Speed of sound
A_b	Main rotor blade area
b_r	Systematic standard uncertainty of the result
b_{Xi}	Standard deviation bias for the measurement of each variable X_i
c	Chord
C	Vertical speed (Rate of Climb), Confidence level
$C_{(MAX)}$	Maximum achievable climb performance
C_D	3-dimensional drag coefficient
c_{dp}	Local blade section profile drag coefficient
C_{Dp}	Mean profile drag coefficient
CG_{cor}	Centre of Gravity correction coefficient
$CG_{cor(lat)}$	Centre of Gravity correction coefficient lateral cyclic position
$CG_{cor(long)}$	Centre of Gravity correction coefficient longitudinal cyclic position
$CG_{cor(pitch)}$	Centre of Gravity correction coefficient pitch attitude
$CG_{cor(roll)}$	Centre of Gravity correction coefficient roll attitude
CG_{lat}	Lateral Centre of Gravity position
$CG_{lat(desired)}$	Desired lateral Centre of Gravity position
CG_{long}	Longitudinal Centre of Gravity position
$CG_{long(desired)}$	Desired longitudinal Centre of Gravity position
c_l	Local blade section lift coefficient
C_L	Mean lift coefficient along the blade
C_{MPV}	Maximum power vertical climb coefficient
C_P	Power coefficient
c_p	Specific heat of air at constant pressure
C_T	Thrust coefficient
c_v	Specific heat of air at constant volume
C_v	Local wind speed coefficient with respect to the relevant anemometers
$C_{v(an)}$	Wind speed coefficient at the anemometer location
$C_{v(hor)}$	Local horizontal wind speed coefficient
$C_{v(loc)}$	Local wind speed coefficient
$C_{v(ver)}$	Local vertical wind speed coefficient
C_v-P	Local wind speed coefficient with respect to the port anemometer
C_v-S	Local wind speed coefficient with respect to the starboard anemometer
D	Diameter
dD_p	Profile drag component of the blade element
D_e	Diameter of the engine at a specified nominal point
dL	Lift force of the blade element
D_p	Profile drag
D_{par}	Parasite drag

dQ/r	Torque component of the blade element
dR	Air force of the blade element
D_r	Diameter of the main rotor
dT	Thrust component of the blade element
g	Acceleration due to gravity (gravitation)
g_0	Standard value for acceleration due to gravity
g_{sl}	Gravity at sea level
H	Geopotential height
h	Height
H_0	Force on the rotor disc as a result of difference in profile drag
h_{AGL}	Height above ground level
H_b	Defined geopotential height
h_{field}	Height field elevation
H_i	Force on the rotor disc as a result of difference inclination lift force
H_p	Pressure height
h_Δ	Vertical change in height for 1 hPa difference
i	Error source
J	Quantity of measured variables
k	Induced drag power factor, number of basic dimensions, error source
L	External aerodynamic moment about the *x*-axis, Lift force, Physical dimension length
l_{tr}	Distance of the tail rotor from the main rotor hub
m	Mass
$\dot{m}$	Mass flow rate
M	External aerodynamic moment about the *y*-axis, Figure of Merit, Physical dimension mass, Number of significant elemental systematic error sources
$\dot{m}_f$	Fuel mass flow through the engine
N	External aerodynamic moment about the *z*-axis, Number of rotor blades, Number of measurements
n	Index parameter
N_f	Free power turbine rotational speed
N_g	Engine gas generator rotational speed
$N_{g,ref}$	Referred engine gas generator rotational speed
$N_{g(LIMIT)}$	Actual engine gas generator rotational speed limiting value
N_r	Main rotor rotational speed
P	Power
p	Rotational velocity component of helicopter about fuselage *x*-axis, Pressure
p_0	Pressure at sea level in standard conditions
p_a	Ambient pressure
P_a	Power available
$P_{a,ref}$	Referred power available
p_b	Ambient pressure at a defined height
P_c	Climbing power
P_{clb}	Power required in vertical climb

P_d	Profile drag power caused by the H_0-force
P_{eng}	Power delivered by the engine
P_{fwd}	Power required in forward flight
P_{hov}	Power required in hover
P_i	Induced power
P_{ideal}	Ideal induced power
P_{misc}	Power needed for miscellaneous items
P_p	Profile drag power caused by the profile drag of the rotor blades
P_{par}	Parasite drag power
p_{ref}	Referred ambient pressure
P_{req}	Power required
$P_{req,ref}$	Referred power required
$P_{req,ref(alt)}$	Referred power required for alternative grouping
q	Rotational velocity component of helicopter about fuselage *y*-axis
Q	Torque
$Q_{(LIMIT)}$	Actual transmission limiting value
Q_a	Torque available
Q_{eng}	Engine torque
Q_R	Reaction torque
Q_{req}	Torque required
$Q_{req,ref}$	Referred torque required
$Q_{req,ref(alt)}$	Referred torque required for alternative grouping
$Q_{req(desired)}$	Torque required in the desired atmospheric conditions
Q_{trend}	Torque trend factor
Q_{uti}	Torque utilised
R	Gas constant
r	Rotational velocity component of helicopter about fuselage *z*-axis, Radius of a blade element, Experimental result
r_a	Result from model *a*
r_b	Result from model *b*
R_e	Effective rotor radius
Re	Reynolds number
R_r	Rotor radius
S	Equivalent flat plate area
s_r	Random standard uncertainty of the result
s_X	Sample standard deviation
s_{Xi}	Standard deviation scatter for the measurement of each variable X_i
T	Thrust, Physical dimension time, Temperature
t	Value for a given level of confidence
T_0	Temperature at sea level in standard conditions
T_1	Turbine engine inlet temperature
T_{46}	Engine power turbine inlet temperature
$T_{46,ref}$	Referred engine power turbine inlet temperature
$T_{46(LIMIT)}$	Actual engine power turbine inlet temperature limiting value
T_a	Ambient temperature
T_b	Temperature at a defined height

$TR_{actuator}$	Tail rotor actuator position
$TR_{actuator(desired)}$	Tail rotor actuator position in the desired conditions
T_{ref}	Referred ambient temperature
T_{tr}	Thrust delivered by the tail rotor
u	Translational velocity component of helicopter fuselage x-axis, uncertainty
u_c	Combined standard uncertainty with given confidence
U_c	Overall or expanded standard uncertainty with given confidence
u_r	Combined standard uncertainty of the result with given confidence
U_r	Overall or expanded standard uncertainty of the result
U_X	Expanded uncertainty estimate of measurement X
u_X	Uncertainty interval for measurement X
U_{Xi}	Uncertainty in the measured X_i
V	Forward flight speed
v	Mean velocity of the object relative to the fluid
v	Translational velocity component of helicopter fuselage y-axis
V_{an}	Mean wind speed at the height of the anemometer locations above sea level
V_c	Vertical speed (rate of climb)
V_{fd}	Mean wind speed at the height of the flight deck above sea level
v_i	Induced velocity
v_{ih}	Induced velocity in hover condition
V_{loc}	Local wind speed of ship
V_{rel}	Relative wind speed of ship
V_{res}	Resulting flow velocity of the blade
V_{tip}	Rotor tip speed
W	Weight
w	Translational velocity component of helicopter fuselage z-axis, Velocity in the far wake
$W_{(MAX)}$	Actual maximum weight
$W_{(MAX,ref)}$	Referred maximum weight
W_{MTOW}	Maximum take-off weight
W_{ref}	Referred weight
$W_{ref(achieved)}$	Referred weight achieved for the test condition
$W_{ref(desired)}$	Referred weight in the desired atmospheric conditions
X	External aerodynamic forces acting along the x-axis, Measurement
x	Forward orthogonal direction of fuselage axis at the CG
x_a	Input variable model a
x_b	Input variable model b
X_{best}	Best estimate for true value of a measurement
X_{low}	Lowest value of a measurement
x_s	Forward direction of the ship axis, Shared input variable model
X_{true}	True value of a measurement
X_{up}	Highest value of a measurement
Y	External aerodynamic forces acting along the y-axis
y	Starboard orthogonal direction of fuselage axis at the CG

y_a	Input variable to another sub-model from model *a*
y_b	Input variable to another sub-model from model *b*
y_s	Starboard direction of the ship axis
z	Downward orthogonal direction of fuselage axis at the CG
Z	External aerodynamic forces acting along the *z*-axis, Height above ground
Z_{ABL}	Atmospheric boundary layer coefficient
z_{an}	Height of the anemometer locations above sea level
z_{fd}	Height of the flight deck above sea level
z_0	Roughness height of the surface
z_s	Upward direction of the ship axis

Greek variables

ε	Precision error for parent population
α	Angle of attack
α_{tip}	Angle of attack of tip-path plane
β	Relative wave direction, Bias error for parent population
β_{an}	Horizontal wind direction at the anemometer location of ship
β_{loc}	Local horizontal wind direction of ship
β_{rel}	Relative horizontal wind direction of ship
γ	Flight path angle, Ratio of the specific heat of air (adiabatic index)
δ	Relative pressure, Measurement error
δ_i	Error in a specific measurement *i*
Δ_{IGV}	Position Inlet Guide Vanes
δ_{lat}	Lateral cyclic position
$\delta_{lat(desired)}$	Desired lateral cyclic position
δ_{long}	Longitudinal cyclic position
$\delta_{long(desired)}$	Desired longitudinal cyclic position
Δ_{VSV}	Position Variable Stator Vanes
ζ	Relative wind direction
η	Mechanical efficiency
Θ	Physical dimension temperature
θ	Relative temperature
θ_f	Euler angle defining the pitch attitude of the helicopter
$\theta_{f(desired)}$	Euler angle defining the pitch attitude of the helicopter in desired condition
θ_p	Blade pitch angle
λ	Temperature gradient (lapse rate)
λ_i	Inflow ratio
μ	Advance ratio, Viscosity coefficient, Mean value
Π	Dimensionless dependent variable
ρ	Air density
ρ_0	Air density at sea level in standard conditions
ρ_a	Ambient air density
ρ_{ref}	Referred ambient air density

σ	Relative density, Solidity, Standard deviation parent population
υ	Number of degrees of freedom for *t* distribution
φ	Inflow angle, Vertical flow direction with respect to the relevant anemometers
φ_{an}	Vertical wind direction at the anemometer location of ship
ϕ_f	Euler angle defining the bangle angle helicopter, Heat flow of the fuel
φ_{loc}	Local vertical flow direction of ship
ϕ_{RH}	Relative humidity
χ	Local horizontal flow deviation with respect to relevant anemometers
χ_{an}	Horizontal flow deviation at the anemometer location of ship
χ_{loc}	Local horizontal flow deviation of ship
χ-*P*	Local horizontal flow deviation with respect to port anemometer
χ-*S*	Local horizontal flow deviation with respect to starboard anemometer
ψ	Azimuth angle
ψ_f	Euler angle defining the yaw angle helicopter
ω	Relative rotorspeed
Ω	Rotor rotational speed

Abbreviations

ACC	Actuator Control Computer
ADC	Air Data Computer
ADS-33	Aeronautical Design Standard 33
AEO	All Engine Operatives
AFCC	Automatic Flight Control Computer
AFCS	Automatic Flight Control System
AGL	Above Ground Level
AIAA	American Institute of Aeronautics and Astronautics
AOR	Auxiliary Oiler Replenishment
ASME	American Society of Mechanical Engineers
ATC	Air Traffic Control
AUW	All-Up Weight
CFD	Computational Fluid Dynamics
CFE	Candidate Flight Envelope
CG	Centre of Gravity
CPL	Commercial Pilot License
CR	Control Reference
DAU	Data Acquisition Unit
DEP	Design Eye Position
DIMSS	Dynamic Interface Modelling and Simulation System
DIPES	Dynamic Interface Pilot Effort Scale
DKU	Digital Keyboard Unit
DNW	German-Dutch Wind tunnels
DT&E	Development Test & Evaluation
DVE	Degraded Visual Environment
ECS	Environmental Control System
EECU	Engine Electronic Control Unit
EMC	Electro Magnetic Compatibility
EMI	Electro Magnetic Interference
ENG	Engine
EO	Electro Optic
EPNER	École du personnel navigant d'essais et de reception
ESLRP	Engine Speed Limited Referred Power
ETLRP	Engine Temperature Limited Referred Power
ETPS	Empire Test Pilots' School
FADEC	Full Authority Digital Engine Control
FCC	Flight Control Computer
FCCCP	Flight Control Central Control Panel
FCLCP	Flight Control Lateral Control Panel
FCMC	Flight Control Mechanical Characteristics
FCP	Flight Control Processing

FCS	Flight Control System
FCSAU	Flight Control System Auxiliary Unit
FDO	Flight Deck Officer
FLI	First Limit Indicator
FOD	Foreign Object Damage
FOV	Field Of View
FTE	Flight Test Engineer
GPI	Glide Path Indicator
GPS	Global Positioning System
HOSTAC	Helicopter Operations from Ships other Than Aircraft Carriers
ICAO	International Civil Aviation Organization
ICD	Interface Control Document
IEC	Instrument Error Correction
IETP	Integrated Electronic Technical Publication
IGV	Inlet Guide Vanes
IRS	Inertial Reference System
ISA	International Standard Atmosphere
ISO	International Standardization Organization
ITU	Inceptor Transducer Unit
JSHIP	Joint Shipboard Helicopter Integration Process
KNMI	Koninklijk Nederlands Meteorologisch Instituut
LCF	Air defence and Command Frigate
LHV	Lower Heat Value of fuel
LLF	Large Low-speed Facility
LPA	Landing Platform Amphibious
LPD	Landing Platform Dock
$LRP_{(MIN)}$	Lowest limited Referred Power
LWIR	Long Wave Infra Red
MCP	Maximum Continuous Power
MFRI	Multi-purpose frigate
MGB	Main Gear Box
MPV	Maximum Power Vertical
MRA	Main Rotor Actuator
MRH	Multi Role Helicopter
MTE	Mission Task Element
MTOW	Maximum Take-Off Weight
MWIR	Medium Wave Infra Red
NAHEMA	NATO HElicopter Management Agency
NATO	North Atlantic Treaty Organisation
NFH	NATO Frigate Helicopter
NHI	NATO Helicopter Industries
NLDA	Netherlands Defence Academy
NLMoD	Netherlands Ministry of Defence
NLR	National Aerospace Laboratory
NNLN	NFH Netherlands Navy
NVG	Night Vision Goggles

OAT	Outside Air Temperature
OEI	One-Engine Inoperative
OFE	Operational Flight Envelope
OGE	Out-of-Ground Effect
OPV	Ocean Patrol Vessel
OT&E	Operational Test & Evaluation
PEC	Pressure Error Correction
PFCAC	Primary Flight Control Analogue Computer
PFCDC	Primary Flight Control Digital Computer
PFCS	Primary Flight Control System
PMC	Plant Management Computer
PPI	Power Performance Index
PT	Port
QNH	Air pressure with reference to mean sea level
REP	Reference Eye Position
ROC	Rate Of climb
ROSDIS	ROtorcraft Ship Dynamic Interface Simulation
RPM	Revolutions Per Minute
RRM	Risk Reduction Measures
RRR	Rotors Running Refuelling
RTM	Rolls Royce Turbomeca MTU Piaggio engine
SB	Starboard
SFE	Safe Flight Envelope
SHOL	Ship Helicopter Operational Limitation
SI	Système International d'unités
SME	Subject Matter Experts
TAS	True Air Speed
TFCP	Trimmed Flight Control Position
TLRP	Transmission Limiter Referred Power
TRA	Tail Rotor Actuator
TRL	Technology Readiness Level
TSM	Taylor Series Method
UCE	Usable Cue Environment
UMF	Uncertainty Magnification Factor
USCG	United States Coast Guard
USMC	United States Marine Corps
USNTPS	United States Naval Test Pilot School
VAR	Vibration Assessment Rating
VHF	Very High Frequency
VSV	Variable Stator Vanes
WCA	Wind Correction Algorithm
WTU	Winchman Trim Unit

Page intentionally left blank

Chapter 1 **Introduction**

1.1 Background and Relevance

A comprehensive analysis of the current methodologies used for helicopter-ship qualification testing, also known as dynamic interface testing, reveals that the operational capabilities for shipboard operations are evaluated after the ship and helicopter are built independently from each other. The limitations and associated operational envelopes that results from the combination of the independent designs is accepted. This process contrasts sharply with a typical procurement procedure in which a 'system' is designed and built to an agreed set of requirements. At present, the helicopter industry delivers a helicopter that has undergone elaborate in-flight test campaigns performed to demonstrate safe flight within the expected operational envelope for land-based operations. However, establishing the operational capabilities and associated limitations for safe shipboard operations is still considered a responsibility of the operator. For some reason, there are still no internationally agreed regulations or standard procedures to establish the desired helicopter-ship operational limitations. Consequently, the kind of interpretation given to such limitations differs strongly between countries.

Traditionally, each specific helicopter-ship combination is extensively evaluated at sea during varying environmental conditions like, for example, wind speeds, wind directions, sea state and time of day. While this may seem straightforward, there are some significant drawbacks to the exclusive reliance on actual flight tests conducted on board a ship, which include but are not limited to: the indispensable dependency on encountered environmental conditions and major costs associated with readiness of both helicopter and ship, usually for weeks at a time, which requires careful planning over a long period. Moreover, since one is indeed attempting to determine the limitations for a specific helicopter-ship combination, there may be safety issues involved in such experiments. In some current test methodologies, even despite any preliminary efforts before conducting sea trials, the resulting helicopter-ship operational capabilities are still solely based on qualitatively rated test points achieved by the test pilot during dedicated sea trials. However, it occasionally happens that either due to prevailing weather conditions, ship availability or helicopter availability the limits of the helicopter-ship combination can not be fully explored, thereby restricting the operational capability. Furthermore, the number of countries that face large cost reductions is growing, suggesting that defence organizations should be prepared for possible concessions in operational capabilities and/or lowering safety standards for evaluation of the potential boundaries for safe shipboard helicopter operations.

As it is assumed that each country or operator aims for maximum operational capability of a particular helicopter-ship combination, achieved with minimal expenses

and without any concessions to flight safety, this dissertation describes an innovative methodology for helicopter-ship qualification testing. The innovative helicopter-ship qualification testing methodology is aided by a predictive software tool to be developed in this dissertation, named "*SHOL-X*", which eliminates subjective elements as much as possible by determining unambiguous operational envelopes used for in-service conditions in a world-wide theatre for many years to come. This dissertation is aimed at both junior and experienced rotorcraft engineers, researchers, academia, flight test engineers and pilots. But in particular managers who are involved in flight trials of helicopter-ship combinations as part of a complex flight test program for which they are required to plan, conduct and report on ship helicopter operational limitations. This dissertation has the ambition to function as the starting point for international regulations or standard procedures to conduct helicopter-ship qualification testing.

1.2 Literature Review

Full-scale helicopter operations onboard any ship, as opposed to most simulated scenarios, are likely to include a combination of e.g. ship motion, sea spray, turbulence due to the ship's superstructure and various environmental conditions. Although a combination of these aspects is always present in reality, so far most helicopter-ship interface related research considered only individual aspects at a time. Due to the multi-disciplinary character of this research, a complete review of the current developments in the vast field of helicopter-ship dynamic interface would be too elaborate. Nevertheless, the more essential literature describing the exploration of the helicopter-ship operational capabilities will be reviewed in the following.

1.2.1 Dynamic Interface Modelling and Simulation

A potential alternative to traditional at-sea full-scale helicopter-ship qualification testing is the use of pilot-in-the-loop simulation (i.e. pilot-out-the-loop simulation has so far never been seriously considered to define the helicopter-ship operational potential). An obvious benefit from using helicopter flight simulators is the availability of any sea state, wind condition and surface ship, provided one has appropriately detailed mathematical models that characterize their respective influence on the landing and take-off task. However, computer simulation of the dynamic interface environment is very complex due to the need to model all aspects of the test environment that may dictate the boundaries for a specific Ship Helicopter Operational Limitation (SHOL) envelope which defines the operational capabilities. The aspects to simulate in the flight simulator include amongst others: proper modelling of the ship motion in the particular sea-state condition, the atmospheric turbulence generated by the ship's superstructure, the helicopter response to both pilot inputs and airwake disturbances, and the interaction of the helicopter induced velocity with the ship's structure in the landing zone [1,2]. In addition, any pilot-in-the-loop simulation used must have adequate fidelity in terms of flying characteristics, motion, aural and visual cueing [3,4,5,6,7]. The term adequate is vague, and to set the requirements for defining this term is a study by itself. Important is to remember that advances in any particular aspect will not be complete without comparable improvements in modelling accuracy in the related areas and the interactions between them.

An example for developments in the pilot-in-the-loop simulation is the Dynamic Interface Modelling and Simulation System (DIMSS), which was a five-year modelling and simulation project of the Joint Shipboard Helicopter Integration Process (JSHIP) starting in 1998 [8]. The goal of DIMSS was to define a process for defining SHOLs for any helicopter-ship combinations using modelling and simulation. Its specific purpose was to increase the interoperability of joint shipboard helicopter operations for helicopter units that were not specifically designed to go aboard navy ships. A pilot-in-the-loop flight simulator was developed which included integration from several high fidelity models of the ship and ocean environment, helicopter cockpit, flight controls and flight characteristics. The subjective pilot workload ratings given and the encountered helicopter limitations in the simulator were used to define the flight envelope purely by simulation. However, whilst the DIMSS methodology offered a potential characterization of workload trends, there was insufficient real-world data gathered in high sea states and because of that not enough confidence to use the methodology to near full-scale at-sea and simulation test results. Ironically, one of the reasons why modelling and simulation can be of great benefit for developing SHOL envelopes, the ability to test any condition, is the reason why the simulation could not be fully accredited [9]. Other pilot-in-the-loop research activities performed, although at a smaller scale, for example by the University of Liverpool [10] and the National Aerospace Laboratory (NLR) [11] have so far only been used for generic research and not to define a SHOL of a particular helicopter-ship combination.

Therefore, present pilot-in-the-loop simulation models are unlikely to replace experimentally derived operational envelopes in the near future, although they may provide understanding of the airwake and the unique problems that helicopter-ship operations encounter. Only when there is sufficient certainty in the similarity of the simulation for a particular helicopter-ship combination, and when the restraints of simulation in these applications are well understood, can one begin to consider the replacement of in-flight testing and evaluation by these alternative means. More specifically, the main areas that need focus to increase the potential for pilot-in-the-loop simulation are at least the following:

1. The required fidelity and level of complexity for the ship's airwake, as implemented in the simulator, in comparison with a ship at full-scale;
2. The similarity of the implemented flight loop compared with the actual helicopter flight characteristics, with the focus on the low speed region;
3. The combination of the previous items; the accuracy of the methodology applied to ensure representative interaction between the ship's airwake and the flight loop;
4. The similarity in visual references with the ship, for example, the Field Of View (FOV) as caused by the cockpit structure and the visual aids as applied for take-off and landing on board the ship.

1.2.2 Full-Scale Helicopter-Ship Qualification Testing

Helicopter-ship qualification testing is considered complex and should only be performed by agencies that have specialized flight test crew and engineering teams that

are knowledgeable of this type of testing. These conditions are fulfilled only in a limited numbers of countries amongst which are the United States of America, the United Kingdom and the Netherlands [12]. So far, worldwide, even despite all the preliminary efforts in determination of the environment near the ship deck [13,14,15], the resulting operational capabilities of any helicopter-ship combination are still solely based on subjectively assessed test points by the test pilot during dedicated sea trials. The progression of the test is primarily driven by subjective pilot workload ratings as shown in Figure 1-1.

For each condition tested, the results are evaluated and subsequently the required increase in difficulty of the next test condition is determined. However, a prediction of the increase in pilot workload is only possible to a certain extent. If, for example, the workload in a certain condition is "*low*", the permitted increase in difficulty of the next test condition will be greater than in the case for "*high*" workload. The same rule is applied (in reverse) in the case a condition is considered "*unacceptable*". If it is "*beyond unacceptable*" (occurring sporadically), a large decrease in difficulty is applied whereas if the condition is considered "*just unacceptable*" a small decrease in difficulty is applied. The most common test technique is to proceed in steps of 5 knots or 15 degree increments from existing "*safe*" conditions towards the next test point. At night only tests within the limits of "*safe*" day testing are performed.

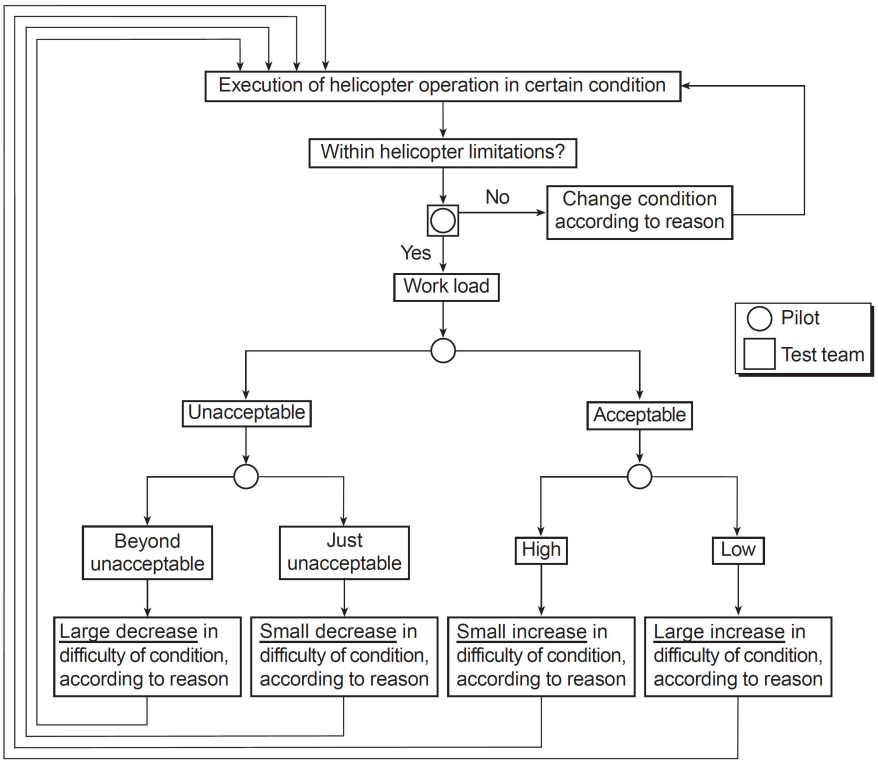

Figure 1-1; Flight test procedure on board ship [12]

A somewhat more sophisticated approach, although at the end still only based on the outcome of dedicated sea trials, is developed by the NLR as shown in Figure 1-2 [16]. This approach includes wind tunnel tests on a scale model of the ship, full-scale ship's wind climate tests and shore-based hover trials to determine some helicopter flight characteristics. Wind tunnel tests on ship models are carried out to determine the airflow characteristics (i.e. airflow deviations with respect to the undisturbed oncoming relative wind) above the flight deck and in the possible approach and departure paths of the helicopter at the ship as a function of the relative wind. The relative wind is the wind vector resulting from the true wind and ship's course and speed. Thereafter, full-scale airflow trials are conducted for every ship type prior to helicopter tests on board. With the information obtained, a relation between the anemometer readings, the air flow conditions above the flight deck, in the helicopter approach and departure paths, and the undisturbed relative wind conditions can be determined.

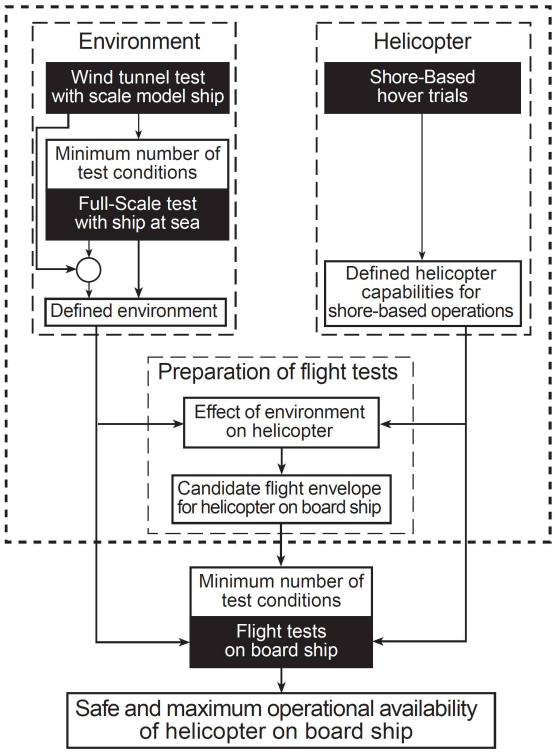

Figure 1-2; Set-up of helicopter-ship qualification programme [16]

The purpose of the shore-based hover trials is to establish power margins and controllability limits in an omni-directional wind envelope to complement the flight manual information, as these are generally lacking detailed information. The test is performed at several altitudes Above Ground Level (AGL), yawing the helicopter relative to the ambient wind in steps of 45 degree increments and when necessary in smaller increments. Starting with head winds (wind on the nose of the helicopter) and working around from 0° to 405° (i.e. 360° + 45°). When a stable hover condition is

obtained, engine torque, rotor rpm, helicopter attitudes, and flight control positions are recorded in addition to ambient conditions (pressure altitude, Outside Air Temperature (OAT), ambient winds, etc.). The data obtained should indicate where, within the land-based envelope, regions exist where the margin between available and required helicopter performance is small. Unfortunately, the shore-based hover trials are conducted by performing hover turns in actual wind conditions. Therefore, testing is required over long periods (i.e. months) and only the limited number of wind speeds encountered during the shore-based hover trials can be used to estimate the potential flight envelope for shipboard operations.

The starting point for the sea trials then results by the best guess of combining the manufacturer's land-based low speed flight envelope and a huge amount of data gathered for the ship's environment and during the shore-based hover trials. Thereby, the real challenge by using this approach is to define the limitations imposed by the environment in quantitative terms. Often it is not a matter of demonstrating the capability to operate the helicopter at the condition specified, but to obtain data at differing conditions and interpolating or extrapolating the results to the conditions required. Unfortunately, despite the preliminary effort to define the ship environment and helicopter-flight characteristics the final result is still only based on the outcome of dedicated sea trials. Concluding, there are some major drawbacks in this approach whilst primarily relying on subjective pilot ratings:

1. It occasionally happens that either due to prevailing weather conditions, ship availability or helicopter availability the limits of the helicopter-ship combination can not be fully explored, thereby restricting the operational capability.
2. The increase in difficulty of the next test conditions is vague, and has more than once resulted in exceeding helicopter limitations and/or hazardous situations for the aircrew (later to be told passionately at the bar with a beer).
3. The possible limitations for any helicopter-ship combination have to be approached with a conservative incremental approach. In this way, losses are likely of valuable time and/or useful environmental conditions which could not be compensated for at a later stage of the test campaign.
4. It has been demonstrated that the pilot(s) used for SHOL development either at-sea or in a simulator will have an impact on the envelopes released to operational service for a large diversity of squadron pilots [9]. The variations in subjective pilot workload ratings underline the requirement for a flight test instrumented helicopter to be used for helicopter-ship qualification testing. The flight test instrumentation suite should record the helicopter flight characteristics and ship parameters, to be analyzed during post-flight analysis, in order to verify any pilot comments, although this is definitely not common standard.
5. The flight trials are mainly driven by momentarily decisions, based on qualitative judgement, to increase the difficulty of the next test conditions. However, a test conditions can only be assessed after it has be flown, as such there may be safety issues involved.

1.2.3 Cross-Ops Envelopes

If helicopter-ship qualification testing has not yet been performed for a specific combination, for example operations with a Dutch helicopter on board a foreign naval vessel, they may, under restrictive conditions, be operated in a pre-determined operational envelope. These kind of pre-determined operational envelopes are known as "*Cross-Ops*". For operations between countries within the North Atlantic Treaty Organization (NATO), the procedures to construct such envelopes are briefly described in the Helicopter Operations from Ships other Than Aircraft Carriers (HOSTAC) [17]. It is obvious that these "*Cross-Ops*" envelopes are necessarily conservative and restrict the operational capability of the ship. Therefore, circumstances can occur in which other operational tasks from the ship have priority over flight operations, and thus the helicopter will not be able to take-off or land as the ship can not provide the appropriate conditions for helicopter operations. Moreover, since one is indeed attempting to determine the limitations for a specific helicopter-ship combination by rules of thumb without scientific basis, there may be safety issues involved as there are huge subjective elements in the construction of it. This dissertation does not further discuss the construction of "*Cross-Ops*" envelopes, as without the proper knowledge to conduct helicopter-ship qualification testing, and the subsequent data analysis to define operational limitations, its construction is pure speculation.

1.3 Research Objectives

The research objectives are derived from the key motivation to optimize for cost and time efficiency of helicopter-ship qualification testing.

1.3.1 Key Motivation

The helicopter is required to perform within the user-defined Operational Flight Envelope (OFE), or a specific combination of airspeed, temperature and other limiting parameters that bind the helicopter dynamics required to fulfil the user's intended operation. Outside this envelope lies the manufacturer-defined Safe Flight Envelope (SFE), which sets the limits to safe flight, normally in terms of the same parameters as the OFE, but representing the physical limits of structural, aerodynamic, powerplant, transmission or flight control capabilities. The margin between the OFE and the SFE needs to be large enough so that inadvertent transient excursions beyond the OFE are tolerable. Due to the unique characteristics of each specific helicopter-ship combination and the innumerable combinations possible, it is understandable that in most cases no (extensive) testing has been carried out by the helicopter manufacturer for every combination that could potentially be of interest. To determine these particular operational limitations a dedicated helicopter-ship qualification test program needs to be executed. It would be an obvious advantage to have a predictive engineering software tool capable of performing early evaluations of safety limits for helicopters operating on ships in a wide range of in-service conditions. In this way, the qualification process will be less dependent on the successful outcome of several dedicated sea trials. More importantly, the predictive tool can be used to allow a well-considered assessment of the gap between the SFE, as determined by the helicopter

manufacturer, and the user-defined OFE (overcoming the major drawbacks in the current approaches). Additionally, such a predictive tool allows initial assessment of the impact of design changes to both helicopter and ship after the SHOLs have been released to service with regard to flight performance and control capability.

1.3.2 Overview Objectives

The objectives of the research are threefold, whilst of course aiming to engineer for safety, by combining the outcomes of the following:

1. The first objective is to increase the knowledge in the behaviour of the helicopter in the shipboard environment. This is required as the use of a predictive tool to increase the knowledge of the helicopter-ship interface necessitates not only development, but also verification, calibration and validation of this tool. Only after these laborious tasks the predictive tool can be rightfully used to make predictions prior to, or instead of full-scale measurements with a helicopter at sea.
2. As a next step, the second objective is to improve trial efficiency of helicopter-ship qualification testing for various operational conditions at sea. However, regardless of what pre/post test data manipulation is performed, the fleet is likely to remain required for testing of some relative wind conditions and ship motions to assess the pilot workload and visual references acceptability. Therefore, the requirements of what is acceptable as a bare minimum for sea trials should be determined in order to evaluate a particular helicopter-ship combination.
3. The third objective is to investigate the effects of atmospheric conditions on the performance of the helicopter by means of full-scale trials. This is required to determine to which extent results from sea trials performed in the North Sea, can be used to construct operational limitations for Hot & Heavy conditions by desk-top analysis alone, i.e., above approximately 25 °C outside air temperature (hot) with maximum weight of the helicopter (heavy).

More specifically, the objectives and their related research questions are summarized as follows:

1. Create a predictive software tool that represents reality accurately enough to make it useful to evaluate the operational capability of any helicopter-ship combination. The questions to be answered are:
    a. What is the validity of this tool with respect to: helicopter performance, flight characteristics and other limitations?
    b. To what extent can this tool be used to evaluate the operational capabilities of a specific helicopter-ship combination objectively?
2. Use the predictive software tool to develop a test methodology that aims at a bare minimum in flight hours and the lowest possible demand on sailing periods for ships without any concessions to flight safety. This requires the following questions to be answered:

a. How should the predictive software tool be used in order to have maximum benefit during the construction and exploration of a practically applicable operational flight envelope?
b. How should a newly developed predictive software tool be tested in order to assess its accuracy in the predictions made?
c. How much actual at-sea testing is required as a bare minimum for a specific helicopter-ship combination?
d. How should any regulations for helicopter-ship qualification testing be defined, in order to be applied as an international standard?

3. Investigate the effects of variations in the atmospheric conditions on the performance of the helicopter during shipboard operations in a world-wide theatre. The questions to be answered are:
   a. What are the effects of variations in the atmospheric conditions on the boundaries of the operational flight envelope?
   b. What are the most restricting aspects for the operational flight envelope?
   c. What is the impact of a particular ship type (due to for instance airwake disturbances or ship motion) on the operational flight envelope?

1.4 Research Limitations

This research is mainly focussed on the development of safe operational envelopes for the take-off and landing of a helicopter during shipboard operations. It is concerned with optimizing helicopter-ship qualification testing without reducing safety, rather than how to design and build ships and/or helicopters to achieve the defined level of quality. It cannot, nor does it intend to, ignore design issues; however requirements can be credible only if they are achievable with the available hardware. The research does not include a pilot model (e.g. pilot-in-the-loop simulations) as only when there is sufficient certainty in the similarity of the simulation for a particular helicopter-ship combination, and when the restraints of simulation in these applications are well understood, it can be considered to replace in-flight testing and evaluation by a pilot model in the future. In addition, as wind tunnel measurements of the ship's airwake were readily available, of which the author had access, no alternative means for ship airwake simulation has been considered.

Furthermore, this research does not include any deck handling of the helicopter once on the flight deck. In general, once the helicopter has landed, it is secured to ensure that it does not slide across the flight deck. On deck, limitations are imposed for example for spreading and folding the main rotor blades, engaging and disengaging of the main rotor blades during start-up and shut-down, and for moving the helicopter from the landing spot towards the hangar and vice versa. The corresponding limitations for deck handling may have already been demonstrated by the industry and the results presented in the flight manual. In that case, the operator of the helicopter is restricted to operate within these limitations; otherwise a dedicated test campaign should be

scheduled to demonstrate the boundaries of the envelope. However, defining the deck handling limitations is considered a different discipline and is not further considered in this research project.

1.5 Proposed Approach

The limitations for land-based operations determined after extensive factory testing, are based amongst others on a rigid and unobstructed landing site. On the other hand, the limitations for ship-borne operations are to be based on an obstructed landing site (i.e. flight deck) which may show random oscillatory movement and where strong turbulent wind conditions can prevail. Sometimes an almost marginal facility is provided for take-off, landing and deck handling. Yet, helicopter operations may be required in a wide range of operational conditions (day, night, sea-state, wind, visibility, etc.) with the highest possible payload. Nowadays, in line with the increasing importance of helicopter/ship operations the helicopter manufacturer sometimes provides limitations of a general nature for helicopter-ship operations. However, because of the unique characteristics of each helicopter-type/class-of-ship combination and the innumerable combinations possible it is understandable that usually no (extensive) testing has been carried out by the helicopter manufacturer for all combinations that may be of interest for each operator. It follows that the limitations given, if any, must be considered as general guidelines, with large safety margins with respect to the helicopter capabilities and pilot ability to control the helicopter, and thus do not provide the maximum operational capability of the helicopter on board the ship. It is expected that the actual limitations, i.e. those that allow maximum operational capability of the helicopter within the constraints of safety, are lying somewhere between the limitations for land-based and those for shipboard operations as given by the manufacturer. To determine these limitations a dedicated helicopter-ship qualification programme is to be executed. An innovative three-phase approach for establishing SHOLs, aided by a predictive software tool to be developed in this dissertation named "*SHOL-X"* is developed as shown in Figure 1-3.

The proposed approach eliminates subjective elements by determining unambiguous operational envelopes by merging the huge amount of data gathered in the phase prior to the embarked sea trials, whilst making the merging process transparent for everybody involved in the test campaign and the authorizing authorities. In *Phase I* the ship-environment (green box in figure) in which the helicopter will operate is determined by conducting wind tunnel measurements of the airflow in the take-off and landing paths of the ship. This is (still) followed by a validation with full-scale measurements of the airflow above the flight deck of the ship. For the helicopter (yellow box in figure), a ground assessment and shore-based hover trials with a pace-car are carried out to verify precisely the helicopter limitations, including aspects such as e.g. pilot workload in cross-wind conditions, engine performance and control margins resulting in objectively predicted flight capabilities and engine characteristics. Thereafter, in *phase II* (blue box in figure), the so-called "*Candidate Flight Envelope*" (CFE) is obtained by the predictive tool "*SHOL-X*", to be developed in dissertation, combining the behaviour of the isolated helicopter, the specific environmental

conditions for a particular ship type and other miscellaneous items. The CFE is a diagram giving the likely combinations of indicated wind speed (in radial coordinates) and direction (in angular coordinates) for safe take-offs and landings from a particular ship type. The miscellaneous items (red box in figure) could be added to optimize the CFE, for example experience from previous test campaigns with either the helicopter or the ship under test. Once the CFE is developed, the associated uncertainty and adequate safety margins are established prior commencing sea trials. Finally, in *phase III*, based on the CFE, a (partial) flight test campaign on board the ship is conducted preferably in a range of weather conditions by day and by night (black outlined white boxes in figure). This is to determine for the particular helicopter-ship combination the effects on the pilot workload from, for example, visual references, ship motion and turbulence.

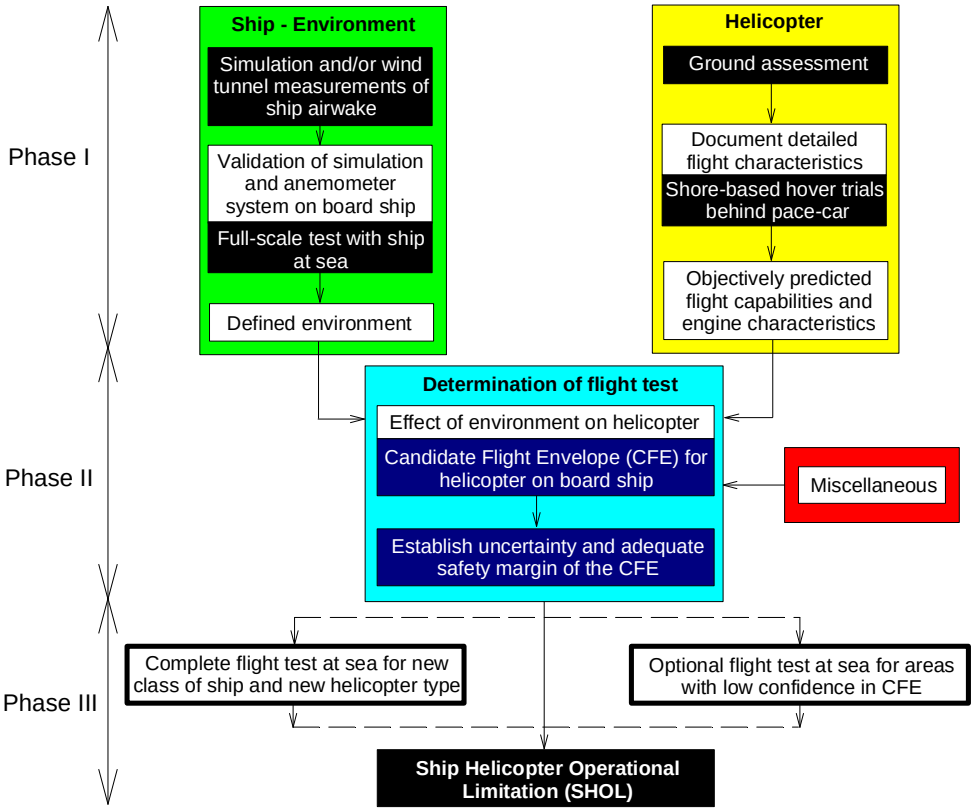

Figure 1-3; Innovative flow chart SHOL development

The finally determined operational limitations for safe take-off and landing from a particular ship type, known as SHOL, are presented as a set of diagrams (i.e. polar plot) giving the combination of ship motion with indicated wind speed (in radial coordinates) and direction (in angular coordinates) as shown for example in Figure 1-4. Note that for security reasons, the axes from the remaining polar plots presented in this dissertation have been removed. There are separate SHOLs developed for a range of

weights of the helicopter, varying take-off and landing procedures and day or night conditions. The boundaries of these operational envelopes are either defined when approaching and/or exceeding quantitative helicopter limitations, or when the pilot's workload becomes too high to consistently make safe take-off and landings. The proper merging of the quantitative and qualitative assessment is what now defines the operational capacities for a particular helicopter-ship combination. For example, a helicopter with a low thrust margin or inadequate vertical agility is in danger of unintentional contact with the flight deck in high sea states. Alternatively, in strong cross-winds, the limit of tail rotor thrust can be reached such that the pilot cannot maintain heading. Therefore, the SHOL envelopes are equally reliant on an acceptable envelope based on objective helicopter limitations, as on acceptable piloting workload to perform the task. During operational scenarios the combination of ship motion, wind speed and wind direction must be within the relevant SHOL envelope. If they are not, an alternative take-off and landing procedure or different helicopter weight category must be chosen, or the ship must be forced to change course and speed to achieve the environmental conditions within the defined envelope.

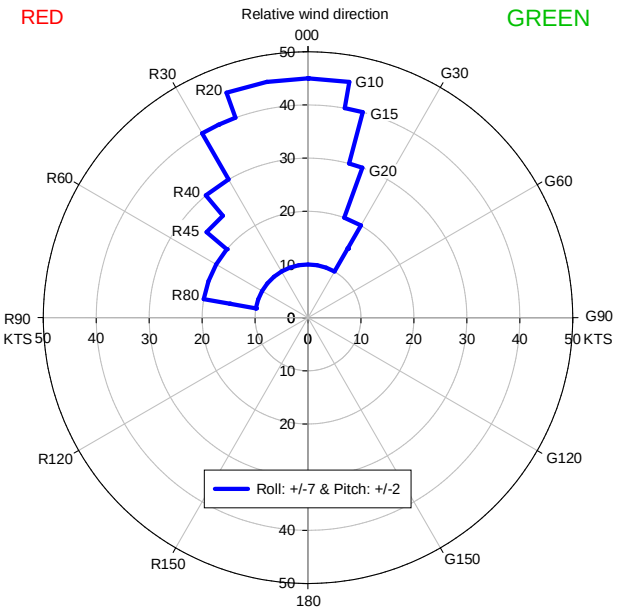

Figure 1-4; Example SHOL envelope

1.6 Technology Readiness Level

A Technology Readiness Level (TRL) is the results from a systematic, metrics-based process that assesses the maturity of, and the risk associated with, critical technologies to be used [18,19,20]. The outcome helps to answer the question: "*readiness for what*"? This question might seem debatable for an academic research; although the reader should fully understand that the aim of this research is to reduce the number of flight hours for helicopter-ship qualification testing without reducing safety. To make

rightful conclusions of this ambitious research objective, the test methodology and consequential software model to be developed in this dissertation, needs to be available and validated to make full-scale predictions. The definitions for TRL, with some change in terminology (as to better reflect the meaning), are summarized in Table 1-1. In contrast, to most academic research that turns out somewhere between TRL 2 (i.e. technology concept and/or application formulated) and TRL 4 (i.e. model and/or sub-models validation), the ambition of this research project is to aim at TRL 7 (i.e. model demonstration in an operational environment). This implies focus and discussion on a consequential amount of operational aspects in this dissertation. The reason why TRL 8 (i.e. actual model completed through test and demonstration) is not aimed for is that it requires most user documentation, training documentation and engineering support in place to support the test methodology and developed model. Although this dissertation hopefully functions as the basis for any future efforts in that direction, it is considered outside of the scope of this research project to include and develop a software tool to be readily available for commercial purposes.

1.7 Simple Guide to the Dissertation

This dissertation is structured into 7 chapters. First in Chapter 2, an introductory tour of the relevant aspects and operational procedures required for a basic understanding of helicopter-ship qualifications testing is given. Chapter 3 explains the possible model and measurement uncertainties and how these uncertainties propagate in the predictions made by the predictive tool. Furthermore, the safety margins and confidence levels of the various helicopter parameters are discussed. The test methodology to be developed consists of three distinctive phases. In *phase I* as discussed in Chapter 4, the ship-environment in which the helicopter will operate is determined by conducting wind tunnel measurements of the airflow in the take-off and landing paths of the ship. For a specific helicopter, a ground assessment and shore-based hover trials are described to verify precisely the helicopter limitations, including aspects such as e.g. pilot workload in cross-wind conditions, engine performance and control margins. These initial chapters are necessary to rightfully support use of the predictive tool to assess the likely operational capability for take-off and landing of a particular helicopter-ship combination. Thereafter, in *phase II* as discussed in Chapter 5, the potential operational limitations are derived by combining the behaviour of the isolated helicopter and the environmental conditions for a particular ship type. The outcome is used as the starting point for sea trials. Finally, in *phase III* as discussed in Chapter 6, a (partial) flight test campaign on board the ship is described to be conducted preferably in a range of weather conditions by day and by night. This is to determine for the particular helicopter-ship combination the effects on the pilot workload from, for example, visual references, ship motion and turbulence. In addition, the flight test results from various sea trials are used to validate the predictions made by the predictive tool. This dissertation concludes with Chapter 7, in which the results are summarized, conclusions are drawn, and recommendations are given.

TRL	Definition	Description	Exit Criteria
1	Basic principles observed and reported.	Basic properties software architecture, mathematical formulations, and general algorithms.	Peer reviewed publication with proposed concept and application.
2	Technology concept and/or application formulated.	Basic properties of algorithms, representations and concepts defined.	Description of the application and concept with feasibility and benefit.
3	Analytical and experimental critical function and/or proof of concept.	Scientific feasibility is demonstrated through analytical studies or experimental results.	Analytical or experimental results validating predictions of key parameters.
4	Model and/or sub-models validation.	Functionally critical software components are integrated. Relevant environment defined.	Test performance demonstrating agreement with a full-scale problem.
5	Model and/or sub-models validation in a relevant environment.	Experiments with realistic problems. System software architecture established.	Test performance demonstrating agreement with a full-scale problem.
6	Model and/or sub-models validation in a relevant end-to-end environment.	Limited documentation available. Engineering feasibility fully demonstrated.	Comparisons between tested and operational environment understood.
7	Model demonstration in an operational environment.	Software exists having most functionality available for demonstration and test.	Critical technological properties measured against operational environment.
8	Actual model completed through test and demonstration.	All user and training documentation completed. All functionality tested in operational scenarios.	Published documentation and product technology.
9	Actual model proven through operational capabilities.	All documentation verified. Engineering support in place. System successfully operated.	Documented mission results in operational environment.

Table 1-1; Technology Readiness Level (TRL) definition; modified from [19,20]

Chapter 2 Helicopter-Ship Qualification Testing – *an introductory tour*

2.1 Introduction

This chapter is intended to guide the reader on a tour of the subject of the dissertation with the aim of instilling increased motivation by sampling and linking the wide range of subtopics that make the whole. The tour topics will range from relatively simple subjects such as how different approaches and take-offs are made in a shipboard environment, through to more complex topics such as the helicopter flight characteristics, the disturbances caused by the superstructure of the ship and the subsequent effects of these disturbances on helicopter flight performance. All these topics lie within the domain of helicopter-ship qualification testing and within the scope of this dissertation. This chapter is required reading for the reader who wishes to benefit most from the dissertation as a whole. Many topics are introduced and developed in fundamental form here in this chapter, and the material in later chapters will draw on the resulting understanding gained by the reader. One feature is re-emphasized here. This dissertation is concerned with optimizing helicopter-ship qualification testing without reducing safety, rather than how to design and build ships and/or helicopters to achieve the defined level of quality. It cannot, nor is it wished to, ignore design issues; however requirements can be credible only if they are achievable with the available hardware.

2.2 Four Reference Points

First, four useful reference points are introduced for developing an appreciation of the factors resulting in an operational flight envelope for shipboard operations. These reference points are summarized in Figure 2-1 and comprise the following:

1. The helicopter flight characteristics and limitations;
2. The atmospheric conditions;
3. The ship environment;
4. The pilot and pilot-helicopter interface.

With this perspective, the helicopter characteristics and limitations can be regarded as the internal attributes, the atmospheric conditions and the ship environment as the external influences and the pilot and pilot-helicopter interface as the connecting human factors. While these initially need to be discussed separately, it is their interaction and interdependence that widen the scope of the subject of helicopter-ship qualification testing to reveal its considerable scale. The disturbances in airwake caused by the ship's superstructure on the helicopter flight characteristics, the influence of the ship motion on the pilot's workload, and the effects of the atmospheric conditions in terms

of Outside Air Temperature (OAT) and pressure on engine performance are profound. In many ways these are key concerns and primary drivers for the boundaries of the operational flight envelopes to be released to service.

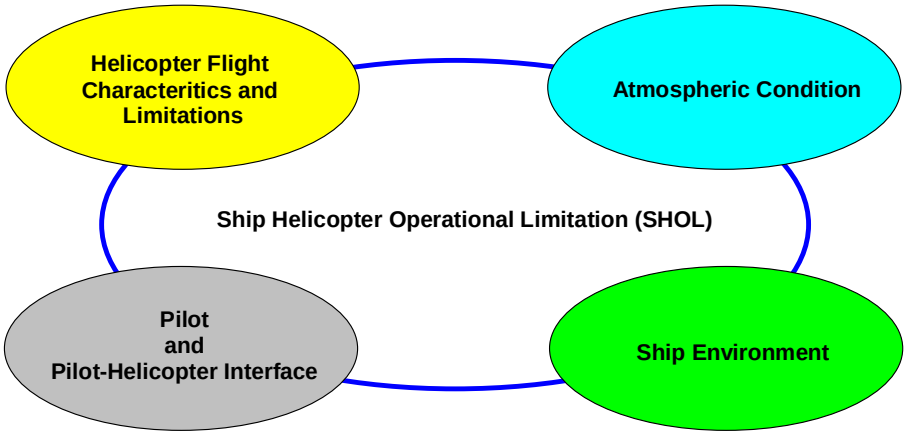

Figure 2-1; Four reference points

2.2.1 The Helicopter Flight Characteristics and Limitations

As an introduction, in this section the reader is given an overview of the basics of the helicopter: its principles of flight, its means of control and its general design features. Most current helicopters are of the single four-bladed main rotor configuration with a separate tail rotor. For this reason, this type of helicopter will be focused on with specific emphasize on the NH90 NATO Frigate Helicopter (NFH) which is in service within the Netherlands Ministry of Defence (NLMoD) and many other countries worldwide. The NH90 NFH is a twin engine medium weight transport helicopter with a fully articulated four-bladed counter-clockwise turning main rotor, when seen from above, and a bottom-forward rotating tail rotor. Its maximum take-off weight is 11 000 kg. Conventional cyclic, collective and yaw pedals are fitted, assisted by a fly-by-wire computer and a hydraulic system. The helicopter has Rolls-Royce RTM 322-01/9 engines, including Full Authority Digital Engine Controller (FADEC) software. A more detailed description of the NH90 NFH helicopter is contained in Appendix A.

2.2.1.1 Body Axes System

The helicopter dynamics are referred according to the orthogonal body axes system, fixed at the Centre of Gravity (CG) location of the helicopter as shown in Figure 2-2. Strictly speaking, the CG will move as the rotor blades flap, but it is assumed that the CG is located at the mean position, relative to a particular trim state. Note that at this level of complexity the rotor dynamics are ignored. The body axes system (x, y, z) is fixed to the helicopter with its origin at the CG. The components of force along the body axes are (X, Y, Z). For the case that six rigid-body degrees of freedom are considered, the three translational velocity components are (u, v, w), and the three rotational velocity components are (p, q, r). The moments about the same axes are (L, M, N). Furthermore, the Euler angles which define the orientation of the fuselage

with respect to the earth fixed axes system are as follows: the roll attitude ϕ_f is positive to the right, the pitch attitude θ_f is positive upwards, and the yaw angle ψ_f is positive to the right.

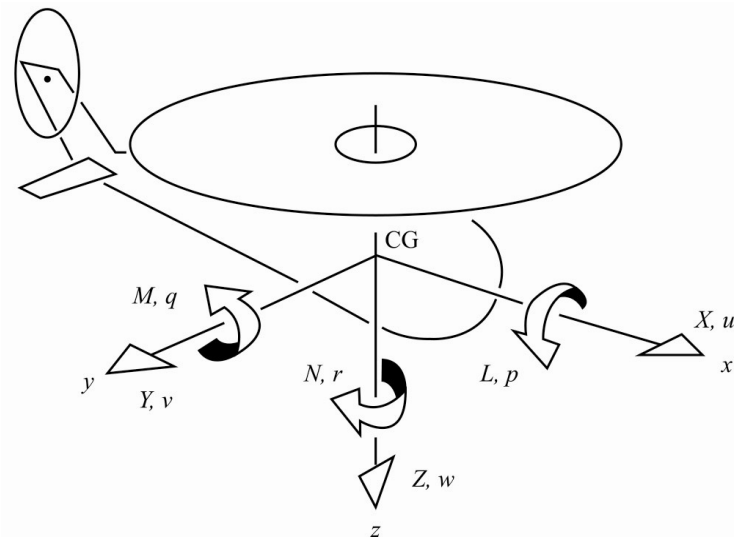

Figure 2-2; Body axes system; modified from [1]

2.2.1.2 Propulsion System

The RTM 322-01/9 is a front drive, free power turbine turboshaft engine, as shown in Figure 2-3, which is representative for most helicopter engines. The operating principle of the turboshaft gas turbine engine is that a continuous and successive process takes place such that it generates heat energy by internal combustion of jet fuel with oxygen from the air flowing through the engine. The gas generator section initially consists of an annular air inlet to make sure that the inlet air reaches the compressor under the desired conditions. If required the intake region can be configured to prevent ingestion of ice, sand and Foreign Object Damage (FOD).

The function of the compression section is to force the air flow through a continuously decreasing cross-sectional area, which increases pressure and temperature. There are two types of compressor used: a three stage axial-flow compressor and a single stage centrifugal compressor. The three stage axial-flow compressor is a rotor with a number of sequential blade rows. In between each rotor blade row, there is a row of stator blades attached to the compressor casing. The first stage of the stationary components consists of anti-iced variable Inlet Guide Vanes (IGV), followed by one stage of Variable Stator Vanes (VSV) and finally two stages of stator vanes. The IGV/VSV can modify their angle of attack due to a specific electro-hydraulic actuator controlled by the Engine Electronic Control Unit (EECU) to avoid blade stall when they are at off-design speed. The IGV direct the air to the first compressor stage blades at an optimum angle. The VSV have the same function, although in addition, slow the air down to provide a higher static pressure.

The single stage centrifugal compressor accelerates the air by means of centrifugal effect. The centrifugal compressor consists essentially of a stationary casing containing a rotating impeller which imparts a high velocity to the air, and a number of fixed diverging passages in which the air is decelerated with a consequent rise in static pressure. A reason to use a centrifugal compressor is that with current technology, the equivalent flow axial compressor will be less efficient due primarily to a combination of rotor and variable stator tip-clearance losses. Furthermore, they offer the advantages of simplicity of manufacture and relatively low cost, requiring fewer stages to achieve the same pressure rise. Part of the compressed airflow is diverted to cool the gas generator turbine; another part can be used to deliver bleed air to onboard systems like the Environmental Control System (ECS). The aim of the reverse flow combustion chamber is then to burn fuel to increase the temperature and impact energy to the airflow.

A two stage gas generator axial flow turbine extracts mechanical energy from the hot gasses leaving the combustion chamber. This energy is used to drive the compressor. In front of the turbine and in between the rotor blades, radial stator blades attached to the engine casing ensure a proper flow direction towards the rotor blades. The stator vanes increase gas flow velocity and optimize the flow direction to the turbine blades enabling the blades to extract the energy required to drive the compressor. The separate free power turbine is a two stage axial flow turbine whose coaxial shaft extends to the front end of the engine for transmission of the power to the Main Gear Box (MGB). The free power turbine speed can be controlled independently from the gas generator operation, allowing the engine to respond more rapidly to variations in the fuel flow. After passing through the free power turbine the air leaves the engine via the gas exhaust, which can also include a system for mixing hot and cold flows to reduce the heat signature for military helicopters. The accessory gearbox provides the drive for the engine accessories i.e. oil pumps, fuel pumps and alternator.

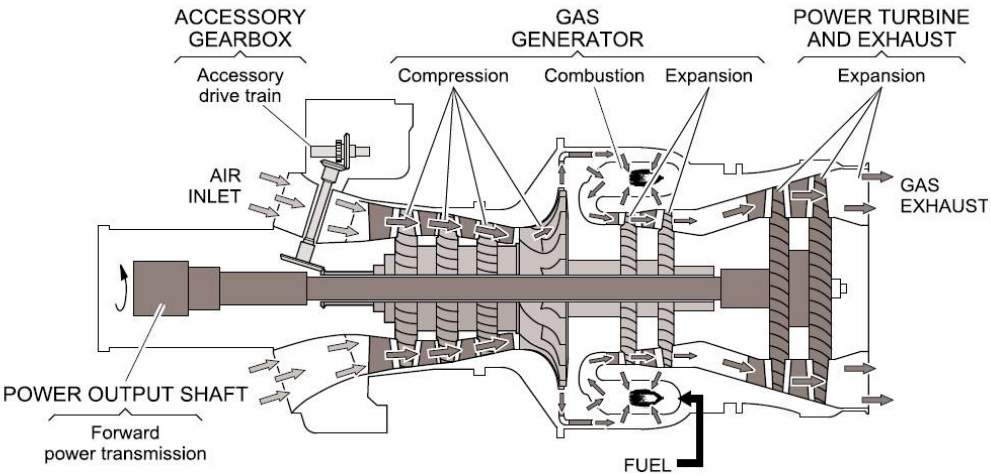

Figure 2-3; RTM 322-01/9 engine [2]

Engine / rotor control system

The ability in a controlled free-shaft power turbine engine to vary both the quantity of fuel that is being burnt (thus combustion temperature) and the air mass flows allows a wide range of energy that is being released to match the power requirements, whilst the free power turbine runs at a sensibly constant speed. Therefore, this type of turbine engine is well suited to multi-engine helicopter applications as it is essential that both engine characteristics are matched. However, the characteristics of a free power turbine engine, particularly its characteristics during acceleration, are such that some form of engine control is essential if protection against surge is to be provided and the main rotor rotational speed N_r is to be maintained sensibly constant without creating an unacceptable workload for the pilot. For this reason, the engine/rotor control system provided by the FADEC software in the EECU, ensures by altering the gas generator rotational speed N_g that the free power turbine rotational speed N_f, and hence main rotor rotational speed N_r, are maintained constant or within the allowable limits. The basic purpose of the EECU is to control fuel flow and air flow into the engine by means of a fuel metering unit, and IGV/VSV position actuators whilst maintaining free power turbine rotational speed N_f within the limits for a range of power demands.

Engine limitations

The engine/rotor control system provides protection and set limits on e.g. free power turbine rotational speed N_f, gas generator rotational speed N_g, engine power turbine inlet temperature T_{46}, torque Q, combustion chamber flame propagation, vibration levels and surge. The relevant governing factors to prevent exceeding engine limitations are described below:

1. *Speed of rotation*. This is a limiting factor for two reasons: (1) forces acting on the compressor blades in normal operation corrected for atmospheric conditions, and (2) the need to avoid overspeed and subsequent destruction of the free power turbine.
2. *Temperatures*. All engine parts have temperatures above which their performance degrades, particularly where oil or hydraulic fluid is involved. These problems can be resolved with adequate cooling. Usually, if the engine power turbine inlet temperature T_{46} can be increased, the kinetic energy available for conversion to mechanical energy can be increased simply by burning more fuel at the same Revolutions Per Minute (RPM). Temperature affects the turbine blades in two ways: (1) stress due to cycles of alternating temperature, and (2) creep. Creep, or deformation, of any material will occur when it is subjected to heat under load. Initially it will expand, returning to its original form when cooled; this is called the primary or elastic stage. If heated further or for longer, the deformation will be permanent: the secondary or plastic stage. Finally, the material will rupture and break. This sequence will be more rapid if the temperature is higher and, therefore, time limits are necessary for operation at high power settings such as maximum continuous power.
3. *Combustion chamber limits*. There are certain airflow velocity limits to ensure adequate flame propagation, and to limit the rate of fuel flow reduction.

4. *Vibration*. Axial compressors are particularly prone to vibration, both of the blades and shaft. These vibration levels should be maintained within acceptable limits.
5. *Surge*. A main purpose of the EECU is to control airflow into the engine by means of the IGV and VSV position actuators. The computed data allows the system to avoid the suspected surge area of the compressor. An alternative option used for other engines would be to install bleed control valves located close to the compressor outlet. They act by increasing the mass flow through the compressor section, normally at low gas generator rotational speed N_g, and then dumping excess airflow overboard before it enters the combustion chamber.

2.2.1.3 Transmission System

The transmission system provides the mechanical power transfer from the engines to the main rotor, tail rotor and to all the mechanically driven accessories. The engine of a helicopter operates at a relatively high rotational speed, while the main rotor rotational speed N_r is much lower at approximately 266 RPM. The speed reduction from the engine is accomplished through high power reduction gears in the MGB which is located directly under the rotor centre. The mechanical power transfer is limited by the maximum loading tolerable before structural damage occurs, expressed in a percentage of torque Q. Note that the engine is connected to the MGB via a freewheel coupling. The freewheeling coupling provides for autorotative capabilities by automatically disconnecting the MGB from the engine in case of an engine failure in flight. With a disconnected engine the main rotor drives the tail rotor and accessories via the MGB. This permits the pilot to maintain directional control and use the (electrically driven) instruments and other necessary systems in autorotation.

2.2.1.4 Power Required and Power Available

Power required

Accurate data concerning the power required P_{req} in different flight phases of the helicopter is of primary importance for mission planning. The power required P_{req} is built up from the following four contributions as demonstrated in Appendix B.

1. *The induced power* P_i: is determined by the induced velocity v_i, which is smaller in forward flight than during hovering and the thrust T required by the main rotor, often taken to be approximately equal to the helicopter weight. The induced velocity reduces with increasing forward flight speed because the air mass flow trough the rotor increases. Therefore, the induced power P_i increases according to the following equation where k is the induced drag power factor:

$$P_i = kTv_i \qquad \textbf{(Eq. 2-1)}$$

2. *The parasite drag power* P_{par}: is for a given altitude the power needed to overcome the parasite drag D_{par}. It is proportional to the forward flight speed V to the third power and to the helicopter's parasite drag area $(C_D S)_{par}$, where ρ is the density of the air:

$$P_{par} = D_{par}V = \sum (C_D S)_{par} \frac{1}{2}\rho V^3 \quad \textbf{(Eq. 2-2)}$$

3. *The profile drag power $P_p + P_d$*: the first term P_p originates from the profile drag of the rotor blades. The second contribution of the profile drag P_d arises because there will be a hub force acting rearward which must be matched by a component of the rotor thrust. The hub force appears because there is an asymmetry of drag acting on opposing blades. When a blade reaches the advancing side, it will see increased drag, a component of which will act rearwards. An opposing blade will see reduced drag as it enters the retreating side. Although a component of the drag on the retreating side acts forwards, it will be less than on the advancing side and a net rearward hub force will result. This result in the following expression, where σ is the relative density (relative to international standard atmosphere), C_{Dp} is the mean profile drag coefficient, Ω is the main rotor rotational velocity, R_r is the rotor radius and μ is the advance ratio:

$$P_p + P_d = \frac{\sigma C_{Dp}}{8}\rho(\Omega R_r)^3 \pi R_r^2 (1 + 4.65\mu^2) \quad \textbf{(Eq. 2-3)}$$

4. *The climbing power P_c*: is the product of the helicopter weight W and the rate of climb C as shown below, where γ is the flight path angle:

$$P_c = WC = WV \sin\gamma \quad \textbf{(Eq. 2-4)}$$

Now the power required for the most general condition in forward climbing flight P_{fwd} can be expressed in:

$$P_{fwd} = P_i + P_{par} + P_p + P_d + P_c \quad \textbf{(Eq. 2-5)}$$

For the total power required P_{req}, the power for the tail rotor system, transmission losses from the engine towards the rotor systems, and power requirements for on-board systems should be added as well P_{misc}. The power required for flight is the energy absorbed by the helicopter to keep it flying according to:

$$P_{req} = P_i + P_{par} + P_p + P_d + P_c + P_{misc} \quad \textbf{(Eq. 2-6)}$$

Power required curve

The power required for level forward flight is captured in a representative curve for a given helicopter weight, atmospheric condition and altitude of which an example is shown for a medium weight helicopter in Figure 2-4. The induced power P_i dominates the hover and low speed regime but is continuously decreasing because the mass flow through the rotor is increasing. In contrast, the parasite drag power P_{par} is negligible in the hover but is continuously increasing with forward flight speed. This increase is proportional to the third power of the true airspeed and it dominates at high speeds. The profile drag power $P_p + P_d$ rises only slowly with true airspeed, unless and until the compressibility drag rise begins to be shown at high speeds and/or at high weights and altitudes. The tail rotor power required is initially high in hover, but it quickly decreases as true airspeed builds up, the vertical fin at the tail of the helicopter becomes

more effective and the main rotor torque requirements decrease. In high forward flight speeds, the tail rotor power required increases again as the main rotor torque increases to overcome parasite drag. As a result of these variations with true airspeed, the power required curve has a typical 'bucket' shape, high in the hover, falling to a minimum at moderate speed, and rising rapidly at high speed to levels above the hover value.

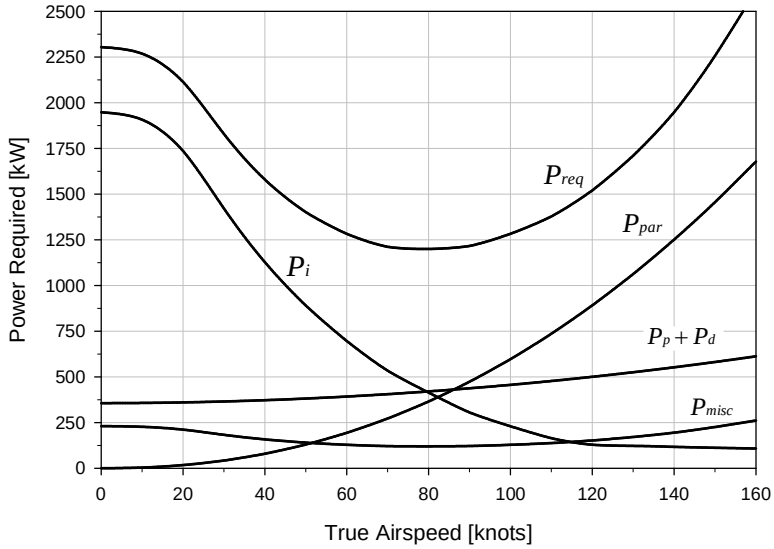

Figure 2-4; Example power required curve for medium weight helicopter

Power available

The engines have a shaft power P_{eng}. However, not all this power can be transmitted to the rotors as part of it will be lost in the transmission system. The available power P_a is the power usable by the main rotor that is developed by the engine(s) and delivered via the transmission system. The power available P_a is found by multiplying the engine power P_{eng} with a mechanical efficiency η, thus:

$$P_a = P_{eng}\eta \qquad \textbf{(Eq. 2-7)}$$

Effect of atmospheric conditions

In addition to the effects of forward speed on power required P_{req}, this important performance parameter, is also influenced by the atmospheric conditions in which the helicopter operates and of course the gross weight of the helicopter. For example, less density requires a higher induced flow speed to maintain mass flow through the rotor. Blade pitch angles, angles of attack and inflow angles must be greater. This causes the induced power curve to rise as shown in Figure 2-5. In general, a decrease in density or an increase in gross weight causes the power required curve to move up and to the right, while an increase in density or a decrease in gross weight causes the power required curve to move down and to the left. The power available P_a may also be affected by the atmospheric conditions (e.g. less power available with reduced air density).

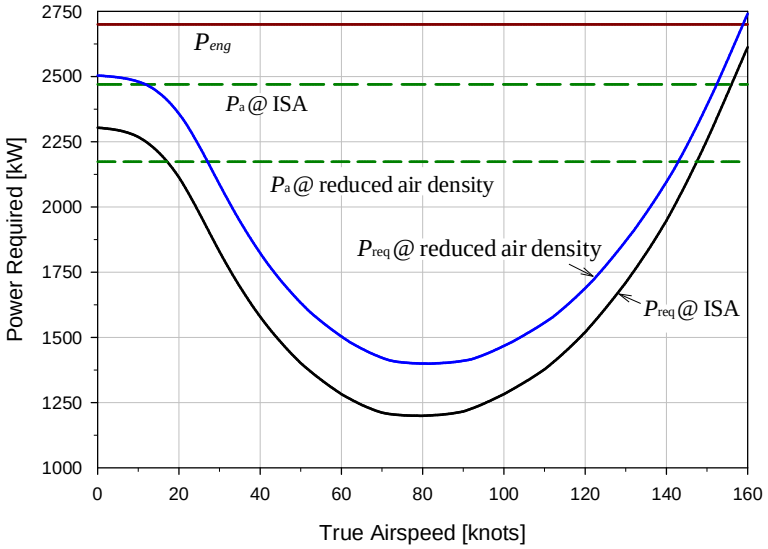

Figure 2-5; Example effect of atmospheric conditions

The performance of a gas turbine engine is dependent on the mass flow through it and the consequent release of heat energy from the rate of fuel burnt. At a constant rotational speed, the compressor pumps approximately a constant volume of air into the engine with no regard for air mass or density. If the density of the air decreases, the same volume of air will contain less mass, so less fuel may be injected and thus less power is produced. If air density increases, power output also increases as the air mass flow increases for the same volume of air. Thus the atmospheric conditions affect the performance of the engine since the density of the air will be different under different conditions. For example, on a cold day, the air density is high, so the mass of the air entering the compressor is increased. As a result, more fuel can be burnt and more power is available. In contrast, on a hot day, or at high altitude, air density is decreased, resulting in a decrease of output shaft power. Should the power available P_a become lower than the power required P_{req}, and the helicopter already be in flight, it will incur a descent as the helicopter cannot maintain straight and level flight anymore. The power available can be limited by the maximum engine gas generator rotational speed N_g, engine power turbine inlet temperature T_{46}, control of the fuel flow and the maximum permissible physical loading of the engine structure. In contrary, on a cold day the engine may produce more thrust or power than it or the airframe can safely take. Apparently for the NH90 NFH, the permissible gas generator rotational speed N_g is controlled by the FADEC and increases with OAT and pressure height [3], which is required to maintain the same power available at high ambient temperatures and low air density. The engine is thus so-called "*flat-rated*". Flat-rating means that the engine will produce a certain horsepower, but once density decreases the engine itself starts working harder to maintain the output shaft power.

One-engine inoperative

It is assumed that all performance test methods remain valid in an One-Engine Inoperative (OEI) situation, as under normal circumstances the power required will not

change between OEI and All Engine Operatives (AEO) performance. As a first estimate it may be permissible to use data gathered during AEO testing and simply apply the OEI limits to get the desired performance information. However, in any case the OEI performance should be verified with the flight manual data.

2.2.1.5 Controlling the Helicopter in Flight

To fully control the position and attitude of the helicopter requires control of forces and moments about all three-body axes. This would require six independent controls. However, the control of forces and moments in the longitudinal and lateral direction can be coupled to achieve the desired motion. So, actually four independent controls are adequate for the helicopter. The conventional way of controlling the motion of the helicopter, i.e. by means of the so-called "*swashplate*" mechanism of the main rotor is presented in Figure 2-6. Basically, the swashplate consists of a fixed part attached to the control actuators, which is controlled by the pilot, and a rotating part attached to the main rotor blades with pitch link rods, which is connected to the blades that have to be controlled. By controlling the swashplate the pilot command is transmitted to the main rotor blades.

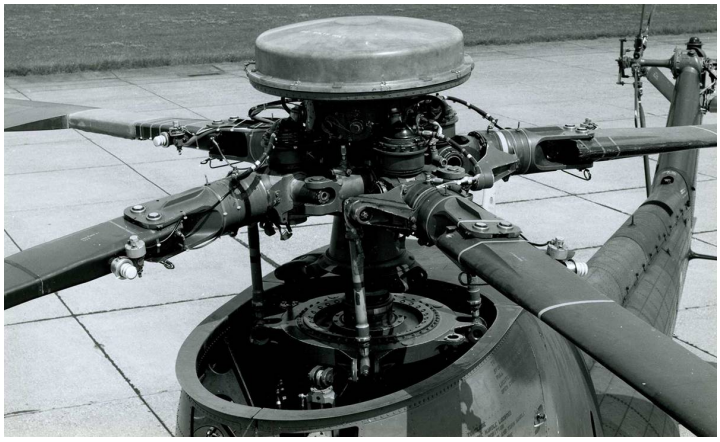

Figure 2-6; Example main rotor control through swashplate and pitch link rods [4]

Flight controls

With the collective lever the vertical position of the helicopter can be controlled. The pilot can accomplish this by vertically moving the collective lever: up for more rotor thrust (thus climbing), down to lower the thrust (thus descending). When the blade lift is varied for controlling the rotor thrust, the blade drag and the required shaft power respectively increase or decrease as well. For this reason, for a gas turbine engine the fuel supply and the collective pitch θ_p are linked such that the main rotor rotational speed N_r remains constant for a higher or lower output. Pedals are used for directional control of the helicopter into the desired direction. With pedal inputs the pilot changes the tail-rotor thrust by increasing or decreasing the collective pitch angle of the tail rotor blades. For controlling the position of the helicopter in longitudinal and lateral direction the pilot uses the cyclic stick into the desired direction.

Principle of operation

A detailed description of the principle of operation is given by Padfield [1], whilst in this section only a brief overview is given. If the collective lever is moved, the lower disc of the swashplate will shift up or down. The upper disc moves along. This means that all pitch rods are controlled at the same time, and all blades get the same change in pitch angle and therefore a change in angle of attack. The rotor thrust will change. If the cyclic stick is moved the lower disc will tilt, it will not move in vertical direction. Also the upper disc tilts. Now the pitch rods will not be moved all at the same time in the same manner, but the opposite blades will move in an opposite way. This implies that the angle of attack is changed cyclically. An adjustment of the angle of attack and thus the lift on each blade is the result. This way there is an inclination of the thrust. Note that the rotor blades are free to flap about the hinge. The rotor blades will flap in a way such that there will be no resulting moment about the hinge. The flapping of the blades is cyclic as well. There is a phase lag though between the change in cyclic pitch angle and the change in flapping angle – that is, between control input and flap response. Actually it is the flapping of the blades that are the cause of the tilting of the rotor disc. The tilting is about 90° out-of-phase with the cyclic adjustment of the blades. An overview of the helicopter flight controls and its effects are summarized in Table 2-1.

Effects	**Cyclic lateral**	**Cyclic longitudinal**	**Collective**	**Pedals**
Directly controls	Varies main rotor blade pitch fore / aft	Varies main rotor blade pitch left / right	Collective pitch angle for the rotor main blades via the swashplate	Collective pitch supplied to tail rotor blades
Primary effect	Induces roll motion in direction moved	Induces pitch nose up or down in direction moved	Increase / decrease pitch angle of rotor blades causing climb / descend	Yaw rate
Secondary effect	Induces pitch nose up or down (due to x-coupling)	Induces roll motion (due to x-coupling)	Increase / decrease torque	Increase / decrease torque
Used in forward flight	To turn the helicopter	Control attitude	To adjust power through rotor blade pitch setting	Adjust sideslip angle
Used in hover flight	To move sideways	To move forwards / backwards	To adjust hover height / vertical speed	Control yaw rate / heading

Table 2-1; Overview flight controls and effects

2.2.2 The Atmospheric Conditions

Aeronautics focuses mainly on the state variables of air, because variations in for example altitude and temperature have an impact on helicopter flight. The most important state variables of air are pressure, temperature, density and the speed of sound as discussed in more detail in Appendix B. In summary, a force perpendicular to a body's surface exerted by a gas is called pressure p. Pressure is caused by moving air molecules, colliding with the body's surface. This results in a transfer of momentum between the air and the body. In a stationary atmosphere, the static pressure is only dependent on the height above the earth's surface. The air temperature T has a strong influence on state variables such as density and viscosity. In airflow, the temperature is a local property. The density ρ is the amount of mass per unit of volume. The density of a gas is derived by dividing the mass present in a very small element by its volume. The relation between pressure p, density ρ and temperature T of a perfect gas is determined by the equation of state:

$$p = \rho RT \qquad \textbf{(Eq. 2-8)}$$

where R denotes the specific gas constant. The gas constant R varies from one type of gas to another, depending on the molecular mass. Small pressure disturbances in a medium are transmitted at the speed of sound a. The propagation of sound is closely related to the transfer of momentum between colliding molecules, thus with the average speed of the molecules. Since the average kinetic energy of molecules is proportional to the temperature T, the speed of sound a is proportional to the square root of the temperature:

$$a = \sqrt{\gamma RT} \qquad \textbf{(Eq. 2-9)}$$

Here, γ is the adiabatic index, which is the ratio of the specific heats of air at constant pressure c_p and constant volume c_v, respectively:

$$\gamma = c_p / c_v \qquad \textbf{(Eq. 2-10)}$$

For atmospheric air the adiabatic index amounts to γ = 1.4. Note that the speed of sound depends only on the temperature, provided the values for specific heat remains constant.

International Standard Atmosphere

Because the condition of the atmosphere changes constantly, it is impossible to define helicopter performance precisely unless the state of the atmosphere, in which a particular parameter is measured, is defined first. There is also the need to calibrate helicopter instruments in order to measure the performance of the helicopter. This leads to the fact that to standardize performance information some type of standardized atmosphere must be used. Therefore, a fictitious model of the actual atmosphere is used that defines mean values of pressure, temperature, density and other state variables solely as functions of the altitude above mean sea level. For this reason, the International Standardization Organization (ISO) has defined the International Standard Atmosphere (ISA) based on the model that has been established by the International

Civil Aviation Organization (ICAO) [5]. The basic properties of the standard atmosphere are summarized in Appendix B.

Relative quantities

It is convenient to express the pressure p, temperature T and density ρ as the appropriate fraction of their ISA mean sea level values, p_0, T_0 and ρ_0 respectively:

Relative pressure: $$\delta = p/p_0 \quad \textbf{(Eq. 2-11)}$$

Relative temperature: $$\theta = T/T_0 \quad \textbf{(Eq. 2-12)}$$

Relative density: $$\sigma = \rho/\rho_0 \quad \textbf{(Eq. 2-13)}$$

The relative quantities are used throughout performance analysis as reference values, where H_p is the pressure height to be inserted in the equation for relative pressure, and OAT to be inserted in the equation for relative temperature:

Relative pressure: $$\delta = (1 - 6.8756 \times 10^{-6} \times H_p)^{5.2559} \quad \textbf{(Eq. 2-14)}$$

Relative temperature: $$\theta = \frac{273.15 + OAT}{288.15} \quad \textbf{(Eq. 2-15)}$$

Relative density: $$\sigma = \frac{\delta}{\theta} \quad \textbf{(Eq. 2-16)}$$

2.2.3 The Ship Environment

In comparison to most land-based take-off and landing, ship-board take-off and landing occur in winds from any direction relative to the helicopter, onto a moving platform, usually in close proximity to the hangar in front of the flight deck. Optimal relative wind conditions for take-offs and landings may be constrained by the ship's operational requirements, forcing the helicopter to land in non-ideal conditions. Separately, the individual elements of the ship environment (e.g. relative wind, ship motion and sea spray) are complex and difficult to predict, however, the ship environment is even more challenging due to the interaction of these elements.

2.2.3.1 Ship Airwake

To perform safe and efficient shipboard helicopter operations, it is required to have a proper knowledge of the airflow characteristics in the vicinity of the ship, known as the ship airwake. The airwake in the vicinity of the ship is complex and chaotic in nature, and may be significantly disturbed due to the ship's superstructure in comparison to the undisturbed airwake far away from the ship. For example the complexity over the flight deck is shown in Figure 2-7, with three distinct flow features highlighted [6]. Feature (a) is the starboard deck-edge vortex, formed as flow travelling along the lower starboard side of the superstructure meets freestream flow at the starboard deck edge.

The top of this structure is roughly in line with the hangar, reaching its maximum height in the middle of the flight deck. Feature (b) is the starboard hangar edge shear layer, which is formed as the flow attached along the starboard edge of the superstructure separates from the vertical edge of the hangar. In Computational Fluid Dynamics (CFD) animations this feature is seen to be unsteady in nature, with a flapping motion commonly seen in bluff-body separation. This is a major contributing factor to turbulence over the flight deck, particularly in regions below the hangar. Feature (c) is the secondary superstructure vortex identified above, which appears to break up and shed helical vortical structures as it encounters the flight deck. This flow feature is responsible for most of the turbulence encountered over the flight deck at locations above hangar height and could therefore pose significant difficulties to helicopters operating to and from such a ship. The interactions between the flow features identified above result in a highly complex, unsteady flow-field over the flight deck. Unfortunately, this level of complexity in the ships airwake is still labour intensive to acquire and not readily available at regular one degree increments in azimuth, which is preferably used to predict the operational limitations of any helicopter-ship combination. Therefore, although from less complexity, mean flow fields as determined in the windtunnel are used throughout this dissertation.

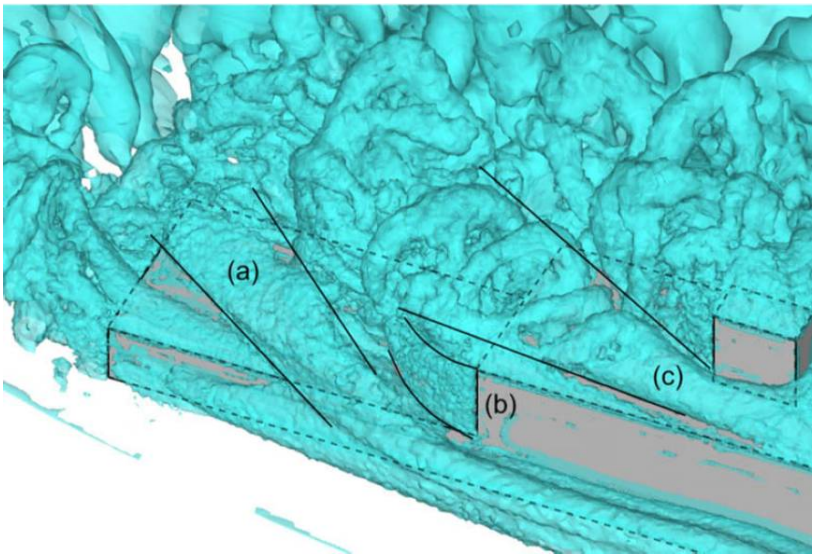

Figure 2-7: Example complexity airwake over the flight deck [6]

The coordinate system for the different azimuths and velocities, used to define the airwake as determined in the windtunnel is shown in Figure 2-8. The ship reference system is fixed to the ship (x_s, y_s, z_s). The relative wind speed V_{rel} and the relative horizontal wind direction β_{rel} are the resultant of the ship's course and speed with the true wind conditions. The local wind properties as measured at different locations in the take-off and landing paths are defined as: the local wind speed V_{loc}, the local horizontal wind direction β_{loc} and the local vertical wind direction φ_{loc}. The horizontal flow deviation from the local wind compared to the relative wind is defined as χ_{loc}.

The wind properties at the anemometer locations are defined as: the wind speed at the anemometer location V_{an}, the horizontal wind direction at the anemometer location β_{an} and the vertical wind direction at the anemometer location φ_{an}. The horizontal flow deviation from the wind at the anemometer location compared to the relative wind is defined as χ_{an}. In addition, a red and green terminology is used throughout this dissertation to refer to winds coming from either the port or starboard side of the ship, respectively.

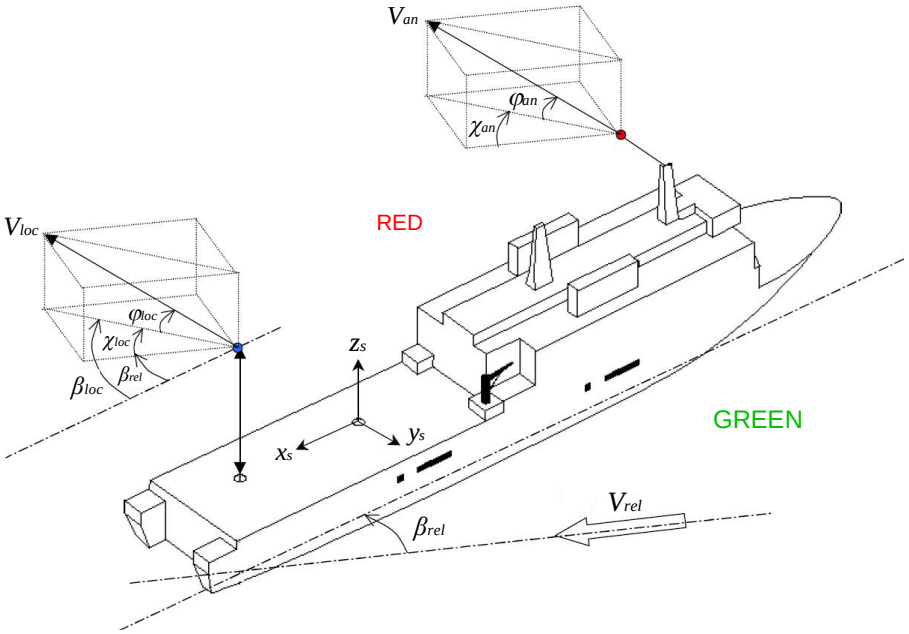

Figure 2-8: Coordinate system ship's airwake; modified from [7]

General overview ship airwake characteristics

Several distinct features are consistent and play a significant role in the ship environment. Generally, the wind influenced by the ship's superstructure can be divided into four groups based on the relative wind direction with each their own characteristics:

1. Head winds +/- (0° to 25°);
2. Quartering winds +/- (25° to 60°);
3. Beam winds +/- (60° to 120°);
4. Aft quartering winds and tail winds +/- (120° to 180°).

1. *Head winds* +/- (0° to 25°): For winds in this sector the flow over the flight deck is strongly influenced by the superstructure and the dimensions of the hangar as shown in Figure 2-9. The hangar generates an area over the flight deck, in which a turbulent airflow with low wind speeds or even a reverse flow region may be present. When the height of the hangar and/or the relative wind speed increases the recirculation zone

behind the hangar generally also increases in strength. The origin is on the centre line of the ship just aft of the hangar. On entering this air bubble the helicopter can loose height and move forward due to sudden loss of wind speed combined with the reversed flow. To compensate for the sudden loss of wind speed there is a risk in exceeding performance margins. Flight operations from the aft landing spot (furthest away from the hanger) are usually less hampered, and as a result flight operations can be conducted at higher wind speeds than the forward spot. Note that there is usually no difference whether the hangar door is open or closed.

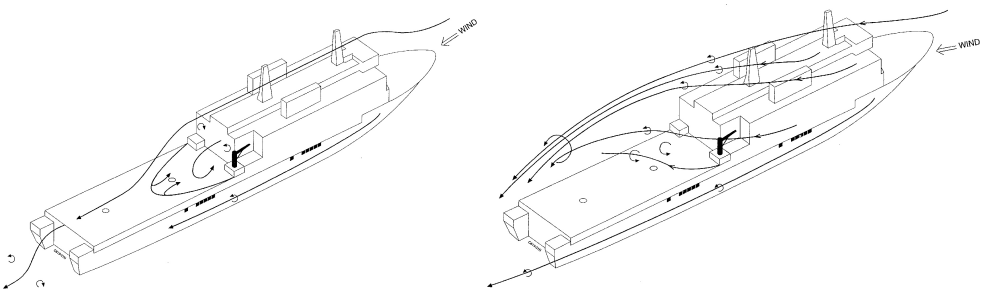

Figure 2-9: Example main vortices for angles 0° and 25° [7]

2. *Quartering winds* +/- (25° to 60°): For winds from port or starboard side in this sector the sharp hangar edges and also the ships superstructure generate a dominant vortex, which could roll over the flight deck as shown in Figure 2-10. Flight operations to the aft spot are generally less hampered by hull vortices. As a result, flight operations in these wind sectors might be possible at higher wind speeds than the forward spot. At the leeward side of the ship high down flow, so-called "*downdraft*", can be observed which may exceed 400 ft/min depending on the height and type of the superstructure [7].

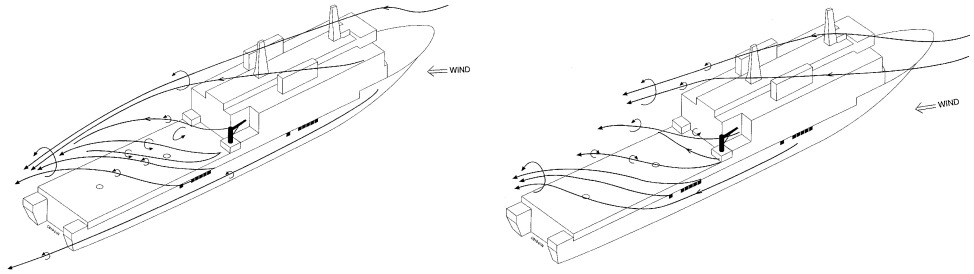

Figure 2-10: Example main vortices for side slip angles 45° and 60° [7]

3. *Beam winds* +/- (60° to 120°): For beam winds there is an up-flow and down-flow close to the ship observed as shown in Figure 2-11. Also for beam winds, at the leeward side of the ship high down flow can be observed. The sharp flight deck edges generate a vortex over the whole deck length noticeable on the leeward side of the ship, which is also noticeable in the approach towards the ship causing large fluctuation in torque utilised (i.e. torque spikes).

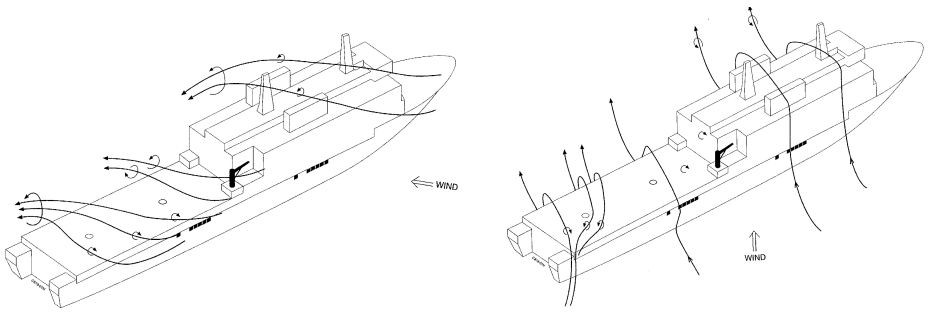

Figure 2-11: Example main vortices for side slip angles 75° and 120° [7]

4. *Aft quartering winds and tail winds* +/- (120° to 180°): For aft quartering winds and tail winds the rear flight deck edge could generate a relatively strong vortex as shown in Figure 2-12. The intensity of the vortex increases with height of the flight deck above sea level and relative wind speed. Generally, flight operations from the forward landing spot (closest to the hangar) are less hampered by the vortex generated by the rear edge of the flight deck. However, this effect is less pronounced due to the lower wind speeds usually included in the operational flight envelopes for tail wind.

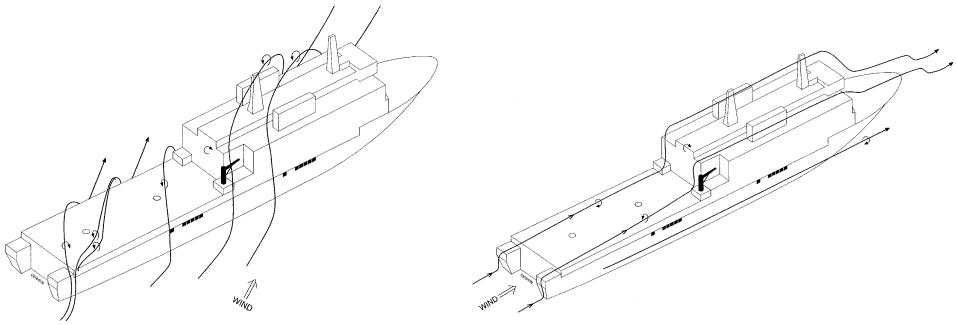

Figure 2-12: Example main vortices for side slip angles 150° and 180° [7]

Turbulence levels associated with ship airwake

The turbulence levels associated with the ship airwake generally increase in intensity with increasing relative wind speed, and vice versa, as shown for example in Figure 2-13. In addition, the turbulence levels are related to the relative wind direction, as shown for red quartering winds, where the turbulence levels are generally higher than for head winds at the same relative wind speed. The areas with increased turbulence levels in the vicinity of the ship may cause torque spikes, increased yaw instability, considerable pitch and roll motion of the helicopter and higher pilot workload.

2.2.3.2 Ship Motion

The ship motion limitations in an operational flight envelope are defined in terms of absolute pitch and roll angle of the ship. The coordinate system for the ship motion is shown in Figure 2-14. The ship reference system is fixed to the ship (x_s, y_s, z_s). Pitch

is the rotation of a ship about its transverse (side-to-side) axis. Roll is the rotation of a ship about its longitudinal (front/back) axis. Yaw is the rotation of a vessel about its vertical axis. Sway is the linear lateral (side-to-side) motion. Surge is the linear longitudinal (front/back) motion. Heave is the linear vertical (up/down) motion.

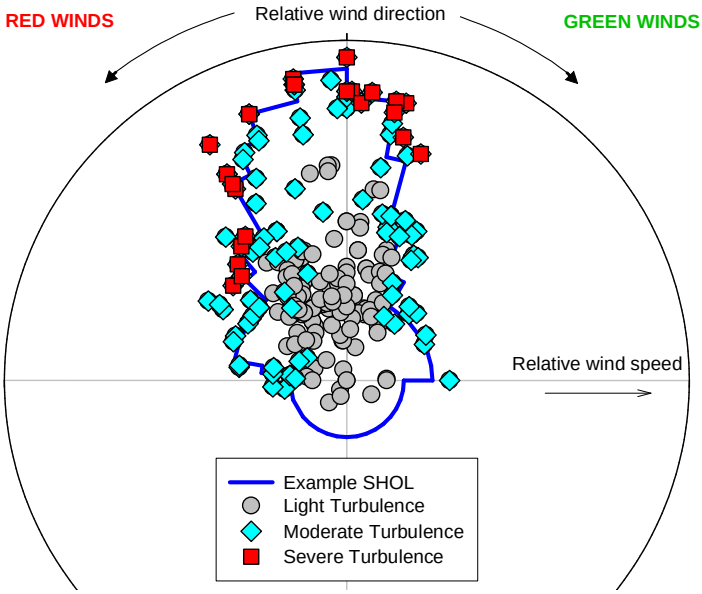

Figure 2-13: Example turbulence levels due to ship airwake

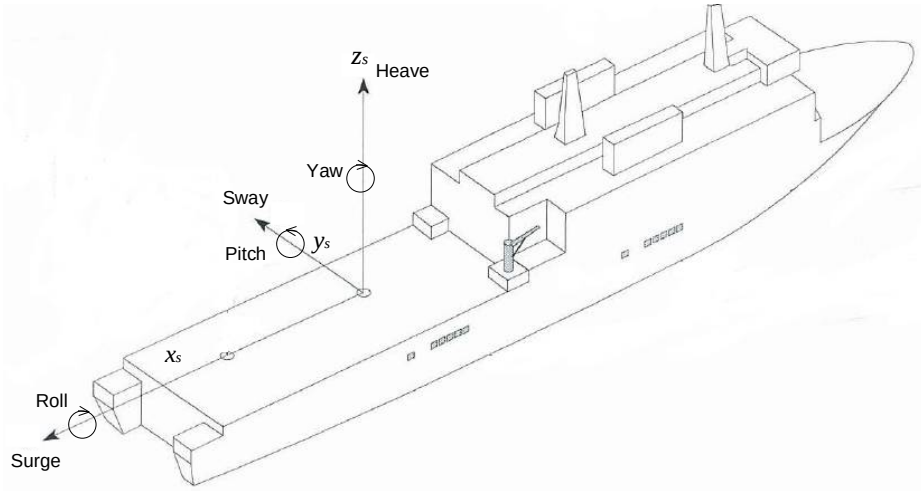

Figure 2-14; Coordinate system ship motion

The pitching and rolling motion of the ship is changing with the course and speed of the ship in relation to the relative wave direction β as shown for example in Figure 2-15. In general, there is more pitch motion of the ship sailing into the wave direction with

high speeds (i.e. β = 0˚), and there is more roll motion of the ship once sailing perpendicular to the wave direction at low speeds (i.e. β = 90˚). Note that for every ship type there will be different ship motion characteristics in similar sea state conditions.

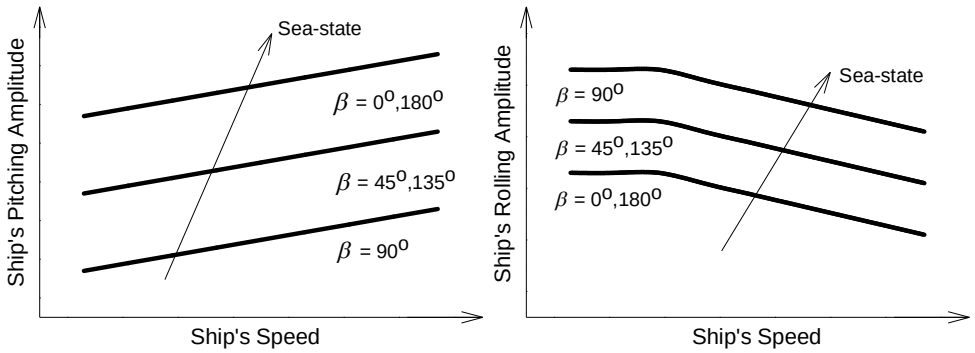

Figure 2-15; Example ship motion with relative wave direction; modified from [8]

2.2.3.3 Sea Spray

Sea spray can result from either the main rotor downwash of the helicopter, or might originate at the bow of the ship in high sea states and hamper flight operations all the way back in the vicinity of the flight deck. Helicopter sea spray occurs during take-off and landing due to the main rotor downwash, especially in low relative wind speeds with high helicopter weights as shown for example in Figure 2-16. In any case, the sea spray impacting on the cockpit windows reduces the visibility towards the flight deck for the pilots. A rough guideline for the areas in which sea spray potentially hinders flight operations is shown in Figure 2-17, i.e., low wind speeds for sea spray resulting from the main rotor downwash of the helicopter and high wind speeds for sea spray originating at the bow of the ship in high sea states.

Figure 2-16; Sea spray caused by the main rotor downwash

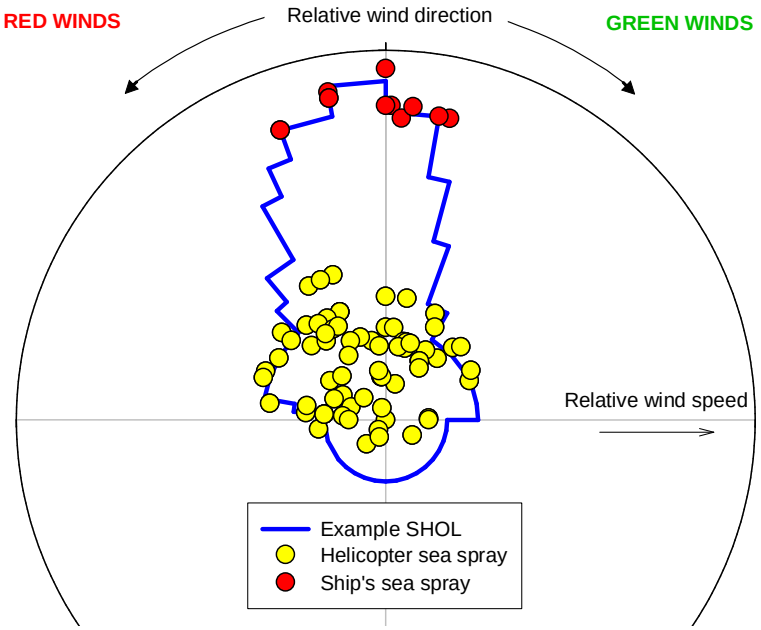

Figure 2-17; Example potential areas with sea spray

2.2.4 The Pilot and Pilot-Helicopter Interface

This aspect draws its conceptual and application boundaries from the engineering, physiological and psychological facets of the human factors discipline. This dissertation is concerned with the take-off and landing task and hence with only that function in the crew station; the crew have other, perhaps more important, mission-related duties, but the degree of spare capacity with which the pilot has to share these will depend critically on the pilot workload. Controlling the helicopter in the conditions encountered during shipboard operations is a demanding task. The pilot workload depends amongst others on the helicopter flying qualities, the amount of ship motion, the turbulence levels encountered, the visual cues and the ambient lighting conditions (e.g. day or night).

2.2.4.1 Pilot Workload

In making an assessment, the assessing pilot(s) concentrate on their own judgment or reactions, and do not attempt to explain or analyze the reasons for the helicopter's behaviours. The intention of a flying qualities assessment is to predict the helicopter's capability in the hands of a so-called "*average fleet pilot*". The task performance achieved is an expression of the amount of pilot workload, be it physical and/or mental, which is required to achieve a particular standard or level of task performance. Pilot compensation is a measure of the additional pilot workload necessary to achieve a given level of task performance in the face of helicopter handling deficiencies. In other words, compensation is effort over and above that which would be required if the helicopter was perfectly adapted for the task. For sustained periods the pilot can only provide a small degree of compensation. The degree of pilot compensation and hence

workload, necessary to overcome a handling difficulty could be used as a measure of the helicopter's suitability for a role. The pilot workload in the shipboard environment may, amongst other reasons, increase as a result of one or more of the following factors:

- *Helicopter limitations*; operating near the physical limits of the helicopter;
- *Increased turbulence*; piloting difficulty arises due to oscillations of the helicopter around all three axes;
- *Increased ship motion*; the pilot may tend to follow or tend to compensate for ship motion, or insufficient vertical climb performance of the helicopter;
- *Insufficient visual cues*; decreasing visual references with the ship due to environmental conditions, or inadequate visual cues provided to the pilot by the ship's design;
- *Loss of sight with the flight deck officer*; the take-off and/or landing instructions by the flight deck officer can not be seen by the pilot;
- *Hindrance of sea spray*; causing deteriorated visual reference with the ship.

The pilot workload rating is not only prescribed by the task tolerance that is required to achieve (i.e. landing on the spot). A workload rating in isolation does not tell the whole story; it must be associated with a verbal description of the extent and nature of the associated pilot compensation. Therefore, this information must be recorded coincidentally with the allocation of the rating itself. The rating should be awarded as soon as feasible after the task has been flown, otherwise it becomes less and less valid as memories and impressions fade. There needs to be a very good reason to change the ratings that are initially assigned. The pilot workload rating scale used is the Deck Interface Pilot Effort Scale (DIPES) which is a 5-point scale as shown in Appendix C. The main advantage of this scale is that it can be used for multiple task evolutions for multiple axis tasks, without specific task tolerances being required.

2.2.4.2 Flying Qualities

Flying qualities is usually one of the two principal regimes in the science of flight test, the other being helicopter performance. In this research flying qualities will be considered an integral part of the testing done for the determination of the helicopter flight characteristics. Flying qualities involve the study and evaluation of the stability and control characteristics of a helicopter. They have a critical bearing on the safety of flight and on the ease of controlling the helicopter in steady flight and in manoeuvres. Flying qualities are normally the product of four elements: the helicopter, the pilot, the mission and the environment. The helicopter dynamics can be regarded as internal attributes, the mission and environment as the external influences and the pilot and pilot-vehicle interface as the connecting human factors. A sub-division is made for the term flying qualities in accordance with Padfield – handling qualities, reflecting the helicopter's behaviour in response to pilot controls, and ride qualities, reflecting the response to external disturbances [1]. The handling qualities investigation of a helicopter is conducted to determine if the pilot-helicopter combination can safely and precisely perform the role for which it is intended (in this case shipboard operations).

If a helicopter exhibits poor handling qualities, for any reason, then the low speed manoeuvre envelope may have to be restricted. The helicopter's response to external disturbances like, for example, gusts and turbulence should be convergent and well-damped to minimize workload in the final phases of the approach and landing towards the ship.

Usually, there has already been extensive flight testing performed by the helicopter manufacturer to provide optimal flying qualities during the Development Test & Evaluation (DT&E) phase, and this process should not be repeated during a helicopter-ship qualification test campaign. The helicopter manufacturer may involve numerous pilots in the process, flying various Mission Task Elements (MTE) to assess the flying qualities. On the other hand, for a helicopter-ship qualification program the helicopter is preferably only evaluated during a brief Operational Test & Evaluation (OT&E), as closely as possible to the intended role it is intended to operate in, by a minimum amount of pilots to reduce the time required for the evaluation. It is the OT&E phase that is focussed on in this dissertation, such that the process is optimized, in order to make it as short and efficient as possible.

2.2.4.3 Visual Cues

Visual cues provide the pilot with the necessary situational awareness and the ability to accurately position the helicopter above the landing spot. Lack of or degraded visual cues are dangerous in the shipboard environment due to the small landing area, usually with only minimal clearances with the ship's superstructure. The visual cues may be restricted because of poor visibility, reduced light levels or a lack of suitable visual references. When the pilot can no longer make aggressive and precise manoeuvres due to the inadequacies of the visual cueing, the pilot is said to be operating in a poor Usable Cue Environment (UCE) according to the definitions within ADS-33 [9]. The UCE is a numerical representation and encompasses all the visual cues available to the pilot, both inside and outside the cockpit, both artificial and natural.

In general, the relevance of visual cues can be divided into two phases: (1) the approach to the ship and (2) the take-off and landing itself. In the approach to the ship the pilot is initially concerned with capturing and holding the flight path. In case required at night, the pilot can be assisted by the Glide Path Indicator (GPI) to ensure the correct glide path is maintained. As the ship is approached, smooth transition to outside visual cues is important to achieve a safe hover alongside the ship or above the landing spot, particularly regarding vertical flight path and power management. In transition to the hover and once established in the hover, ship texture and the relative movement of the ship in the cockpit windows are observed. In addition, the horizon bar provides height cues above the flight deck, and information about the ship motion. The lines painted on the flight deck provide the pilot with cues to position the helicopter above the landing spot. Note that at night for some scenarios, the simplest solution for recoveries to the ship might be to light up the flight deck completely to allow unaided flight operations, but for military operations there are usually operational constraints for this option. For this reason, night flight operations are performed aided by Night Vision Goggles (NVG).

Night Vision Goggles

The NVG is an optical instrument that allows images to be produced in levels of light approaching total darkness. For helicopter operations, it usually consists of two light intensification tubes as shown in Figure 2-18 (left). The NVG's are worn by the pilot and are mounted on the forward part of the helmet. An example of the image visible through the NVG's is shown in Figure 2-18 (right). Along with their advantages, NVG's also have limitations, and pilots and operators must be thoroughly informed about both. The brighter scene provided by NVG's, which makes it possible for pilots to see objects not otherwise visible, increases situational awareness, enhances safety and improves flight capability. However, as impressive as these devices are at increasing the ability to see and fly at night, the technology does not "*turn night into day*". The NVG's reduced Field Of View (FOV) and resolution is probably the most significant limitations. Pilots describe their impression of viewing the outside world through NVG's as "*looking through a straw*". To compensate for this reduced FOV, pilots must continuously scan from side to side, as well as up and down. High resolution requires optimal environmental conditions, including high illumination and contrast, clear weather, and absence of fog, dust and glare sources.

In addition, NVG's have additional limitations that include reduced depth perception, loss of colour information and the presence of image noise, also called scintillation, which looks sparkly and obscures fine detail. When operating in close proximity of a moving ship deck for landing and take-off, the pilot needs to be able to see the ship's deck motion to anticipate any flight control inputs. Due to the NVG's limitations, reduced depth perception, infinite focus, limited FOV and resolution, the pilot will obtain most of the necessary visual cues from the side and "*under-look*" vision. Therefore, maintaining good side and "*under look*" vision without a bright light source (e.g. landing light) makes NVG operations, especially under humid or high main rotor downwash conditions, much safer. For example, low level lights can be applied to the superstructure to enable all the necessary ship motion and positioning cues to be perceived by the pilot through the NVG's combined with side and "*under-look*" vision.

Figure 2-18; Example NVG (left) and NVG image (right)

Horizon bar

The horizon bar consists of dimmable white light bulbs attached in horizontal direction to the hangar, usually just above the hangar doors as shown in Figure 2-19. The horizon bar could be either completely fixed to the hangar, or consist of fixed parts on the outside and a stabilized section in the middle which then represents the horizon. The horizon bar provides visual cues to the pilot to maintain the correct height above the flight deck during lateral transitions and/or hovering above the landing spot prior landing or after take-off. It is also used to assess ship motion in order to assist in timing the most quiescent period for landing.

Figure 2-19: Example horizon bar

Glide Path Indicator

For a recovery at night, the GPI can be used to determine and maintain the correct glide path to the ship, whilst aiding the pilot not to descend below it. An example of a GPI is shown in Figure 2-20, however, there are different versions in use worldwide, and also within the NLMoD. The GPI is usually fixed in a red 155° azimuth from the ship's heading in a 3° glide slope. In this example, the GPI contains a three coloured filter. When the pilot is in a descending approach path and aligned with the correct azimuth the following holds: *Amber*, the pilot is flying too high - *Green*, the pilot is flying on the correct glide path - *Red*, the pilot is flying too low. In some cases, the GPI can be turned towards different azimuths with the ship's heading to allow other landing procedures to be used. Note that there are also other colour filters used to indicate the correct glide slope, including different flashing frequencies of these sectors. Different flashing frequencies of the sectors are essential for flight operations aided by current NVG technology, as whilst looking through the NVG the pilot would be unable to differentiate between steady red, green and amber lights (or differentiate any colours in general as ambient light is only intensified by the goggles).

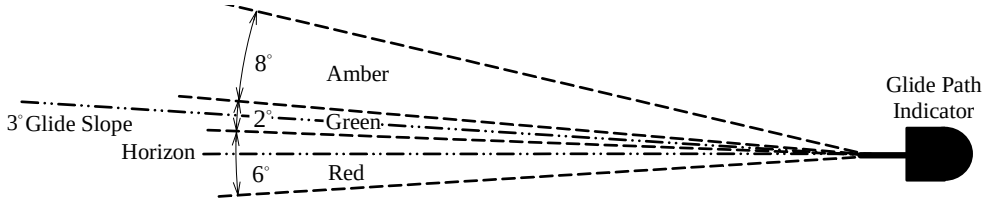

Figure 2-20: Example Glide Path Indicator; modified from [10]

Ship's navigation lights

The ship's navigation lights are designed to alert other traffic, and to indicate the ship's heading for other traffic. The ship's navigation lights consist of a red port and a green starboard sidelight, one or two white masthead lights and a white stern light as shown for example in Figure 2-21. These lights each have their own respective azimuth in which they are visible by other traffic. The red port and green starboard sidelights, and the white masthead lights are only visible in the sector from dead ahead towards 22.5° abaft beam. The white stern light is only visible in the aft sector beyond 22.5° abaft abeam.

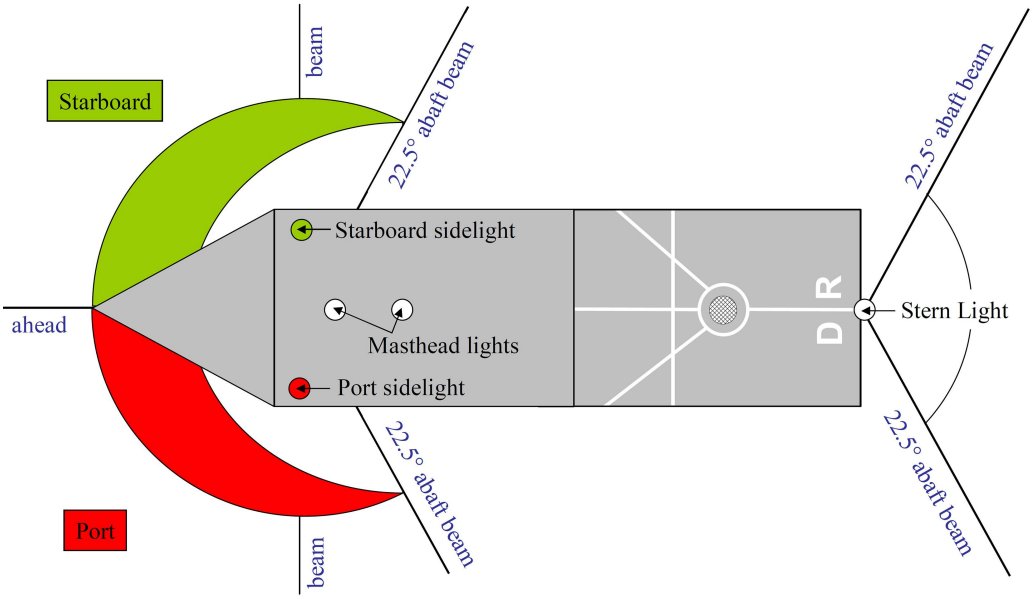

Figure 2-21; Example ship navigation lights

Flight Deck Markings

The white lines painted on the flight deck provide the pilot with visual cues to position the helicopter above the landing spot as shown in Figure 2-22 and Figure 2-23. The line across the flight deck from left to right is positioned such that when the helicopter is in the correct fore and aft position above the spot, the pilot's seat is directly over this so-called "*bum-line*". Lateral position cues are derived from the centreline painted

across the flight deck from aft to forward direction, which is extended onto the hangar doors. For oblique landings in a 45º azimuth with the ship's centreline, the corresponding lines painted on the flight deck are used. In case cross-deck landings are made in a 90º azimuth with the ship's centreline, the "*bum-line*" is used to align the helicopter's heading for landing.

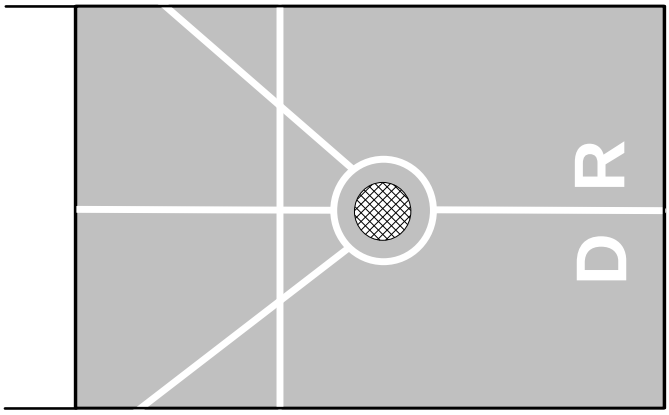

Figure 2-22: Diagram flight deck markings

Figure 2-23: Example flight deck markings

2.2.5 Summary Factors Affecting Shipboard Operations

A summary of the factors affecting shipboard operations is shown in Table 2-2.

Aspect	Group	Factor
Helicopter flight characteristics and limitations	Performance and control	Weight Rotor system Flying qualities Engine performance Control characteristics
	Mechanical	Transmission Structural design loads Control margins Vibration Undercarriage Field of view
Atmospheric conditions	Weather	Natural turbulence Visibility Environment True wind
	Geographical location	Sea motion characteristics
Ship environment	Flight deck	Dynamic motions Obstacles Dimensions Sea spray Distorted airflow Deck markings Deck friction
	Equipment	Deck handling systems Communication facilities Landing aids NVG compatibility
Pilot and pilot-helicopter interface	Capabilities	Training Experience & Skills
	Human factors	Crew co-ordination Physical ability
	Procedures	Standard
	Requirements	Commitments and tasks

Table 2-2; Summary factors affecting shipboard operations

2.3 Dimensional Analysis

Dimensional analysis is used, often unconsciously, by practically everyone who deals with physical problems. It provides a guide to experimental planning and to the correlation of data. Dimensional analysis is concerned with the nature of the relationship between various parameters relating to a physical problem. These parameters consist of groups of relevant dimensional quantities. However, before dimensional analysis can be applied it must be assured that only one relationship exists between a certain numbers of physical quantities, and that no pertinent quantities have been omitted, and no extraneous quantities included. Dimensional analysis is a step toward the goal of describing a physical entity or phenomenon in terms of relationships between groups of parameters. The ultimate goal can never be reached by dimensional analysis alone, and it is therefore not a substitute for complete analysis or for flight test. It is nevertheless a useful tool, especially for improving physical insight. A more detailed overview of dimensional analysis, including the derivations for engine and main rotor performance are given in Appendix B.

Performance flight test involves determining the relationship between pairs of non-dimensional parameters whilst the others are held constant. This experimental method of testing reduces any limitations in the applicability of performance test data. This is because data converted into non-dimensional form can be used to produce information relevant to atmospheric conditions and helicopter masses different from those actually tested. Consequently, with few exceptions, a relatively small number of tests at carefully chosen test sites can produce information relevant to much of the helicopter's flight envelope. However, even if a non-dimensional approach is employed, it is advisable to fly in conditions as near to the envisioned conditions as possible (i.e. the atmospheric conditions as specified in the role specification). As such, any unforeseen issues in atmospheric condition on helicopter performance and/or flying qualities can already be identified before an operational deployment. However, the experimental method with dimensional analysis does have some disadvantages in terms of planning and the choice of the non-dimensional grouping [11]:

- Although the test method can yield large quantities of relevant data from a few test points, it requires detailed and careful pre-flight planning if the full utility of the method is to be achieved;
- The method can appear vague with alternative groupings possible;
- It is possible to require flight conditions, in terms of the non-dimensional groupings, that are outside the limitations of the helicopter;
- Performance limiting factors that depend on actual conditions may not be fully replicated although matching non-dimensional values have been targeted successfully.

Engine performance

The referred quantities for power delivered by the engine P_{eng}, engine gas generator rotational speed N_g, engine power turbine inlet temperature T_{46}, the position of the Inlet

Guide Vanes Δ_{IGV} and the position of the Variable Stator Vanes Δ_{VSV} are all dependent on the heat flow of the fuel ϕ_f and the free power turbine rotational speed N_f as summarized below.

Referred engine power function (controlled engine)

$$P_{eng,ref} = \frac{P_{eng}}{\delta\sqrt{\theta}} = f_1\left(\frac{\phi_f}{\delta\sqrt{\theta}}, \frac{N_f}{\sqrt{\theta}}\right) \quad \textbf{(Eq. 2-17)}$$

Referred gas generator rotational speed function (controlled engine)

$$N_{g,ref} = \frac{N_g}{\sqrt{\theta}} = f_2\left(\frac{\phi_f}{\delta\sqrt{\theta}}, \frac{N_f}{\sqrt{\theta}}\right) \quad \textbf{(Eq. 2-18)}$$

Referred power turbine entry temperature function (controlled engine)

$$T_{46,ref} = \frac{T_{46}}{\theta} = f_3\left(\frac{\phi_f}{\delta\sqrt{\theta}}, \frac{N_f}{\sqrt{\theta}}\right) \quad \textbf{(Eq. 2-19)}$$

Position Inlet Guide Vanes function (controlled engine)

$$\Delta_{IGV} = f_4\left(\frac{\phi_f}{\delta\sqrt{\theta}}, \frac{N_f}{\sqrt{\theta}}\right) \quad \textbf{(Eq. 2-20)}$$

Position Variable Stator Vanes function (controlled engine)

$$\Delta_{VSV} = f_5\left(\frac{\phi_f}{\delta\sqrt{\theta}}, \frac{N_f}{\sqrt{\theta}}\right) \quad \textbf{(Eq. 2-21)}$$

In summary, in the normal operating mode the EECU controls the free power turbine rotational speed N_f in order to keep it as close as possible to the nominal demand throughout the flight envelope regardless of main rotor load variations. This is achieved by varying the gas generator rotational speed N_g by taking into account free turbine rotational speed N_f, collective pitch position and the load sharing between both engines. The gas generator rotational speed N_g is controlled by the collective pitch position input, such that it anticipates the rotor load variations to obtain a fast engine response. The gas generator rotational speed N_g is also corrected by the twin engine load sharing correction exchanged by a direct link between both EECUs. The free power turbine rotational speed N_f output is proportional to the gas generator rotational speed N_g. As a consequence all variables controlled by the EECU and impacting the gas generator rotational speed N_g are related to the same variables.

Main rotor performance

The referred quantities for power required P_{req} and main rotor blade pitch θ_p are both dependent of the helicopter weight W, forward flight speed V, rate of climb V_c, height

above ground level *Z*, main rotor relative rotorspeed ω, and relative wind direction ζ as summarized below.

Referred main rotor power required function (θ_p *controlled*)

$$P_{req,ref} = \frac{P_{req}}{\sigma\omega^3} = f_1\left(\frac{W}{\sigma\omega^2}, \frac{V}{\omega}, \frac{V_c}{\omega}, Z, \frac{\omega}{\sqrt{\theta}}, \zeta\right) \quad \textbf{(Eq. 2-22)}$$

Main rotor blade pitch function (θ_p *controlled*)

$$\theta_p = f_2\left(\frac{W}{\sigma\omega^2}, \frac{V}{\omega}, \frac{V_c}{\omega}, Z, \frac{\omega}{\sqrt{\theta}}, \zeta\right) \quad \textbf{(Eq. 2-23)}$$

Within the dynamic ship environment, the benefits of ground effect can be considered negligible [12]. Hence, only Out-of-Ground Effect (OGE), low speed, conditions are tested without any vertical speed, thus:

Referred main rotor power required function (θ_p *controlled*)

$$P_{req,ref} = \frac{P_{req}}{\sigma\omega^3} = f_1\left(\frac{W}{\sigma\omega^2}, \frac{V}{\omega}, \frac{\omega}{\sqrt{\theta}}, \zeta\right) \quad \textbf{(Eq. 2-24)}$$

Main rotor blade pitch function (θ_p *controlled*)

$$\theta_p = f_2\left(\frac{W}{\sigma\omega^2}, \frac{V}{\omega}, \frac{\omega}{\sqrt{\theta}}, \zeta\right) \quad \textbf{(Eq. 2-25)}$$

The equations above demonstrate that performance of the helicopter is mainly influenced by the referred weight, the relative wind velocity (airwake in the vicinity of the ship), rotorspeed setting and the relative wind direction (airwake in the vicinity of the ship). In which, the referred weight is defined as the helicopter weight divided by the relative density and squared relative rotorspeed. In order to test at the desired referred weight it is necessary to fly at a mass which straddles this value by plus or minus 2%. A 2% margin is chosen so that the helicopter can fly for a sufficient period of time to gain useful data and yet be close enough to the desired value to permit small corrections to be made when the helicopter is either too heavy or too light. Note that as tests are normally planned to allow the widest possible range of referred weight, it may be advantageous to have the helicopter cleared to operate at an overload weight capacity for the purpose of the tests. External ballast is useful as it can be jettisoned should the helicopter encounter a problem which threatens the safety of the helicopter.

The selection of specific values or ranges of non-dimensional parameter will depend on the test results required, the flying time available and the likely atmospheric conditions at the test site. Note that for a particular test point with a defined relative wind speed, relative wind direction and OAT, the referred main rotor power required is solely a function of the weight of the helicopter. This grouping cannot be used, if a test

technique requires maintenance of $\omega/\sqrt{\theta}$ as well as $W/\sigma\omega^2$ since by testing at different locations with other environmental conditions to vary $\omega/\sqrt{\theta}$ the referred weight will also be altered. The requirement to obtain performance information at constant $\omega/\sqrt{\theta}$ and $W/\sigma\omega^2$ occurs, especially during the evaluation of tip effects. A tip effect causes an actual increase in power required arising from a change in rotor speed Ω [11]. Unfortunately, the alternative grouping, although easier to use since it lacks air density, cannot be used for helicopters with fixed rotor speed. However, it is given here for applications in relation with engine performance as derived in Appendix B.

Referred main rotor power required function (θ_p *controlled*)

$$P_{req,ref} = \frac{P_{req}}{\delta\sqrt{\theta}} = f_1\left(\frac{W}{\delta}, \frac{V}{\omega}, \frac{\omega}{\sqrt{\theta}}, \zeta\right) \qquad \textbf{(Eq. 2-26)}$$

Main rotor blade pitch function (θ_p *controlled*)

$$\theta_p = f_2\left(\frac{W}{\delta}, \frac{V}{\omega}, \frac{\omega}{\sqrt{\theta}}, \zeta\right) \qquad \textbf{(Eq. 2-27)}$$

The relationship between $P_{req}/\sigma\omega^3$ and $P_{req}/\delta\sqrt{\theta}$ confirms this alternative grouping as demonstrated below. Therefore, the flight test data gathered for power required $P_{req}/\sigma\omega^3$ can still be converted into the alternative grouping of power required $P_{req}/\delta\sqrt{\theta}$:

$$P_{req,ref\,(alt)} = \frac{P_{req}}{\sigma\omega^3}\cdot\left(\frac{\omega}{\sqrt{\theta}}\right)^3 = \frac{P_{req}}{\sigma\theta\sqrt{\theta}} = \frac{P_{req}}{\delta\sqrt{\theta}} \qquad \textbf{(Eq. 2-28)}$$

2.4 Operational Scenario

This section gives the reader somewhat more background about the operational procedures used on board of the ship. The information is required to understand the terminology used in the remaining of the dissertation. First, a brief description of a typical sortie profile for an embarked helicopter on board a ship is given. Thereafter, the different take-off and landing procedures applied by the NLMoD are discussed, however, it should be noted that there are also other procedures applied worldwide.

2.4.1 Typical Embarked Sortie

A typical sortie for an embarked helicopter onboard a ship (day or night) can be divided into the following phases:

a. *Stowed.* The helicopter is stowed and secured in the hangar. Generally the main rotor and tail are folded as shown for example in Figure 2-24.

b. *Traversing (Ranging).* The helicopter is moved from the hangar to the landing spot on the flight deck using a suitable traversing system as shown for example in Figure 2-25.

c. *Secured (Lashed/Tied Down).* The folded helicopter is secured to the deck using lashings and/or a deck-lock system as shown in Figure 2-26.

d. *Unfolding (Spreading).* Helicopter main rotor blades and tail are unfolded automatically or manually depending on the type of helicopter.

e. *Engine Start and Rotor Engagement.* Engine or engines are started and main rotors are coupled to the driveshaft.

f. *Take-off.* When take-off conditions are inside the SHOL and Command has issued take-off permission, the deck crew removes nylon or chain lashings and the pilot, when applicable, disengages the deck-lock system. The helicopter lifts off into a hover over the flight deck and moves clear of the ship.

g. *Departure.* Once the helicopter is clear of the ship's superstructure, it transitions to forward flight and departs away from the ship.

h. *Mission.* The helicopter crew carries out their mission. During a mission, the helicopter can for example return to the ship to pick up or release external cargo or for Rotors Running Refuelling (RRR) as shown for the latter for example in Figure 2-27.

i. *Approach.* After the mission is completed, either the helicopter flies directly to the landing spot, or a specific pattern may be followed to set-up for a landing. The approach phase ends when the helicopter is hovering in a waiting position in the vicinity of the ship or directly continues the approach towards above the landing spot.

j. *Landing.* The helicopter moves from the waiting position to the flight deck, or continues the approach directly towards a position above the landing spot and lands. On touch down the pilot immediately engages the deck-lock system if fitted. Lashings are employed for further securing.

k. *Engine Shut Down and Rotor Disengagement.* Engine or engines are shut down. The main rotors are disengaged from the driveshaft and stopped, preferably using a rotor brake instead of stopping due to inertia (i.e. to minimize the potential for blade sailing).

l. *Folding.* Helicopter main rotor blades and tail are folded automatically or manually depending on the type of helicopter.

m. *Traversing (Ranging).* The helicopter is moved from the flight deck to the hangar using a suitable traversing system.

n. *Stowed.* The helicopter is stowed and secured in the hangar. Generally the main rotor and tail are folded.

2.4.2 Role of the Flight Deck Officer

The Flight Deck Officer (FDO) instructs the pilot when to take-off or land at a calm period in ship deck motion and is advisory in nature. In case of doubt the pilot may ignore the instructions by holding in position, however, the wave-off and remain on deck instructions are mandatory. In addition to signalling and/or voice marshalling the pilot when to take-off and/or land the FDO has several other tasks during helicopter operations, amongst which are the following:

Figure 2-24; Helicopter stowed and secured in the hangar

Figure 2-25; Helicopter moved towards landing spot (ranging)

Figure 2-26; Helicopter secured and lashed on deck

Figure 2-27; Helicopter conducting Rotors Running Refuelling (RRR)

- The FDO ensures the general safety conditions of the flight deck, to include control of the flight deck crew;
- Acting as safety officer during standard helicopter operations and emergency;
- Communicate to the pilot at the controls, through various hand signals and/or voice directions, for the proper helicopter placement on the flight deck, re-fuelling, and deck handling.

2.4.3 Take-off and Landing Procedures

In general, take-offs and landings with a helicopter are easiest into wind. However, on ships this procedure is not always possible due to other operational requirements, and it does not always account for the presence of obstacles. Therefore, different take-off and landing procedures are used to increase the operational flexibility of the helicopter on board ships. The procedures applied by the NLMoD are given here (i.e. fore-aft, oblique and cross-deck procedures).

Fore-Aft procedure

The fore-aft procedure is applicable if the helicopter centre line is aligned with the ships heading as shown in Figure 2-28 and Figure 2-29. The fore-aft procedure can be applied towards either the port or starboard side of the ship (i.e. fore-aft port or fore-aft starboard). It is at pilot discretion to choose either one; however, as in most cases the pilot flying is positioned in the right seat, the fore-aft port procedure is the most common enabling best visual cues with the ship. The flight path of the approach and landing can be divided into three distinctive segments, namely:

- *Approach;* approach up to the hover wait position abeam of the landing spot. The hover wait position is approximately ¾ rotor diameter next to the ship and approximately 10 ft above the flight deck. The helicopter's longitudinal axis is parallel to the ship's centreline, with its nose in the sailing direction;
- *Transition;* fly side-wards from the hover wait position to hover over the flight deck/landing spot. The hover height is approximately 10 ft above the flight deck;
- *Landing;* make a vertical descend to land-on. If a deck-lock system is fitted, secure on deck by engaging the system immediately after landing.

The take-off is generally carried out as follows:

- *Alignment;* if required align the helicopter with the ship's centreline, with its nose in the sailing direction;
- *Take-off;* vertical take-off to hover position over the flight deck/landing spot. The hover height is approximately 10 ft above the flight deck. The helicopter's longitudinal axis is parallel to the ship's centre line, with its nose maintained in the sailing direction;
- *Transition;* side-wards transition with simultaneous slow climb, until approximately 1.5 main rotor diameter next to the ship, abeam the landing spot. Yaw approximately 30° and climb away from the ship.

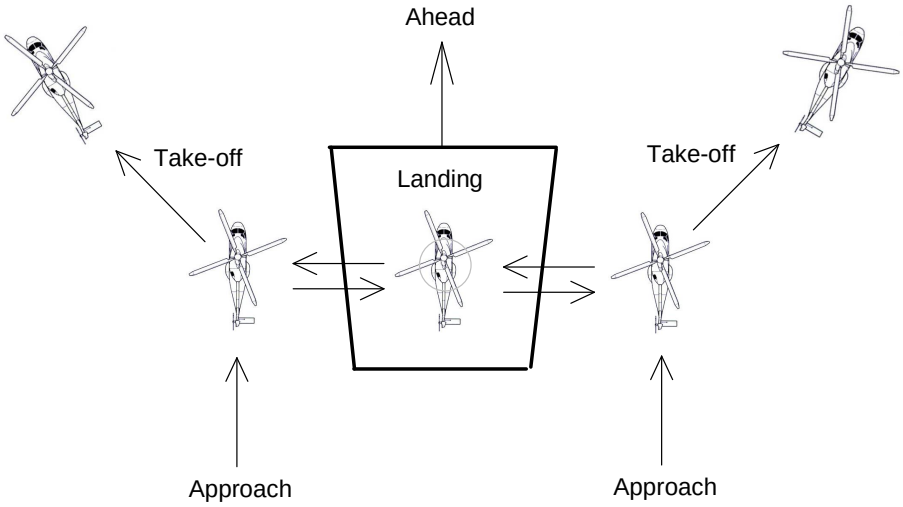

Figure 2-28; Diagram fore-aft procedure

Figure 2-29; Example fore-aft procedure

Oblique procedure

The oblique procedure is applicable if the helicopter centre line is aligned in a 45° angle with the ship's heading as shown in Figure 2-30 and Figure 2-31. The oblique procedure can be applied towards either the port or starboard side of the ship (i.e. oblique facing port or oblique facing starboard). It is at pilot discretion to choose either one. The flight path of the approach and landing can be divided into three distinctive segments, namely:

- *Approach;* approach the ship from the leeward side at a 45° angle with the ship's centreline;
- *Transition;* continue flight up to the hover position above the flight deck/landing spot (helicopter nose maintained in a 45° angle with the ship's centreline). The hover height is approximately 10 ft above the flight deck;
- *Landing;* make a vertical descend to land-on. If a deck-lock system is fitted, secure on deck by engaging the system immediately after landing.

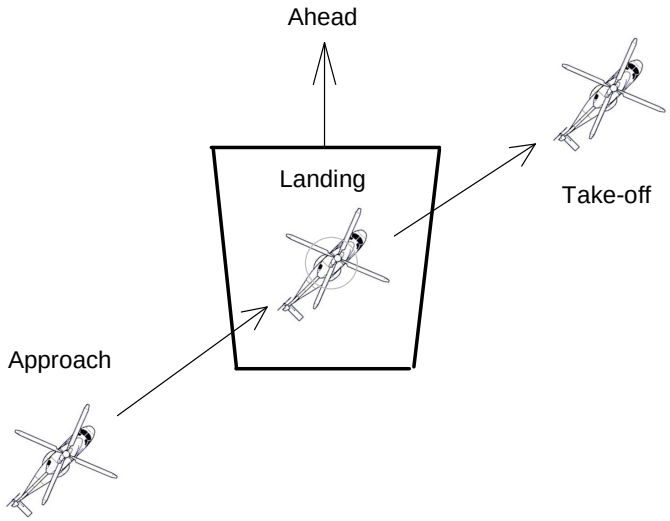

Figure 2-30; Diagram oblique facing starboard procedure

Figure 2-31; Example oblique facing port procedure

The take-off is generally carried out as follows:

- *Alignment;* if required align the helicopter at a 45° angle with the ship's centreline;
- *Take-off;* vertical take-off with the obtained heading to hover position over the flight deck/landing spot. The hover height is approximately 10 ft above the flight deck. The helicopter's longitudinal axis is maintained in a 45° angle with the ship's centreline. If required to avoid obstacles, side-ward flight until the helicopter is clear of the ship's superstructure;
- *Transition;* forward transition with a climb away from the ship.

Cross-deck procedure

The cross-deck procedure is applicable if the helicopter centre line is aligned in a 90° angle with the ships heading as shown in Figure 2-32 and Figure 2-33. The cross-deck procedure can be applied towards either the port or starboard side of the ship (i.e. cross-deck facing port or cross-deck facing starboard). It is at pilot discretion to choose either one. The flight path of the approach and landing can be divided into three distinctive segments, namely:

- *Approach;* approach the ship from the leeward side at a 90° angle with the ship's centreline;
- *Transition;* continue flight up to the hover position above the flight deck/landing spot (helicopter nose maintained at a 90° angle with the ship's centreline). The hover height is approximately 10 ft above the flight deck;
- *Landing;* make a vertical descend to land-on. If a deck-lock system is fitted, secure on deck by engaging the system immediately after landing.

The take-off is generally carried out as follows:

- *Alignment;* if required align the helicopter at a 90° angle with the ship's centreline;
- *Take-off and transition;* vertical take-off with the obtained heading followed by a forward transition with a climb away from the ship.

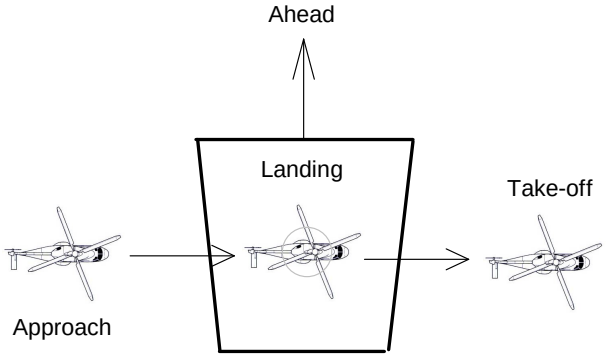

Figure 2-32; Diagram cross-deck facing starboard procedure

Figure 2-33; Example cross-deck facing port procedure

Degraded / single-engine from astern procedure

An additional emergency landing procedure is applied for degraded modes and/or single-engine conditions as shown in Figure 2-34. Note that to reduce power requirements, the helicopter weight should be minimized before starting the approach to the ship. The FDO should position towards either the port or starboard side of the ship's centre line for the landing to maintain visual reference with the pilot (not in front of the helicopter for safety reasons).

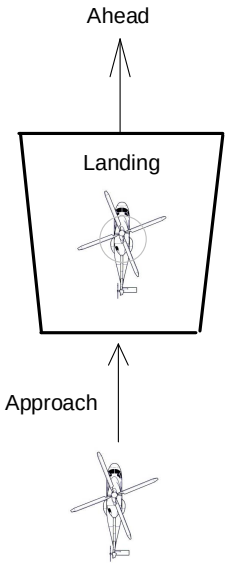

Figure 2-34; Diagram degraded / single-engine from astern procedure

The flight path of the approach and landing can be divided into two distinctive segments, namely:

- *Approach;* approach the ship from the stern along the ship's centreline until above the landing spot;
- *Landing;* make a continuous descend to land-on. If a deck-lock system is fitted, secure on deck by engaging the system immediately after landing.

2.5 Chapter Review

The novelty in this chapter is the systematic approach used to describe the various aspects that interact with each other in the shipboard environment and that are of influence to the behaviour of the helicopter. In this way, the readers understanding of helicopter-ship qualification testing as a whole is increased without the necessity to have access to a large diversity of literature. The subject of helicopter-ship qualification testing is characterized by interplay between theory and experiment. This introductory tour attempts to highlight this interplay in a number of ways. By introducing the four reference points early in the tour – (1) the helicopter flight characteristics and limitations, (2) the atmospheric conditions, (3) the ship environment and (4) the pilot and pilot-helicopter interface – an attempt has been made to reveal the considerable scope of the subject and the skills required to conduct this kind of testing. The theory of dimensional analysis used to plan and analyze the flight test data is highlighted. This theory is important because data converted into referred parameters can be used to produce information relevant to atmospheric conditions and helicopter weights different from those actually tested. Finally, a brief overview of an operational scenario and the applied take-off and landing procedures is given to provide the reader with more background information about shipboard operations and to become familiar with the terminology used in this dissertation.

Chapter 3 Uncertainty Analysis and Safety Margins

3.1 Introduction

Since a model by definition is a simplified representation of reality, differences between model and reality arise simply because of the existence of the model. In addition, no measurement, even when carefully made, can be completely free of errors. All measurements of a variable contain inaccuracies. Since the whole structure and application of flight test depends on measurements, it is therefore crucially important to be able to evaluate the associated uncertainties and to keep errors to a minimum. It is important to realize that errors in this context are not mistakes. It would be impossible to eliminate errors by careful measurements; the best achievable is to ensure that they are as small as reasonably possible and also have some reliable estimate of how large the errors are. This includes the development of (1) methodologies needed to estimate the errors inherent in various types of measurements, and (2) techniques for testing data to find out whether these error estimates are valid, and (3) the understanding of the way errors propagate through calculations made by the model using experimental data, finally resulting in uncertainties of the predictions.

Engineers often tackle such problems on the basis of their past experience of similar problems and seek to resolve any residual scatter "*by eye*". Where it is appropriate to apply margins, this too is usually done intuitively on the basis of past experience and a knowledge of the likely consequences of being "*wrong*", in one direction (over cautious) or the other (over optimistic). This process is so well established that the term "*engineering judgment*" has been used to describe it, and in many cases, it is an entirely appropriate and adequate procedure. However, there are occasions where the use of a more objective numerical method is called for and this dissertation describes some of these methods based on well-established statistical principles. It must be recognized that no single method will give a rigorous, scientifically correct answer for all situations. The method discussed in this dissertation is believed to be most suitable. It is important to appreciate that statistical methods do not entirely replace the use of engineering judgment; rather they should be seen as supplementary to it, providing engineers with the ability to be better judges.

3.2 Basics Uncertainty Analysis

This section gives a framework for uncertainty analysis associated with the data gathering during actual flight tests and the output of a simulation model (e.g. the predictive tool to be developed in this dissertation). This includes, amongst others, a consistent terminology and foundation for a methodology bridging the gap between a practical execution of actual flight tests and well-established statistical principles based

on Isukapalli [1], Coleman [2], Bendat [3], and the Engineering Sciences Data Unit (ESDU) [4]. However, unless stated otherwise, the author used his own interpretation to present the basics of uncertainty analysis and associated definitions as applied throughout this dissertation.

3.2.1 Purpose of Uncertainty Analysis

In computer- and simulation-based design, the output of the mathematical model invariably differs from the assumed true values. These differences arise because of uncertainties in the model with its parameters, and through input values and equations because of the imperfection and assumptions for numerical analysis. The general indication – uncertainty analysis – represents different areas, e.g. measurement uncertainty, model uncertainty and physical parameter uncertainty. The following definition of uncertainty analysis is adopted [1]:

"Uncertainty analysis is the analysis of the difference between the model output and the true values the simulation intends to approach as well as the analysis of all possible causes of the difference."

This definition recognizes the fact that uncertainty analysis is performed to evaluate (complex) computer models and simulations performed with these models. An important aspect of uncertainty analysis is that a lot of uncertainty exists in the input values and results of the uncertainty analysis itself. The uncertainties in the input parameters and measurements could be analyzed and determined to an acceptable level of confidence, but the supposed confidence in any model uncertainty remains arbitrary. Because of this, the objective of uncertainty analysis, at least as used in this dissertation, can be formulated in a general way:

> The objective of uncertainty analysis is to provide a notion of the possible range of the model output in relation with the assumed 'true' values.

3.2.2 Origins of Uncertainties

It is considered that the experimental values of measurement X will contain errors, and so an uncertainty should also be associated with X. In addition, the model output also has uncertainties arising from, for example, modelling errors and possibly errors from algorithms used to numerically solve the simulation equation. The causes of the uncertainties, as shown in Figure 3-1, with some change in terminology (as to better reflect the meaning) are summarized as follows [1]:

1. Theory uncertainty;
2. Model uncertainty:
    a. Model structure;
    b. Model detail;
    c. Extrapolation
    d. Model resolution.
3. Parameter / variable uncertainty:

a. Input variable uncertainty;
b. Model parameter uncertainty;
c. Physical parameter uncertainty.

4. Measurement uncertainty.

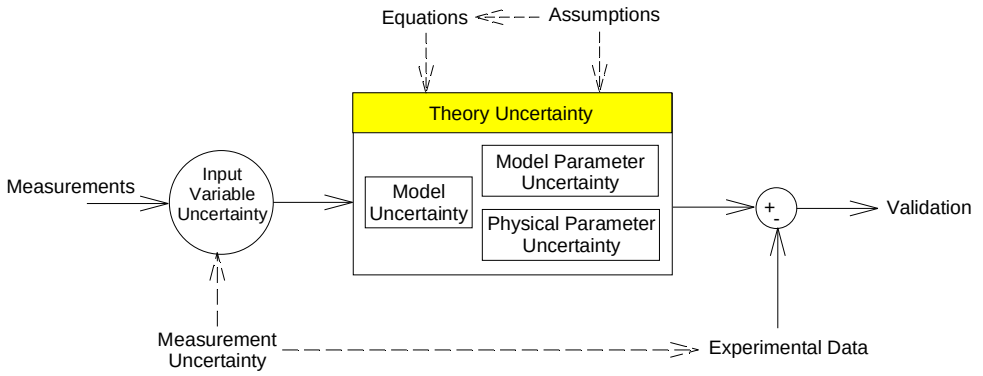

Figure 3-1; Origins of uncertainties; modified from [5]

Closely related to these origins of uncertainty is the process of verification, calibration and validation. In short, verification involves the initial evaluation of the model structure and whether the model predicts expected trends. Calibration is the process of adjusting numerical or physical modelling parameters in the computational model for the purpose of improving agreement with experimental data to be further discussed in Chapter 5. Finally, the model is validated by comparing the results with an independent set of measurements from experimental data to be further discussed in Chapter 6.

3.2.2.1 Theory Uncertainty

Theory uncertainty is the uncertainty in the underlying fundamental physical principles of the model caused by the applied assumptions and utilized equations. In this dissertation, the following fundamental principles are adopted and considered to be fully certain:

- Newton's law of motion and gravitation;
- Conservation of mass;
- The ideal gas law;
- The constancy for the ratio of specific heats (γ).

All other models referred to in this dissertation are considered to be uncertain to some extent. This uncertainty falls into the category 'model uncertainty'.

3.2.2.2 Model Uncertainty

Since a model by definition is a simplified representation of reality, differences between model and reality arise simply because of the existence of the model. The causes of model uncertainty can be divided into three categories:

a. Model structure: The model structure reflects the physical principles and assumptions that have been adopted and applied when constructing the model. If alternative models or sub-models are available, uncertainty arises when these alternative models produce different results. In combination with experimental flight test data, the differences make it possible to accept or discard model alternatives and to assess the physical assumptions. For example, the benefit of ground effect for helicopter performance has not been implemented in the predictive tool, as this is neglected for mission planning purposes due to the dynamic ship environment [6]. However, in reality the helicopter is likely positively influenced by the ground effect above the flight deck such that a lower power requirement may be required.

b. Model detail: Often models are simplified in order to speed up simulation or to keep the model tractable. Uncertainty in the predictions of simplified models can sometimes be characterized by comparison of their predictions to those of more detailed, inclusive models or with actual flight test data. The predictive tool developed in this dissertation relies to a large extent on actual flight test data for steady-state conditions, and although it is simple, the predictive tool provides adequate model detail whilst being transparent in its predictions.

c. Extrapolation: If the choice of model in a certain region of operation proves to be accurate and returns satisfying results, it remains to be seen what the accuracy is if the model is outside this region. In order to minimize any extrapolation in results, two shore-based hover trials were conducted at different test location with different atmospheric conditions. The atmospheric conditions were chosen such that they would capture the extremes in operational scenario's in which the helicopter would operate during shipboard operations. Therefore, the predictions made by the predictive tool can actually be considered a structured interpolation between actual flight test results.

d. Model resolution: The resolution of the model - both spatial and temporal - usually dictates the trade-off between computation time and prediction accuracy. The governing equations in the novel predictive tool are as simple as possible and as complex as necessary, whilst assuring quick results and adequate prediction accuracy. The step size between the test conditions during the shore-based hover trials (i.e. speed and azimuth), and between the data points used from the flight manual to construct certain graphs are considered sufficient to construct a Candidate Flight Envelope (CFE).

Although a classification of the causes for model uncertainty is easily achieved, actual estimation of the uncertainty is another matter. Model detail, extrapolation and model resolution uncertainty are still relatively easily estimated by comparing the model output with actual flight test data, but estimating the model structure uncertainty might prove difficult. To get a definite result, it would be required to recognize all technical and physical assumptions in the model, and formulate all possible alternative assumptions and compare the results. Since this is impossible, the model structure is not evaluated in terms of uncertainty but is only accepted or rejected. The objective of the validation then is to locate the parts of the model structure that require improvement.

3.2.2.3 Parameter / Variable Uncertainty

Regarding the uncertainty in parameters and variables, the following sub-division is made: input variable uncertainty, physical parameter uncertainty and model parameter uncertainty.

a. Input variable uncertainty: Each sub-model has up to three types of input variables as shown in Figure 3-2. The sub-models share the input variables x_s with the associated uncertainties. A number of input variables are unique to a certain sub-model (x_a and x_b), again with their uncertainties. Finally, some output variables from one sub-model may serve as input variables to another sub-model (y_a and y_b). This last type of input variable makes it such that the overall uncertainty (the uncertainties in r_a and r_b) can only be determined if the uncertainties associated with y_a and y_b are known. This is only really possible if the total model is available. If only the sub-model is available, the uncertainty in y_a or y_b has to be estimated.

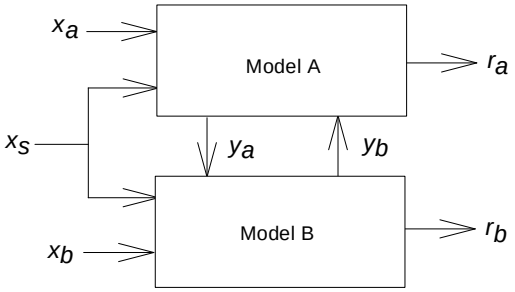

Figure 3-2; Relation between sub-models; modified from [5]

b. Physical parameter uncertainty: The physical parameters are associated with material properties, physical dimensions etc., each with their own uncertainty. The physical parameters can often be measured directly and remain constant during the simulation.

c. Model parameter uncertainty: Model parameters arise from the assumed physical model. The difference between the physical parameters and the model parameters is the fact that physical parameters are associated with physical objects and always exist while the model parameters only exist because of the model (i.e. the physical assumptions). This parameter is the result of the adopted model structure and often cannot be directly measured. Instead, they have to be deduced using measurements during the calibration procedure. If sufficient measurements are available, the uncertainty in the model parameters can be expressed in a statistical way. In case experiments are unavailable, one has to rely on expert opinions.

3.2.2.4 Measurement Uncertainty

The measurement uncertainties inherent to all forms of data gathering influence the input variables of the predictive tool. In addition, measurement uncertainties have an influence on the experimental flight test data necessary to calibrate and validate the model output. If enough measurements are available, the uncertainty can be

determined rather than estimated. The determination of the uncertainty of a measurement allows amongst others: (1) meaningful comparison of equivalent results from different flight trials, and/or (2) comparison of the result with reference values given in specifications or standards. Availability of this information can allow the equivalence of results to be judged by the user and avoid unnecessary repetition of tests if differences are not significant.

3.2.3 Assumption for Uncertainty Propagation in Model Output

An important aspect of multi-disciplinary modelling is the actual propagation of the uncertainties and especially of the distribution associated with this uncertainty. The simplest way to obtain this would be to vary the model parameters and physical parameters along their range, run the model with each (combination of) parameters and record the model output. However, such a direct method may prove impracticable and most research is directed in finding efficient ways of performing this analysis (e.g. by using the Taylor series method for propagation of uncertainties). Therefore, in this dissertation, the following assumptions have been made:

1. The uncertainty in the input parameters and variables is considered to have a normal distribution with a 95% confidence level;
2. The cumulated uncertainty of the model output due to the uncertainties in the input variables and parameters is also considered to have a normal distribution with a 95% confidence level.

Because of these assumptions, one has to be careful in judging the model output with its uncertainty. The uncertainty interval itself is uncertain due to the two assumptions mentioned above. However, the purpose of this dissertation is not necessarily to have the exact distribution of the uncertainty in the answer as well as an exact value of this uncertainty. The objective of the uncertainty analysis is to identify those parameters and variables that have a large influence on the model output (and therefore require the most attention) and to locate those parts of the model that produces results that are not in agreement with validation measurements.

3.2.4 Mathematics

The mathematics involved in uncertainty analysis which are relevant for helicopter-ship qualification testing is summarized for convenience [2,3,4]. The basic knowledge required to properly understand these mathematics and some example calculations are contained in Appendix D. Contrary to laboratory tests, where the same measurement can be repeated multiple times to determine statistical distributions, flight time is expensive and consequently statistical distributions usually need to be determined from single time histories. A single time history representing a random phenomenon is called a sample function (or sample record when observed over a finite time interval). When a physical phenomenon is considered in terms of a random process, the properties of the phenomenon can hypothetically be described at any instant of time by computing average values over the collection of sample functions that describe the random process. If the random process is stationary and the mean value does not differ when computed over different sample functions, the random process is so-called "*ergodic*". For ergodic random processes, the time-averaged mean values (as well as

other time-averaged properties) are equal to the corresponding ensemble-averaged values. It is for this reason that the properties of stationary random phenomena can be measured properly, in most cases, from a single observed time history record e.g. shore-based hover trials and wind tunnel measurements.

A distinction is made between an uncertainty u and an error δ. The uncertainty u is an estimate of a range within which it is believed that the actual (but unknown) value of an error lies. An error δ is a quantity that has particular sign and magnitude, and a specific error δ_i is the difference caused by an error source i between a quantity (measured or simulated) and its true value X_{true}. It is generally assumed that corrections will be or have been made for errors of known sign and magnitude in the calibration phase. Any remaining error is thus of unknown sign and magnitude. Therefore, an uncertainty u is introduced with the idea that $\pm u$ characterizes the range containing all error sources. Errors from some sources vary during the period when measurements are taken and so are different for each measurement, while others do not vary and so are the same for each measurement. For this reason, the error sources are divided in systematic errors, also known as bias, b, that remain constant during all measurements and in precision errors, also known as random errors or scatter, s, which are random in nature and vary for each measurement.

Statistical parameters of sample function

For N measurements of X, the standard deviation s_X of the sample function can be calculated as:

$$s_X = \left[\frac{1}{N-1} \sum_{i=1}^{N} (X_i - \overline{X})^2 \right]^{1/2} \qquad \textbf{(Eq. 3-1)}$$

where the mean value of X is calculated from:

$$\overline{X} = \frac{1}{N} \sum_{i=1}^{N} X_i \qquad \textbf{(Eq. 3-2)}$$

Uncertainty in a result determined from multiple variables

In many experiments or flight test programs the experimental result is not directly measured but is determined by combining multiple measured variables in a data reduction equation. Examples are the dimensionless groups, such as referred torque required, referred engine gas generator rotational speed, and referred engine power turbine inlet temperature that are often used to present the results of a flight test. The Taylor Series Method (TSM) is applied for propagating the uncertainties of the variables into the determined result. In this dissertation, the TSM expression is an approximation that includes only the first-order terms from the Taylor series expansion. Also, the derivatives are evaluated at the measured values of, for example, x and y instead of at x_{true} and y_{true}, which would be required for a normal Taylor series expansion. For most engineering and scientific applications, these approximations are reasonable, and the resulting combined standard uncertainty u_r is a good estimate of the

standard deviation for the parent population of the result, *r*. Consider a general case in which an experimental result *r* is a function of *J* measured variables X_i:

$$r = r(X_1, X_2, ..., X_J) \quad \textbf{(Eq. 3-3)}$$

The combined standard uncertainty is given by:

$$u_r^2 = \sum_{i=1}^{J} \left(\frac{\partial r}{\partial X_i} \right)^2 b_{X_i}^2 + \sum_{i=1}^{J} \left(\frac{\partial r}{\partial X_i} \right)^2 s_{X_i}^2 \quad \textbf{(Eq. 3-4)}$$

where b_{Xi} and s_{Xi} values are the standard deviations for the measurement of each variable X_i. Using the defined systematic standard uncertainty of the result (bias) b_r and random standard uncertainties of the result (scatter) s_r, the combined standard uncertainty becomes:

$$u_r = \left(b_r^2 + s_r^2 \right)^{1/2} \quad \textbf{(Eq. 3-5)}$$

In order to associate a level of confidence with the uncertainties for the variables, a coverage factor is applied such that:

$$U_r = t_{\%} u_r \quad \textbf{(Eq. 3-6)}$$

where U_r is the overall or expanded uncertainty at a given percent level of confidence. The ± U_r band around the variable *X*, or the mean value of *X*, will contain the true value of the variable with the given percent level of confidence. Normally, a number of degrees of freedom (i.e. the number of independent measurements minus the number of parameters calculated from these measurements) are needed in order to select the *t* value for a given level of confidence. However, it has been demonstrated that the degrees of freedom will be generally large enough to consider the *t* value to be constant, known as the "*large-sample approximation*" [2]. This constant will be approximately equal to the Gaussian value for a given level of confidence (i.e. 1.96 for 95%) which is applicable for a parent population with an infinite number of measurements. For example, the resulting large-sample approximation for a 95% level of confidence using the *t* distribution as shown in Table D-1 in Appendix D can be used ($t_{95} \approx 2$) resulting in:

$$U_{95} = 2 \cdot \left[\sum_{i=1}^{J} \left(\frac{\partial r}{\partial X_i} \right)^2 \left(b_{X_i}^2 + s_{X_i}^2 \right) \right]^{1/2} \quad \textbf{(Eq. 3-7)}$$

If reasonably assumed that there are no correlated systematic or random errors within the flight test data, then all of the b_{Xi} and s_{Xi} terms are independent. Taking the coverage factor inside the summation, results in:

$$U_{95} = \left[\sum_{i=1}^{J} \left(\frac{\partial r}{\partial X_i} \right)^2 U_i^2 \right]^{1/2} \quad \textbf{(Eq. 3-8)}$$

where each U_i is the large-sample 95% expanded uncertainty for the variable X_i. This equation describes the propagation of the overall uncertainties in the measured variables into the overall uncertainty of the result. The application of this equation is termed general uncertainty analysis.

Application in experimentation

Consider again the general case in which an experimental result r is a function of J measured variables X_i. The expanded uncertainty in the result is given by the data reduction equation used for determining r from the measured values of the variable X_i:

$$U_r^2 = \left(\frac{\partial r}{\partial X_1}\right)^2 U_{X_1}^2 + \left(\frac{\partial r}{\partial X_2}\right)^2 U_{X_2}^2 + \cdots + \left(\frac{\partial r}{\partial X_J}\right)^2 U_{X_J}^2 \qquad \textbf{(Eq. 3-9)}$$

where the U_{Xi} are the expanded uncertainties in the measured X_i. The partial derivatives are called absolute sensitivity coefficients. These values should have all the same level of confidence, in most cases 95 % confidence. To obtain a useful form for the application in experimentation, divide each term in the equation by r^2, and multiply each term on the right-hand side by $(X_i / X_i)^2$ which of course is equal to one, so:

$$\frac{U_r^2}{r^2} = \left(\frac{X_1}{r}\frac{\partial r}{\partial X_1}\right)^2\left(\frac{U_{X_1}}{X_1}\right)^2 + \left(\frac{X_2}{r}\frac{\partial r}{\partial X_2}\right)^2\left(\frac{U_{X_2}}{X_2}\right)^2 + \cdots + \left(\frac{X_J}{r}\frac{\partial r}{\partial X_J}\right)^2\left(\frac{U_{X_J}}{X_J}\right)^2 \qquad \textbf{(Eq. 3-10)}$$

where U_r / r is the relative uncertainty of the result. The factors U_{Xi} / X_i are the relative uncertainties for each variable. The factors in the parentheses that multiply the relative uncertainties of the variables are so-called "*uncertainty magnification factors*" [2]. The Uncertainty Magnification Factors (UMF) are defined as:

$$UMF_i = \frac{X_i}{r}\frac{\partial r}{\partial X_i} \qquad \textbf{(Eq. 3-11)}$$

The UMF for a given X_i indicates the influence of the uncertainty in that variable on the uncertainty in the result. An UMF value greater than one indicates that the influence of the uncertainty in the variable is magnified as it propagates through the data reduction equation into the result. An UMF value of less than one indicates that the influence of the uncertainty in the variable is diminished as it propagates through the data reduction equation into the result. Since the UMFs are squared their signs are of no importance, thus only the absolute values of the UMFs are considered for the general uncertainty analysis.

The expression that arises for the propagation of errors is represented by the percentage error. In each case, a calculation is performed to identify any dominant error. One

should always concentrate on reducing the dominant error, and not to waste time trying to reduce the error on parameters which do not contribute significantly to the error. An important lesson to be learned is that error analysis not only tells the size of the errors but also helps to pinpoint the contributions from the individual measured parameters. Thus, if, for example, the reduction of raw data involves parameters raised to high powers, such parameters need to be measured with a high degree of precision if the calculated result is not to be unduly degraded in probable error. An analysis of measured errors and required computation may affect the choice of instrumentation for a given trial. Although specialist instrumentation may raise the cost of a trial the alternative is to repeat the measurements until an acceptable confidence in the results is attained. However, increased flying time is likely to be a more expensive option than an improved instrumentation fit.

An example calculation for the uncertainty in referred torque required is shown in the following. The function for referred torque required $Q_{req,ref}$ is given by:

$$Q_{req,ref} = \frac{Q_{req}}{\sigma\omega^2}$$

The variables are torque required Q_{req}, relative density σ (relative to international standard atmosphere) and ω is the relative rotorspeed (relative to a standard rotor speed value). Using the general uncertainty analysis expression for the referred torque required, the uncertainty is determined as:

$$U^2_{Q_{req,ref}} = \left(\frac{\partial Q_{req,ref}}{\partial Q_{req}}\right)^2 U^2_{Q_{req}} + \left(\frac{\partial Q_{req,ref}}{\partial \sigma}\right)^2 U^2_{\sigma} + \left(\frac{\partial Q_{req,ref}}{\partial \omega}\right)^2 U^2_{\omega}$$

To obtain a useful form for the application in experimentation, divide each term in the equation by $Q^2_{req,ref}$, and multiply each term on the right-hand side by $(X_i / X_i)^2$ which of course is equal to one, so:

$$\frac{U^2_{Q_{req,ref}}}{Q^2_{req,ref}} = \left(\frac{Q_{req}}{Q_{req,ref}}\frac{\partial Q_{req,ref}}{\partial Q_{req}}\right)^2\left(\frac{U_{Q_{req}}}{Q_{req}}\right)^2 + \left(\frac{\sigma}{Q_{req,ref}}\frac{\partial Q_{req,ref}}{\partial \sigma}\right)^2\left(\frac{U_{\sigma}}{\sigma}\right)^2 + \left(\frac{\omega}{Q_{req,ref}}\frac{\partial Q_{req,ref}}{\partial \omega}\right)^2\left(\frac{U_{\omega}}{\omega}\right)^2$$

The UMFs can be determined in this case by replacing $Q_{req,ref}$ with its function:

$$\text{UMF}_{Qreq} = \frac{Q_{req}}{Q_{req,ref}}\frac{\partial Q_{req,ref}}{\partial Q_{req}} = \frac{Q_{req}}{Q_{req,ref}}\left(\frac{1}{\sigma\omega^2}\right) = \frac{Q_{req}}{Q_{req,ref}\sigma\omega^2} = 1$$

$$\text{UMF}_{\sigma} = \frac{\sigma}{Q_{req,ref}} \frac{\partial Q_{req,ref}}{\partial \sigma} = \frac{\sigma}{Q_{req,ref}} \left(-\frac{Q_{req}}{\sigma^2 \omega^2} \right) = -\frac{\sigma Q_{req}}{Q_{req,ref} \sigma^2 \omega^2} = -1$$

$$\text{UMF}_{\omega} = \frac{\omega}{Q_{req,ref}} \frac{\partial Q_{req,ref}}{\partial \omega} = \frac{\omega}{Q_{req,ref}} \left(-2 \cdot \frac{Q_{req}}{\sigma \omega^3} \right) = -2 \cdot \frac{\omega Q_{req}}{Q_{req,ref} \sigma \omega^3} = -2$$

with the UMFs now substituted in the equation and taking the square root gives:

$$\frac{U_{Q_{req,ref}}}{Q_{req,ref}} = \sqrt{\left(\frac{U_{Q_{req}}}{Q_{req}} \right)^2 + \left(\frac{U_{\sigma}}{\sigma} \right)^2 + \left(2 \cdot \frac{U_{\omega}}{\omega} \right)^2}$$

The application of this equation for the general uncertainty analysis is useful for application in experimentation and is used throughout this dissertation.

3.3 Sources of Uncertainties

Measurements of the variable *X* are influenced by a number of elemental error sources such as:

1. The errors in the standard used for calibration and from an imperfect calibration process (i.e. systematic errors);
2. The errors due to undesired interactions of the transducer with the environment (i.e. systematic errors);
3. The errors due to imperfect installation of the transducer (i.e. systematic errors);
4. The errors caused by variations in for example ambient temperature, humidity, pressure, vibrations and electromagnetic influences (i.e. precision errors);
5. Unsteadiness in the "*steady-state*" test condition being measured (i.e. precision errors).

The measurement process is the totality of all the individual sub-processes and steps in the measurement system. That is, the process is the total of all the calibrations, all data acquisitions and all data reductions. Therefore, the systematic error (i.e. bias) in each sub-process is a systematic error in the total process. The precision error (i.e. scatter) in each step of each sub-process is reflected as a precision error in the total process. Then, it must be determined how the systematic and precision errors are related to the relevant parameter. The uncertainties associated with the measurement process for the wind tunnel, shore-based hover trials and sea trials are discussed in this section in more detail. The statistical data used for data analysis associated with these measurements are initially estimated by engineering judgement based on subject matter expertise of the author amongst a large diversity of helicopter types. To find out whether these error estimates are valid, where applicable, the precision error (i.e. scatter) is determined from the measurements, of which the latter value is then used to derive the

combined standard uncertainty as summarized in Table 3-1. A more detailed description of the test techniques and test instrumentation is contained in Appendix E and Appendix F, respectively.

3.3.1 Wind Tunnel Measurements

The wind tunnel measurements were performed on scale models of the ships within the entire Dutch fleet in the German Dutch Wind Tunnels Large Low-speed Facility (DNW-LLF). The size of the scale models was dependent on the actual size of the ships in relation to the available dimensions of the wind tunnel, and varied between 1:70 and 1:100 [7,8,9,10,11,12]. In general, for every wind tunnel measurement, a number of items are relevant to consider for the measurement uncertainty, for example, Reynolds number (Re), blockage effect and boundary layer. The probe was calibrated at flow angles up to ± 30°. If the vertical flow direction φ or horizontal flow deviation χ did exceed this range, flow angles nor local wind speed were calculated. Based on the calibration results and validation tests (with the calibration set-up) the instrument accuracy was determined. The accuracy of the vertical flow direction φ or horizontal flow deviation χ obtained by the measurements was about ± 0.5°. The accuracy in the measured wind speed was about ± 0.25 m/s. The wind tunnel measurements have been spot-checked by full-scale measurements at the respective ships and therefore are considered validated [13,14,15,16,17,18]. For this reason, only the wind tunnel measurements are used to construct the CFE in this dissertation.

Reynolds number (Re)

The ratio of inertial forces to viscous forces in the fluid is given by Re:

$$\mathrm{Re} = \frac{\rho v L}{\mu} \qquad \textbf{(Eq. 3-12)}$$

where ρ is the density of the fluid, v is the mean velocity of the object relative to the fluid, L is the characteristic linear dimension and μ is the dynamic viscosity of the fluid. The numerator represents the inertial force. The denominator is a viscous force. For an ideal fluid, Re is effectively infinite. However, when viscous forces are dominant, the Re is a small value. The Re is one of the governing similarity parameters for the simulation of flow in a wind tunnel. For Mach numbers less than 0.3, it is the primary parameter that governs the flow characteristics. However, it has been demonstrated that for the Re of interest for a ship with a bluff body consisting of rectangular surfaces and sharp edges, the flow is largely Re independent [19,20,21]. Therefore, the wind tunnel speed can be chosen to suit the test optimally, and the measurement can be scaled linearly to other speeds of interest for the same relative wind angle. To obtain a reasonable quality of the test data in disturbed wind sections, a high tunnel speed is preferred, which increases the measured pressures and allows accurate pressure measurements. However, vibrations of the probe support and aerodynamic loads on the ship model limit the applicable wind tunnel speed. A wind tunnel speed of 30 m/s has proven to be a good practical value, and this value was applied for all pressure probe tests on the scale models within the entire Dutch fleet.

Blockage Effect

For a ship at full-scale there is a certain amount of divergence in the airflow around it. However, wind tunnel walls obstruct a free displacement of the oncoming flow, and any divergence in the airflow around the scale model of the ship is confined by the wind tunnel walls. The blockage effect by the wind tunnel walls becomes more critical as the characteristic linear dimensions of the scale models increase in relation to the available dimensions of the wind tunnel. The blockage effects of the airflow around the scale model of the ship may increase the dynamic pressure at the measurement locations in the vicinity of the scale model. Consequently, higher pressures can result that increase the local wind speed measurement in the vicinity of the ship [19].

Boundary Layer

In the wind tunnel, the airflow measurements are carried out in a uniform airflow condition, i.e. the wind is assumed not to vary with height or at least there is a very thin boundary layer compared to the size of the scale model of the ship [22]. In reality, the wind speed increases with height due to the effects of the atmospheric boundary layer. To compare full-scale wind climate data with wind tunnel data, corrections for atmospheric boundary layer effects should be accounted for [23]. However, it should be noted that the relative wind speed which is solely caused by the speed of the ship at full-scale will be an uniform airflow condition as well, whilst the relative wind speed resulting from the course and speed of the ship in combination with the actual wind will not. Unfortunately, during operational scenarios the relative wind speed could result from any combination in course and speed of the ship in relation to the actual wind. Furthermore, when sailing into the wind the calculated correction factor could approximate the theoretical value, although when in the same conditions sailing with the wind from astern, a different calculated correction factor may be approximated. In addition, the airflow around the ship and the associated indicated wind as determined by the ship's anemometers is likely to be influenced by ship motion in various sea states. Therefore, it is expected that this accounts for a certain amount of variance between the wind tunnel measurements and full-scale results at sea.

3.3.2 Shore-Based Hover Trial Measurements

The purpose of the shore-based hover trials is to determine helicopter flight characteristics, for example, power required, Trimmed Flight Control Positions (TFCP), helicopter attitude, controllability limits and pilot workload in an omni-directional relative wind envelope. A dedicated pace-car is used to set up the required relative wind conditions in addition to the actual wind encountered. The flight test data from the helicopter is recorded with an instrumentation suite via the 1553-data bus and/or direct ARINC lines. Unfortunately, the systematic error (i.e. bias), is usually not provided by industry for the various sensors in the helicopter and has to be estimated.

Data qualification

Prior to detailed data analysis, it is important that data qualification is performed. Each test condition is maintained for a period of approximately 90 seconds, to ensure that all trends of the factors that have a significant influence on the data and contribute to the random uncertainty are captured within a single sample record. A period of 90 seconds

is chosen as a compromise between the available runway length for the pace-car to operate, and sufficient time to capture random sources that vary during the measurement period and which effects are included in the precision error. The data is checked for any anomalies indicative of data acquisition errors by careful inspection of the time histories. If anomalies are identified during the data qualification, and feasible, those time history records should be edited to remove the anomalies. This data qualification procedure can range from purely subjective techniques to sophisticated techniques using specialized computer programs. For the flight test data analyses used in this dissertation, the data is presented in graphical format and then only analyzed by a subjective technique. Thereby, a time interval within the sample record is chosen in which the flight test conditions are most representative for the helicopter flight characteristics, reducing the unwanted effects of the phenomena listed below:

- Wind direction and wind speed fluctuations by gusts with strong natural winds (e.g. scatter of approximately 3 seconds time periods);
- Wind speed variations along the runway due to variation in landscape and/or pace-car drivers ability to hold speed (e.g. scatter of approximately 5 seconds time periods);
- The flight crew's ability to judge their speed relative to that of the pace car (e.g. scatter of approximately 5 seconds time periods);
- Variations in the flight path, speed and attitude of the helicopter by unintentional pilot inputs (e.g. scatter of approximately 3 seconds time periods).

Randomness individual test conditions

Provided all test conditions are reasonably similar and the same method is used for each one, it can reasonably be expected that there is the same uncertainty in the measurements for each individual test condition. For this reason, unless stated otherwise, the average standard deviation is taken from the sum of all the standard deviations and not for each individual test condition. However, it is required that for each parameter areas with excessive excursions from the mean value, representative for a specific helicopter type, are identified and considered for further data analyses. Therefore, graphs are produced for each parameter within which areas with high scatter (i.e. more than two average standard deviations from the mean) are indicated by the predictive tool as shown for pedal and tail rotor actuator position in Figure 3-3. In this case, certain combinations of cross-wind speed and flow through the tail rotor are forming a so-called "*region of roughness*" for the NH90 NFH. Within this region there is an oscillatory yawing motion leading to a high scatter in pedal deflections. For such areas with higher scatter around the trimmed flight condition, a larger standard deviation around the mean is applied for further calculations (i.e. the average standard deviation for the specific group of test points).

3.3.3 Sea Trials Measurements

The main objective of the sea trials is to confirm the CFE, by collecting quantitative test data to validate the predictions whilst ensuring that within the released operational envelope no helicopter limitations are exceeded. In addition, a confirmation is required

based on qualitative elements to determine the effects on pilot workload from, for example, visual references, ship motion and turbulence. The operational envelopes are established by validation of the predicted boundaries by various take-off and landings in different relative wind conditions.

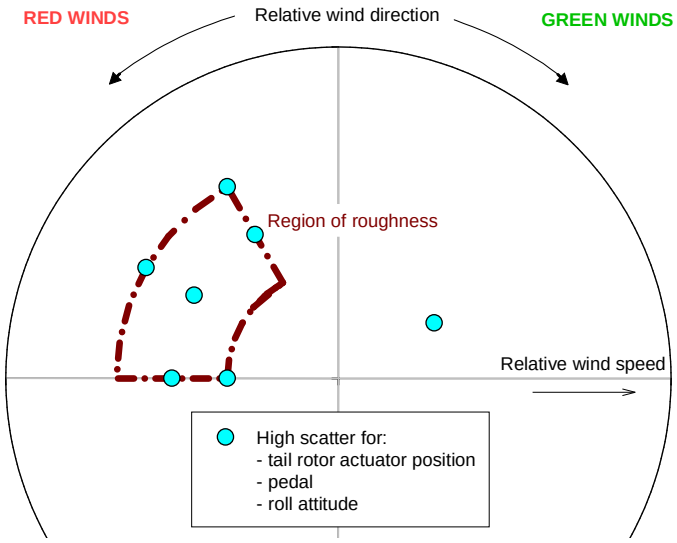

Figure 3-3; Example area with high scatter, so-called "*region of roughness*"

In addition to helicopter parameters, the ship's parameters are recorded to set the operational limitations in pitch and roll motion of the ship. Prior to detailed data analysis, it is important that data qualification is performed. Contrary to the shore-based hover trials, not the steady-state flight characteristics are relevant during the sea trials, but the proximity of the measurements to any limitations, i.e. maximum and/or minimum values of the measurements. However, it is unlikely that even for the same relative wind condition, identical time histories are produced to allow a direct comparison. There are too many variables that influence the behaviour of the helicopter in the vicinity of the ship, for example, ship motion, the airwake disturbed by the ship's superstructure and the pilot's control inputs. For this reason, each test condition at the potential boundaries of the operational envelope is flown at least two times to allow some comparison. In addition, any comments noted during the flight test are taken into account to ensure the correct data is used for further data analysis.

An important consideration for the data qualification, are the take-off and landing techniques applied by the pilot, as these have a considerable impact on the maximum and minimum values. For example, torque required during the shore-based hover trials is for a steady-state condition to allow the helicopter to maintain level flight. In case the pilot performs a take-off from the ship he or she may utilise much more torque than required for the climb away from the ship, i.e. pull the collective towards the maximum allowed power setting as indicated on the First Limit Indicator (FLI). The FLI is in modern helicopters a common representation of the power margin, and as such a useful tool.

Measurement	Units	Bias *estimated*	Scatter *estimated*	Scatter *determined*	Combined uncertainty
Torque	%	0.1	5.0	5.2	5.2
Engine speed, N_g	%	0.1	0.5	0.5	0.5
Engine temp, T_{46}	°C	0.1	10.0	9.8	9.8
Tail rotor actuator	%	0.1	3.0	3.2	3.2
Pedal	%	0.1	3.0	3.2	3.2
Cyclic longitudinal	%	0.1	2.5	2.5	2.5
Cyclic lateral	%	0.1	2.5	2.0	2.0
Pitch attitude	deg	0.1	1.0	1.0	1.0
Roll attitude	deg	0.1	1.0	1.2	1.2
Nr	%	0.1	0.1	-	0.1
OAT	°C	0.1	0.0	-	0.1
Pressure (QNH)	mbar	0.1	0.0	-	0.1
Rate of Climb	ft/min	10.0	100.0	-	100.5
Weight	kg	20.0	0.0	-	20.0
Height above ground	ft	1.0	3.0	-	3.2
Longitudinal CG	cm	1.0	0.0	-	1.0
Lateral CG	cm	1.0	0.0	-	1.0
Ship pitch	deg	0.1	N/A	-	0.1
Ship roll	deg	0.1	N/A	-	0.1
Relative wind direction at ship	deg	0.1	5.0	-	5.0
Relative wind speed at ship	knots	0.1	3.0	-	3.0
Wind direction in wind tunnel	deg	0.5	5.0	-	5.0
Wind speed in wind tunnel	knots	0.25	3.0	-	3.0

Table 3-1; Statistical data measured parameters

However, the torque utilised may not be representative for that particular test condition. A similar effect is seen for the roll attitude of the helicopter. A pilot may use much more roll attitude during the take-off than during the landing. During the landing the pilot is worried about the visual references with the ship, assessing the ship motion and considering the impact with the flight deck during landing. However, during the departure the pilot only has to manoeuvre the helicopter safely away from the ship. For this reason, there are sound engineering skills required to take the appropriate maximum and minimum values for the data analysis of the sea trials as explained in more detail in Appendix F. Once these values are determined, it is assumed that the scatter is already included, as no mean but only maximum and/or minimum values are considered. These values are used to validate the predictions in the CFE. Note that transient margins are not used in the construction of the operational limitations. This allows these transient margins to be used for safety reasons if operational scenario's dictate.

3.4 Data Analysis, Regression, and Reporting of Results

Once data are acquired during a flight test campaign, it must be decided how the data can most effectively be analysed and presented. Data can be reduced manually or, as is normally the case, processed through a suitable computer program or spreadsheet which may produce results in tabulated or graphical form. As a minimum, a report presenting experimental data should contain the value (single reading or average), the estimated systematic error (i.e. bias), the estimated or calculated precision error (i.e. scatter) and the uncertainty analysis with the level of confidence indicated. The graphical representation of data, including a trend line, is the most efficient method of analyzing and reporting experimental measurements. Graphs are an effective visual aid and can be used to (1) highlight trends in, and relationships between, experimental data, (2) test theories, (3) enable comparisons between various data sets to be made, (4) look for evidence of systematic errors and (5) extract additional parameters which characterise the data set.

Confidence bands

A method is needed to indicate the uncertainty in each data point and also to ensure that any curve fitted to the plotted data is the best estimate of the relationship governing the measured parameters. One accepted method of achieving both of these aims is to add so-called "*confidence bands*" to the data points representing the uncertainty interval. This is because a plot in isolation would not give the reader any idea of experimental errors or whether the discrepancy between a data point and the plotted line is significant. If however the uncertainty ranges for the errors are added to each data point in the form of a vertical and horizontal line extending either side of the data point, the reader can see at a glance that all the differences between the data points and the plotted lines are insignificant, and that the extension is directly proportional with the perceived errors. The confidence bands in the graphs presented in this dissertation represent plus/minus one standard deviation, the 68% confidence limit for the value of the ordinate, and do not reflect the full safety margins.

Regression trend line

At the completion of an experimental program, the relationship among the results might be shown by using a regression trend line. When attempting to fit a trend line to some data points, the errors bars should be taken into account which indicates the uncertainty in the position of the points. A line should then be drawn that encompasses a majority of points and passes as close to all of them as possible, taking into account the errors bars. This "*best*" line is usually a graphical estimate of the "*average*" of the data; by determining how far on either side of this "*best*" line you can draw other acceptable lines. Note that not all points need to lie on the line; a scatter of points around a theoretical curve is to be expected in the real world. Deliberately ignoring a few points without a good reason, just because they spoil a perfect fit to the other points should be avoided at all times. In general, the uncertainty for individual data points is larger than the uncertainty associated with the regression model, as the individual data points are then combined to determine trends in the measurements. This is reasonable, since the regression uncertainty interval at a given point includes information from the N data points used in the regression, while the uncertainty interval for a single data point includes information from that point only. However, all computer-produced curves should be manually verified; the program's idea of a best fit may not be realistic.

Obviously, an additional error may be introduced if the "*wrong*" regression model is used (although this is likely not known to the user), for example, if a third-order regression model is used and the true relationship is first order. This is the classical problem of incorrectly fitting the data, over-fitting, or under-fitting. A potential error introduced by the choice of an inappropriate regression model is not included in the methods discussed. It is assumed that the correct regression trend lines are being used, and the only uncertainties in the regression model are those due to the uncertainties in the original experimental information. The types of regression trend lines applied for each graph are indicated in Chapter 4 and Chapter 5 (e.g. polynomial, linear, etc.) and are considered an adequate representation of the helicopter flight characteristics. However, more sophisticated regression trend lines could be considered for future application of the predictive tool (e.g. sine functions). These trend lines should for example be able to prevent the discrepancy in downward versus upward trends for the same data points at -180˚ and 180˚.

Outliers outside the expected range

All data should be inspected for unexpected points (i.e. outliers) as a continuing quality control check on the measurement process as shown in Figure 3-4. The outliers may be caused by e.g. temporary or intermittent malfunctions of the measurement system, or they may represent actual variations in the measurement. The outliers should be subjected to a comprehensive engineering analysis. This routine is intended to be used in scanning small samples of data from a large number of parameters in various time histories. The work of processing considerable volumes of data can be reduced to a manageable job with this approach. In this dissertation all outliers, if present, have been subjected to such a review process and only included once these are considered representative for the actual helicopter flight characteristics.

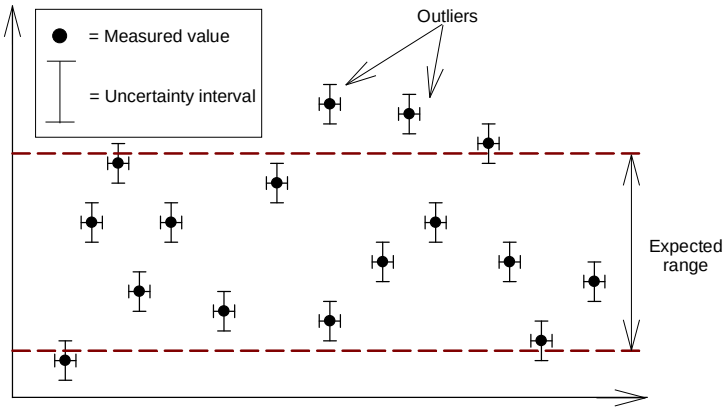

Figure 3-4; Example outliers outside the acceptable range

3.5 Safety Margins and Confidence Level

A safety margin is applied to allow the helicopter to be handled without exceeding any limitations, for example, maximum continuous power limitations whilst influenced by the ship's airwake and/or ship motion during shipboard operations. The magnitude of the safety margins are either based on internationally agreed values (i.e. margins for control positions) or are initially determined by flight test data gathered during the shore-based hover trials (i.e. power margins), as some evaluation experience is required in order to make sound judgements concerning the safety margins that need to be applied for a specific helicopter type. The safety margins are at least one standard deviation (i.e. combined uncertainty of the measurements as summarized in Table 3-1) as shown in Table 3-2. This is required to ensure a minimum 95% confidence level is achieved in the predictions made by the software tool (i.e. one standard deviation in the confidence bands of the measurements, and at least one standard deviation included in the safety margins). If necessary, the safety margins can be further fine-tuned during the sea trials. The limitations for pitch and roll attitude are the combined result of the limitations mentioned in the flight manual for a specific helicopter type (e.g. maximum pitch-up attitude for landing) and qualitative assessments from the flight trials (e.g. loss of visual cues with the landing site). As the limitations for pitch and roll attitude already contain a qualitative assessment, the safety margins are considered incorporated in these values.

The flight test data from the shore-based hover trials and sea trials are compared against the applicable limitations including the associated safety margin unless stated otherwise. The helicopter performance limitations adhered to are maximum continuous values and only important if the top limits are exceeded (i.e. one tailed), with a transient margin available which can temporarily be utilised. The limitations for control position can be exceeded both for the top and bottom limit (i.e. two tailed), and are based on the maximum deflections and as such are larger than for the performance limitations. The limitations for the helicopter attitudes, already including a safety

margin, are initially determined during the shore-based hover trials and verified during the sea trials. The resulting confidence levels for each parameter are listed, indicating the number of combined standard uncertainties included in the confidence band and safety margin together. These confidence levels are representative for the prediction accuracy of the helicopter parameters by the software tool *"SHOL-X"*.

Parameter	Limitation	Combined uncertainty	Safety margin	Confidence level
Torque required	104.0 % [a]	5.2 %	5.2 %	2.0σ = 97.5 % [b]
Engine gas generator rotational speed N_g	Varies with OAT [24]	0.5 %	0.5 %	2.0σ = 97.5 % [b]
Engine power turbine inlet temperature T_{46}	863.0 °C [a]	9.8 °C	9.8 °C	2.0σ = 97.5 % [b]
Tail rotor actuator position	Maximum deflection	3.2 %	± 10.0 % [c]	4.1σ = 99.9 % [d]
Pedal position	Maximum deflection	3.2 %	± 10.0 % [c]	4.1σ = 99.9 % [d]
Longitudinal cyclic position	Maximum deflection	2.5 %	± 10.0 % [c]	5.0σ = 99.9 % [d]
Lateral cyclic position	Maximum deflection	2.0 %	± 10.0 % [c]	6.0σ = 99.9 % [d]
Pitch attitude	10.0° pitch-up [e]	1.0°	Included in limitation	N/A
Roll attitude	± 10.0° [e]	1.2°	Included in limitation	N/A

[a] Maximum Continuous Power (MCP) limitations [25]; additional transient margins are available which could be temporarily used (e.g. 113.0 % for torque required)
[b] One-tailed confidence level (i.e. only top limit is relevant)
[c] International agreed value of 10% control margin
[d] Two-tailed confidence level (i.e. both top and bottom limit are relevant)
[e] Limitations qualitatively determined from flight test with specific helicopter type

Table 3-2; Helicopter limitations, safety margins and confidence levels NH90 NFH

Assessing compliance of measurements

The newly developed *"SHOL-X"* tool verifies whether an output value, including the errors bars, exceeds any of the safety margins. If the safety margins for the parameter are not exceeded (top or bottom limits as applicable) by the calculated result, then compliance with the specification is achieved as shown by example 1 in Figure 3-5. If the calculated result exceeds either the top or bottom limit (i.e. example 2 and 3), or falls close enough to either top or bottom tolerance limit such that the combined standard uncertainty interval overlaps the limit (i.e. example 4 and 5) non-compliance occurs.

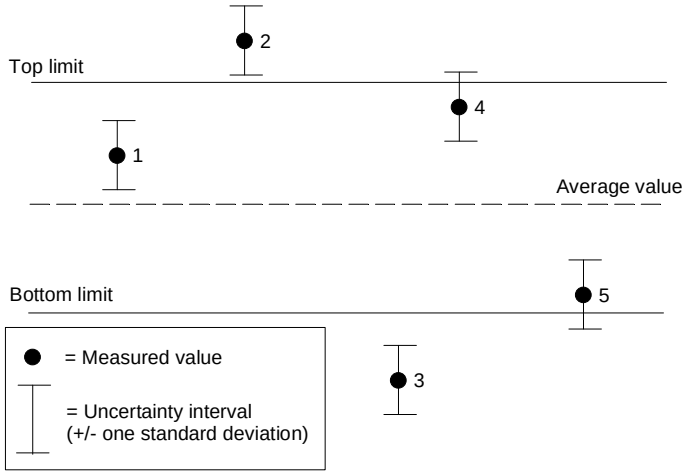

Figure 3-5; Assessing compliance of measurements

3.6 Chapter Review

The novelty for uncertainty analysis in this chapter is the sound and transparent methodology applied for the predictive tool, which enables the user of the model to understand the basics without the necessity to become an expert in the vast field of uncertainty analysis. No measurement, even when carefully made, can be completely free of uncertainties. All measurements of a variable contain inaccuracies. Since the whole structure and application of flight test depends on measurements, it is therefore crucially important to be able to evaluate these uncertainties and to keep errors to a minimum. A framework is given for uncertainty analysis associated with the data gathering during actual flight tests and the output of a simulation model (e.g. the predictive tool to be developed in this dissertation). This includes, amongst others, the terminology and foundation for a methodology bridging the gap between a practical execution of actual flight tests and well-established statistical principles. The mathematics involved in uncertainty analyses which are relevant for helicopter-ship qualification testing is summarized for convenience. In addition, the data analyses performed and assumptions made for the predictive tool are discussed.

Page intentionally left blank

Chapter 4 *Phase I*, Preliminary Investigation of Ship and Helicopter

4.1 Introduction

This chapter discusses the two aspects of the preliminary investigation in *Phase I* of the innovative three-phase approach for determining Ship Helicopter Operational Limitations (SHOLs), namely the ship-environment and the helicopter as shown in Figure 4-1. First, the ship-environment (green box in figure) in which the helicopter will operate is determined by conducting wind tunnel measurements of the airflow in the take-off and landing paths of the ship. This is (still) followed by a validation with full-scale measurements of the airflow above the flight deck of the ship. For the helicopter (yellow box in figure), a ground assessment and shore-based hover trials with a pace-car are carried out to verify precisely the helicopter limitations, including aspects such as e.g. pilot workload in cross-wind conditions, engine performance and control margins resulting in objectively predicted flight capabilities and engine characteristics. Note that some helicopter flight characteristics may have already been determined by the manufacturer during the qualification of the helicopter, however, these are usually not provided to the customer and/or conducted in the desired step-size between test conditions for the prediction of operational limitations on board of a ship.

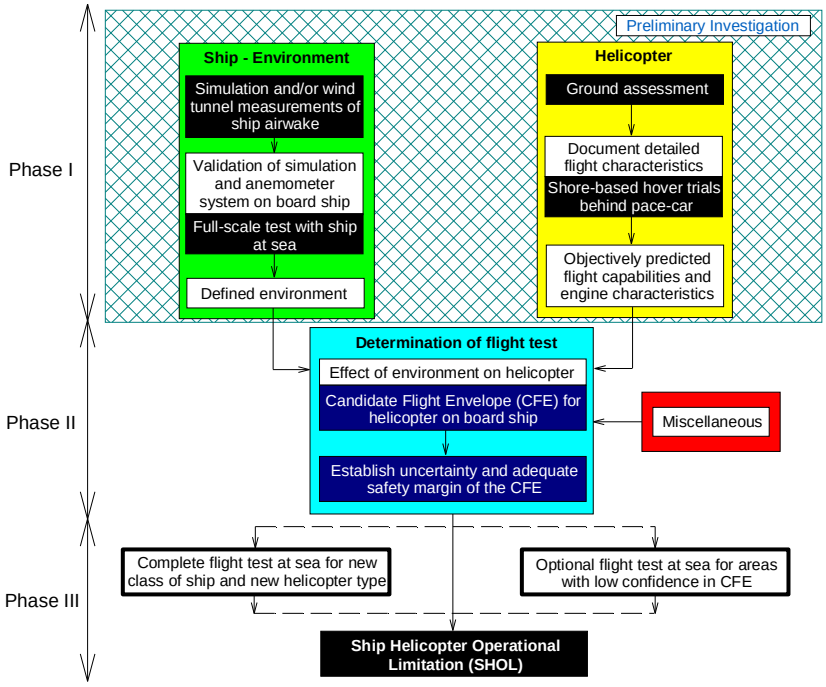

Figure 4-1; Innovative flow chart SHOL development

4.2 Ship-Environment Aspects

The superstructure of a naval ship is cluttered with constructions of different sizes and shapes (e.g. hangar, antennas and exhaust stakes) due to which the state of the wind after passing through these differs from the undisturbed relative wind. The undisturbed relative wind is the vector summation of the actual wind with the course and speed of the ship. However, the airwake encountered by the helicopter near or over the flight deck during take-off and landing may strongly deviate in speed and direction from it, and could be highly complex with both steady (low frequency) and unsteady (high frequency) airflow effects interacting. In addition, high up-flow and down-flow caused by the ship's hull may be encountered. In this section, a novel approach is demonstrated how wind tunnel measurements are used for an objective assessment of the ship-environment prior to conducting sea trials.

The wind tunnel measurements were not performed as part of the data gathering campaign required for this dissertation. It is intended to give the reader the required background information to understand the process required for the data analysis. The data sets used were readily available within the Netherlands Ministry of Defence (NLMoD), of which the author had access, due to previous contract requirements [1,2,3,4,5,6]. In this dissertation all figures related to ship airwake are from measurements as performed by the National Aerospace Laboratory (NLR); however the author performed his own data analysis to present the corresponding figures. The figures as presented are the output from the predictive tool "*SHOL-X*". Note that the effects of ship motion on pilot workload for take-off and landing are determined as part of the flying routine during sea trials, and for that reason are discussed in Chapter 6.

4.2.1 Distinctive Wind Conditions

The helicopter flight characteristics determined by shore-based hover trials are based on the relative wind conditions encountered by either hovering in natural wind conditions or by using a pace-car. However, near and above the flight deck the relative wind is disturbed by the large ship's superstructure. This disturbed wind is what the helicopter encounters when operating from the ship and is known as local wind. The local wind conditions are determined by wind tunnel measurements at different locations and heights above the flight deck and in the approach and departure paths of the helicopter. Unfortunately, the undisturbed relative wind and local wind conditions are unknown for the operational crew after the test campaign, as the indicated wind by the ship anemometers is their only reference source. The latter is unreliable since by mounting anemometers on a ship with a bluff body, the local air flow at the anemometer location also deviates from the undisturbed relative wind conditions. For this reason, the undisturbed relative wind should be known to the test team, and applicable corrections made to the indicated wind speed on board the ship in order to construct a usable Candidate Flight Envelope (CFE). Therefore, in this dissertation a distinction has been made between the following three different wind conditions:

1. *Relative wind.* The shore-based hover trials are performed in undisturbed relative wind, and this is the free air stream near the ship.

2. *Indicated wind.* The relative wind with the anemometer indication errors taken into account. The operational envelopes are based on this wind condition.
3. *Local wind.* The local wind conditions are different for each position near and above the flight deck. These are the wind conditions the helicopter will encounter during ship board operations.

4.2.2 Ship Airwake Test Methodology

Wind tunnel tests on ship models are carried out to determine the airflow characteristics (i.e. airflow deviations with respect to the undisturbed oncoming relative wind) above the flight deck and in the possible approach and departure paths of the helicopter to the ship as function of the relative wind. In addition, the position error of the ship's anemometers are determined which is needed to establish the relationship between the undisturbed relative wind conditions. The wind tunnel measurements were performed, on scale models of the ships in service within the entire Dutch fleet, in the German Dutch Wind Tunnels Large Low-speed Facility (DNW-LLF) as shown for example for the Ocean Patrol Vessel (OPV) in Figure 4-2. The size of the scale models was dependent on the actual size of the ships in relation to the available dimensions of the wind tunnel, and varied between 1:70 and 1:100. The wind tunnel was equipped with an interchangeable aeronautical test section and a fixed non-aeronautical test section. The interchangeable test section was 3.0 meters wide and 2.25 meters high and had a length of 5.75 meters. Downstream of this interchangeable aeronautical test section was the fixed non-aeronautical test section with a length of 3.0 meters. The latter test section was equipped with a turntable, which was flushed into the floor.

Figure 4-2; Ocean Patrol Vessel wind tunnel model [6]

A wind tunnel speed of 30 m/s was applied for all pressure tests with a 5-hole probe in continuous testing mode. A practical wind tunnel speed of 30 m/s was chosen to suit the test optimally, as the flow is considered Reynolds number (Re) independent [7,8,9]. The continuous testing mode means that the scale model rotated continuously at a rotational rate of the turntable of approximately 0.3 °/s and did not stop in order to take data points. The probe pressures were registered roughly every degree in azimuth. The pressures of the 5-hole probe were measured with differential pressure transducers.

The five pressures of the probe were combined to obtain the local flow velocity vector. The local airflow properties were measured at the two anemometer positions, above the helicopter flight deck, in the helicopter approach and departure paths and at a reference position on top of the jack staff on the bow of the ship. The tip of the probe was always positioned above the centre of rotation of the turntable and the probe was always aligned with the tunnel axis. The vertical position of the probe was set according to the height of the applicable measurement location.

Data processing

The relative wind speed V_{rel} and the relative horizontal wind direction β_{rel} are the resultant of the ship's course and speed with the actual wind. The local wind properties as measured at different location in the take-off and landing paths are defined as: the local wind speed V_{loc}, the local horizontal wind direction β_{loc} and the local vertical flow direction φ_{loc}. The horizontal flow deviation from the local wind compared to the relative wind is defined as χ_{loc}. The local wind speed V_{loc} is expressed as a fraction of the relative wind speed V_{rel} by defining the local wind speed coefficient $C_{v(loc)}$:

$$C_{v(loc)} = V_{loc} / V_{rel} \qquad \textbf{(Eq. 4-1)}$$

The local horizontal wind direction β_{loc} is calculated as the sum of the relative horizontal wind direction β_{rel} and the horizontal flow deviation χ_{loc}:

$$\beta_{loc} = \beta_{rel} + \chi_{loc} \qquad \textbf{(Eq. 4-2)}$$

The wind speed at the anemometer location V_{an} is expressed as a fraction of the relative wind speed V_{rel} by defining the wind speed coefficient at the anemometer location $C_{v(an)}$:

$$C_{v(an)} = V_{an} / V_{rel} \qquad \textbf{(Eq. 4-3)}$$

The horizontal wind direction at the anemometer location β_{an} is calculated as the sum of the relative horizontal wind direction β_{rel} and the horizontal flow deviation at the anemometer location χ_{an}:

$$\beta_{an} = \beta_{rel} + \chi_{an} \qquad \textbf{(Eq. 4-4)}$$

For practical purposes, it is convenient to correlate the local airflow properties with the data measured at the ship's anemometer locations. The local wind speed V_{loc} is expressed as a fraction of the wind speed at the anemometer location V_{an} by defining the wind speed coefficient C_v:

$$C_v = V_{loc} / V_{an} \qquad \textbf{(Eq. 4-5)}$$

The horizontal flow deviation χ follows from the subtraction of the horizontal wind direction at the anemometer location β_{an} from the local horizontal wind direction β_{loc}:

$$\chi = \beta_{loc} - \beta_{an} \qquad \textbf{(Eq. 4-6)}$$

Note that these properties need to be calculated twice: once for the port and once for the starboard anemometer. The addition '*P*' or '*S*' defines correlation with the port or starboard anemometer system respectively, i.e. C_v-*P* for the port anemometer. The vertical flow direction φ follows from the subtraction of the vertical flow direction at the anemometer location of the ship φ_{an} from the local vertical flow direction φ_{loc}:

$$\varphi = \varphi_{loc} - \varphi_{an} \qquad \textbf{(Eq. 4-7)}$$

Calculation of the vertical flow direction with respect to the relevant anemometers is not relevant, as the anemometer systems applied on board of the ships do not account for vertical air flow angles. The local horizontal and vertical speed (i.e. up-flow and down-flow) are presented as a component of the local wind speed coefficient $C_{v(loc)}$. The local speed components are divided into the local horizontal wind speed coefficient $C_{v(hor)}$ and the local vertical wind speed coefficient $C_{v(ver)}$ as follows:

$$C_{v(hor)} = C_{v(loc)} \cos\varphi_{loc} \qquad \text{(horizontal component)} \qquad \textbf{(Eq. 4-8)}$$

$$C_{v(ver)} = C_{v(loc)} \sin\varphi_{loc} \qquad \text{(vertical component)} \qquad \textbf{(Eq. 4-9)}$$

Examples of local wind properties above the landing spot

Once the data reduction is performed, the data is presented in graphical format. In these graphs the port anemometer is used for red wind conditions and the starboard anemometer is used for green wind conditions. This red and green terminology is used throughout this dissertation to refer to winds coming from either the port or starboard side of the ship, respectively. Some examples are shown for wind speed coefficient C_v and horizontal flow deviation χ at different heights above the landing spot as a function of the indicated wind direction in Figure 4-3 and Figure 4-4, respectively.

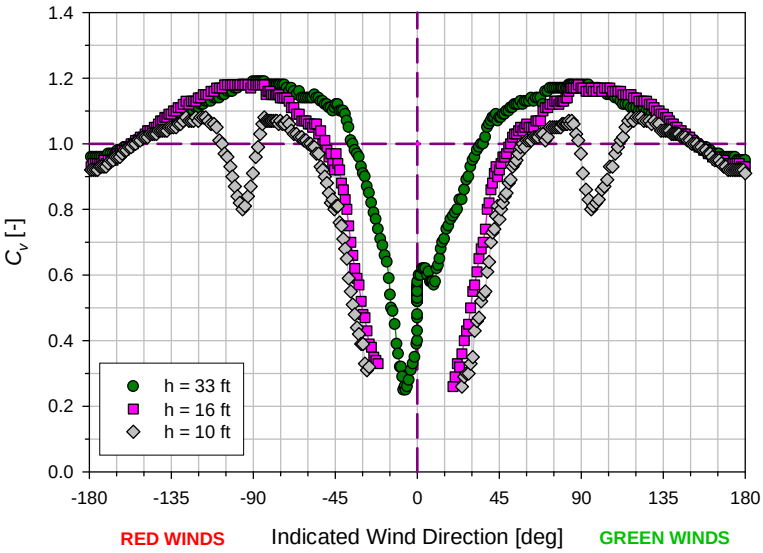

Figure 4-3; Example wind speed coefficient C_v

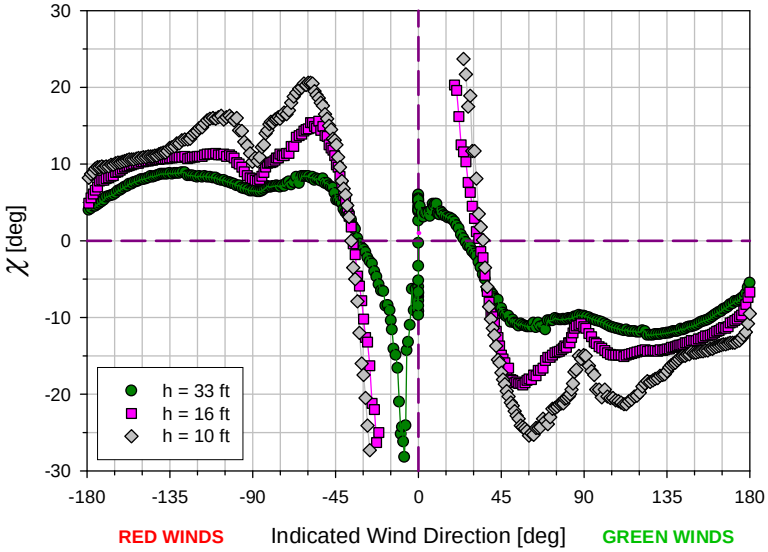

Figure 4-4; Example horizontal flow deviation χ

In case $C_v < 1$, the indicated wind speed is higher than the local wind speed which the helicopter encounters when operating from the flight deck, and vice versa. The helicopter encounters the local airspeed and wind direction, and thus the flight characteristics in the CFE should be based on the local wind conditions instead of on the indicated wind conditions by the anemometers. The decrease in local wind speed between red 45° and green 45° is caused by the air bubble generated by the hangar in front of the landing spot. There was no reliable data measured in the wind tunnel for winds in the sector between red 30° and green 15° at 16 ft (purple line in figures) and 10 ft (grey line in figures) and thus not presented. In general, a symmetrical airflow pattern is observed. However, the position of an electronic warfare jammer on the starboard side of the ship caused anti-symmetrical airflow at 33 ft above the flight deck (green line in figures). In this case, the electronic warfare jammer has a positive effect on the airflow for winds in the sector between dead-ahead and green 15°, i.e. higher wind speeds and smaller deviations in flow direction.

Both for green and red wind conditions, the local winds have a larger angle when seen from the bow of the ship as indicated by the anemometers (i.e. the wind moves inboard behind the hangar). Once the relative wind is more from abeam and aft, other factors might influence the local wind direction. In the sector between 30° and 150° (both for red and green winds) an over-speed (up to 20 %) occurs. This over-speed is caused by the flow being deflected over the ship's hull; above the hull the streamlines will be compressed, leading to higher wind speeds. For a height of 16 ft the flow for head and stem winds is more or less identical to the flow pattern at 33 ft. For a height of 10 ft, the airflow in the sector 80° to 110° (both for red and green winds) is strongly influenced by vortices generated by the ship's hull. There is a sharp gradient between red 45° and red 15° and between green 15° and green 45° with possibly unpredictable wind speed and wind direction in case the helicopter flies within either of these regions.

Areas with vertical flow deviations φ from the horizontal plane are shown at different heights above the landing spot as a function of indicated wind direction in Figure 4-5. The disturbances in air flow are more or less identical to the effects described for wind speed coefficient C_v and horizontal flow deviation χ. For a height of 10 ft, the airflow in the sector 80° to 150° (both for red and green winds) is strongly influenced by vortices generated by the ship's hull. The areas with a large negative angle (i.e. downward airflow velocities) in combination with high wind speeds may create problems in performance requirements. Note that although not shown, the limitations due to downward airflow velocities are most pronounced on the leeward side of the ship, for example port side with green wind conditions, as the wind drops down on the leeward side after being disturbed by the ship's superstructure. Up to 400 ft/min to 600 ft/min downdrafts can be expected at high wind speeds [2]. In most cases these downward airflow velocities are the cause of the SHOL boundaries for fore-aft take-offs and landings towards the leeward side of the ship.

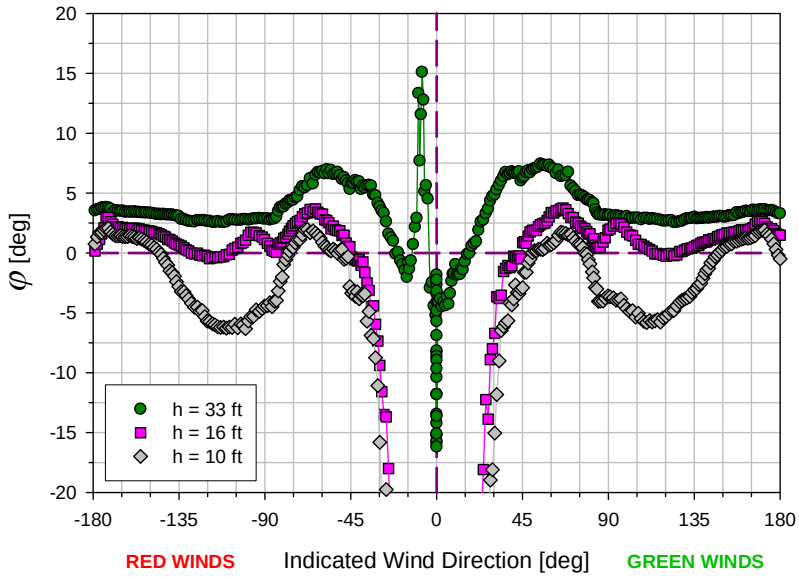

Figure 4-5; Example vertical flow direction φ

Examples of wind properties at the anemometer locations

The SHOLs are based on the indicated wind conditions as presented by the anemometers on board each ship type. The anemometer systems are usually positioned somewhere in the mast of the ship or on top of the roof of the navigation bridge, preferably as much as possible outside the disturbances in the airwake caused by the ship's superstructure. Therefore far away from the flight deck, this is also not ideal. In order to correlate the helicopter flight characteristics with a particular ship type, it is essential to understand the disturbances in airflow at each anemometer location in relation to the undisturbed relative wind. The ship's anemometers can be subjected to various influences, which in turn will lead to erroneous reading and interpretation when not properly handled. These influences are categorized as follows:

1. *Position errors.* By mounting a system on a bluff body, the local air flow (speed and direction) at the system's location will deviate from the free air stream. These deviations can generally be measured beforehand in for example a wind-tunnel.
2. *Installation error.* This error is caused by the misalignment of the system with respect to the centre line of the ship.
3. *System errors.* These are the calibration and system deviations. These deviations can be provided by the manufacturer, or can be determined on for example a test bench.

Some examples of the disturbances at the anemometer location for the Auxiliary Oiler Replenishment (AOR) ship, Air defence and Command Frigate (LCF), Landing Platform Dock (LPD No.1), Landing Platform Dock (LPD No.2), M-Frigate (MFRI), and the Ocean Patrol Vessel (OPV) are shown for wind speed coefficient at the port anemometer location $C_{v(an)}$-*P* and the horizontal flow deviation at the port anemometer location χ_{an}-*P* as a function of the relative wind direction in Figure 4-6 and Figure 4-7, respectively. The differences between these ship types in wind speed coefficient at the anemometer location $C_{v(an)}$ for red wind conditions are up to approximately 0.3, hence for 30 knots already a difference exists of up to 9 knots between the actual and indicated wind speed. The differences in horizontal flow deviation at the anemometer location χ_{an} are up to approximately 30º in azimuth in the sector red 45° to red 30° between the OPV (blue line in figures) and the LCF (purple line in figures). If for whatever reason, the port anemometer is selected for green wind conditions, the "*invalid sector*" is presented and the readings would be unreliable. The same effects, although in opposite direction, are noted for wind speed coefficient at the starboard anemometer location $C_{v(an)}$-*S* and the horizontal flow deviation at the starboard anemometer location χ_{an}-*S* as shown as a function of the relative wind direction in Figure 4-8 and Figure 4-9, respectively. In case, these relations between undisturbed relative wind and indicated wind are unknown to the test crew, it is questionable whether efficient sea trials can be conducted and/or read-across performed between operational limitations for different ships types.

In operational scenario's, the port anemometer is selected for red winds and the starboard anemometer is selected for green winds to ensure that the windward anemometer is used during flight operations. In case an anemometer system would be out of service, it is advised to provide either red or green winds for flight operations to ensure that the windward anemometer system could be used, or to use the emergency SHOL envelope. The emergency SHOL envelope should contain sufficient margins to allow shipboard operations with the downwind anemometer system selected. Note that as the disturbances at the anemometer locations are already known for each ship type, a Wind Correction Algorithm (WCA) is applied on most new ships within the Royal Netherlands Navy. The WCA calculates the relative wind from the anemometer readings, which are subject to local disturbances at the anemometer locations, and in addition applies dampening to these relative wind data streams. As a result, undisturbed relative wind is presented onboard these ships and less variation is present in the indicated wind information.

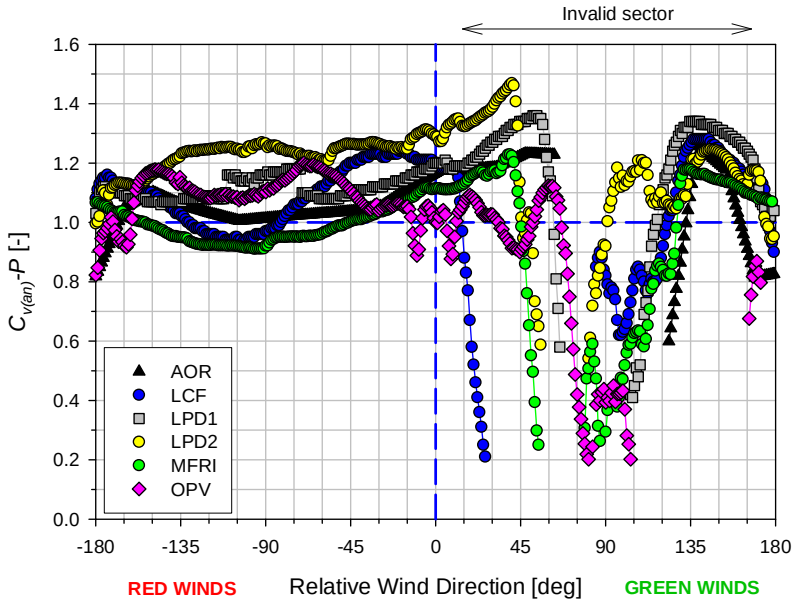

Figure 4-6; Example port anemometer locations $C_{v(an)}$-*P*

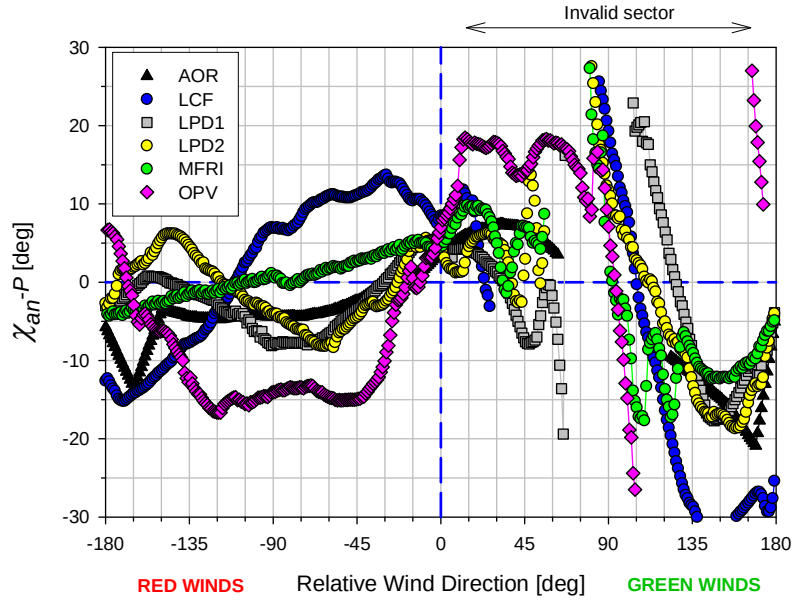

Figure 4-7; Example port anemometer locations χ_{an}-*P*

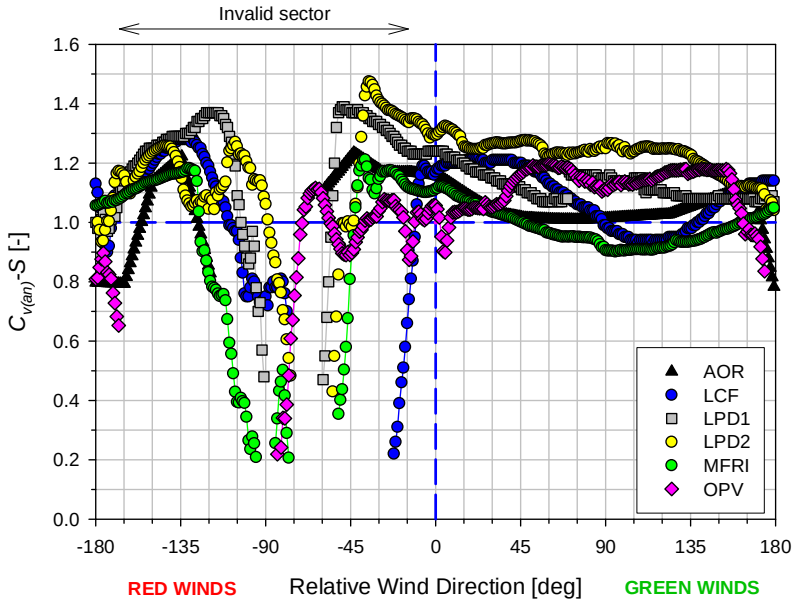

Figure 4-8; Example starboard anemometer locations $C_{v(an)}$-S

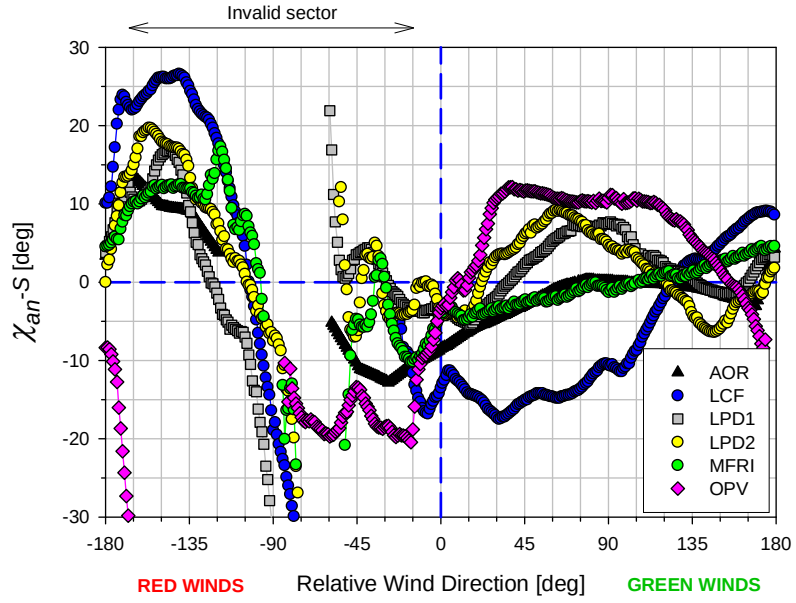

Figure 4-9; Example starboard anemometer locations χ_{an}-S

4.2.3 Lessons Learned for the Ship-Environment

The following lessons learned for the ship environment related to shipboard operations are observed:

1. A distinction should be made between relative, indicated and local wind conditions;
2. The relation between undisturbed relative wind and indicated wind should be known for each ship type, as there are large variations;
3. The port anemometer should be selected for red winds and the starboard anemometer selected for green winds, to ensure that the windward anemometer is used during flight operations;
4. An atmospheric boundary layer coefficient should be determined to correlate wind tunnel measurements with full-scale airwake data from the ship (to be discussed in Chapter 5);
5. The effects of ship motion on pilot workload for take-off and landing should be determined as part of the flying routine during the sea trials (to be discussed in Chapter 6).

4.3 Helicopter Aspects

The ground assessment and shore-based hover trials are carried out to verify precisely the helicopter limitations, including aspects such as pilot workload in cross-wind conditions, engine performance and control margins. There is a distinction made between "*rejection criteria"* for each helicopter type, and their "*dependencies*" in the ship environment as previously defined by the author [10]:

- *Rejection criteria* are quantitative and qualitative helicopter parameters which, once exceeded, prevent safe execution of a flight phase;
- *Dependencies* are variables in a flight phase which directly influence their related rejection criteria.

The subdivision is made to be less dependent on the dedicated sea trials. More specifically, the subdivision of test data in rejection criteria and dependencies enables (1) assessing other possible conditions for in-service operations and (2) accurate exclusion of test points. Rejection criteria, and how they are influenced by dependencies, are determined for every new type of helicopter or are a consequence of significant changes to an old aircraft, which might affect low-speed performance and/or pilot workload. Since the steady-state helicopter flight characteristics are valid for trimmed conditions without any difference between land- or sea-based operations [11], the measured helicopter data from the shore-based hover trials can be saved into lookup tables and used for future helicopter-ship qualification trials. There is a distinction made between subjective, performance, control position, and aircraft attitude related issues. An overview of the rejection criteria and their dependencies is summarized in Table 4-1. Note that these rejection criteria and their dependencies are considered applicable for most current helicopters with a single main rotor configuration and a separate tail rotor; although for each helicopter type other specific characteristics might have to be taken into account.

Item	Rejection criteria	Dependencies
	Subjective rejection criteria	
1	Pilot workload	Relative wind (airwake), Referred weight, Visual cues, Ship motion, Flying qualities
2	Vibration levels	Relative wind (airwake), Referred weight
3	Turbulence levels	Relative wind (airwake), Ship motion, Atmospheric conditions
	Performance rejection criteria	
4	Torque required	Relative wind (airwake), Referred weight, Visual cues, Ship motion, Atmospheric conditions, Helicopter configuration, Main rotor rotational velocity Ω
5	Engine gas generator rotational speed N_g	Relative wind (airwake), Referred weight, Torque required, Atmospheric conditions
6	Engine power turbine inlet temperature T_{46}	Relative wind (airwake), Referred weight, Torque required, Atmospheric conditions
7	Climb performance	Relative wind (airwake), Referred weight, Torque required, Atmospheric conditions, Helicopter configuration, Power available
	Control position rejection criteria	
8	Tail rotor actuator position	Relative wind (airwake), Referred weight, Torque required
9	Pedal position	Relative wind (airwake), Control envelope
10	Longitudinal Cyclic	Relative wind (airwake), Control envelope, Centre of Gravity (CG) location
11	Lateral Cyclic	Relative wind (airwake), Control envelope, Centre of Gravity (CG) location
	Aircraft attitude rejection criteria	
12	Pitch attitude	Relative wind (airwake), Centre of Gravity (CG) location
13	Roll attitude	Relative wind (airwake), Centre of Gravity (CG) location

Table 4-1; Overview rejection criteria and dependencies

4.3.1 Ground Assessment

There are numerous items to consider when operating a specific helicopter type from a ship, and the limitations for each helicopter-ship combination may vary accordingly. Some of the helicopter limitations are already identified by industry and usually documented in the flight manual. In any case, the helicopter's capabilities for embarked operations from a ship at sea should be verified. During the ground assessment it is required to identify the relevant limitations and organize these such that the operational capabilities of the specific helicopter are identified and/or the items which need to be tested during actual flight tests are determined. The ground assessment starts with collecting all the relevant information from the helicopter under test, for example, flight performance data, previous experience with the helicopter on board ships, and documenting whether the helicopter is fitted with for example a rotor brake, floatation gear and/or deck-lock system. There are no "*a priori*" items that prevent a helicopter to operate from ships. The operational capabilities are a consideration of the amount of risk the operator is willing to take for shipboard operations, and a reflection of the experience level of the pilots. A more detailed description of the items to consider during the ground assessment to determine the initial test considerations is contained in Appendix E.

4.3.2 Shore-Based Hover Trials

The purpose of the shore-based hover trials is to determine the helicopter flight characteristics, for example, pilot workload, engine performance, Trimmed Flight Control Positions (TFCP), controllability limits and helicopter attitudes in an omni-directional relative wind envelope. This is done in order to complement the flight manual information, which only provides torque required for dead-ahead conditions. These tests are executed within the limitations for land-based operations as given by the helicopter manufacturer. The flight test data obtained from the shore-based hover trials indicates - within the low speed hover envelope - which regions exist where safety margins between available and required helicopter rejection criteria are marginal or even exceeded. This is required for safety reasons, as in these regions, limitations are likely to be exceeded by the operational aircrew during shipboard operations. The shore-based hover trials for the NH90 NFH of the NLMoD were conducted at two different test locations at 10 000 kg, 11 000 kg and 11 750 kg referred weight, the latter simulated by 11 000 kg maximum take-off weight at an Outside Air Temperature (OAT), equivalent to 34.6 ºC at sea level [12,13]. The flight tests were performed at the required values of referred weights, $W/\sigma\omega^2$, where W is helicopter weight, σ is relative density (relative to international standard atmosphere), and ω is the relative rotorspeed (relative to a standard rotor speed value). The targeted referred weights are set as the operational weight bands for shipboard operations.

A dedicated pace-car, as shown in Figure 4-10, is used to set up the required relative wind conditions in addition to the actual wind conditions encountered. Note that a pace-car or alternative low-speed measuring device is required as the airspeed indications of a helicopter are generally only reliable above 40 knots with winds on the nose of the helicopter. The pace-car is equipped with a calibrated speed measurement system, a display on top of the dashboard to present the relative wind to the driver, and

a wind vane to provide the pilot with a visual reference of the relative wind direction. A more detailed description of the pace-car and test instrumentation is contained in Appendix F.

Figure 4-10; Pace-car used for shore-based hover trials

4.3.3 Subjective Rejection Criteria

For subjective ratings, three scales are used as presented in Appendix C: the Deck Interface Pilot Effort Scale (DIPES) is used to describe pilot workload, the Vibration Assessment Rating (VAR) scale is used to describe vibration levels and the turbulence rating scale is used to indicate the intensity of the turbulence encountered and its associated helicopter reactions [14]. However, these subjective ratings should be used with care, as there are different visual cues between a formation with a vehicle travelling over the runway and a formation with a ship at sea. In addition, natural winds are always accompanied by some degree of turbulence which is not fully replicated by the pace-car tests. Note that the DIPES scale is used during the shore-based hover trials, although it is originally developed for the helicopter-ship interface. The main reason to use the DIPES scale as well for the shore-based hover trials is to ensure that the same rating scale for pilot workload is used throughout. This avoids potential error introduced by converting pilot workload from one scale to another. Further research should aim for development of a suitable rating scale applicable to both the shore-based hover trials and the sea trials, allowing a direct comparison for these dynamic multiple axis task without specific task tolerances being required.

4.3.3.1 Pilot Workload

In general, the pilot workload is low for the NH90 NFH, with two exceptions as shown in Figure 4-11. One exception is for red 90° relative wind conditions for higher winds speeds, where the high roll attitude is considered uncomfortable by the pilot increasing the workload up to DIPES 3 (i.e. highest tolerable pilot compensation required). For some reason, the other exception is for green wind conditions at a somewhat lower wind speed, which corresponds with a test condition with high scatter in pedal deflection. There are no restrictions in the CFE due to pilot workload. Note that the relatively low pilot workload ratings are typical for the NH90 NFH with good handling qualities throughout. For other helicopter types there may be more pronounced areas with higher workload ratings which in that case should be further investigated.

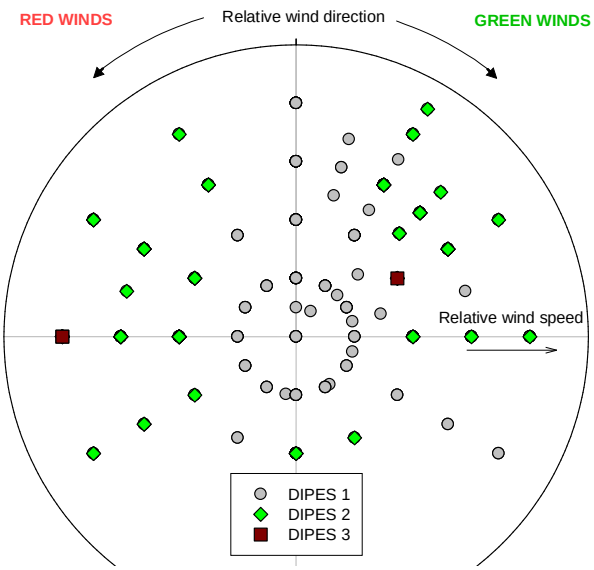

Figure 4-11; Overview DIPES ratings for shore-based hover trials

4.3.3.2 Vibration Levels

The vibration levels can be uncomfortable and fatiguing for the aircrew and may also affect the reliability and operation of e.g. onboard systems such as vision aids. The results for vibration levels are shown in Figure 4-12. The vibration level increased up to a VAR moderate level 5 (i.e. experienced aircrew are aware of the vibration but it does not affect their work, at least over as short period). There are no restrictions in the CFE due to vibration.

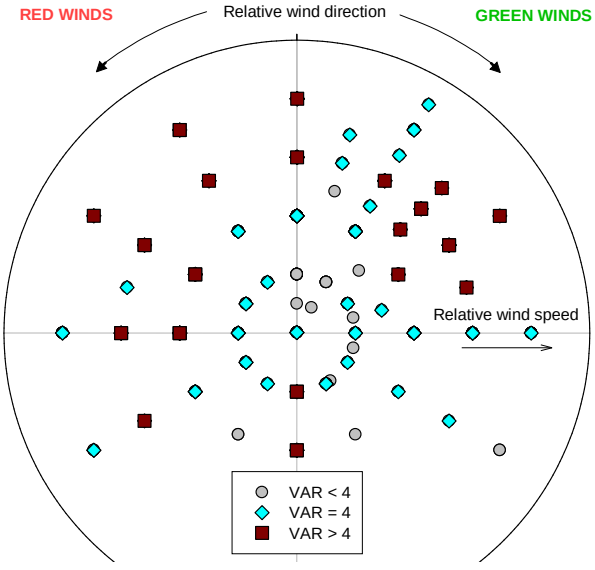

Figure 4-12; Overview vibration levels for shore-based hover trials

4.3.4 Objective Rejection Criteria

The pilot opinion on how close a test point is to the potential boundaries of the envelope is usually as varied as the number of pilots, because each one may look for different cues and concentrate on different aspects. In helicopter-ship qualification testing, there are usually only one or two pilots involved in defining the flight envelope. Based on the pilot differences, it is possible that different operational envelopes might be produced. This has already been demonstrated in the past, and it proves that different SHOLs could be released for operational use [15]. The obvious trade-off is expressed in terms of authenticity versus economy. Three pilots seems to be the bare minimum with four or five likely to lead to a more reliable result and six being optimal for establishing confidence in the average pilot workload ratings. Alternatively, using objective rejection criteria in conjunction with subjective rejection criteria from usually the two pilots in the cockpit provides a robust means for defining flight envelope restrictions without increasing the time required for the test campaign. The objective test data thereby shows whether subjective ratings were made with consistency. The confidence bands, regression trend lines, safety margins, and associated confidence levels of the rejection criteria as used for the construction of the figures in this section is discussed in Chapter 3.

4.3.4.1 Performance related rejection criteria (power required)

Helicopter performance is measured in terms of power required to maintain steady flight for various atmospheric conditions, over a range of weight and, if necessary, external configurations. The main objective is to determine the parameter that will limit the helicopter performance under the atmospheric conditions in a role specification. Note that under certain atmospheric conditions, usually hot and high, the engines, rather than the transmission will limit helicopter performance. Therefore, it is necessary to determine the limiting factor(s) for the conditions specified, for example, in order to compare test conditions flown during different missions of the test campaign with each other.

Torque required

The flight test results for torque required at 20 knots, as a function of the relative wind direction are shown in Figure 4-13. The torque required increases for higher referred weights, and depends on the relative wind direction. The increase in torque required between 11 000 kg and 11 750 kg referred weight, is caused by variations in OAT and air pressure, as the maximum take-off weight of the helicopter is limited to 11 000 kg. It shows that the effect for increased take-off weight of the helicopter has a larger effect on torque required, than increasing the OAT whilst maintaining the same take-off weight. As the main rotor turns counter-clockwise, when seen from above, more tail rotor thrust and thus torque required, is necessary to prevent the nose to turn into the wind in the sector between dead-ahead and green 90°. The tendency for the nose of the helicopter to turn into the wind is known as the ‘weather-cock effect’. For this reason the torque required is highest at relative winds from the direction green 60° to green 120°. An opposite effect occurs for red wind conditions in the sector between red 90° and dead-ahead, with a slightly less or equal demand for tail rotor thrust and thus torque required. Once past the abeam position for either red or green wind

conditions, the same effects occur although in opposite direction as the nose of the helicopter wants to turn now in the other direction. The areas that exceed the applicable safety margin for All Engine Operatives (AEO) continuous power are to be excluded from the CFE, which in this case is the sector between green 30° and green 150° for 11 000 kg and 11 750 kg referred weight. Although not shown, for the lower relative wind speeds at 11 000 kg and 11 750 kg referred weight, the torque required exceeds the safety margin and/or the maximum continuous power limitation of 104% torque. Therefore, these low speed relative wind conditions are removed from the respective CFE's.

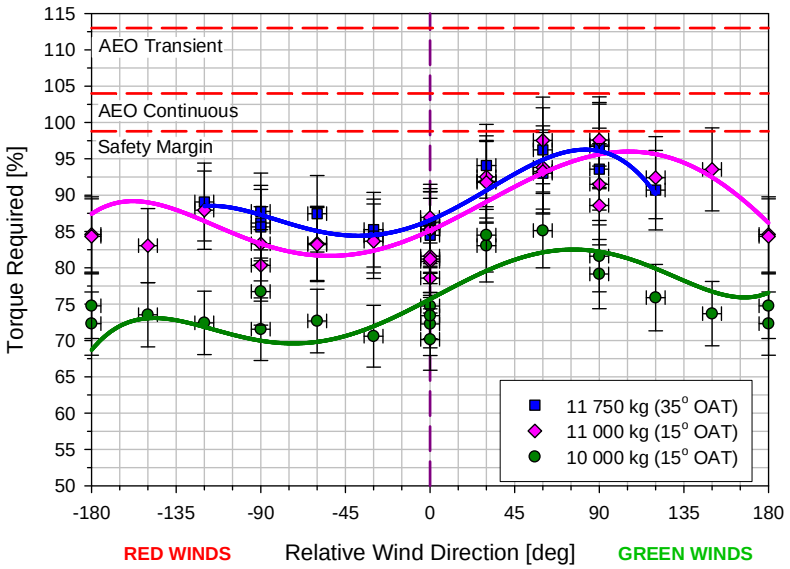

Figure 4-13; Torque required at 20 knots
(*regression trend line is* $y = a + bx + cx^2 + dx^3 + ex^4 + fx^5$)

Engine gas generator rotational speed N_g

The flight test results for engine gas generator rotational speed N_g at 20 knots, as a function of the relative wind direction are shown in Figure 4-14. The engine gas generator rotational speed increases for higher referred weight, and depends on the relative wind direction. The increase in engine gas generator rotational speed N_g between 11 000 kg and 11 750 kg referred weight, is caused by variations in OAT and air pressure, as the maximum take-off weight of the helicopter is limited to 11 000 kg. It shows that the effect for a higher OAT has a comparable effect on engine gas generator rotational speed N_g, as increasing the take-off weight of the helicopter whilst maintaining the same OAT. In general, the same variations in engine gas generator rotational speed N_g with relative wind direction are noticed as for torque required. For this reason, the engine gas generator rotational speed N_g is highest at relative winds from the direction green 60° to green 120°. The areas that exceed the applicable safety margin for AEO continuous power are to be excluded from the CFE, which in this case is between green 90° to green 120°. Note that the presented limitations change with

varying atmospheric conditions [16]. There are no additional restrictions in the CFE's due to engine gas generator rotational speed N_g (i.e. torque required is more restrictive in this case).

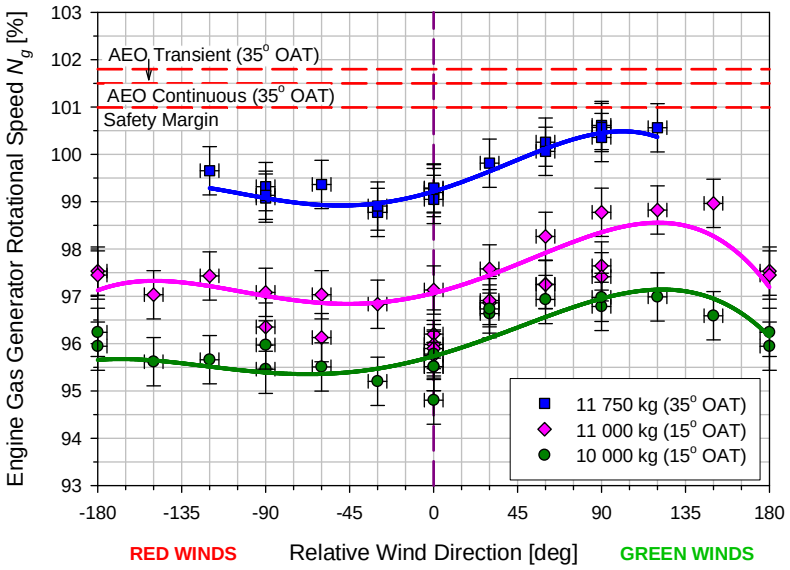

Figure 4-14; Engine gas generator rotational speed N_g at 20 knots
(*regression trend line is* $y = a + bx + cx^2 + dx^3 + ex^4$)

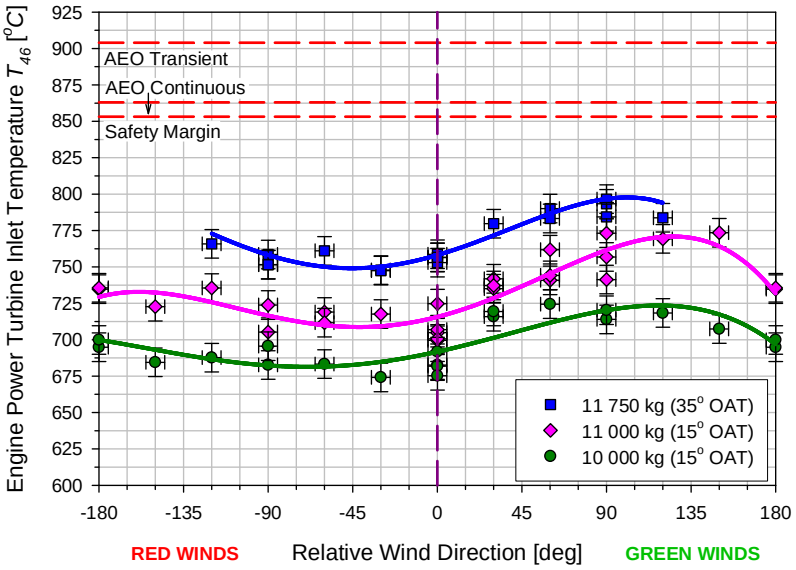

Figure 4-15; Engine power turbine inlet temperature T_{46} at 20 knots
(*regression trend line is* $y = a + bx + cx^2 + dx^3 + ex^4$)

Engine power turbine inlet temperature T_{46}

The flight test results for engine power turbine inlet temperature T_{46} at 20 knots, as a function of the relative wind direction are shown in Figure 4-15. The engine power turbine inlet temperature increases for higher referred weight, and depends on the relative wind direction. The increase in engine power turbine inlet temperature T_{46} between 11 000 kg and 11 750 kg referred weight, is caused by variations in OAT and air pressure, as the maximum take-off weight of the helicopter is limited to 11 000 kg. It shows that the effect for a higher OAT has a comparable effect on power turbine inlet temperature T_{46}, as increasing the take-off weight of the helicopter whilst maintaining the same OAT. In general, the same variations in engine power turbine inlet temperature T_{46} with relative wind direction are noticed as for torque required. For this reason, the engine power turbine inlet temperature T_{46} is highest at relative winds from the direction green 60° to green 120°. The areas that exceed the applicable safety margin for AEO continuous power are to be excluded from the CFE, which in this case is not applicable. There are no restrictions in the CFE's due to engine power turbine inlet temperature T_{46}.

4.3.4.2 Performance related rejection criteria (climb performance)

There is little need to emphasize the importance of knowing the climb performance of a helicopter. Information about power required and power available is needed to determine the helicopter's suitability for a given role, to check performance against requirements, and to provide data for inclusion in a substantiated database from which the CFE's are derived. Estimating climb performance from level flight data is not straightforward in practice. The difficulty lies in determining the percentage of excess power that is available as climb power. For an accurate estimate it is necessary to determine the precise amount of power wasted through transmission losses and in generating the extra anti-torque force needed as a consequence of the greater collective pitch applied to the main rotor blades. The simplest approach of assuming that all the excess power available is taken up as climb power will typically lead to an overestimate of the actual rate of climb.

The helicopter's maximum achievable climb performance is assessed, using a technique known as Maximum Power Vertical (MPV), at different true airspeeds of which the test techniques are explained in more detail in Appendix E. The achieved Rate Of Climb (ROC) is shown as a function of the true airspeed in Figure 4-16. For each test point the achieved ROC, *C*, is expressed against the deltas (i.e. the differences) in torque required, between the torque required in hover Q_{req} and the maximum torque utilised Q_{uti} in the climb as shown in Figure 4-17. The result is called the maximum power vertical climb coefficient C_{MPV}:

$$C_{MPV} = \frac{C}{(Q_{uti} - Q_{req})} \qquad \textbf{(Eq. 4-10)}$$

The maximum achievable ROC increased with true airspeed, and decreased with an increase in referred weight. The increase in maximum achievable ROC with true airspeed corresponds with the initial decrease in power required with true airspeed,

which is typical for helicopters (i.e. increased power margin between torque required and torque available). The decrease in achieved ROC between 11 000 kg and 11 750 kg referred weight is smaller than between 10 000 kg and 11 000 kg referred weight, which corresponds to the larger increase in power required for the latter, and thus reduction in the power margin.

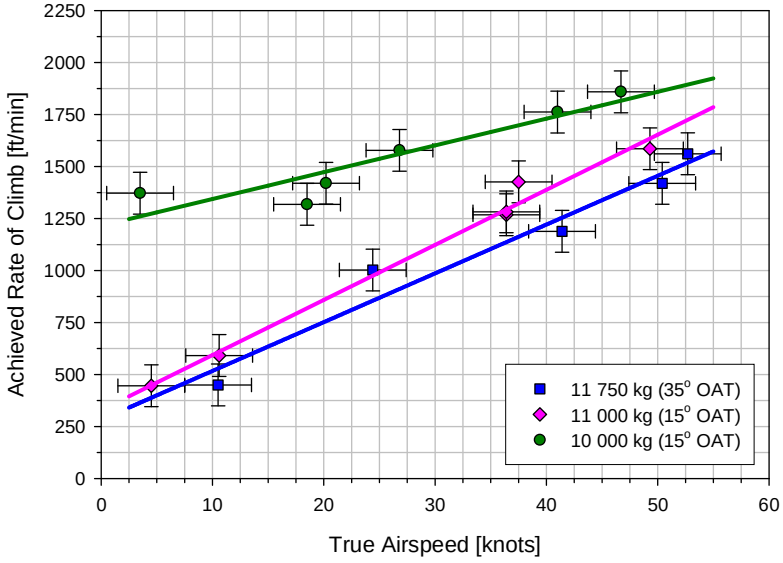

Figure 4-16; Achieved rate of climb
(*regression trend line is* $y = a + bx$)

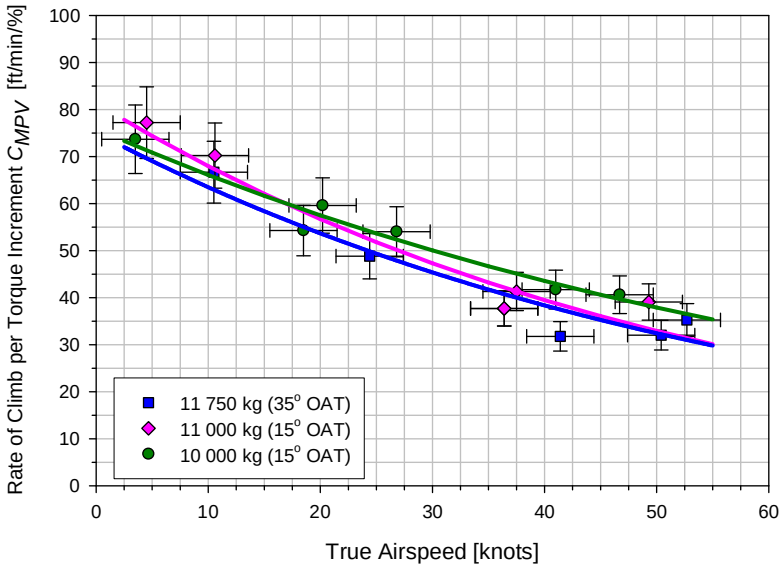

Figure 4-17; Rate of climb per torque increment C_{MPV}
(*regression trend line is* $y = ae^{bx}$)

It was observed that achieved ROC per 1% torque increment decreased with an increase in true airspeed (i.e. ΔQ increases faster with true airspeed than climb rate), and showed minimal changes between the referred weights. This is a very convenient result since it means that the extra power required to climb can be simply added to that required for level flight, which is consistent with simple modelling techniques used to predict rates of climb in forward flight. The values for achieved ROC per torque increment C_{MPV} can be correlated with the downward flow components of the airwake in the vicinity of the ship, to indicate areas where the climb performance of the helicopter might be inadequate to maintain level flight. These areas with inadequate power margin have to be avoided during the sea trials or if required approached very carefully with an incremental approach in difficulty of the test condition.

4.3.4.3 Centre of Gravity

Cyclic control positions and helicopter attitudes are affected by changes in the longitudinal and/or lateral CG position, and could be affected by the All-Up Weight (AUW) of the helicopter. To determine the effects of changes in CG, flight tests were performed at the three representative values of referred weight at the extremes of both longitudinal and lateral CG position. The cyclic control positions and helicopter attitudes were measured in cross-winds up to 40 knots, both for green and red winds, and from 20 knots tailwind towards 40 knots headwind. The resulting cyclic position and attitude offsets are expressed in control position or attitude changes per shift in CG position, the so-called "*CG correction coefficient*". These CG correction coefficients CG_{cor} are determined from a linear curve fit for longitudinal cyclic, lateral cyclic, pitch attitude and roll attitude, respectively. The results for displacements in cyclic positions and helicopter attitudes are summarized in Table 4-2.

Parameter	Effect	Cause
Longitudinal cyclic	± 0.27 %/cm	Fore-aft movement CG
Lateral cyclic	± 0.97 %/cm	Left-right movement CG
Pitch attitude	± 0.08 °/cm	Fore-aft movement CG
Roll attitude	± 0.24 °/cm	Left-right movement CG

Table 4-2; Displacements due to CG changes, CG_{cor} (per cm)

The following effects in displacements are noted, and vice versa:

- An aft cyclic movement is caused by a more forward CG;
- A left cyclic movement is caused by a more right CG;
- A pitch-down movement is caused by a more forward CG;
- A roll movement to the right is caused by a more right CG.

The procedure is used to identify potential problem areas (for further testing) rather than to determine an absolute result. If the application of CG correction coefficients leads to a clear indication that control margin problems will be absent in a particular flight condition, then a reduction in the amount of testing may be possible. For example, testing might proceed directly from mid-CG to maximum aft-CG, without an

intermediate step, as a result of confidence gained by the use of CG corrections. Or sea trials can be conducted only at one CG position, whilst applying appropriate corrections to ensure adequate control authority throughout the complete CG envelope for operational aircrew.

4.3.4.4 Control Position Related Rejection Criteria

The TFCP provide extensive information about the stability characteristics of the helicopter. In addition, it can be verified whether control margins are approached or exceeded at any point. During flight there must be a margin of control authority remaining to enable the helicopter to be manoeuvred, and to allow the pilot to overcome for example disturbances due to the ship's airwake. The helicopter inertia, control power and the expected degree of turbulence during shipboard operations will all affect the control margin required. For ease of understanding, an internationally agreed value of 10 % control margin is used as being representative of this value.

Tail rotor actuator position

The flight test results for tail rotor actuator position at 40 knots, as a function of the relative wind direction are shown in Figure 4-18. The tail rotor thrust increases for higher referred weights, and depends on the relative wind direction. The increase in tail rotor thrust between 11 000 kg and 11 750 kg referred weight, is mainly caused by the variation in torque required due to OAT, as the maximum take-off weight of the helicopter is limited to 11 000 kg.

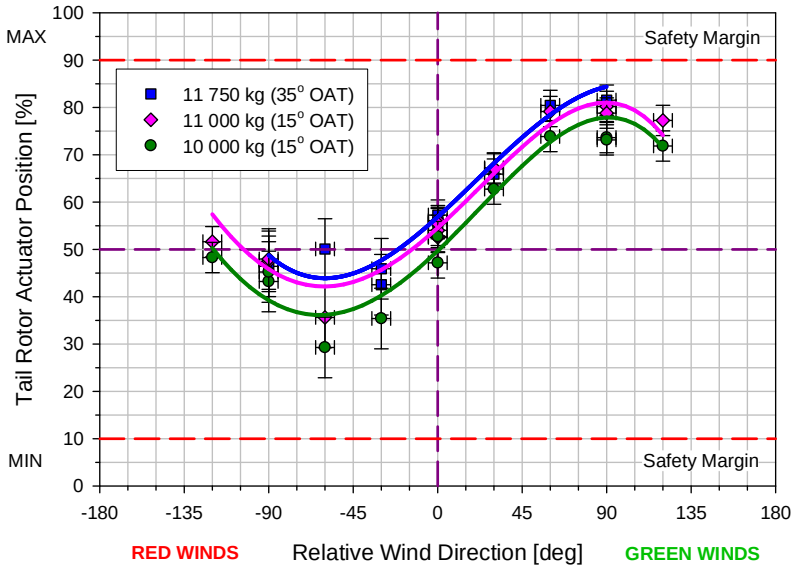

Figure 4-18; Tail rotor actuator position at 40 knots
(*regression trend line is* $y = a + bx + cx^2 + dx^3 + ex^4$)

The tail rotor thrust is dependent on referred weight, thus torque required, as the tail rotor has to deliver more or less anti-torque to maintain helicopter heading. As the main rotor turns counter-clockwise, when seen from above, more tail rotor thrust and

thus torque required, is necessary to prevent the nose to turn into the wind in the sector between dead-ahead and green 90°. The tendency for the nose of the helicopter to turn into the wind is known as the 'weather-cock effect'. For this reason the highest tail rotor actuator position is required at relative winds from the direction green 60° to green 120°. An opposite effect occurs for red wind conditions in the sector between red 60° and dead-ahead, with less demand for tail rotor thrust and thus torque required to maintain helicopter heading. Once past the abeam position for either red or green wind conditions, the same effects occur although in opposite direction as the nose of the helicopter wants to turn now in the other direction. The areas that exceed the applicable safety margin for tail rotor actuator position are to be excluded from the CFE, which in this case is not applicable. With a relative wind from port, the tail rotor has the potential to generate a vortex ring state, as the thrust vector has the same direction as the cross-wind vector. In particular, sideways flight, rapid spot turns or out-of-wind hovering are situations when the tail rotor is operating in a state equivalent to either a climbing or descending rotor. Certain combinations of cross-wind speed and flow through the tail rotor in this state are forming a so-called "*region of roughness*". In this condition the air flowing through the tail rotor is deflected sideways and re-circulates. This leads to unsteady flow conditions, erratic thrust variation, unsteady helicopter attitudes and high scatter in yaw control (i.e. larger combined standard uncertainties).

Pedal position

The flight test results for pedal position at 40 knots, as a function of the relative wind direction are shown in Figure 4-19. The pedal position changes with the relative wind direction.

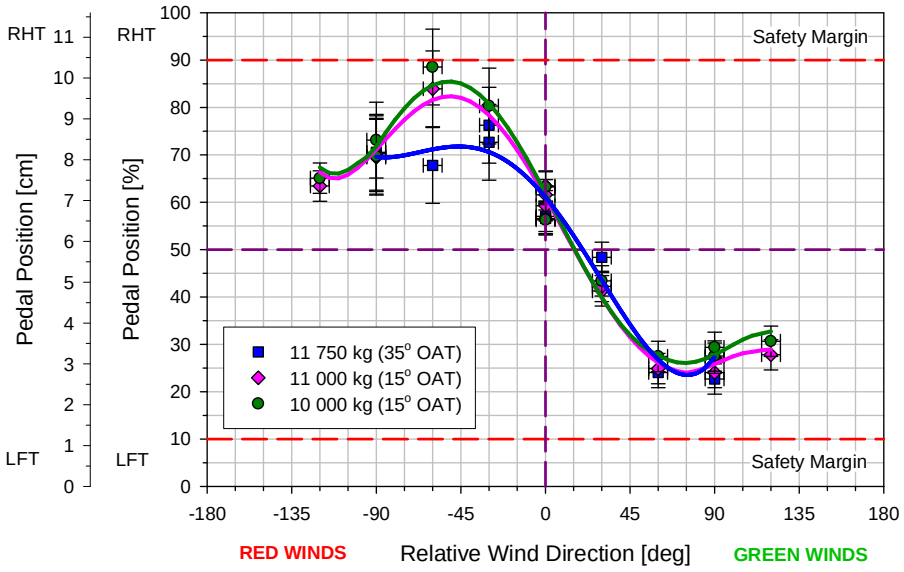

Figure 4-19; Pedal position at 40 knots
(*regression trend line is* $y = a + bx + cx^2 + dx^3 + ex^4 + fx^5$)

The pedal position is largely independent of referred weight, thus torque required, as the fly-by-wire flight control system acts as a collective-yaw interlink which compensates for variations in pedal deflection caused by changes in torque. As the main rotor turns counter-clockwise, when seen from above, more tail rotor thrust and thus left pedal (i.e. power pedal in this case), is necessary to prevent the nose to turn into the wind in the sector between dead-ahead and green 90°. For this reason the most left pedal position is required at relative winds from the direction green 60° to green 120°. An opposite effect occurs for red wind conditions in the sector between red 60° and dead-ahead, with less demand for tail rotor thrust and thus more right pedal to maintain helicopter heading. Once past the abeam position for either red or green wind conditions, the same effects occur although in opposite direction as the nose of the helicopter wants to turn now in the other direction. A region of roughness is noted between red 90° and red 30° with an erratic oscillatory yawing motion leading to a high scatter in pedal deflections (i.e. larger combined standard uncertainties). It was noted that the pedal position at red 60° for 11 750 kg referred weight is less towards the right as for the lower referred weights, and thus should be further investigated during the sea trials. The areas that exceed the 10 % safety margin for pedal position are to be excluded from the CFE, which in this case is around red 60°.

Longitudinal and lateral cyclic position

The flight test tests results for longitudinal and lateral cyclic position at 20 knots with a longitudinal aft and lateral mid CG (i.e. most common situation for operational scenarios), as a function of the relative wind direction, are shown in Figure 4-20 and Figure 4-21 respectively. There are negligible differences in cyclic position with referred weight, whilst the cyclic position changes with relative wind direction.

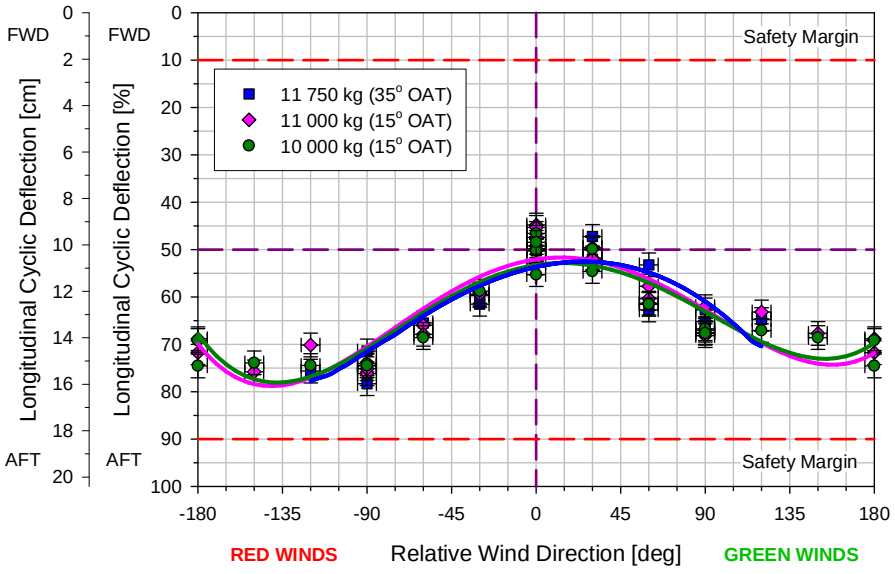

Figure 4-20; Longitudinal cyclic position at 20 knots (aft CG)
(*regression trend line is* $y = a + bx + cx^2 + dx^3 + ex^4 + fx^5$)

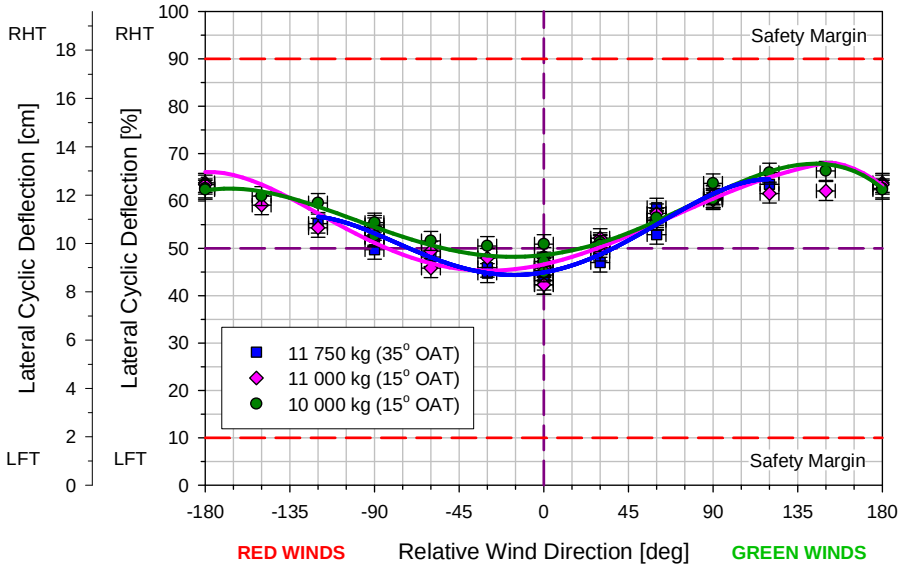

Figure 4-21; Lateral cyclic position at 20 knots (mid CG)
(*regression trend line is* $y = a + bx + cx^2 + dx^3 + ex^4$)

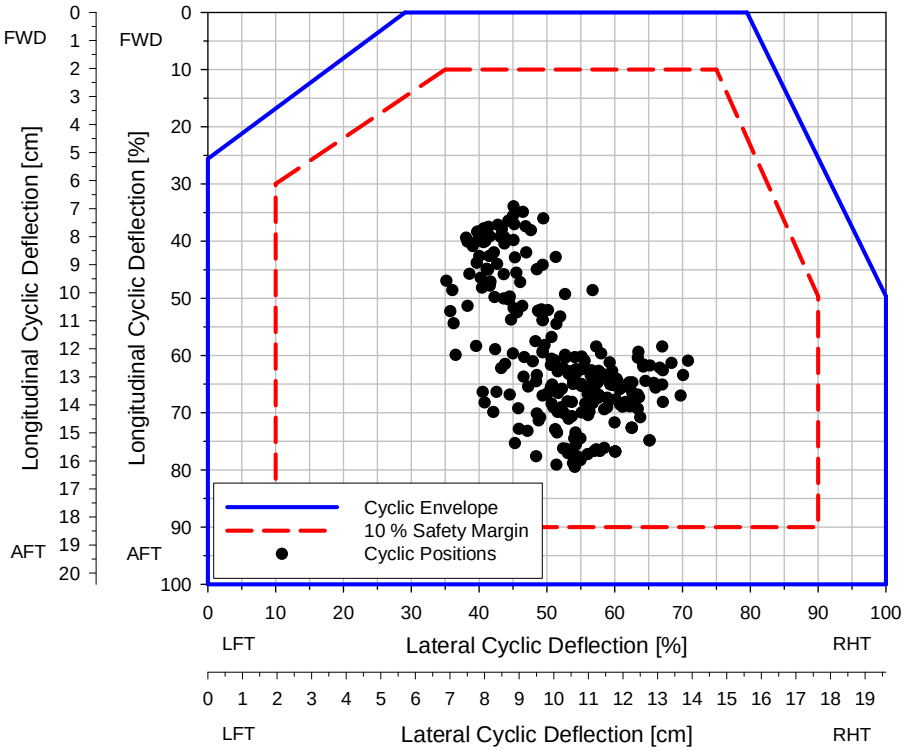

Figure 4-22; Overview cyclic positions within cyclic control envelope

A complete overview of the cyclic positions measured during the shore-based hover trials for all relative wind conditions and different CG positions, is presented as longitudinal cyclic position vs. lateral cyclic position, including the cyclic control envelope restrictions in Figure 4-22. In some areas, the cyclic control envelope restrictions could result in more stringent margins than only the 10 % safety margin or a particular longitudinal and lateral cyclic position. Therefore, these additional restrictions in the cyclic control envelope have to be taken into account during the construction of the CFE for the tested aircraft. No discontinuities, control margins, handling issues or other abnormalities are noted. There are no restrictions in the CFE due to longitudinal and/or lateral cyclic positions.

4.3.4.5 Helicopter Attitude Related Rejection Criteria

An increased nose-down pitch attitude for increased airspeed (and vice versa for rearward velocities) is desirable to give the pilot attitude cues to airspeed, however, the pitch attitude change with airspeed should not be excessive such that it is uncomfortable to the crew or adversely affects the Field Of View (FOV). Similarly, side-force cues are particularly important during low speed flight as the role of the helicopter may require prolonged flight maintaining a relative lateral airspeed. If the side-force is excessive then the helicopter would need to be kept at a high roll attitude which would be uncomfortable for the crew and passengers and might also affect for example the use of role equipment or weapon systems. Weak side-force cues might also be undesirable in that the pilot would not receive any feedback of lateral airspeed through the roll attitude of the helicopter when visual cues are weak such as when hovering aided by Night Vision Goggles (NVG).

Pitch attitude

The flight test results for pitch attitude of the helicopter at 30 knots, as a function of the relative wind direction are shown in Figure 4-23. There are no noticeable differences in pitch attitude with referred weight, although the pitch attitude changes with relative wind direction. The pitch-up attitude, at aft-CG, increases to high values of approximately 10° in a wind direction around green 30° at 30 knots (occasionally increasing towards approximately 11°), whilst knowing that the maximum pitch-up attitude for landing according to the flight manual is 12° [17]. The high pitch-up attitudes result in reduced visual cues with the ship and would increase the risk of a tail strike during shipboard take-offs and landings. The green wind conditions with high pitch-up attitudes up to approximately 10° (occasionally increasing towards approximately 11°) around green 30° at 30 knots are removed from the CFE.

Roll attitude

The flight test results for roll attitude at 40 knots, as a function of the relative wind direction are shown in Figure 4-24. There are negligible differences in roll attitude with referred weight, although the roll attitude changes with relative wind direction. As the main rotor turns counter-clockwise, when seen from above, the tail rotor thrust once applied at the CG, causes a side drift of the helicopter to the right. To cancel the drift an equal force directed in the opposite direction must be opposed to the tail rotor thrust.

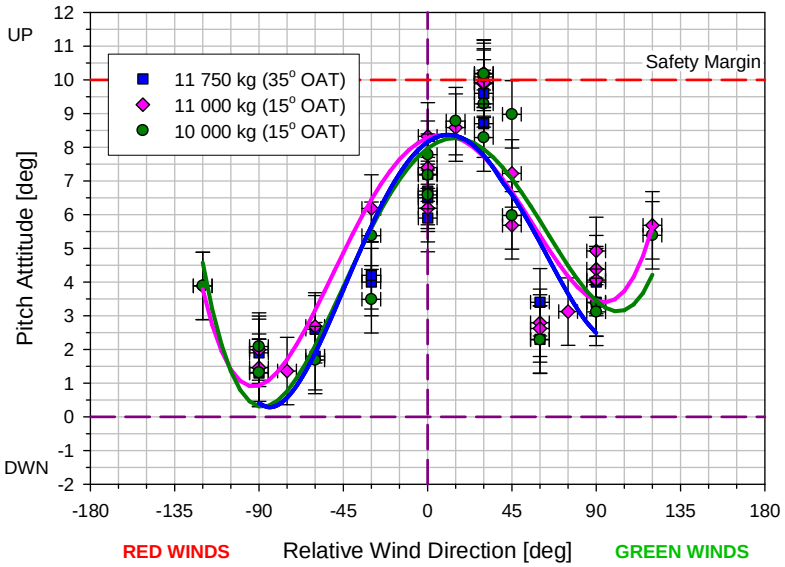

Figure 4-23; Pitch attitude at 30 knots (aft CG)
(*regression trend line is* $y = a + bx + cx^2 + dx^3 + ex^4$)

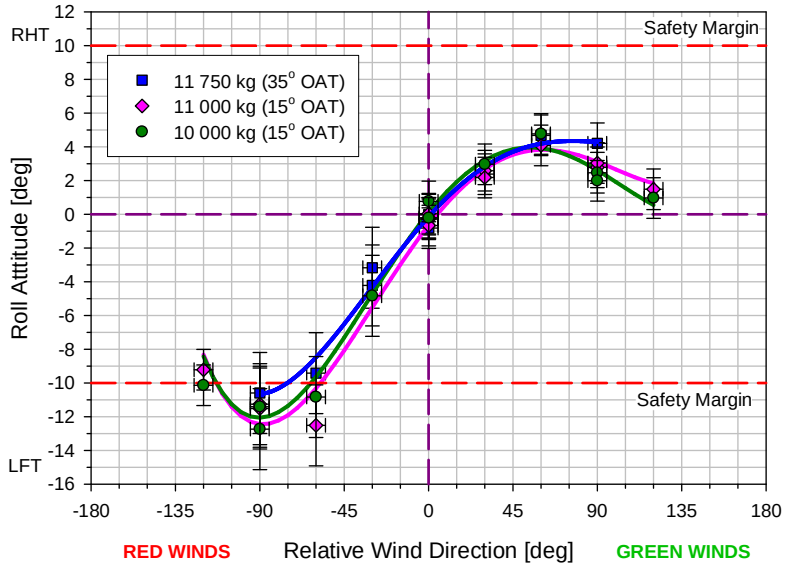

Figure 4-24; Roll attitude at 40 knots (mid CG)
(*regression trend line is* $y = a + bx + cx^2 + dx^3 + ex^4$)

In general, more roll attitude to the left is necessary to prevent the helicopter from drifting to the right in the low speed region. The changes in roll attitude towards the right in green winds conditions are relatively small up to approximately 5°. The changes in roll attitude towards the left for red wind conditions are such that for red 90° winds at 40 knots the roll attitude is approximately 13° (occasionally increasing

towards approximately 15°), and this is considered uncomfortable by the aircrew. The large roll attitude for red wind conditions, between red 120° and red 60°, would likely restrict ship board operations. The restrictions are dependent on, for example, the capacity of the landing gear to absorb the impact from the landing, the tendency of the helicopter to bounce on the flight deck once landed with one wheel first, and the comfort level of the pilot to manoeuvre the helicopter above a moving flight deck with a tilted view of the horizon. The relative wind conditions between red 120° and red 60°, with large roll attitudes of the helicopter up to approximately 13°, are removed from the CFE for the higher relative wind speeds.

4.3.5 Lessons Learned for the Helicopter Flight Characteristics

The following lessons learned for the helicopter flight characteristics related to shipboard operations are observed:

1. The flight test data should be converted into referred parameters, so that it can be used to produce information relevant to atmospheric conditions and helicopter masses different from those actually tested;
2. The precise limiting factor(s) for the specified operational conditions should be known, for example, in order to compare test conditions flown during different missions of the test campaign with each other;
3. The flight test data should be accompanied by a comprehensive uncertainty analysis (as discussed in Chapter 3);
4. If the main rotor turns counter-clockwise, when seen from above, more torque required is necessary to prevent the nose to turn into the wind for green winds conditions;
5. An increase in referred weight results in an increase in torque required, engine gas generator speed, engine power turbine inlet temperature and tail rotor thrust. As a result, for higher referred weights, an associated minimum relative wind speed is required to perform flight operations;
6. An increase in referred weight has negligible influence on pedal position, longitudinal cyclic, lateral cyclic, pitch attitude and roll attitude;
7. The likely problem areas, in terms of cyclic control margins and helicopter attitudes, can be identified by applying a CG correction coefficient (i.e. cyclic and helicopter attitude changes per cm shift in CG).

4.4 Chapter Review

The novelty of the preliminary investigation is the systematic approach to the assembly of the database for the construction of the CFE in the next phase, related to the concept of rejection criteria and their quantification. As such any issues can be properly investigated before being embarked on board the ship whilst under huge pressure to provide the widest operational capabilities within the least amount of time. The preliminary investigation includes an assessment of the expected environment conditions near the ship, and the determination of the helicopter flight characteristics in

an omni-directional relative wind envelope. For the ship environment, there are three different and distinct wind conditions defined that are important during shipboard operations: relative, indicated and local wind. The relative wind is considered the undisturbed wind in this case, which is the vector summation of the actual wind with the course and speed of the ship. The indicated wind is the wind presented to the ship's crew, although it is subject to disturbances in the airwake at the anemometer locations and varies between each ship type. The local wind is different at each location in the take-off and landing path, however, this wind is what the helicopter will encounter during shipboard operations. Therefore, the aim is to correlate for the various take-off and landing procedures, the local wind and the indicated wind by the ship's anemometers, for the construction of the CFE.

For the determination of the helicopter flight characteristics, shore-based hover trials are conducted. A distinction is made between rejection criteria and dependencies, to be less dependent on dedicated sea trials. More specifically, the subdivision of test data in rejection criteria and dependencies enables (1) assessing other possible conditions for in-service operations and (2) accurate exclusion of test points. A distinction is made between subjective, performance, control position, and aircraft attitude related issues. The flight test data is converted into referred parameters, so that it can be used to produce information relevant to atmospheric conditions and helicopter masses different from those actually tested. In any case, the precise limiting factor(s) for the specified operational conditions should be known, for example, in order to compare test conditions flown during different missions of the test campaign with each other. In general, the following effects are noted of variations in the environmental conditions to the helicopter flight characteristics in a world-wide theatre. An increase in referred weight results in an increase in torque required, engine gas generator speed N_g, engine power turbine inlet temperature T_{46} and tail rotor thrust. As a result, for higher referred weights, an associated minimum relative wind speed is required to perform flight operations. An increase in referred weight has negligible influence on pedal position, longitudinal cyclic, lateral cyclic, pitch attitude and roll attitude.

Page intentionally left blank

Chapter 5 *Phase II*, The Prediction of the Candidate Flight Envelope

5.1 Introduction

This chapter discusses the construction of the Candidate Flight Envelope (CFE) of the innovative three-phase approach for determining Ship Helicopter Operational Limitations (SHOLs) as shown in Figure 5-1. The prediction of the CFE, aided by a novel analytical tool developed by the author, named "*SHOL-X*", is based on the fundamental understanding and correct merging of the ship environment and helicopter flight characteristics [1]. The CFE (blue box in figure) is obtained by combining the behaviour of the isolated helicopter, the local environmental conditions for a particular ship and other miscellaneous items. The miscellaneous items (red box in figure) could be added to optimize the CFE, for example, experience from previous test campaigns with either the helicopter type or the ship type under test. Once the CFE is developed, the associated uncertainty and adequate safety margins are established prior commencing sea trials.

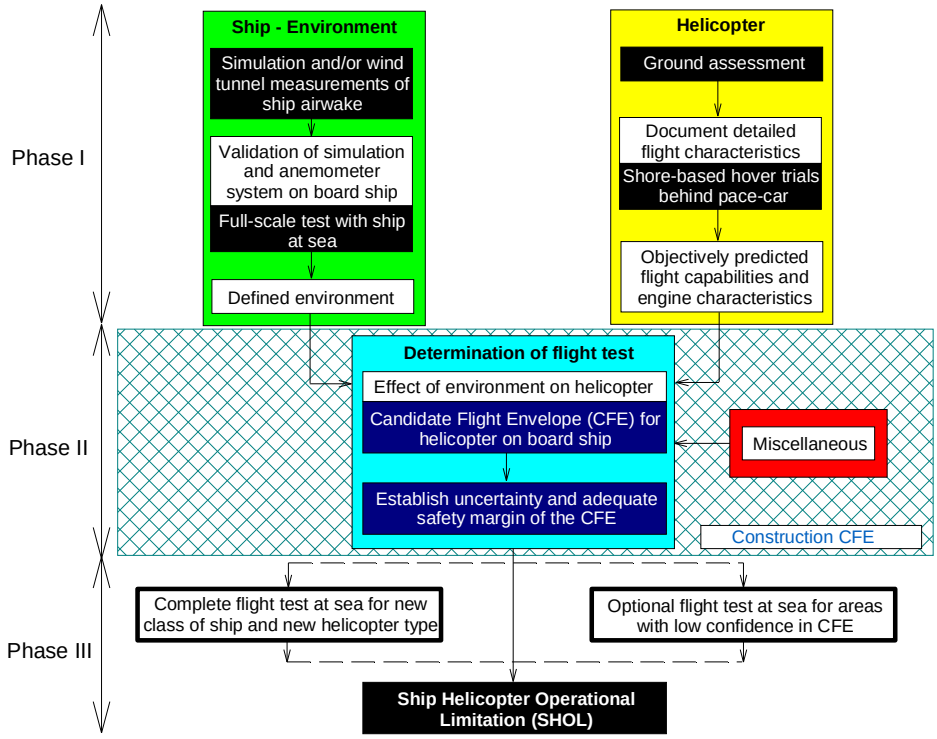

Figure 5-1; Innovative flow chart SHOL development

5.2 Development Cycle

This section gives a framework for quality assurance guidelines in the development cycle of the predictive tool. This includes a consistent terminology and foundation for a methodology bridging the gap between scientific philosophy and pragmatic modelling based on Refsgaard [2] and the American Society of Mechanical Engineers (ASME) [3]. However, unless stated otherwise, the author used his own interpretation to present the development cycle and associated definitions as applied in this dissertation.

5.2.1 Terminology and Methodological Framework

The simulation environment is divided into four basic elements: (1) the conceptual model, (2) the model code, (3) the specific model and (4) the reality as shown in Figure 5-2. The inner arrows describe the processes that relate the four basic elements to each other, whilst the outer circle refers to the procedures that evaluate the credibility of these processes. In general terms, a model is understood as a simplified representation of the natural system it attempts to describe. However, in the terminology a distinction is made between three different meanings of the general term model, namely the conceptual model, the model code and the model itself. The conceptual model is a description of reality that constitutes the scientific hypothesis or theory that is assumed for the particular modelling study. The model code is a mathematical formulation in the form of a computer program that is so generic that, without program changes, it can be used to establish a model with the same basic type of equations (but allowing different input variables and parameter values) for different types of helicopter and/or ship. The model is then established for a particular helicopter-ship combination, including input data and parameter values. The credibility of the descriptions or the agreements between reality, conceptual model, model code and model are evaluated in the development cycle by confirmation, verification, calibration and validation:

1. *Model confirmation:* Determination of adequacy of the conceptual model to provide an acceptable level of agreement for the domain of its intended application. This is in other words the scientific confirmation of the theories/hypotheses included in the conceptual model, which are confronted with actual experimental data and be subject to critical peer reviews.
2. *Code verification.* The process of determining that a computational model accurately represents the underlying mathematical model and its solution. The methodologies used are comparing a numerical solution with an analytical solution or with experimental data.
3. *Model calibration*. The process of adjusting numerical or physical modelling parameters in the computational model for the purpose of improving agreement with experimental data. It should be kept in mind that short sighted use of model calibration may result in the right model output for the wrong reason.
4. *Model validation*. The process of determining the degree to which a model or simulation is an accurate representation of reality, or some other meaningful

referent, from the perspective of the intended uses of the model or simulation. The credibility of the model's capability to make predictions about reality must be evaluated against independent data, not been used during calibration.

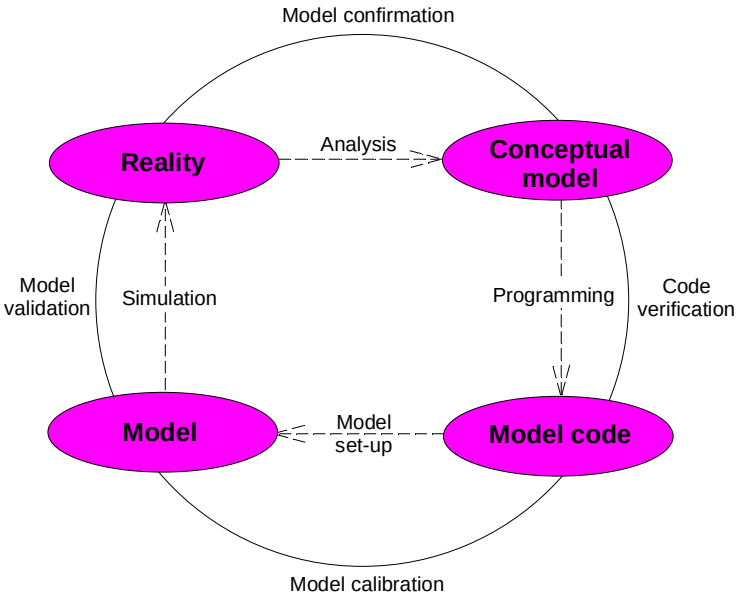

Figure 5-2; Elements of a modelling terminology [2]

5.2.2 Performance Criteria and Application Domain

A critical issue in relation to the methodological framework is how to define the level of acceptable agreement between the model and reality, known as performance criteria. The performance criteria apply both for model calibration and model validation. As mentioned by Beven [4] any conceptual model is known to be wrong, and hence any model will be falsified if investigated in sufficient detail and specified according very high performance criteria. Clearly, if one attempts to establish a model that should simulate the truth it would always be falsified. However, this is not useful information. Therefore, the validation should be restricted to the domain of applicability.

A good test for model performance is to compare it with the available experimental data. If the model performance is within the associated uncertainty range of the experimental data, the model is often characterised as good enough. However, usually it is not so simple as it should be decided how wide the confidence bands may be in order to be accepted as observational uncertainties – usually ranges corresponding to 65%, 95% or 99%. A question to be answered is whether the model should always be rejected if it cannot perform within the observational uncertainty range. In many cases even results from less accurate models may be very useful. Therefore, the answer is that the decision on what is good enough generally must be taken in a socio-economic context. Thus, the accuracy criteria cannot be decided universally by modellers or researchers, but must be different from case to case depending on how much is at stake

in the decision to depend on the support from model predictions. This implies that the performance criteria must be discussed and agreed between the stakeholders and the modeller beforehand. However, as the modelling process and the underlying study progresses with improved knowledge on the data and model uncertainties, as well as on the risk perception of the concerned stakeholders, it may well be required to adjust the performance criteria in a sort of adaptive project management context. For this reason, the following domains of applicability are distinguished:

- *Domain of applicability (of conceptual model):* Prescribed conditions for which the conceptual model has been tested, i.e. compared with reality to the extent possible and judged suitable for use (by model confirmation).
- *Domain of applicability (of model code):* Prescribed conditions for which the model code has been tested, i.e. compared with analytical solutions, other model codes or similar to the extent possible and judged suitable for use (by code verification).
- *Domain of applicability (of model):* Prescribed conditions for which the helicopter-ship model has been tested, i.e. compared with reality to the extent possible and judged suitable for use (by model validation).

The purpose of defining the application domain is to increase the confidence in non-validated model predictions. The better the overlap between the validated domain and the application domain, and the better the understanding of the underlying physical principles, the stronger the inference with respect to model prediction can be [5]. The effect of validation and application domain on the strength of inference is illustrated in Figure 5-3. The understanding of the predictive tool should be at such a level that quite strong inferences with respect to predictions outside the validated environmental conditions are justified in order to be used. Predictions outside the validated domain should (as always) be considered with care.

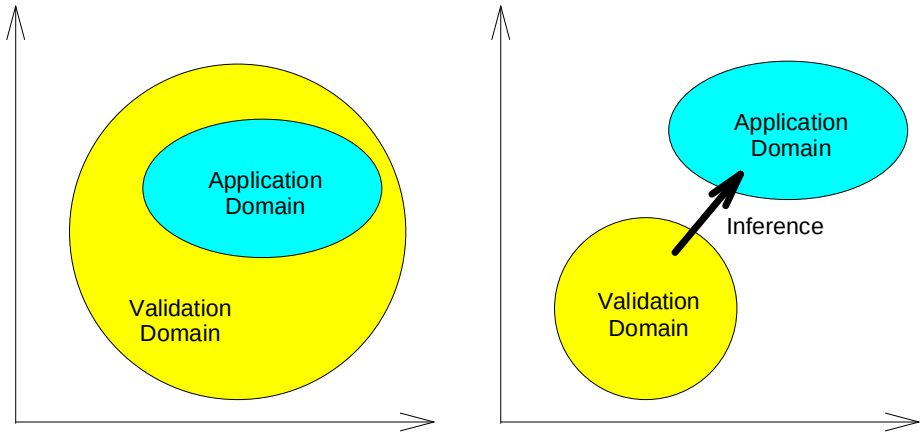

Figure 5-3; Relationship of validation to application domain; modified from [6]

In order to ensure that the validation domain covers the application domain as much as possible, dimensional analysis are applied. Data converted into non-dimensional form

can be used to produce information relevant to atmospheric conditions and helicopter masses different from those actually tested. Consequently, with few exceptions, a relatively small number of tests at carefully chosen test sites can produce information relevant to much of the helicopter's flight envelope. However, even though a non-dimensional approach is employed, it is advisable to fly in conditions as near to the standard conditions (at which results are required) as possible. As such, any unforeseen issues due to varying atmospheric conditions on helicopter performance and/or flying qualities could be identified already before an operational deployment. For this reason, the shore-based hover trials were conducted at different test locations with different atmospheric conditions (i.e. approximately 15 °C and 35 °C).

5.2.3 Goals of the Predictive Tool

The simulation goals of the predictive tool should be driving the extraction of the conceptual model from reality. This might seem trivial, but often modellers are tempted to use legacy codes that were developed earlier, sometimes by others, with other goals in mind, which can easily lead to non-adequate computer codes. For rough estimates of main system performance one can often use a system model based on simplified concepts. In such cases the trends are more important than the actual quantitative results. On the other side of the spectrum, where interest goes out to in-depth analysis of complex processes, one needs to model these complex processes in detail. However, when detailed physical processes have a big effect on the overall system behaviour, it should be considered whether a simplified sub-model of the complex part can still give good overall results. The predictive tool developed in this dissertation is built with these considerations on necessary model complexity in mind. On an abstract level the goal of the predictive tool can be summarized as follows:

> Create a predictive software tool that represents reality accurate enough to make it useful in order to evaluate the operational capability of any helicopter-ship combination. In addition, the tool should allow to investigate the effects of variations in the environmental conditions on the performance of the helicopter during shipboard operations in a world-wide theatre.

This abstract goal includes the somewhat vague descriptions: "*accurate enough*", "*useful*", and "*operational in a world-wide theatre*". To clarify these and turn them into specifications for the simulation model an interpretation of the high level goal is made here:

> Create a model to assess the helicopter flight characteristics in the shipboard environment containing the following sub-models: helicopter performance, helicopter control positions and helicopter attitudes.

More specifically:

- The accuracy of the predictions in helicopter performance should be such that conclusions with respect to power required and power available can be drawn in the shipboard environment;

- The accuracy of the predictions in helicopter control positions should be such that conclusions with respect to the sufficiency in control authority can be drawn in the shipboard environment;
- The accuracy of the predictions in helicopter attitudes should be such that conclusions with respect to potential limiting helicopter attitudes can be drawn in the shipboard environment.

These specifications give a starting point for setting up the predictive engineering tool. Whether the resulting total simulation model gives outputs with sufficient accuracy cannot easily be said beforehand due to uncertainty propagation through the various sub-models.

5.3 Overview of the Predictive Tool

There are various inputs required in the predictive tool, i.e. helicopter flight characteristics and limitations, helicopter and ship parameters, atmospheric conditions and the ship environment as shown in Figure 5-4. There are sub-models for the atmospheric boundary layer, ship airwake, subjective pilot ratings, helicopter performance, helicopter control positions and helicopter attitudes.

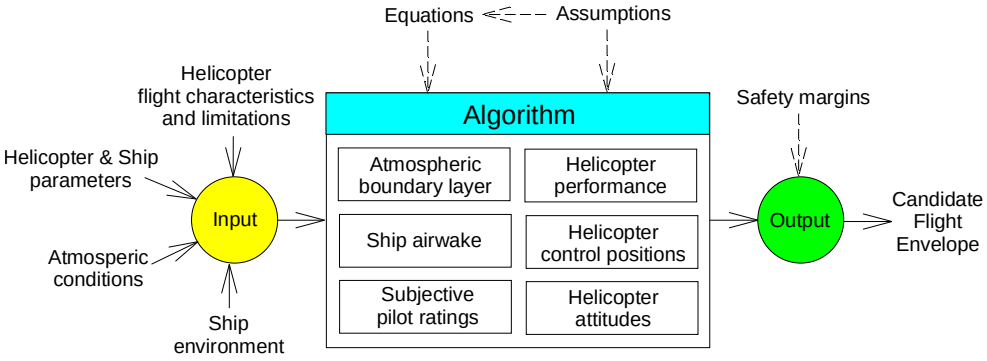

Figure 5-4; Overview elements predictive tool

The algorithm is based on assumptions and the consequential equations that together form the fundamental basis of the predictive tool as discussed in this chapter. Furthermore, the algorithm processes the input data such that all relevant rejection criteria and dependencies interact with each other. For this reason, maximum and minimum values of local wind conditions near and above the flight deck are applied to helicopter rejection criteria, stored in lookup tables, for example, to ensure that there remains sufficient power and control margin available to perform safe shipboard operations throughout various operational scenarios. The output from the predictive tool results in the CFE, based on the indicated wind as presented by the ship's anemometers, which can likely be released to in-service operations for each particular helicopter-ship combination, whilst taking adequate safety margins into account. Unfortunately, there are uncertainties associated with the measurements used as input

for the predictive tool, and uncertainties associated with the algorithm itself. Therefore, the output of the predictive tool is validated to determine the degree of representation of the reality from the perspective of constructing the CFE, used as a starting point for the sea trials, as further discussed in Chapter 6.

5.4 Ship Environment Simulation

There are various inputs required for the ship environment simulation, i.e. boundary layer profile, wind tunnel measurements, ship parameters, desired take-off and landing procedure, and the desired take-off and landing spot on the flight deck as shown in Figure 5-5. There are sub-models for the determination of the atmospheric boundary layer and the ship airwake. Furthermore, the algorithm processes the input data such that it interacts with each other. The output from the ship environment simulation results in detailed knowledge about the ship environment in the take-off and landing paths for the desired procedure towards the desired spot on the flight deck which are relevant for the construction of the CFE. The code verification for the ship environment simulation was mainly performed by engineering judgement. In addition, spot checks were performed with full-scale test data from the sea trials; no model calibration at sub-model level is performed. Note that the effects of ship motion on pilot workload for take-off and landing are determined as part of the flying routine during the sea trials, and for that reason are discussed in Chapter 6.

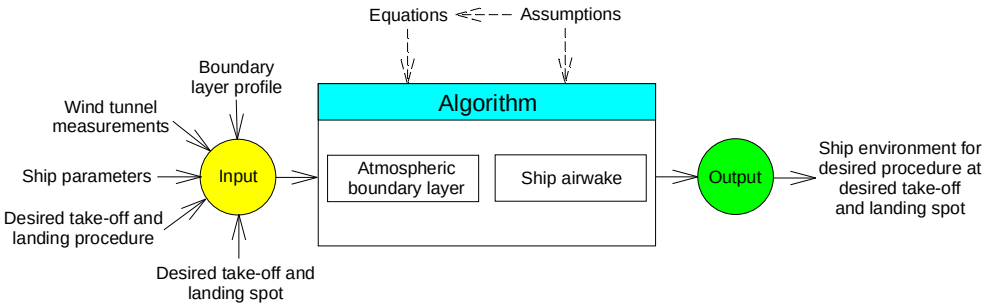

Figure 5-5; Overview elements ship environment simulation

5.4.1 Sub-Model Atmospheric Boundary Layer

In the wind tunnel, the airflow measurements are carried out in a uniform airflow condition, i.e. the wind is assumed not to vary with height or at least there is a very thin boundary layer compared to the size of the scale model of the ship [7]. In reality, the wind speed increases with height due to the effects of the atmospheric boundary layer as shown for example in Figure 5-6. The atmospheric boundary layer extends from the Earth's surface up to an altitude where the wind is no longer influenced by the roughness of the ground and the mean wind speeds increase with height up to the gradient height, usually defined as the height above ground where surface friction has a negligible effect on wind speed. The applicable increase in mean wind speeds with height depends on the local surface obstructions. On, or very close to the ground, a

helicopter will be travelling through an area where the gradient in mean wind speeds is significant. Therefore, to correlate the local wind speeds near and above the flight deck with the indicated wind speeds measured at the anemometer locations, the airflow velocities should be increased by an amount dependent on the vertical distance between the flight deck and anemometer locations as shown for example in Figure 5-7.

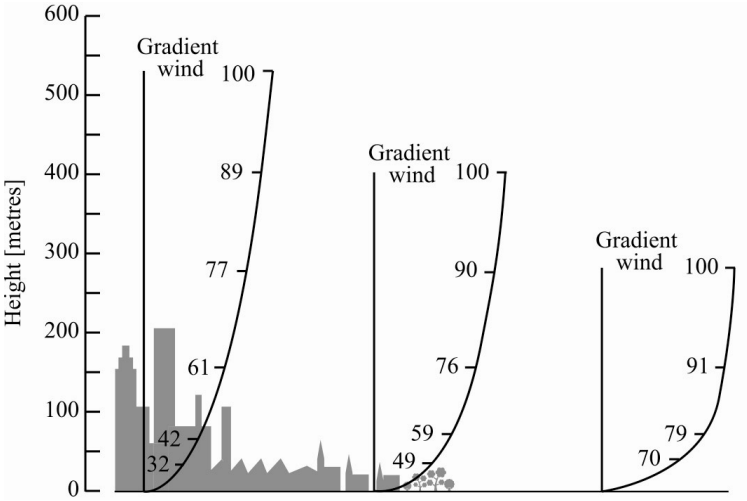

Figure 5-6; Example atmospheric boundary layer; modified from [8]

Figure 5-7; Example vertical distances; modified from [9]

To apply wind tunnel measurements for the construction of a CFE, valid for a ship at full-scale, corrections for the atmospheric boundary layer are made. An approach is chosen based on the knowledge of the wind speed profile above a sea surface at various wind speeds. This model has been developed by the Koninklijk Nederlands Meteorologisch Instituut (KNMI) [10]. The local wind speeds near and above the flight deck are correlated with the indicated wind speeds measured at the anemometer locations by the exponential function:

$$\frac{V_{fd}}{V_{an}} = \frac{\ln(z_{fd} / z_0)}{\ln(z_{an} / z_0)} \qquad \textbf{(Eq. 5-1)}$$

where V_{fd} is the mean wind speed at the height of the flight deck above sea level z_{fd}, V_{an} is the mean wind speed at the height of the anemometer locations above sea level z_{an}, and z_0 is the roughness height of the surface. The roughness height z_0 of a calm sea at the North Sea is approximated to be 0.0001 m, a developed sea is approximated to be 0.0016 m and in case of a rough sea this factor is approximated to be 0.01 m. In general, the estimates for wind speeds at the anemometer locations with a roughness height z_0 for a developed sea match with full-scale test data and this factor is used for further calculations. Note that wind speeds solely caused by the speed of the ship will be an uniform airflow condition as well, whilst the relative wind speeds resulting from the course and speed of the ship in combination with the actual wind conditions will not. Unfortunately, during operational scenarios the relative wind speeds can result from any combination in course and speed of the ship in relation to the actual wind. Therefore, to ensure maximum operational flexibility of the ship, only the relative wind speed with the atmospheric boundary layer taking into account is used for the construction of the CFE (i.e. the highest presented wind speeds by the ship's anemometers).

The atmospheric boundary layer coefficients Z_{ABL} for every ship type within the entire Dutch fleet including: the Auxiliary Oiler Replenishment (AOR) ship, the Air defence and Command Frigate (LCF), the Landing Platform Dock No. 1 (LPD1), the Landing Platform Dock No. 2 (LPD2), the Multi-purpose frigate (MFRI) and the Ocean Patrol Vessel (OPV) are summarized in Table 5-1. The highest atmospheric boundary layer coefficients Z_{ABL}, to be taken into account to correlate the local wind speeds near and above the flight deck with the indicated wind speeds measured at the anemometer locations is for the MFRI with 1.208, whilst the lowest Z_{ABL} to be taken into account is for the LPD1 "Zr.Ms. Rotterdam" with 1.119. The main reason for the differences in Z_{ABL} between these ship types is the exponential gradient in mean wind speeds very close to the ground, thus in this case ships with a low flight deck and a proportionally high location for the anemometers.

Item	AOR	LCF	LPD1	LPD2	MFRI	OPV
Anemometer	26.1 m	24.0 m	39.0 m	37.9 m	27.4 m	15.9 m
Flight deck	8.0 m	5.0 m	13.3 m	11.4 m	5.1 m	5.6 m
Z_{ABL}	1.139	1.195	1.119	1.135	1.208	1.128

Table 5-1; Examples atmospheric boundary layer coefficients Z_{ABL} (developed sea)

An example calculation to correlate the local wind speeds near and above the flight deck V_{fd}, with the indicated wind speeds at the anemometer locations V_{an}, is given for the MFRI:

z_{an} = 27.4 m

z_{fd} = 5.1 m

z_0 = 0.0016 m (developed sea)

V_{fd} = 45.5 knots

The atmospheric boundary layer coefficient Z_{ABL} is:

$$Z_{ABL} = \frac{\ln(z_{an}/z_0)}{\ln(z_{fd}/z_0)} = \frac{\ln(27.4/0.0016)}{\ln(5.1/0.0016)} = 1.208$$

The indicated wind speeds at the anemometer locations V_{an} are:

$$V_{an} = V_{fd} \cdot Z_{ABL} = 45.5 \cdot 1.208 = 55.0 \text{ knots}$$

5.4.2 Sub-Model Ship Airwake

The ship airwake sub-model organizes and fills-up look-up tables for the ship's airwake with wind tunnel measurements. The applied three-dimensional local wind conditions are dependent on the approach towards, and departure path from the ship, as shown for example for a fore-aft port take-off and landing in Figure 5-8. The blue circles represent available and relevant locations of the wind tunnel measurements. These local wind conditions are applied towards the helicopter flight characteristics, such that the maximum and minimum encountered wind conditions are used whilst taking the valid (windward) anemometers corrections into account. The applied local wind conditions are visualized in graphical format, as a function of the indicated wind conditions, to make the ship airwake sub-model transparent for the user. Note that the unsteady airwake components or a spatially distributed flow field as seen for the various blade sections of the rotor in the ship airwake are not included here.

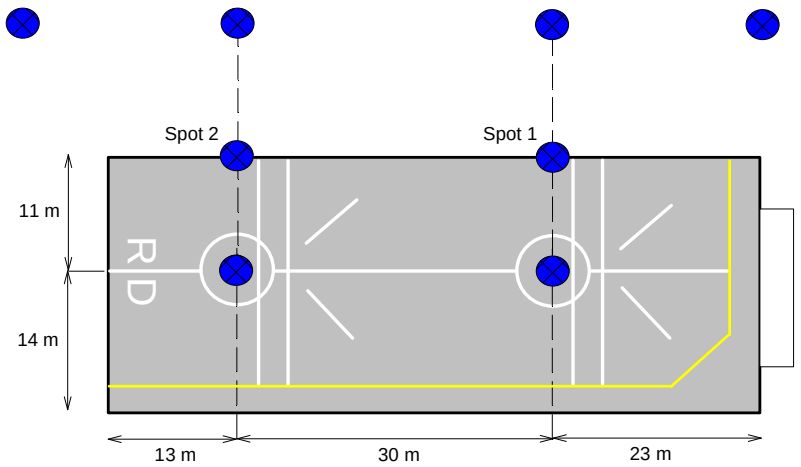

Figure 5-8; Example fore-aft port locations wind tunnel measurements

5.5 Helicopter Flight Characteristics and Limitations Simulation

The simulation of the helicopter flight characteristics consists of sub-models for the subjective pilot ratings, helicopter performance, helicopter control positions and the

helicopter attitudes as described in this section. The code verification for the helicopter flight characteristics simulation was mainly performed by engineering judgement. In addition, spot checks were performed with the data gathered during the shore-based hover trials, and for torque required also a validation has been performed with the performance graphs in the flight manual; no model calibration at sub-model level is performed.

5.5.1 Sub-Model Subjective Pilot Ratings

There are various inputs required for the subjective pilot ratings sub-model, i.e. pilot workload, helicopter vibration levels and turbulence levels as shown in Figure 5-9. For these subjective pilot ratings, three scales are used as presented in Appendix C: the Deck Interface Pilot Effort Scale (DIPES) is used to describe pilot workload, the Vibration Assessment Rating (VAR) scale is used to describe vibration levels and the turbulence rating scale is used to indicate the intensity of the turbulence encountered and its associated helicopter reactions [11]. The output from the subjective pilot ratings sub-model results in knowledge about the subjective rejection criteria which are relevant for the construction of the CFE as shown in Figure 4-11 and figure 4-12 in Chapter 4. Note that the NH90 NFH helicopter showed good handling qualities throughout. However, for other helicopter types there may be more pronounced areas with higher workload ratings which in that case should be further investigated.

The subjective pilot ratings gathered during the shore-based hover trials should be used with care, as there are different visual cues between a situation with a vehicle travelling over the runway and a situation with a ship at sea. In addition, flight operations on board the ship may be performed in a Degraded Visual Environment (DVE) which could increase pilot workload. Furthermore, natural winds on board the ship are always accompanied by some degree of turbulence which is not fully replicated by the pace-car tests. For this reason, no further corrections are made by the predictive tool towards the subjective ratings as assigned during the shore-based hover trials, as these results are only used as a rough guideline for potential areas to be tested during the sea trials. It is recommended to keep up a database belonging to each specific helicopter type under evaluation, to determine if, and to which level of complexity a pilot model can and should be incorporated in the predictive tool at a later stage.

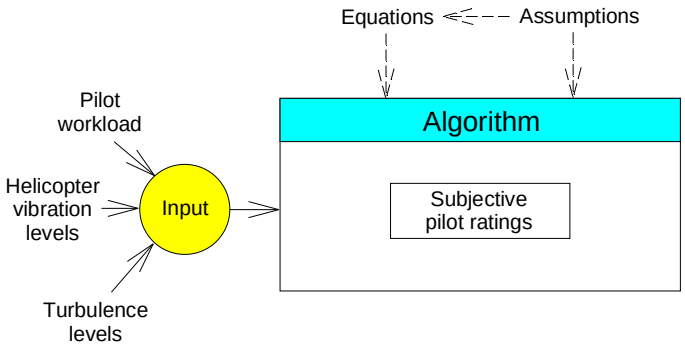

Figure 5-9; Overview elements subjective pilot ratings sub-model

5.5.2 Sub-Model Helicopter Performance

The useful performance of any helicopter depends on the amount by which the power required relates to the power available. This can be determined by the helicopter performance sub-model for various operational scenarios. In addition, the helicopter configuration can be adapted to assess its impact on the CFE, i.e. jet delusion devices (un)installed, sand filters (un)installed, infra-red suppressors (un)installed and/or main rotor speed increase functions enabled or disabled. There are various inputs required for the helicopter performance simulation, i.e. torque required Q_{req}, engine gas generator rotational speed N_g, engine power turbine inlet temperature T_{46}, helicopter weight, atmospheric conditions, helicopter parameters and helicopter configuration as shown in Figure 5-10. There are sub-models for the determination of the power required, power available and achievable climb performance. Furthermore, the algorithm processes the input data such that it interacts with each other. The output from the helicopter performance sub-model results in detailed knowledge about the helicopter capabilities for the desired atmospheric conditions, helicopter weight and helicopter configurations which are relevant for the construction of the CFE, i.e. desired torque required $Q_{req(desired)}$, desired engine gas generator rotational speed $N_{g(desired)}$, desired engine power turbine inlet temperature $T_{46(desired)}$, performance limiting parameter and the maximum achievable climb performance $C_{(MAX)}$.

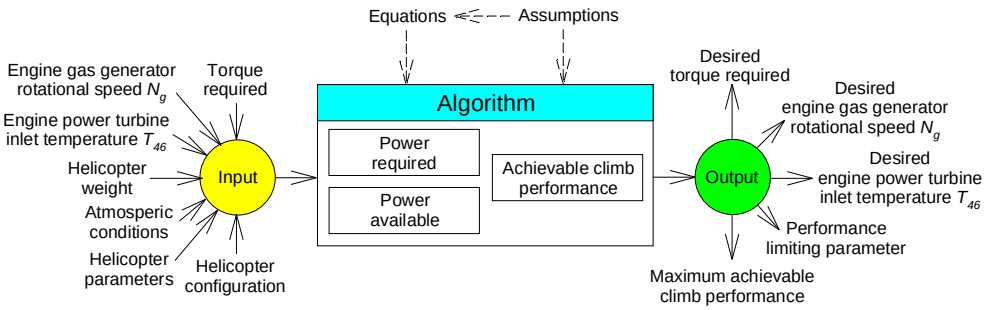

Figure 5-10; Overview elements helicopter performance sub-model

5.5.2.1 Part for Power Required Calculations

The part for power required calculations of the helicopter performance sub-model is divided into: torque required, engine gas generator rotational speed N_g, and engine power turbine inlet temperature T_{46}. This part of the sub-model for helicopter performance is used to adjust the performance parameters towards the desired referred weights and atmospheric conditions for release to operational service. The corrections between desired and achieved referred weights are made to compensate for the fluctuations during the flight test campaign in, for example, helicopter weight due to fuel burn and Outside Air Temperature (OAT). In addition, the impact for the power required by various helicopter configuration changes can be added and/or subtracted.

Torque required

The referred quantity for power required $P_{req,ref}$ depends on the helicopter weight W, forward flight speed V, rate of climb V_c, height above ground level Z, main rotor

relative rotorspeed ω (relative to a standard rotor speed value), and relative wind direction ζ as summarized below:

$$P_{req,ref} = \frac{P_{req}}{\sigma\omega^3} = f\left(\frac{W}{\sigma\omega^2}, \frac{V}{\omega}, \frac{V_c}{\omega}, Z, \frac{\omega}{\sqrt{\theta}}, \zeta\right) \quad \textbf{(ref Eq. 2-22)}$$

where σ is relative density (relative to international standard atmosphere), and θ is relative temperature (relative to international standard atmosphere). Within the dynamic ship environment, the benefits of ground effect can be considered negligible [12]. Hence, only Out-of-Ground Effect (OGE), low speed, conditions are tested without any vertical speed. Thus, for a defined test condition in relative wind speed and relative wind direction, the factors affecting the performance of a family of geometrically similar helicopters with similar rotor blade profiles are reduced to:

$$P_{req,ref} = \frac{P_{req}}{\sigma\omega^3} = f\left(\frac{W}{\sigma\omega^2}, \frac{\omega}{\sqrt{\theta}}\right) \quad \textbf{(Eq. 5-2)}$$

The power required P_{req} is thus directly proportional to the relative density σ and the relative rotorspeed ω. It is indirectly dependent on the helicopter weight W and relative rotorspeed ω. Furthermore, the power required P_{req} is equivalent to the torque required Q_{req} multiplied by the relative rotorspeed ω:

$$P_{req} = Q_{req} \cdot \omega \quad \textbf{(Eq. 5-3)}$$

Thus:

$$Q_{req,ref} = \frac{Q_{req}}{\sigma\omega^2} = f\left(\frac{W}{\sigma\omega^2}, \frac{\omega}{\sqrt{\theta}}\right) \quad \textbf{(Eq. 5-4)}$$

The resulting equation for referred torque required indicates which items affect the torque required, although does not exactly tell how much these items influence it, as dimensional analysis will not predict the mathematical form of the equation nor the numerical constants in any way. In case the manufacturer's performance data is not available then the effects of varying $\omega/\sqrt{\theta}$ and other engine configuration parameters, such as variable Inlet Guide Vanes (IGV) and Variable Stator Vanes (VSV) on torque required should be considered. To simplify this process, it is assumed that the flight manual performance graphs incorporate any of these unforeseen effects. As such, without performing dedicated flight tests, these graphs are a reliable source of performance data and will be used in the calculations of the torque required at the desired helicopter referred weight and atmospheric conditions to be used for construction of the CFE (e.g. alternatively data from the shore-based hover trials can be used). The data of the flight manual performance graphs are inserted in the predictive tool "*SHOL-X*", and allow a linear interpolation at these discrete values to determine the torque trend factor Q_{trend} for a range of OAT at standard pressure at sea level as shown in Figure 5-11. The torque trend factor enables to determine the torque required at the desired conditions $Q_{req(desired)}$ of the various CFE's.

An example calculation for the torque required, at a specific test condition as determined during the shore-based hover trials, towards the desired helicopter referred weight and atmospheric conditions, to be used for construction of the CFE is given in the following:

Field elevation, h_{field}	= 158.0 ft
Hover height above ground level, h_{AGL}	= 60.0 ft
Air pressure with reference to mean sea level, QNH	= 1 012.5 mbar
Vertical change in height for 1 mbar difference, h_{Δ}	= 27.0 ft/mbar
OAT	= 16.0 °C
Main rotor rotational speed, Ω	= 104.0 % (default value)
Q_{req}	= 86.8 % (actual value)
W	= 10 050 kg (actual value)

Calculation of pressure height

Pressure height: $H_p = h_{field} + h_{AGL} + (QNH_{ISA} - QNH) \cdot h_{\Delta}$

$= 158.0 + 60.0 + (1013.25 - 1012.5) \cdot 27.0 = 231.5$ ft

Calculation of relative quantities

Relative pressure: $\delta = (1 - 6.8756 \times 10^{-6} \times H_p)^{5.2559} = 0.99166$

Relative temperature: $\theta = \dfrac{273.15 + \mathrm{OAT}}{288.15} = 1.00347$

Relative density: $\sigma = \dfrac{\delta}{\theta} = \dfrac{0.99166}{1.00347} = 0.98823$

Relative rotorspeed: $\omega = \dfrac{\Omega}{\Omega_0} = \dfrac{104.0}{104.0} = 1.00000$

Calculation of referred parameters

The referred torque required is:

$$Q_{req,ref} = \frac{Q_{req}}{\sigma\omega^2} = \frac{86.8}{0.98823 \cdot 1.00000^2} = 87.8\,\%$$

The actual achieved referred weight $W_{ref(achieved)}$ is:

$$W_{ref\,(achieved)} = \frac{W}{\sigma\omega^2} = \frac{10\,050}{0.98823 \cdot 1.00000^2} = 10169.7 \text{ kg}$$

Calculation towards desired referred weight and atmospheric conditions

In order to use the flight test data from this particular test point for other atmospheric conditions at sea level, the desired torque required is calculated as follows:

h_{field}	= 0.0 ft
h_{AGL}	= 0.0 ft
QNH	= 1 000.0 hPa
OAT	= 30.0 °C
$W_{desired}$	= 10 000 kg

Calculation of the desired pressure height

Pressure height: $H_{p(desired)} = h_{field} + h_{AGL} + (QNH_{ISA} - QNH) \cdot h_{\Delta}$

$= 0.0 + 0.0 + (1013.25 - 1000.0) \cdot 27.0 = 351.0$ ft

Calculation of the desired referred parameters

Relative pressure: $\delta_{(desired)} = (1 - 6.8756 \times 10^{-6} \times H_{p(desired)})^{5.2559} = 0.98738$

Relative temperature: $\theta_{(desired)} = \dfrac{273.15 + \text{OAT}}{288.15} = 1.05206$

Relative density: $\sigma_{(desired)} = \dfrac{\delta_{(desired)}}{\theta_{(desired)}} = \dfrac{0.98738}{1.05206} = 0.93852$

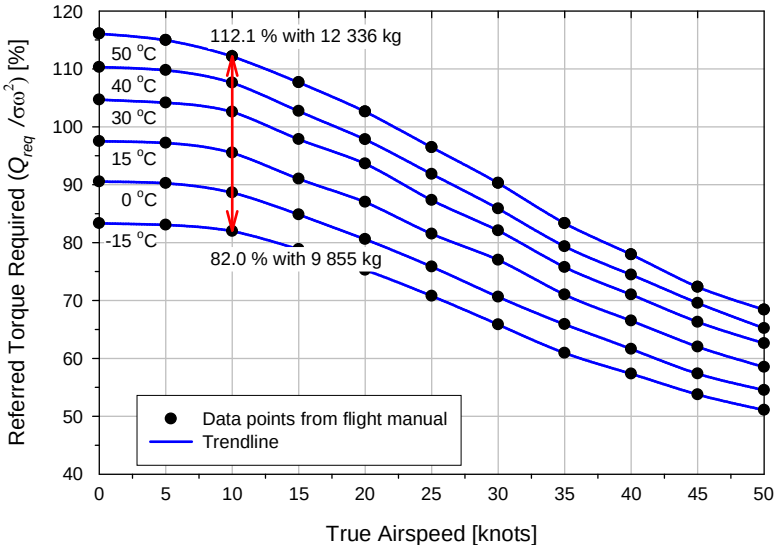

Figure 5-11; Example interpolation Q_{trend} at 11 000 kg (standard pressure)

(*regression trend line is* $y = a + bx + cx^2 + dx^3$)

The level flight performance graphs from the flight manual are used to ensure the correct trends are applied for the performance calculations towards the desired atmospheric conditions using referred parameters. For the maximum weight of the helicopter (i.e. 11 000 kg), an interpolation between referred weight $W/\sigma\omega^2$ and referred torque required $Q_{req}/\sigma\omega^2$ for the highest (i.e. 50 °C) and lowest (i.e. -15 °C) OAT, in standard conditions at sea level at the desired True Air Speeds (TAS) is performed as shown in Figure 5-11. In this case, for 100 % actual torque required (according flight manual) at 10 knots TAS with 50 °C gives 12 336 kg referred weight and 112.1 % referred torque required (i.e. σ = 0.89169), and at -15 °C with 91.5 % actual torque required (according flight manual) gives 9 855 kg referred weight and 82.0 % referred torque required (i.e. σ = 1.11621). The torque trend factor Q_{trend} is then calculated as follows:

$$Q_{trend} = \frac{dW}{dQ} = \frac{W_{ref\,(50^\circ C)} - W_{ref\,(-15^\circ C)}}{Q_{ref\,(50^\circ C)} - Q_{ref\,(-15^\circ C)}} = \frac{12\,336 - 9\,855}{112.1 - 82.0} = 82.2\ \text{kg/\%}$$

The referred weight in the desired atmospheric conditions $W_{ref(desired)}$ is:

$$W_{ref\,(desired)} = \frac{W}{\sigma\omega^2} = \frac{10\,000}{0.93852 \cdot 1.00000\text{^}2} = 10\,655.0\ \text{kg}$$

The actual torque required in the desired atmospheric conditions $Q_{req(desired)}$ is:

$$Q_{req(desired)} = \left(\frac{W_{ref\,(desired)} - W_{ref\,(achieved)}}{Q_{trend}} + Q_{req,ref} \right) \cdot \sigma\omega^2$$

$$= \left(\frac{10\,655.0 - 10\,169.7}{82.2} + 87.8 \right) \cdot 0.93852 \cdot 1.00000^2 = 88.0\,\%$$

Engine gas generator rotational speed N_g

The referred quantity for engine gas generator rotational speed $N_{g,ref}$ (see Eq. 2-18) for a helicopter with a constant main rotor speed, and thus free power turbine rotational speed N_f, only depends on the heat flow of the fuel ϕ_f as summarized below:

$$N_{g,ref} = \frac{N_g}{\sqrt{\theta}} = f\left(\frac{\phi_f}{\delta\sqrt{\theta}} \right) \qquad \textbf{(Eq. 5-5)}$$

where δ is relative pressure (relative to international standard atmosphere). The engine gas generator rotational speed N_g is thus dependent on the square root of the relative temperature θ, and is controlled by the collective pitch position input. The relation between the alternative groupings for referred torque required $Q_{req}\omega/\delta\sqrt{\theta}$ (see Eq. 2-28), commonly used for engine performance and referred engine gas generator rotation speed $N_{g,ref}$, follows from the flight test data of the shore-based hover trials as shown in Figure 5-12.

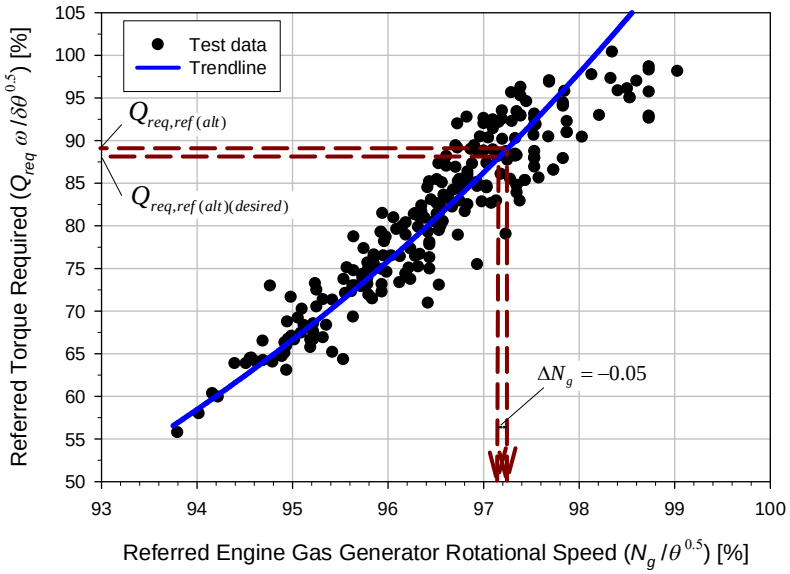

Figure 5-12; Example determination for ΔN_g
(*regression trend line is* $y = ax^b$)

An example calculation for the gas generator rotational speed N_g at a specific test condition as determined during the shore-based hover trials, towards the same desired conditions as for torque required is given in the following:

N_g = 97.2 %

Calculation of referred parameters

$$N_{g,ref} = \frac{N_g}{\sqrt{\theta}} = \frac{97.2}{\sqrt{1.00347}} = 97.0\,\%$$

The referred torque required for the alternative grouping $Q_{req,ref(alt)}$ results from combining Eq. 2-28 with Eq. 5.3:

$$Q_{req,ref\,(alt)} = \frac{Q_{req}\omega}{\delta\sqrt{\theta}} = \frac{86.8 \cdot 1.00000}{0.99166 \cdot \sqrt{1.00347}} = 87.4\,\%$$

$$Q_{req,ref\,(alt)(desired)} = \frac{Q_{req(desired)}\omega}{\delta_{(desired)}\sqrt{\theta_{(desired)}}} = \frac{88.0 \cdot 1.00000}{0.98738 \cdot \sqrt{1.05206}} = 86.9\,\%$$

The corresponding differences in referred gas generator rotational speed ΔN_g are determined using a figure of referred torque required $Q_{req}\omega/\delta\sqrt{\theta}$ against referred engine gas generator rotational speed $N_g/\sqrt{\theta}$, as shown in Figure 5-12. The desired gas generator rotational speed $N_{g\,(desired)}$ is now calculated as follows:

$$N_{g(desired)} = \left(N_{g,ref} + \Delta N_g\right) \cdot \sqrt{\theta_{(desired)}}$$
$$= \left(97.0 - 0.05\right) \cdot \sqrt{1.05206} = 99.5\,\%$$

Engine power turbine inlet temperature T_{46}

The referred quantity for engine power turbine inlet temperature $T_{46,ref}$ (see Eq. 2-19) for a helicopter with a constant main rotor speed, and thus free power turbine rotational speed N_f, is only dependent of the heat flow of the fuel ϕ_f as summarized below:

$$T_{46,ref} = \frac{T_{46}}{\theta} = f\left(\frac{\phi_f}{\delta\sqrt{\theta}}\right) \qquad \textbf{(Eq. 5-6)}$$

The engine power turbine inlet temperature is thus dependent on the relative temperature θ, and is indirectly controlled by the collective pitch position input. The relation between the alternative grouping for referred torque required $Q_{req}\omega/\delta\sqrt{\theta}$ (see Eq. 2-28) commonly used for engine performance and referred engine power turbine inlet temperature $T_{46,ref}$ follows from the flight test data of the shore-based hover trials as shown for example in Figure 5-13.

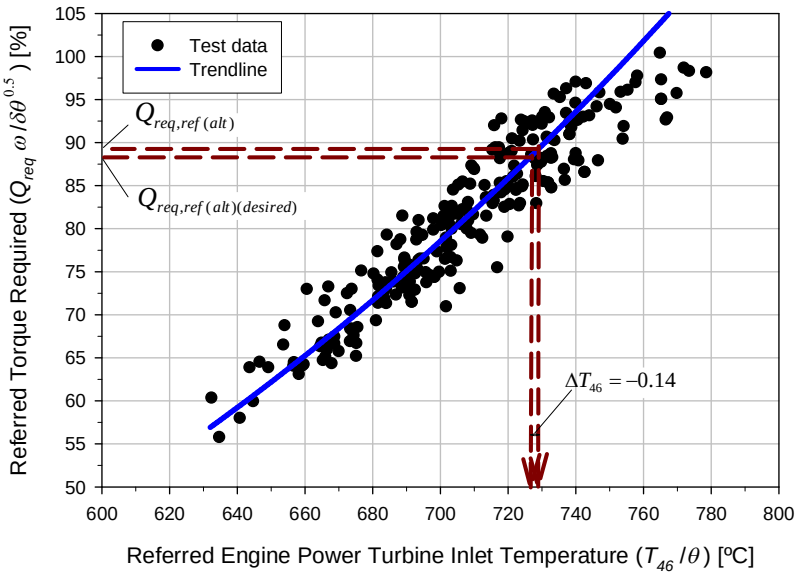

Figure 5-13; Example determination for ΔT_{46}
(*regression trend line is* $y = ax^b$)

An example calculation for the power turbine inlet temperature T_{46}, at a specific test condition as determined during the shore-based hover trials, towards the same desired conditions as for torque required is given in the following:

T_{46} = 731.2 ˚C

Calculation of referred parameters

$$T_{46,ref} = \frac{T_{46}}{\theta} = \frac{731.2}{1.00347} = 728.7\ ^{\circ}\mathrm{C}$$

The referred torque required for the alternative grouping $Q_{req,ref(alt)}$ results from combining Eq. 2-28 with Eq. 5.3:

$$Q_{req,ref\,(alt)} = \frac{Q_{req}\omega}{\delta\sqrt{\theta}} = \frac{86.8 \cdot 1.00000}{0.99166 \cdot \sqrt{1.00347}} = 87.4\,\%$$

$$Q_{req,ref\,(alt)(desired)} = \frac{Q_{req(desired)}\omega}{\delta_{(desired)}\sqrt{\theta_{(desired)}}} = \frac{88.0 \cdot 1.00000}{0.98738 \cdot \sqrt{1.05206}} = 86.9\,\%$$

The corresponding differences in referred power turbine inlet temperature ΔT_{46} are determined using a figure of referred torque required $Q_{req}\omega/\delta\sqrt{\theta}$ against referred engine power turbine inlet temperature T_{46}/θ, as shown in Figure 5-13. The desired power turbine inlet temperature $\Delta T_{46(desired)}$ is now calculated as follows:

$$T_{46(desired)} = \left(T_{46,ref} + \Delta T_{46}\right) \cdot \theta_{(desired)}$$

$$= \left(728.7 - 0.14\right) \cdot 1.05206 = 765.1\ ^{\circ}\mathrm{C}$$

5.5.2.2 Part for Power Available Calculations

The part for the power available calculations of the helicopter performance sub-model is divided into two items. First, the calculation of the performance limiting parameter(s) for specific environmental conditions. Secondly, the construction of a weight correction chart to be used by operational crew to determine which SHOL envelope they have to use. In addition, although not further discussed, the impact for the power available by various helicopter configuration changes can be added and/or subtracted.

Performance limiting parameter(s)

The objective is to determine the performance parameter(s) that will limit the helicopter capabilities under the atmospheric conditions in a role specification. The analysis requires access to engine performance data, i.e. flight manual performance graphs, performance flight test data form shore-based hover trials, transmission and engine limitations [13,14,15,16]. The analysis starts by obtaining the actual limiting values for the Maximum Continuous Power (MCP) of the transmission and engine parameters: $Q_{(LIMIT)}$, $N_{g(LIMIT)}$ and $T_{46(LIMIT)}$. Using the pressure height and specified air temperature, the performance limiting parameters are calculated as follows [17]:

The Transmission Limited Referred Power (TLRP) is calculated by:

$$TLRP = \frac{Q_{(LIMIT)}\omega}{\delta\sqrt{\theta}} \qquad \textbf{(Eq. 5-7)}$$

Note that the alternative non-dimensional group is used for torque available (applicable to engine performance). The Engine Speed Limited Referred Power (ESLRP) is determined using a figure of referred power required $P_{req}/\delta\sqrt{\theta}$ against referred engine gas generator rotational speed $N_g/\sqrt{\theta}$, as shown for example in Figure 5-14, and the value:

$$ESLRP = \frac{N_{g\,(LIMIT)}}{\sqrt{\theta}} \qquad \textbf{(Eq. 5-8)}$$

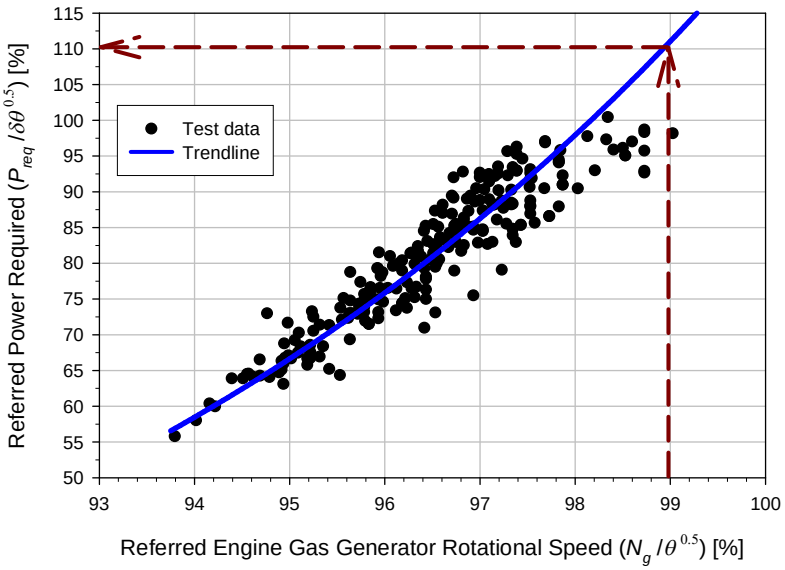

Figure 5-14; Example engine test data - N_g
(*regression trend line is* $y = ax^b$)

The Engine Temperature Limited Referred Power (ETLRP) is determined using a figure of referred power required $P_{req}/\delta\sqrt{\theta}$ against referred engine power turbine inlet temperature T_{46}/θ, as shown in Figure 5-15, and the value:

$$ETLRP = \frac{T_{46\,(LIMIT)}}{\theta} \qquad \textbf{(Eq. 5-9)}$$

If either the ETLRP or the ESLRP is less than the TLRP, then the helicopter performance will be engine limited under the conditions specified. It is now possible to determine the maximum performance available P_a, for the most conservative parameter by choosing the lowest limited referred power, now called $LRP_{(MIN)}$, and calculate the maximum available referred power $P_{a,ref}$ from:

$$P_{a,ref} = \frac{P_a}{\sigma\omega^3} = LRP_{(MIN)}\left(\frac{\sqrt{\theta}}{\omega}\right)^3 \qquad \textbf{(Eq. 5-10)}$$

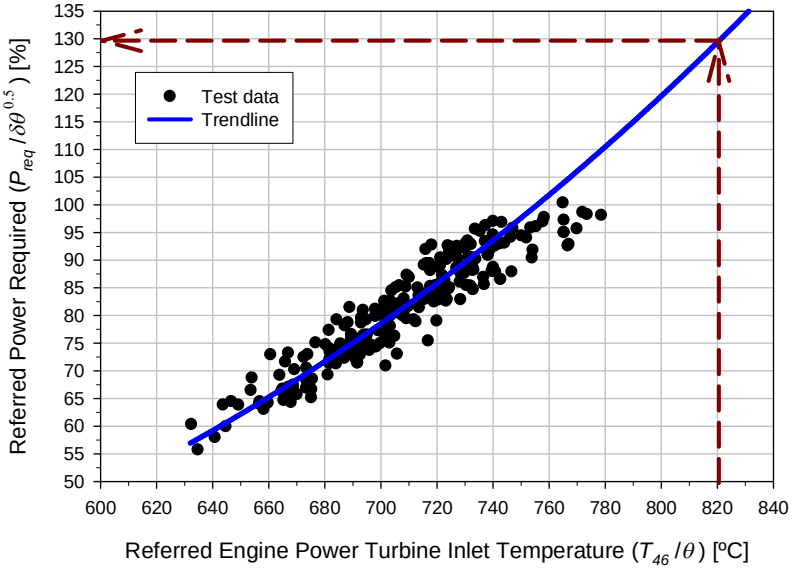

Figure 5-15; Example engine test data - T_{46}
(*regression trend line is* $y = ax^b$)

Using a figure of referred power required $P_{req}/\sigma\omega^3$ against referred helicopter weight $W/\sigma\omega^2$, constructed from the flight manual graphs, determines the maximum referred weight $W_{(MAX,ref)}$ for hover Out-of-Ground Effect (OGE) using the maximum available referred power $P_{a,ref}$ determined with Eq. 5-10 as shown in Figure 5-16. Note that this is a cross-section from Figure 5-11 at 0 knots. It shows that for small correction in torque required a linear interpolation is reasonable, although for large variations a more complex interpolation would be required. Therefore, to minimize any errors introduced by the linear interpolation for torque required within "*SHOL-X*", the flight test data from the shore-based hover trials are corrected towards the nearest applicable referred weight band (e.g. 10 000 kg, 11 000 kg and 11 600 kg referred weight).

Power margins are obtained by comparing the maximum available power P_a, found by de-referring $P_{a,ref}$ with the actual power required for hover OGE at the mission weight under the atmospheric conditions specified. The actual maximum weight $W_{(MAX)}$ can then be calculated:

$$W_{(MAX)} = W_{(MAX,ref)} \cdot \sigma_{(desired)} \cdot \omega^2_{(desired)} \qquad \textbf{(Eq. 5-11)}$$

This value is used to determine a variety of performance limiting parameters as shown for example in Figure 5-17. This figure indicates the performance limiting parameters for a range of OAT at standard pressure at sea level, including the performance limiting

parameters in case a safety margin is applied of one standard deviation due to the randomness in the flight test data (red dashed line in figure).

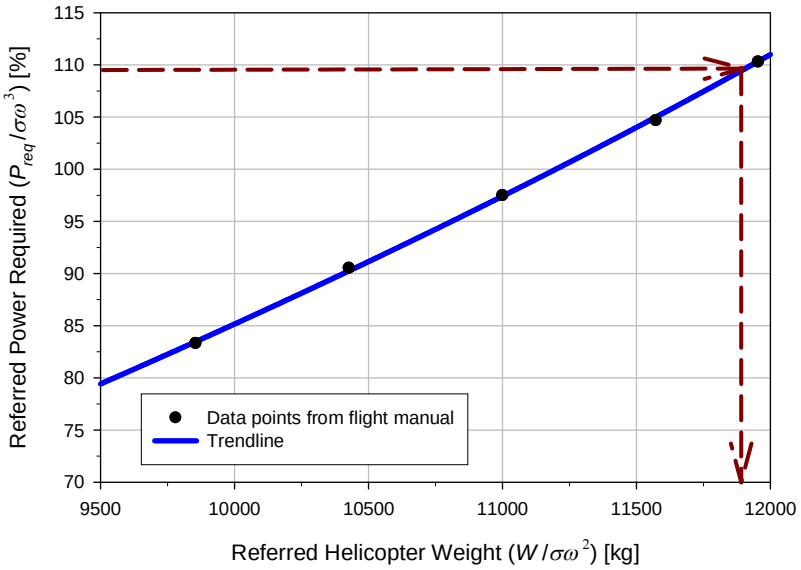

Figure 5-16; Example of limiting performance for hover
(*regression trend line is* $y = a + bx + cx^2$)

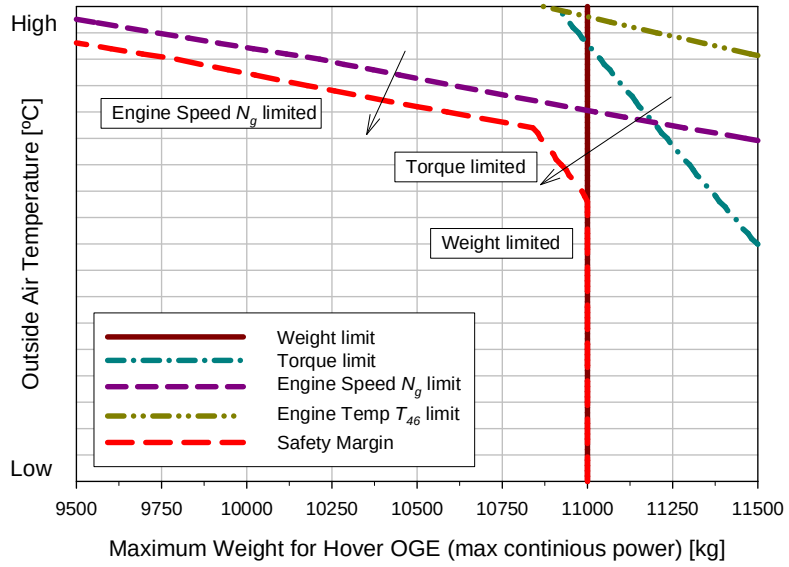

Figure 5-17; Example limits for hover OGE with MCP at sea level

Initially, the Maximum Take-Off Weight (MTOW) as determined by the helicopter manufacturer restricts the performance of the helicopter (i.e. weight limited). For higher OAT the helicopter performance, and thus maximum weight for hover OGE,

will be restricted by the engine gas generator rotational speed N_g (i.e. engine speed N_g limited). Note that the line for engine gas generator rotational speed N_g is not straight, due to the variations in actual limitations with OAT. In this case, the engine power turbine inlet temperature T_{46} causes no restrictions. The torque required causes no restriction in case the MCP values are applied. However, in case a safety margin of one standard deviation is taken into account (e.g. 5.2 % for torque required), it shows that for a certain range in OAT, the helicopter performance will be restricted by the torque required (i.e. torque limited). This information about the limiting performance parameter(s) is essential for the construction of the CFE.

An example calculation for the performance limiting parameter(s) at maximum continuous power, without a safety margin applied, at sea level with standard pressure is shown in the following:

OAT	= 30.0 °C
Main rotor rotational speed, Ω	= 104.0 % (default value)
$Q_{(LIMIT)}$	= 104.0 %
$N_{g(LIMIT)}$	= 101.5 % at 30.0 °C (varies with OAT)
$T_{46(LIMIT)}$	= 863.0 °C

Calculation of pressure height

Pressure height: $H_{p_{(desired)}} = h_{field} + h_{AGL} + (QNH_{ISA} - QNH) \cdot h_{\Delta}$

$$= 0.0 + 0.0 + (1013.25 - 1013.25) \cdot 27.0 = 0.0 \text{ ft}$$

Calculation of relative quantities

Relative pressure: $\delta_{(desired)} = (1 - 6.8756 \times 10^{-6} \times H_p)^{5.2559} = 1.00000$

Relative temperature: $\theta_{(desired)} = \dfrac{273.15 + \text{OAT}}{288.15} = 1.05206$

Relative density: $\sigma_{(desired)} = \dfrac{\delta}{\theta} = \dfrac{1.00000}{1.05206} = 0.95052$

Relative rotorspeed: $\omega_{(desired)} = \dfrac{\Omega}{\Omega_0} == \dfrac{104.0}{104.0} = 1.00000$

Calculation of performance limiting parameters

The TLRP is calculated as follows:

$$TLRP = \frac{Q_{(LIMIT)}\omega_{(desired)}}{\delta_{(desired)}\sqrt{\theta_{(desired)}}} = \frac{104.0 \cdot 1.00000}{1.00000 \cdot \sqrt{1.05206}} = 101.4\,\%$$

The ESLRP follows from the referred gas generator rotational speed $N_{g,ref}$ and Figure 5-14:

$$N_{g,ref\,(LIMIT)} = \frac{N_{g\,(LIMIT)}}{\sqrt{\theta_{(desired)}}} = \frac{101.5}{\sqrt{1.05206}} = 99.0\,\%$$

Gives:

$$ESLRP = 110.5\,\%$$

The ETLRP follows from the referred engine power turbine inlet temperature $T_{46,ref}$ and Figure 5-15:

$$T_{46,ref\,(LIMIT)} = \frac{T_{46\,(LIMIT)}}{\theta_{(desired)}} = \frac{863.0}{1.05206} = 820.3\ ^{\circ}\mathrm{C}$$

Gives:

$$ETLRP = 129.5\,\%$$

The LRP_{MIN} is then caused by the limitations in torque required:

$$LRP_{(MIN)} = 101.4\,\%$$

The maximum available referred power $P_{a,ref}$ is then:

$$P_{a,ref} = \frac{P_a}{\sigma\omega^3} = LRP_{(MIN)}\left(\frac{\sqrt{\theta_{(desired)}}}{\omega_{(desired)}}\right)^3 = 101.4\cdot\left(\frac{\sqrt{1.05206}}{1.00000}\right)^3 = 109.4\,\%$$

The maximum referred weight $W_{(MAX,ref)}$ follows from Figure 5-16:

$$W_{(MAX,ref)} = 11888.7\ \mathrm{kg}$$

The actual maximum weight $W_{(MAX)}$ can then be calculated:

$$W_{(MAX)} = W_{(MAX,ref)}\cdot\sigma_{(desired)}\cdot\omega^2_{(desired)}$$

$$= 11888.7\cdot 0.95052\cdot 1.00000^2 = 11300.4\ \mathrm{kg}$$

Since the MTOW of the helicopter is 11 000 kg, there are no additional restrictions due to helicopter performance at 30.0 °C at sea level with standard pressure (i.e. $W_{(MAX)}$ = 11 000 kg). This corresponds with being weight limited as shown in Figure 5-17.

Weight correction chart

To accommodate for varying atmospheric conditions, a weight correction chart can be used by operational squadron pilots as shown in Figure 5-18. To calculate the values

for the weight correction, the maximum take-off weight W_{MTOW} (i.e. 11 000 kg) is chosen as the representative referred weight at the desired environmental conditions $W_{MTOW,ref}$ as specified in the previous example calculation (i.e. 11 572 kg referred weight for 30 ˚C with σ = 0.95052). The weight correction, giving the same power margin as for the MTOW, can now be calculated as:

$$\Delta W = W_{MTOW,ref} - W_{(MAX)} \qquad \textbf{(Eq. 5-12)}$$

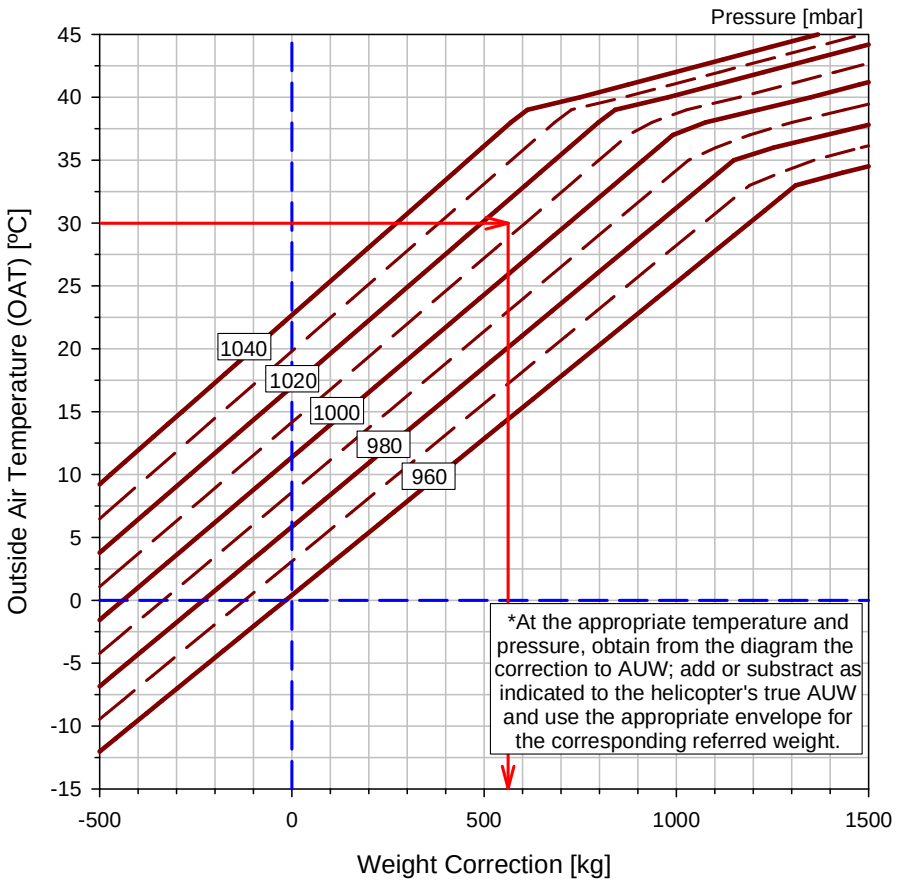

Figure 5-18; Weight correction chart

By calculating the actual maximum weight $W_{(MAX)}$ for different combinations of temperature and pressure the weight correction chart is constructed. This is shown for different lines of constant pressure allowing one graph for the operator to decide in which band their helicopter falls and to use the appropriate SHOLs with the corresponding referred weight. The weight correction chart allows a means for determining the appropriate SHOL for a given OAT, ambient air pressure and All-Up Weight (AUW). Alternatively, the weight correction chart can be used during flight planning to determine the MTOW for a given OAT, ambient air pressure and particular SHOL. This method is required as converting the operational AUW to referred weight

will not retain the transmission torque margins and engine power margins as seen during the trials, as power available is not a simple function of the relative density σ.

5.5.2.3 Part for Achievable Climb Performance Calculations

This part of the sub-model for helicopter performance is used to calculate the achievable climb performance. For each test point the achieved Rate Of Climb (ROC), *C*, is expressed against the deltas (i.e. the differences), between the torque required in hover Q_{req} and the maximum torque utilised Q_{uti} in the climb. This is determined with the Maximum Power Vertical (MPV) tests during the shore-based hover trials. The result is called the maximum power vertical climb coefficient C_{MPV}:

$$C_{MPV} = \frac{C}{(Q_{uti} - Q_{req})} \qquad \textbf{(ref Eq. 4-10)}$$

This result allows that the extra power required to climb can be simply added to that required for level flight by a linear relationship to calculate the maximum achievable climb performance $C_{(MAX)}$:

$$C_{(MAX)} = (Q_a - Q_{req}) \cdot C_{MPV} \qquad \textbf{(Eq. 5-13)}$$

In case, the maximum achievable climb performance $C_{(MAX)}$ is less than the vertical component of the airwake in the vicinity of the ship, it is indicated in the CFE. These areas have to be avoided during the sea trials or progressed towards very carefully with small steps in difficulty (i.e. incremental approach).

An example calculation for the maximum achievable climb performance, at 20 knots true airspeed, is shown in the following:

C_{MPV} = approximately 55.0 ft/min/% (see Fig 4-17 in Chapter 4)
Q_a = 104.0 %
Q_{req} = 85.4 %

Thus, to calculate the maximum achievable climb performance $C_{(MAX)}$:

$$C_{(MAX)} = (Q_a - Q_{req}) \cdot C_{MPV} = (104.0 - 85.4) \cdot 55.0 = 1023.0 \text{ ft/min}$$

5.5.3 Sub-Model Helicopter Control Positions

There are various inputs required for the helicopter control positions sub-model, i.e. torque required, tail rotor actuator position, pedal position, longitudinal cyclic, lateral cyclic and Centre of Gravity (CG) as shown in Figure 5-19. The algorithm takes into account the torque required as calculated by the helicopter performance sub-model such that it interacts with the tail rotor actuator position. The output from the helicopter control positions sub-model results in detailed knowledge about the remaining control authority for the desired torque required and CG positions which are relevant for the construction of the CFE, i.e. desired tail rotor actuator position, desired pedal position, desired longitudinal cyclic position and desired lateral cyclic position.

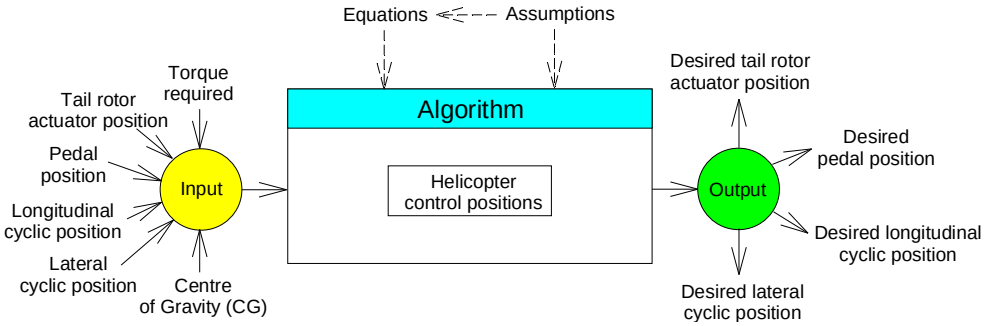

Figure 5-19; Overview elements helicopter control positions sub-model

Tail rotor actuator position

For a particular test condition with a defined relative wind speed and relative wind direction (thus defined yawing moment on the fuselage and fin), the tail rotor actuator position depends on the referred weight, i.e. torque required, as with changes in torque required the tail rotor has to deliver more or less anti-torque to maintain helicopter heading. In case the torque required is adjusted to the desired conditions by the helicopter performance model, changes are made by a linear relationship to assess the remaining tail rotor control authority. The changes in tail rotor actuator position $TR_{actuator}$, are proportional to the torque required in the desired conditions $Q_{req(desired)}$ divided by the torque required Q_{req} at the tested condition. For the tail rotor actuator position in the desired conditions $TR_{actuator(desired)}$ follows:

$$TR_{actuator(desired)} = \frac{Q_{req(desired)}}{Q_{req}} \cdot TR_{actuator} \qquad \textbf{(Eq. 5-14)}$$

An example calculation for the tail rotor actuator position in the desired condition $TR_{actuator(desired)}$ is shown in the following:

$Q_{desired}$ = 88.0 %

Q_{req} = 86.8 %

$TR_{actuator}$ = 68.0 %

Thus, to calculate the tail rotor actuator position in the desired conditions:

$$TR_{actuator(desired)} = \frac{Q_{req(desired)}}{Q_{req}} \cdot TR_{actuator} = \frac{88.0}{86.8} \cdot 68.0 = 68.9\,\%$$

Pedal position

For a particular test condition with a defined relative wind speed and relative wind direction, the pedal position has negligible influence from the referred weight, i.e. torque required, as the fly-by-wire flight control system acts as a collective-yaw interlink which compensates variations in pedal deflection caused by torque variations. Therefore, there are no changes made to the pedal position as determined during the shore-based hover trials by the predictive tool.

Longitudinal and lateral cyclic position

For a particular test condition with a defined relative wind speed and relative wind direction, both the longitudinal cyclic δ_{long} and lateral cyclic δ_{lat} position depend on the CG location. The longitudinal and lateral cyclic positions can be adjusted towards the desired CG position, with a linear relationship by multiplying with the respective cyclic CG correction coefficients, $CG_{cor(long)}$ and $CG_{cor(lat)}$. In addition, the maximum achievable deviations in forward and aft cyclic positions, and left and right cyclic positions, achievable within the CG envelope, are determined to assess adequate cyclic control authority throughout the compete cyclic control envelope. The longitudinal cyclic position in the desired condition $\delta_{long(desired)}$ is calculated by the longitudinal cyclic position δ_{long}, subtracted with the longitudinal distance between the desired CG location $CG_{long(desired)}$ and the tested CG location CG_{long}, multiplied with the CG correction coefficient for longitudinal cyclic $CG_{cor(long)}$:

$$\delta_{long(desired)} = \delta_{long} - (CG_{long(desired)} - CG_{long}) \cdot CG_{cor(long)} \qquad \textbf{(Eq. 5-15)}$$

The lateral cyclic position in the desired condition $\delta_{lat(desired)}$ is calculated by the lateral cyclic position δ_{lat}, subtracted with the lateral distance between the desired CG location $CG_{lat(desired)}$ and the tested CG location CG_{lat}, multiplied with the CG correction coefficient for lateral cyclic $CG_{cor(lat)}$:

$$\delta_{lat(desired)} = \delta_{lat} - (CG_{lat(desired)} - CG_{lat}) \cdot CG_{cor(lat)} \qquad \textbf{(Eq. 5-16)}$$

An example calculation for the longitudinal cyclic position at the desired condition $\delta_{long(desired)}$ is shown in the following:

δ_{long} = 65.9 %

$CG_{long(desired)}$ = 713.0 cm

CG_{long} = 704.7 cm

$CG_{cor(long)}$ = 0.27 %/cm (see Table 4-2 in Chapter 4)

$$\delta_{long(desired)} = \delta_{long} - (CG_{long(desired)} - CG_{long}) \cdot CG_{cor(long)}$$
$$= 65.9 - (713.0 - 704.7) \cdot 0.27 = 63.6\,\%$$

The desired CG location is more aft of the CG position as tested during the shore-based hover trials. Consequently, the more aft CG position causes a corresponding forward cyclic movement.

5.5.4 Sub-Model Helicopter Attitudes

There are various inputs required for the helicopter attitudes sub-model, i.e. pitch attitude, roll attitude and CG as shown in Figure 5-20. The output from the helicopter attitudes sub-model results in detailed knowledge about the limiting helicopter attitudes which are relevant for the construction of the CFE, i.e. desired pitch attitude and desired roll attitude. For a particular test condition with a defined relative wind speed and relative wind direction, both the pitch attitude θ_f and roll attitude ϕ_f of the helicopter depend on the CG location. The pitch attitude and roll attitude can be

adjusted towards the desired CG position, by multiplying with the respective attitude CG correction coefficients, $CG_{cor(pitch)}$ and $CG_{cor(roll)}$. In addition, the maximum achievable deviations in pitch-up and pitch-down attitude, and left and right roll attitude, achievable within the CG envelope, are determined to assess the impact on flight operations.

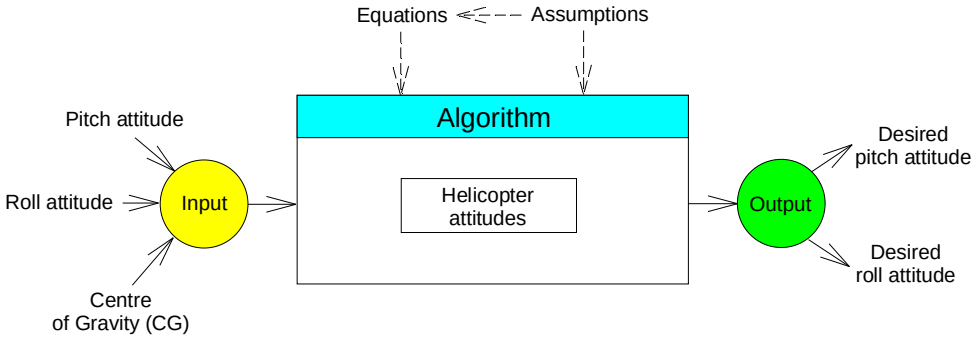

Figure 5-20; Overview elements helicopter attitudes sub-model

The pitch attitude in the desired condition $\theta_{f(desired)}$ is calculated by the pitch attitude θ_f, added with the longitudinal distance, between the desired CG location $CG_{long(desired)}$ and the tested CG location CG_{long}, multiplied with the CG correction coefficient for pitch attitude $CG_{cor(pitch)}$:

$$\theta_{f(desired)} = \theta_f + (CG_{long(desired)} - CG_{long}) \cdot CG_{cor(pitch)} \qquad \textbf{(Eq. 5-17)}$$

The roll attitude in the desired condition $\phi_{f(desired)}$ is calculated by the roll attitude ϕ_f, added with the lateral distance, between the desired CG location $CG_{lat(desired)}$ and the tested CG location CG_{lat}, multiplied with the CG correction coefficient for roll attitude $CG_{cor(roll)}$:

$$\phi_{f(desired)} = \phi_f + (CG_{lat(desired)} - CG_{lat}) \cdot CG_{cor(roll)} \qquad \textbf{(Eq. 5-18)}$$

An example calculation for the pitch attitude at the desired condition $\theta_{f(desired)}$ is shown in the following:

θ_f	= 3.3 °
$CG_{long(desired)}$	= 713.0 cm
CG_{long}	= 704.7 cm
$CG_{cor(pitch)}$	= 0.08 °/cm (see Table 4-2 in Chapter 4)

$$\theta_{f(desired)} = \theta_f + (CG_{long(desired)} - CG_{long}) \cdot CG_{cor(pitch)}$$

$$= 3.3 + (713.0 - 704.7) \cdot 0.08 = 4.0\ ^\circ$$

The desired CG location is more aft of the CG position as tested during the shore-based hover trials. Consequently, the more aft CG position causes a corresponding pitch-up movement of the helicopter.

5.6 Summary Inputs and Outputs of the Predictive Tool

A summary of the inputs and outputs for the various sub-model of the predictive tool is shown in Table 5-2.

Input	Output
Sub-model atmospheric boundary layer	
Boundary layer profile Ship parameters	Correlation between local wind speeds near and above flight deck V_{fd} with the indicated wind speeds at the anemometer locations V_{an}
Sub-model ship airwake	
Wind tunnel measurements Desired take-off and landing procedure Desired take-off and landing spot	Three-dimensional ship environment for desired procedure at desired take-off and landing spot
Sub-model subjective pilot ratings	
Pilot workload Helicopter vibration levels Turbulence levels	Rough guideline for potential areas to be tested during the sea trials with regard to pilot workload
Sub-model helicopter performance	
Torque required Engine gas generator rotational speed N_g Engine power turbine inlet temperature T_{46} Helicopter weight Atmospheric conditions Helicopter parameters Helicopter configuration	Desired torque required Desired engine gas generator rotational speed N_g Desired engine power turbine inlet temperature T_{46} Performance limiting parameter Maximum achievable climb performance
Sub-model helicopter control positions	
Torque required Tail rotor actuator position Pedal position Longitudinal cyclic position Lateral cyclic position Centre of Gravity (CG)	Desired tail rotor actuator position Desired pedal position Desired longitudinal cyclic position Desired lateral cyclic position
Sub-model helicopter attitudes	
Pitch attitude Roll attitude Centre of Gravity (CG)	Desired pitch attitude Desired roll attitude

Table 5-2; Summary inputs and outputs of the predictive tool

5.7 Predictions of the Candidate Flight Envelope

When the behaviour of the isolated helicopter and the local environment conditions of a particular ship type are combined by the predictive tool, it results in the CFE. The CFE is a diagram giving the likely combinations of indicated wind speed (in radial coordinates) and direction (in angular coordinates) for safe take-offs and landings from a particular ship type. The CFE is used to increase trial effectiveness as it functions as the starting point for sea trials. The aim of the CFE is the smallest possible number of flying hours that does not affect the quality of the results and/or safety standards. Subsequent flight tests are then concentrated at and around the potential boundaries, reducing flight test time, and for example easing the difficulties of ship availability and the vagaries of the weather. In fact, the CFE is the preliminary envelope, whilst the SHOL is the result of sea trials and is the ultimate version defining the safe operational limitations.

5.7.1 Model Calibration of the Predictive Tool

With the model code verified, and validated at sub-model level, the next step is to calibrate the predictive tool as a whole. Based on the sub-models calibration results, it might be expected that the connected total model gives approximately the same agreement between computation and experimental data. This is however not necessarily the case due to the propagation of errors. The calibration phase is used to improve agreement between the computational results and the experimental data obtained by actual sea trials. By adjusting uncertain parameters of the predictive tool, the level of agreement can often be improved significantly. It should however be kept in mind that short-sighted use of model calibration (or fine-tuning of the safety margins) may result in the right model output for the wrong reason. Too often, model calibration is (unintentionally) used to cover up the weaknesses of the underlying conceptual (sub) models.

The only noteworthy calibration performed for the predictive tool is an increase in the minimum wind speed as determined during the wind-tunnel tests, and applied towards the helicopter flight characteristics. Possible causes for the discrepancy between the predictive tool and the experimental data could be either:

- The absence of ground effect in the model;
- The absence in the model for the various blade sections of the rotor experiencing a spatially distributed flow field at each instant of time (as seen inside airwake of a ship), compared to the various blade sections of the same rotor experiencing a basically spatially homogenous flow field (as seen in shore-based hover trials);
- Too large safety margins for the rejection criteria;
- Different piloting techniques in case the helicopter is power limited;
- The application of minimum and maximum wind values throughout the whole approach and departure paths whilst certain phases thereof may be more relevant;
- Any combination of the above items.

In addition, any variance in Power Performance Index (PPI) may influence the engine performance. After the simple calibration of the predictive tool by adjusting the minimum wind speed, the agreement seems to be acceptable from a qualitative point of view, which will be quantified in the next chapter about sea trials and validation. Of course, this does not mean that with the simplifications made in the model (e.g. the absence of a spatially distributed flow field for the various blade sections in the ship airwake), it is assumed that the flow fields encountered during the shore-based hover trials and sea trials are very similar from an aerodynamic perspective. However, the model calibration has demonstrated that the effects on e.g. torque required and flight controls is small enough to be captured by the safety margins.

5.7.2 Construction of the Candidate Flight Envelope

To demonstrate the process for the construction of the CFE, two examples for different ship types, that were not used during model calibration, are given for the fore-aft take-off and landing procedure at 10 000 kg, 11 000 kg and 11 600 kg referred weight with an aft-CG. Note that the shore-based hover trials were performed up to 11 750 kg referred weight, whilst the CFE are only developed up to 11 600 kg referred weight. A somewhat lower maximum referred weight is chosen for the Hot & Heavy conditions on board ships, to allow flight operations to be conducted within the speed bracket of the ship's cruise engines in calm wind conditions. Otherwise, the ship's high speed gas turbines would always have to be available in calm wind conditions to operate the helicopter, which unless operational scenarios dictate is not desirable. The first set of examples for a particular ship type is shown for the relevant referred weights in Figure 5-21, Figure 5-23 and Figure 5-25, respectively. The second set of examples for a particular ship type is shown for the relevant referred weights in Figure 5-22, Figure 5-24 and Figure 5-26, respectively. Note that for clarity only the rejection criteria are indicated in the sector between red 110° to green 110° above 10 knots (i.e. not in the aft sector). The following rejection criteria were relevant for construction of the CFE for the NH90 NFH as discussed in Chapter 4:

- Torque required for the lower relative wind speeds;
- It was noted that right pedal position exceeds the 10% safety margin in red wind conditions;
- Pitch attitudes around green 30° at 30 knots;
- Roll attitude in red wind conditions;
- From previous sea trials it was noted that torque required exceeds the rejection criteria in the red 90° azimuth (input miscellaneous items);
- The boundaries for a Hot & Heavy envelope have an additional safety margin due to the more sluggish helicopter response (input miscellaneous items).

For the construction of the CFE the indicated rejection criteria should be excluded as much as possible. In both examples, for all three referred weights, the rejection criteria for pedal position (red wind conditions), pitch attitude (green wind conditions) and roll attitude (red wind conditions) are restricting the CFE (brown dash-dotted line in figure) in similar relative wind conditions.

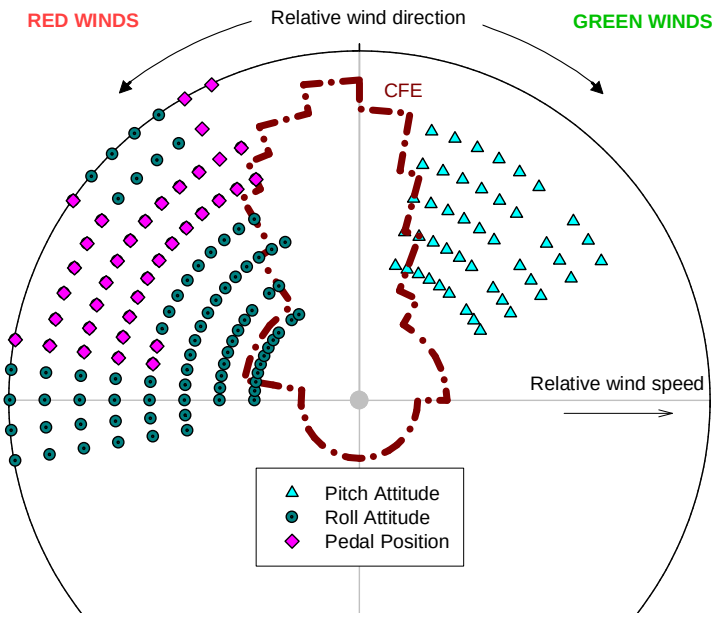

Figure 5-21; CFE for 10 000 kg referred weight - *Example 1*

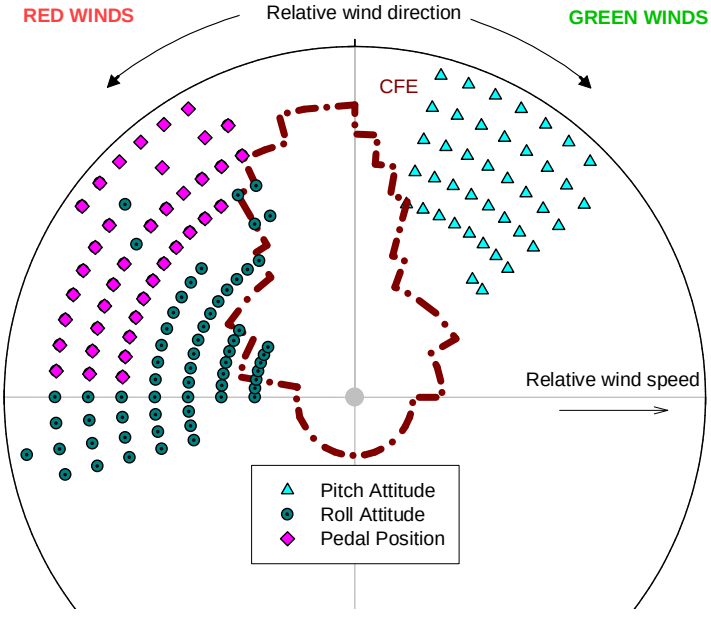

Figure 5-22; CFE for 10 000 kg referred weight - *Example 2*

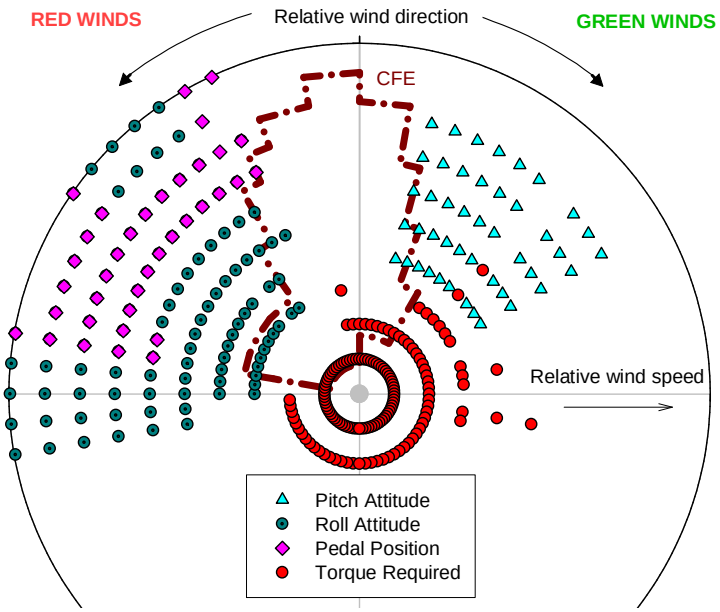

Figure 5-23; CFE for 11 000 kg referred weight - *Example 1*

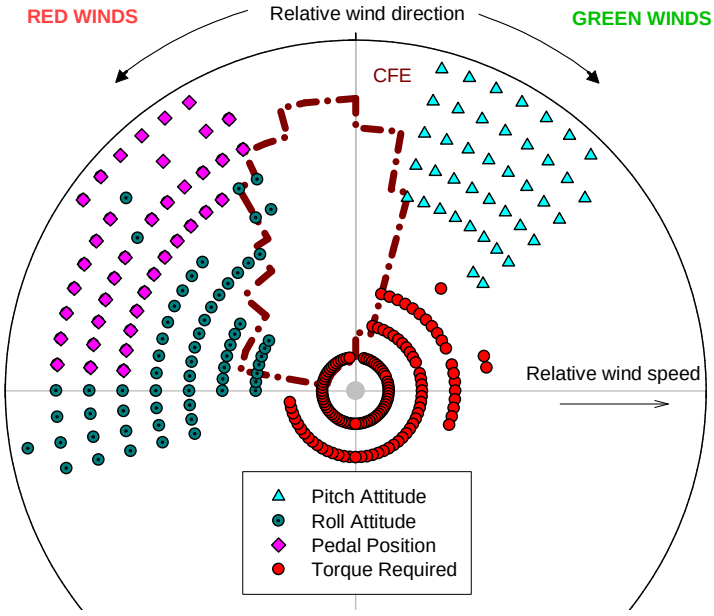

Figure 5-24; CFE for 11 000 kg referred weight - *Example 2*

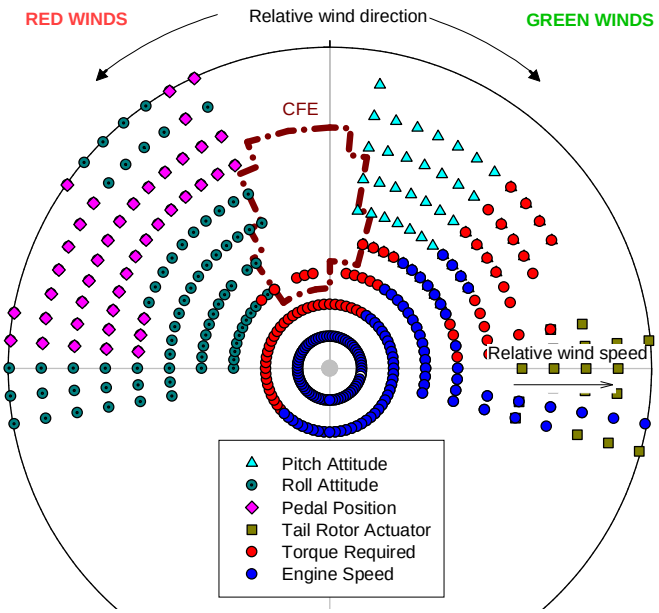

Figure 5-25; CFE for 11 600 kg referred weight - *Example 1*

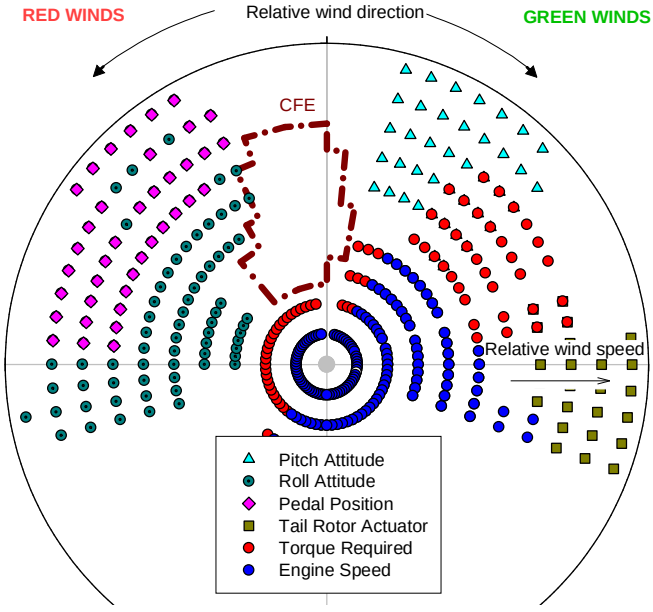

Figure 5-26; CFE for 11 600 kg referred weight - *Example 2*

This is because, as demonstrated by the shore-based hover trials, an increase in referred weight has negligible influence on pedal position, longitudinal cyclic, lateral cyclic, pitch attitude and roll attitude. The differences between the CFE's in referred weight are mainly in the lower speed regions, due to an increase in torque required for the higher referred weights. This is because, as demonstrated by the shore-based hover trials, increases in referred weight results in an increase in torque required, engine gas generator rotational speed N_g, engine power turbine inlet temperature T_{46} and tail rotor actuator position. As a result, for higher referred weights, an associated minimum relative wind speed is required to perform flight operations.

Turbulence level

The wind tunnel measurements used to predict the ship's airwake are average values, which do not take into account the variety in wind speed or wind direction. However, in reality there is an associated turbulence level for a particular relative wind condition for each ship type. Generally, the turbulence level increases with increasing relative wind speed, and vice versa. The turbulence level can increase to such a high level that the helicopter responds violently in pitch and roll attitude, which causes corresponding torque spikes, increased control activity and higher pilot workload. Typically, these high turbulence levels resulting in violent helicopter responses also define the upper boundaries of the SHOL envelope. There is still some engineering judgement required to set the upper boundaries for the CFE of a particular ship type correctly. Unless adequate safety margins are applied, the upper boundaries are the main focus of the sea trials. Further research should thus focus on identifying areas with increased turbulence, including the associated response to helicopter flight characteristics, such that this could be included in the predictions for the CFE.

Night operations

Different envelopes are produced for use by day and by night. The closure rate to the ship during the approach to the ship is more difficult to judge at night, which may result in a last-minute flare to arrest closure rates and potentially leading to an exceedance of power limitations and/or overshooting the approach. This is undesirable and for safety reasons no tail winds are allowed during night operations. In general, this is the main difference between day and night wind envelopes, including some differences that might occur in the upper boundaries due to turbulence intensity.

5.7.3 Alternative Take-off and Landing Procedures

Besides the fore-aft procedure, two alternative take-off and landing procedures are applied by the Netherlands Ministry of Defence (NLMoD): oblique and cross-deck. So far, only the construction of the CFE for the fore-aft procedure has been demonstrated. The simplest solution would now be to turn the CFE in a 45° azimuth for an oblique procedure or a 90° azimuth for a cross-deck procedure. However, these predictions would not take into account the alternative approach and departure paths to the ship and/or the turned helicopter heading in relation to the ship's centreline, and associated encounters with the ships' airwake. For this reason, the predictive tool has the functionality to select the required take-off and landing procedures such that the rejection criteria are correctly applied for the desired procedure with the corresponding

interaction with the ships' airwake. Other factors to be taken into account for an alternative take-off and landing procedure are the different interpretation of ship motion and visual references by the pilot. For example, for a cross-deck take-off and landing, with the helicopter aligned perpendicular to the heading of the ship, the ships' roll motion can be considered as pitch motion. Or instead of having visual references with the superstructure in the forward window for a fore-aft procedure, the visual references are mainly presented in the side window for a cross-deck procedure such that the pilot's head needs to be turned accordingly. Furthermore, strong winds from the forward sector results in a lot of pitch motion with the ship sailing against the waves. When the wind is more from the sideward sector there will be more roll motion from the ship which may be outside the limitations for helicopter operations.

Taking the various factors into account for an alternative take-off and landing procedure, examples for the associated CFE's with a take-off and landing towards the port side are shown in Figure 5-27 (i.e. no procedures facing starboard side are shown for clarity but can generally be considered identical as for the procedures facing port side). The CFE for the fore-aft take-off and landing procedure is considerably larger then for the oblique and cross-deck procedures. The main reasons are the good visual references with the ship for the pilot throughout the approach and landing phase, and it allows the ship to be sailing into the waves such that ship motion can be minimized. Furthermore for oblique and cross-deck procedures a different interaction occurs with the ship's airwake causing more helicopter motion, and in the approach towards the ship from the leeward side the downdraft causes torque spikes that results in smaller envelopes. Some overlap between the CFE's for the alternative procedures is desirable to avoid a sharp distinction between procedures in case of fluctuating wind conditions, and it allows to train pilots more efficiently for different procedures as the ship can remain steady on course and speed whilst allowing different procedures to be practised.

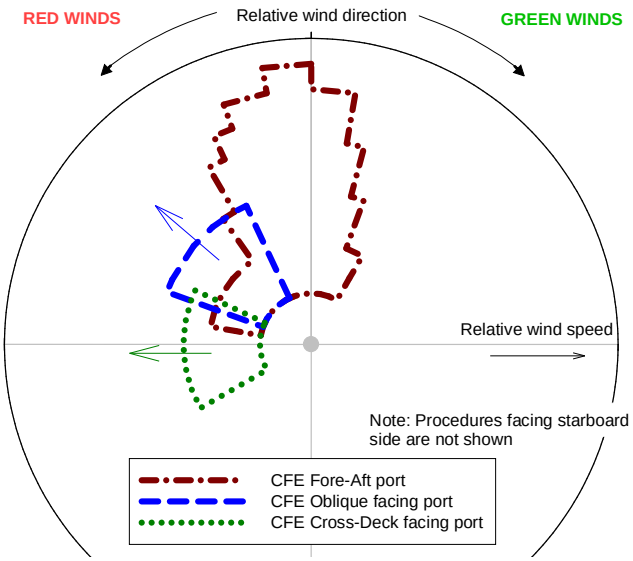

Figure 5-27; Example CFE's for alternative procedures

5.7.4 Lessons Learned for the Candidate Flight Envelope

The following lessons learned for the construction of the CFE's are observed:

1. The predicted CFE is a flight envelope giving the likely combinations of indicated wind speed and direction for safe take-offs and landings from each particular ship type, and is used to increase trials effectiveness as it functions as the starting point for sea trials;
2. The differences in CFE due to increasing referred weight are mainly due to performance related issues;
3. The boundaries for a Hot & Heavy envelope should have an additional safety margin due to a somewhat more sluggish helicopter response.

5.8 Chapter Review

The newly developed predictive tool for the CFE's in this chapter, is considered original, and can be seen as the most important novelty of this work. First, a framework is given for quality assurance guidelines in the development cycle of the predictive tool. This includes a consistent terminology and foundation for a methodology bridging the gap between scientific philosophy and pragmatic modelling. There are various inputs required in the predictive tool, i.e. helicopter flight characteristics and limitations, helicopter parameters and ship parameters, atmospheric conditions and the ship environment. There are sub-models for the atmospheric boundary layer, ship airwake, subjective pilot ratings, helicopter performance, helicopter control positions and helicopter attitudes. Furthermore, the algorithm processes the input data such that all relevant rejection criteria and dependencies interact with each other. For this reason, maximum and minimum values of local wind conditions near and above the flight deck are applied to helicopter rejection criteria, stored in lookup tables, for example to ensure that there remains sufficient power and control margin available to perform safe shipboard operations throughout various operational scenarios.

The output from the predictive tool results in the CFE, based on the indicated wind as presented by the ship's anemometers, which can likely be released to in-service operations for each particular helicopter-ship combination, whilst taking adequate safety margins into account. The CFE is used to increase trial effectiveness as it functions as the starting point for sea trials. The aim of the CFE is to achieve the smallest possible number of flying hours that does not affect the quality of the results and/or safety standards. Subsequent flight tests are then concentrated at and around the potential boundaries, reducing flight test time, and for example easing the difficulties of ship availability and the vagaries of the weather, whilst increasing the effectiveness of sea trials. In fact, the CFE is the preliminary envelope, whilst the SHOL is the result of sea trials and is the ultimate version defining the safe operational limitations.

Chapter 6 *Phase III*, Sea Trials and Validation

6.1 Introduction

This chapter discusses the sea trials and validation of the predictive tool in *Phase III* of the innovative three-phase approach for determining Ship Helicopter Operational Limitations (SHOLs) as shown in Figure 6-1. Based on the Candidate Flight Envelope (CFE), a (partial) flight test campaign on board the ship is conducted, preferably in a range of weather conditions by day and by night (black outlined white boxes in figure). This is to determine for the particular helicopter-ship combination the effects on the pilot workload from, for example, visual references, ship motion and turbulence. The predictive capacity of the predictive tool is validated by comparison against independent data not used for the calibration process.

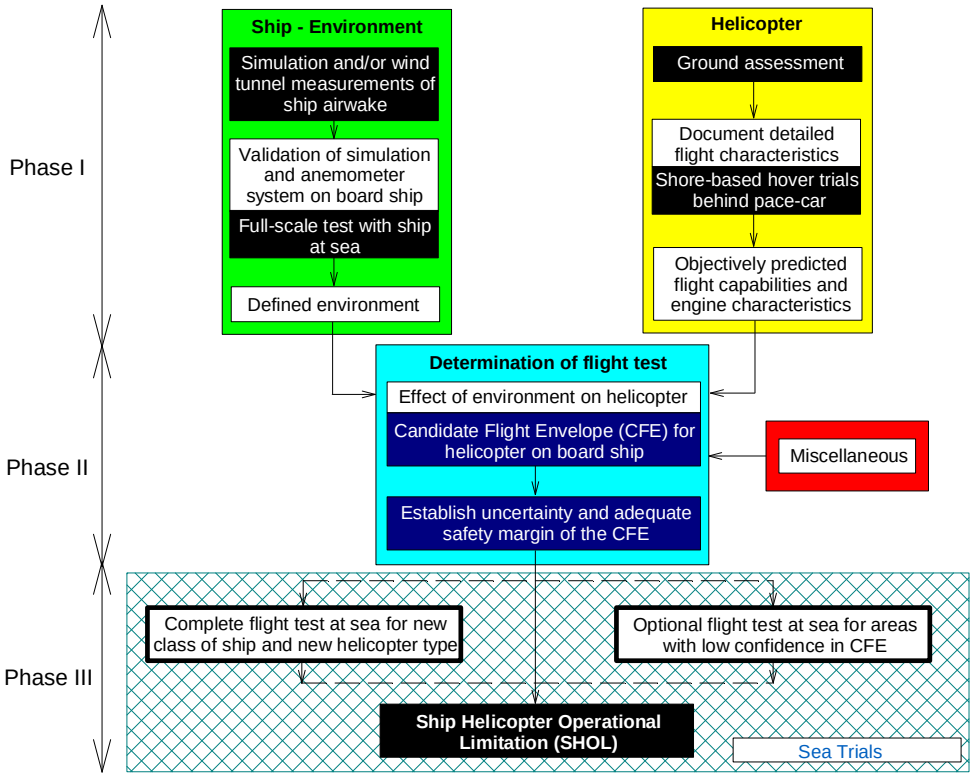

Figure 6-1; Innovative flow chart SHOL development

6.2 Sea Trials

Once the novel test methodology is applied, in *phase III*, the main objective of the sea trials is the confirmation of the CFE by collecting quantitative test data to validate the predictions to ensure that within the released operational envelopes no helicopter limitations are exceeded. In addition, a confirmation is required based on qualitative elements to determine the effects on pilot workload from, for example, visual references, ship motion and turbulence. The flight test are concentrated at and around the potential boundaries, reducing flight test time, and for example easing the difficulties of ship availability and the vagaries of the weather.

6.2.1 Visual References

An important item of the sea trials is to assess the adequacy of the visual references on board each particular ship type (in relation to the flight deck clearances). The visual references are important for the pilot in the take-off and landing phase, to assess ship motion, and to position the helicopter above the landing grid such that, if fitted, the deck-lock system can be immediately engaged once landed on-deck. The visual references should be proportional to the flight deck clearance, e.g., it is easier to miss the landing grid on a large ship than it is on a small ship. However, on a ship with marginal flight deck clearances, the visual references need at least be such that the forward motion towards the hangar is easily assessed and can be prevented by the pilot. Some examples of the lessons learned for visual references that might impact flight safety are summarized in this section [1].

Flight deck markings

The white lines painted on the flight deck provide the pilot with visual cues to position the helicopter above the landing spot. These flight deck markings should be matched with the take-off and landing procedures applied (e.g. fore-aft, oblique and cross-deck). The line across the flight deck from left to right is positioned such that when the helicopter is in the correct fore and aft position above the spot, the pilot's seat is directly over this so-called "*bum-line*". Lateral position cues are derived from the centreline painted across the flight deck from aft to forward, which is extended onto the hangar doors. For oblique landings in a 45º azimuth with the ship's centreline, the corresponding lines painted on the flight deck should be used. In case cross-deck landings are made in a 90º azimuth with the ship's centreline, the "*bum-line*" is used to align the helicopter heading for landing. As the previous naval helicopter for the Royal Netherlands Navy, the SH-14D *Lynx*, used a relative wind procedure instead of a 45º oblique landing procedure, the associated white lines were not painted onto the flight deck. However, it was decided for the NH90 NFH to take-off and land in a fixed 45º azimuth with the ship's centreline, to ensure that with a minimum amount of training the pilot's can quickly memorize the visual cues without reducing operational capability. Due to the change from a relative wind procedure towards an oblique procedure, the corresponding white lines had to be painted on the flight decks across the entire fleet as shown in Figure 6-2. In this case, a simple solution was to paint a line at 45° from the ship's centreline starting from the landing grid running towards the flight deck edge.

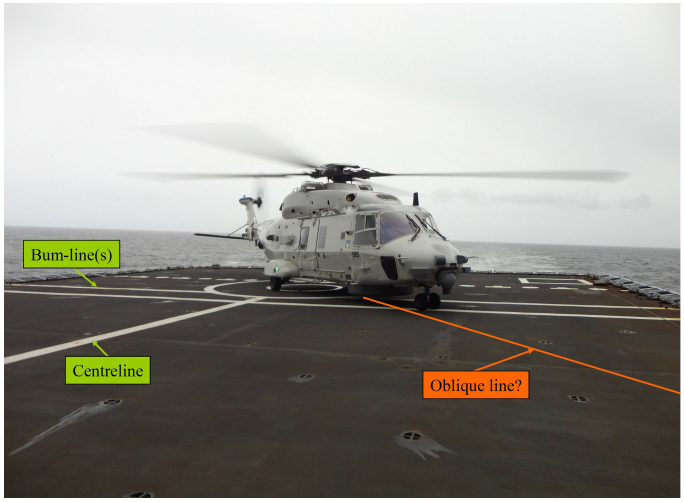

Figure 6-2; Example missing 45° line on the deck

Night vision goggle compatibility

Shipboard lighting poses a significant problem to approaching pilots wearing a Night Vision Goggle (NVG). For example, common ship lights (i.e. stern, masthead, navigation), but also visual landing aids are, if not NVG compatible, usually very bright and cause NVG images to bloom and/or shutdown. Therefore, an approaching NVG aided pilot, in case no adequate ship lighting is present, requires a "*dark*" deck, one with no illumination. A temporary solution that has been applied, in case the light is important for helicopter flight operations, was to tape the green Stop & Go light to indicate the helicopter is cleared for take-off or landing such that is was visible but did not disturb the NVG image as shown in Figure 6-3.

Figure 6-3; Example taped green Stop & Go light

An associated issue is the safety and efficiency of the flight deck crew. It is important that night lighting systems provide the flight deck crew, e.g. Flight Deck Officer (FDO), lashing runners and maintenance personnel with the capability to see the helicopter and surrounding flight deck whilst providing the NVG aided pilot the ability to see the visual cues required to operate the helicopter. An area that is further investigated by the Royal Netherlands Navy, is the application of deck lights to highlight (parts) of the flight deck markings to optimize the available visual cues. The low level lights can be applied to the superstructure to enable all the necessary ship motion and positioning cues to be readable by the pilot through the NVG's combined with side and "*under-look*" vision.

Field of view

The Field Of View (FOV) from the cockpit should be free of obstructions, where possible, to allow the pilot maximum visual references with the ship. If insufficient importance is placed on the FOV in the initial stages of a design it is unlikely that it could easily be improved to a satisfactory standard as this would probably involve expensive modifications to the cockpit structure. Unfortunately, for the NH90 NFH the horizontal bar of the cockpit door window on the right hand side resulted, amongst others, in multiple occasions in temporarily loss of visual reference with the FDO as shown in Figure 6-4. The FDO provides take-off and landing instructions to the pilot and losing sight considerably increases pilot workload. Therefore, it is required during the development phase of a (maritime) helicopter to optimize the field of view such that various take-off and landing procedures are achievable with adequate visual references with the ship throughout.

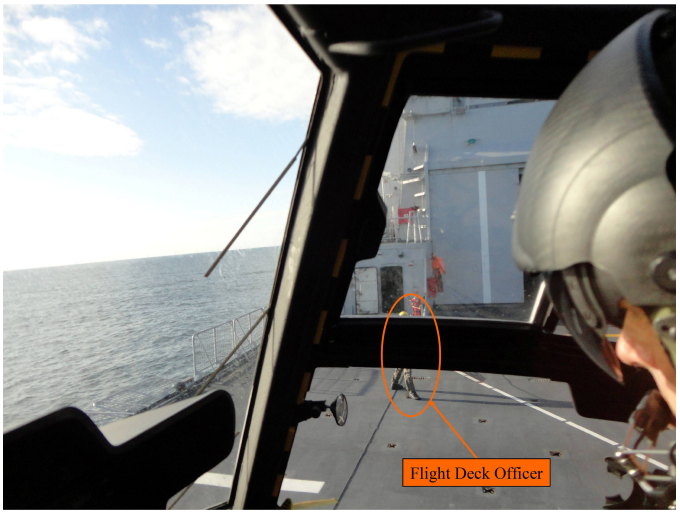

Figure 6-4; Obstruction due to horizontal bar for NH90 NFH

6.2.2 Ship Motion

The limitations in ship motion for deck handling may have already been demonstrated by the industry and the results presented in the flight manual. In that case, the operator

of the helicopter is restricted to operate within these limitations, otherwise a dedicated test campaign should be scheduled to demonstrate the boundaries of the envelope. In case required, the development of deck handling envelopes can be supported by simulation tools and/or mock-ups of the helicopter to determine the maximum operational capability without the risk of damaging the helicopter. It is important to mention that these deck handling envelopes should preferably be larger than the ship motion limitations (and relative wind limitations) for take-off and landing to ensure the maximum operational capability. The aim should be that the helicopter is able to land up to its maximum potential, and once on-deck the helicopter can still be safely moved from the landing spot towards the hangar.

Once the helicopter is on-deck, in case a deck-lock system is fitted, it is secured on deck by engaging the deck-lock. The deck-lock system used for most helicopters is the so-called "*harpoon*". The harpoon is contained in a recess under the fuselage and is extended and retracted hydraulically. When selected to engage, the harpoon extends to engage the locking jaws in the landing grid in the deck of the ship. When the jaws are engaged, the harpoon automatically attempts to retract thus securing the helicopter to the flight deck. A swivel in the harpoon head allows the helicopter to be rotated for the various take-off procedures, whilst remaining secured to the deck. In addition, either nylon or steel chain lashings are applied to secure the helicopter. These lashings are fixated at dedicated strong points of the helicopter and on the flight deck. The ship motion limitations associated with the capacity of the harpoon and/or lashings to prevent the helicopter to turn over to the side should be adhered to. Other deck handling operational aspects to consider are ship motion limitations for: spinning-up and stopping the main rotor blades, spreading and folding the main rotor blades (if possible also the tail boom), and moving the helicopter from the hangar towards the landing spot and vice versa.

In general, ship motion is considered predominantly important for defining the capabilities of a specific helicopter-ship combination once the helicopter is on-deck and not for take-off and landing. The pilot always tries to touch down or take-off the helicopter when the ship is in a quiescent state with minimal deck motion. The corresponding limitations for take-off and landing are determined as part of the flying routine during the sea trials, and if feasible can be read-across from other similar types of ship. The restrictions are dependent on, for example, the capacity of the landing gear to absorb the impact from the landing, the tendency of the helicopter to bounce on the flight deck once landed with one wheel first, and the comfort level of the pilot to manoeuvre the helicopter above a moving flight deck with a tilted view of the horizon.

6.2.3 Turbulence

The wind tunnel measurements used to predict the ship's airwake are average values, which do not take into account the variety in wind speed or wind direction. However, in reality there is an associated turbulence level for a particular relative wind condition for each ship type. Generally, the turbulence level increases with increasing relative wind speed, and vice versa. The turbulence level can increase to such a high level that the helicopter responds violently in pitch and roll attitude, which causes corresponding

torque spikes, increased control activity and higher pilot workload. Typically, these high turbulence levels resulting in violent helicopter responses define the upper boundaries of the SHOL envelope. There is still some engineering judgement required to set the upper boundaries for the CFE of a particular ship type correctly. Therefore, unless adequate safety margins are applied, the upper boundaries are the main focus of the sea trials. The turbulence scale is used as a method to indicate the intensity of the turbulence encountered and the associated aircraft reactions, as shown in Appendix C.

6.2.4 Exploration of the Potential Boundaries

The sea trials consist of take-off and landings, at least two per test condition at the boundaries of the envelope, for different procedures, spots, referred weights and ship motion. Once enough confidence and routine is established for shipboard operations at the lower referred weight (e.g. 10 000 kg) around a number of test points, a higher referred weight is selected (e.g. 11 000 kg). For this higher referred weight the boundaries of the SHOL envelope are established first, and once determined, the original lower referred weight can be re-selected and if possible these boundaries expanded further outwards. This method results in a so-called "*wedding cake*" strategy in which the results for the higher referred weight are also valid for the lower referred weight and the latter do not have to be tested again. The present flight test philosophy and test techniques for the sea trials are discussed in more detail in Appendix E.

The flying qualities of the helicopter will clearly affect task performance but the skill of the pilot will also affect the outcome of the SHOLs for take-off and landing. To take into account the position of the test pilot, it is required that the pilots evaluate pilot workload with respect to the understanding of the lower degree of skill and training existent in a group of operational pilots. In other words, the test pilot must analyze the workload in the context of a less skilled or less experienced pilot. However, it has been demonstrated that the pilot(s) used for SHOL development either at-sea or in a simulator will have an impact on the envelopes released for operational use [2]. For this reason, a test condition is only considered successful in case the pilot gives an acceptable workload rating, whilst at the same time the objective data during post-flight analysis indicates sufficient safety margins. Furthermore, the test pilot is not briefed which test points are flown during a particular mission, such that randomness in test conditions can be assured. The randomness in testpoints avoids a learning curve with potentially lower pilot workloads ratings as the trials progresses.

6.3 Validation of the Predictive Tool

The goal of the predictive tool is to make predictions of real-life system behaviour. Since the predictive tool, or any other simulation model, can never fully capture the complex physical phenomena that contribute to real-life system behaviour, it never perfectly agrees with reality. Nevertheless the predictive tool can still be used, as long as the user has some idea of how well the model predictions are for the intended application of the tool – but to do this with confidence – one must know how good the predictions are at the set points selected for validation, and also how good the

predictions are in the interpolated or extrapolated regions of the application domain for which there are no experimental results. Therefore, a proper understanding of the predictive tool with the potential sources of uncertainties is essential during the validation process.

The estimation of a range within which the simulation modelling errors lie is a primary objective of the validation process and is accomplished by comparing a simulation result (solution) with an appropriate experimental result (data) for specified validation variables at a specified set of conditions. The output of the predictive tool is validated to determine the degree of representation of the reality from the perspective of constructing the CFE as a starting point for the sea trials. Validation takes place by quantification of the agreement between experimental and computational data. It is common practice in all fields of engineering and science for comparisons between computational results and experimental data to be made graphically. In this case, the computational constructed CFE, and the experimental data from the sea trials. If the computational results generally agree with the experimental data, the computational model is declared as validated. The credibility of a helicopter-specific model's capability to make predictions about reality must be evaluated against independent data.

There are various inputs required in the predictive tool, i.e. helicopter flight characteristics and limitations, helicopter parameters and ship parameters, atmospheric conditions and the ship environment as shown in Figure 6-5. There are sub-models for the atmospheric boundary layer, ship airwake, subjective pilot ratings, helicopter performance, helicopter control positions and helicopter attitudes. The algorithm is based on the assumptions and consequential equations that together form the fundamental basis of the predictive tool as discussed in Chapter 5. The output from the predictive tool results in the CFE, based on the indicated wind as presented by the ship's anemometers, which can likely be released to in-service operations for a particular helicopter-ship combination, whilst taking adequate safety margins into account.

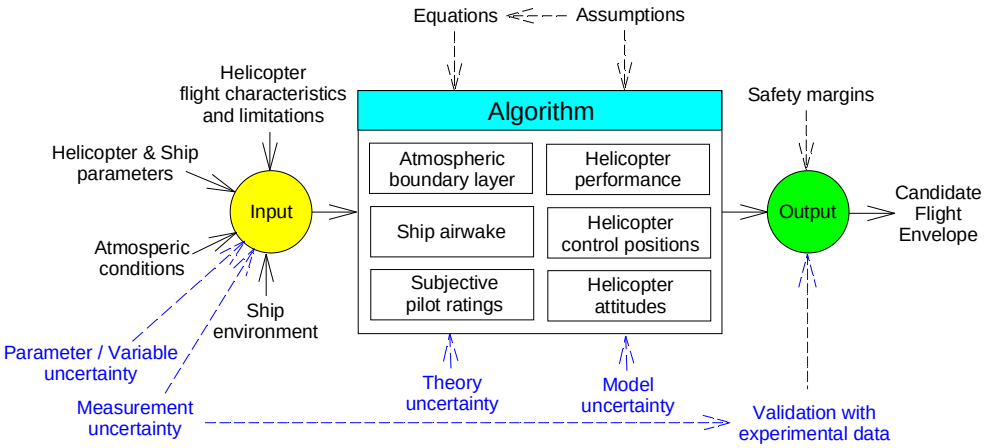

Figure 6-5; Overview elements predictive tool

Unfortunately, there are uncertainties associated with the measurements used as input for the predictive tool, and uncertainties associated with the algorithm itself. As discussed in Chapter 3, there are both parameter / variable uncertainties and measurement uncertainties associated with inputs required for the model. In addition, as the predictive tool is validated against experimental data, the associated measurement uncertainties should be taken into account. Finally, there are uncertainties in the underlying fundamental physical principles of the model caused by the applied assumptions and utilized equations belonging to either the theory uncertainty or model uncertainty.

During the introduction of the NH90 NFH, there were six helicopter capable ship types in-service within the Dutch fleet that all have been certified for helicopter-ship operations as summarized in Appendix A. The sea trials were conducted in the North Sea up to 11 000 kg referred weight (at approximately 15 ºC) [3,4,5,6,7,8]. In addition, for two ship types sea trials were conducted up to 11 600 kg referred weight, which was achieved by 11 000 kg actual weight at an Outside Air Temperature (OAT) equivalent to 30.7 ºC at sea level, in either the Indian ocean or Caribbean Sea [9,10]. For validation purposes, the latter two examples of which the CFE's derived in Chapter 5 are used for the fore-aft procedure at aft-CG.

The validation of the CFE's consists of both a qualitative and a quantitative part. This is required as only the most conservative outcome of the subjective pilot ratings and objective flight test data can be released to service. The qualitative part consists of the pilot workload, with acceptable test points (green colour in figure) and unacceptable test points (red colour in figure) as shown for both examples in Figure 6-6 to Figure 6-11, respectively. There is a distinction made between test points flown during day and night (symbol for day is a square and for night is a circle). In case a quantitative safety margin is exceeded, the respective rejection criteria are indicated in a graph as shown for both examples in Figure 6-12 to Figure 6-17, respectively. As torque is the dominant factor within the atmospheric conditions tested, other performance parameters are not shown for clarity. The CFE is represented as the brown dotted line in these figures. Note that the rejection criteria are only indicated if a safety margin is exceeded. The safety margins for the rejection criteria are initially determined during the shore-based hover trials, and can be fine-tuned as more experience is gained during successive sea trials.

A "*wedding cake*" strategy has been applied in which the results for the higher referred weight are also valid for the lower referred weight and the latter do not have to be tested again. Therefore, unless the test points are not achievable for 11 000 kg referred weight, the required test points are flown for 10 000 kg referred weight. For the examples shown, roll attitude of the helicopter is the main limitation in red wind conditions (which may also result in more torque to manoeuvre the helicopter). The torque utilised is the main limitation for take-offs towards the leeward side of the ship and the lower boundaries of the envelope. Torque utilised, instead of torque required is mentioned, as the pilot may have used temporarily more torque than what would be required. The upper boundaries are mainly defined by the large pitch and roll attitude

deviations of the helicopter due to the turbulence resulting from the ship's superstructure, with a corresponding increase in pilot workload. For the upper boundary in green wind conditions at 11 000 kg referred weight for example 1, as shown in Figure 6-14, the predictions were somewhat too optimistic, as quantitative rejection criteria for pitch and roll attitudes of the helicopter are indicated for some test points within the CFE. Although not for other similar test points around it, and thus these areas may still be included in the SHOL based on engineering judgement after discussion within the test team (note that qualitative rated unacceptable test point may not be included). In contrary, the CFE was somewhat conservative at 11 000 kg referred weight for example 1 in red wind conditions with regard to roll attitude, as shown in Figure 6-14, and this was qualitatively confirmed by Figure 6-8. In all other scenarios, both for the qualitative and quantitative validation, there has proved to be a good agreement between the experimental and computational data. Note that the upper boundaries for 11 600 kg referred weight were not tested due to a lack of sufficient wind and thus cannot be validated with flight test data.

The objective rejection criteria are generally more consistent and restrictive in defining the boundaries of the operational envelopes determined during the sea trials than the subjective ratings given by the test pilots involved (whilst taking into account the skills of the "*average*" fleet pilot). Although there is no straightforward explanation, this is an important conclusion as it supports the philosophy to use objective rejection criteria to accurately predict the likely outcome of the sea trials. In addition, it enables to minimize the amount of test pilots involved in the sea trials, as it makes the qualitative ratings transparent to the test crew (i.e. to determine whether the test pilots were restrictive or conservative in their decisions). The "*SHOL-X"* approach aims to replace some or much of the experimentation at sea with less expensive simulation results that are validated with experimental results at selected set points. In particular, the objective rejection criteria are used to accurately define the boundaries of the potential operational limitations and by an additional feature of the tool during the validation after the sea trials to assess whether actual limits are approached or whether there is still room for expansion of the envelope. The software tool "*SHOL-X"* thereby assists in making fair comparisons between various predictions with any helicopter type for diversity in ship types. This does not mean that expert opinion does not count because quantitative data do not capture all intricacies of model validation.

The user of the predictive tool should be aware of both the advantages and shortcomings to use the predictions optimally such that savings in time and expenses of sea trials are realized without reducing safety. With the appropriate mindset, that the predictive tool does not provide a perfect solution but only the likely outcome of the sea trials, the graphical validation confirms the predictions made by the predictive tool and it is validated. However, this implicates a minimum knowledge level and skill set for the operator of the predictive tool, which should be provided by dedicated training to ensure all prior phases to construct the CFE are executed correctly. The course contents should be used to develop international regulations for the minimum training and currency requirement required for any test crew (and managers involved in flight trials) to conduct helicopter-ship qualification testing.

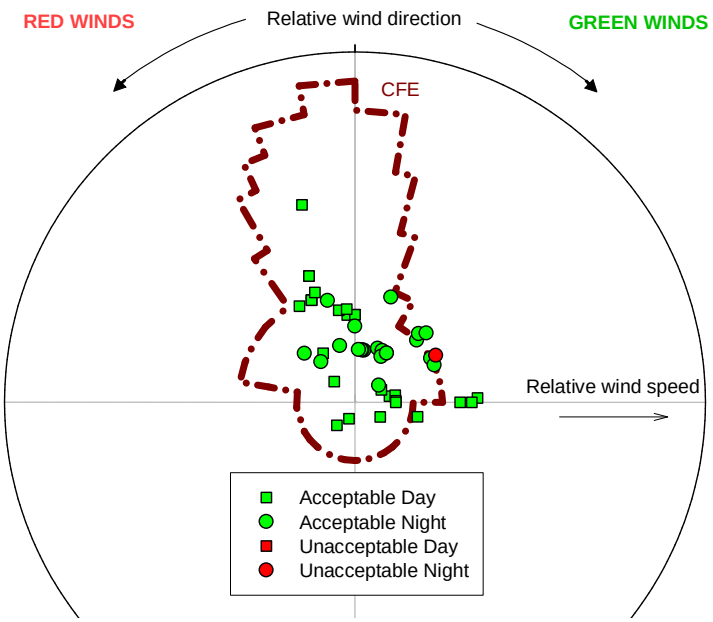

Figure 6-6; Subjective 10 000 kg referred weight - *Example 1*

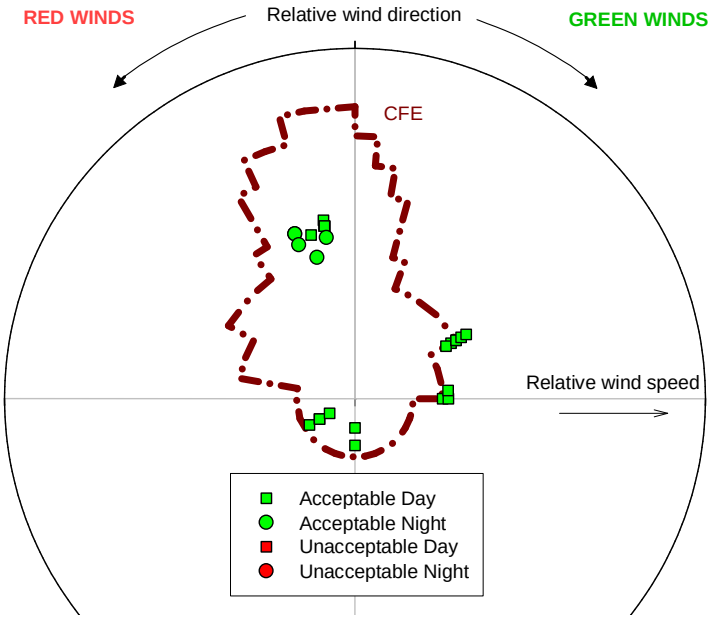

Figure 6-7; Subjective 10 000 kg referred weight - *Example 2*

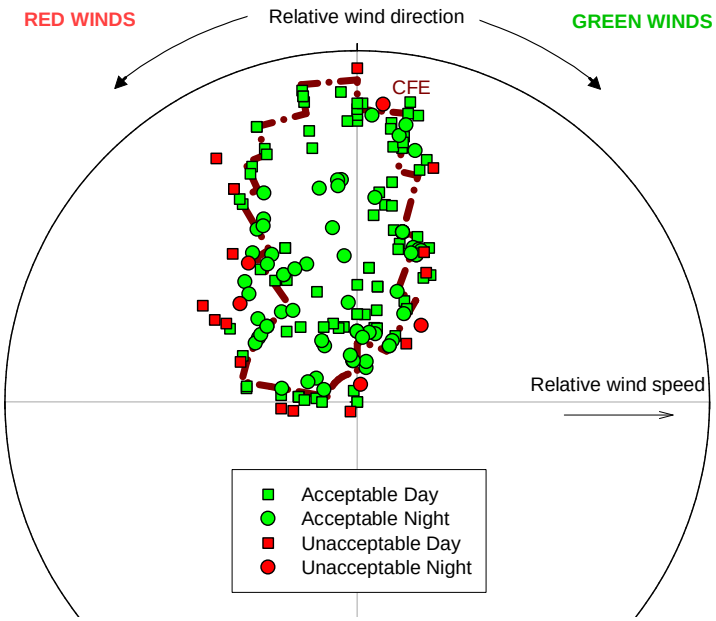

Figure 6-8; Subjective 11 000 kg referred weight - *Example 1*

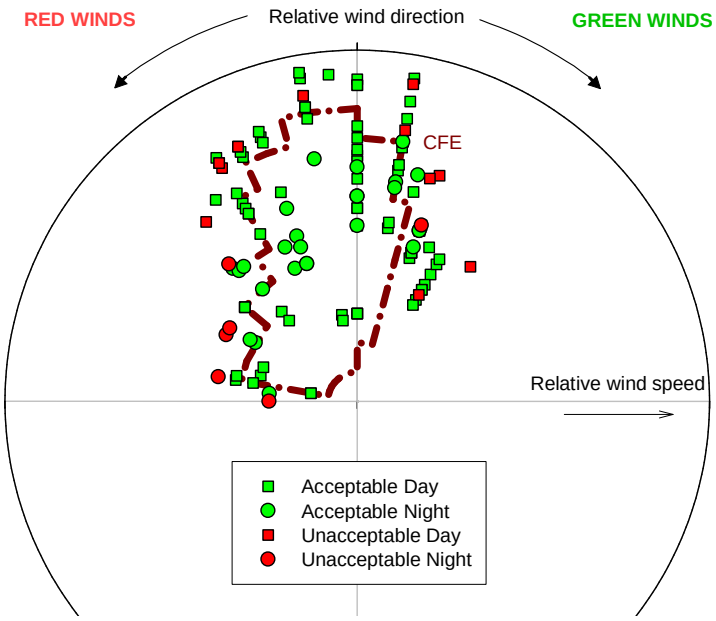

Figure 6-9; Subjective 11 000 kg referred weight - *Example 2*

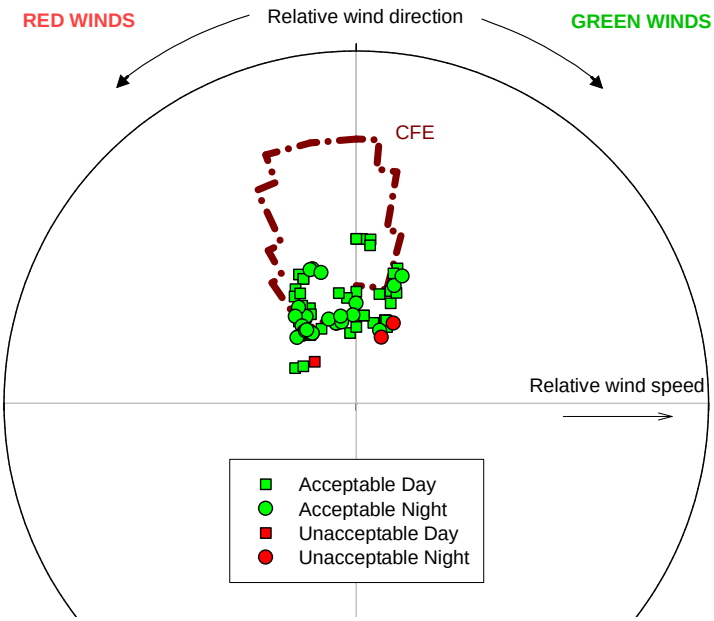

Figure 6-10; Subjective 11 600 kg referred weight - *Example 1*

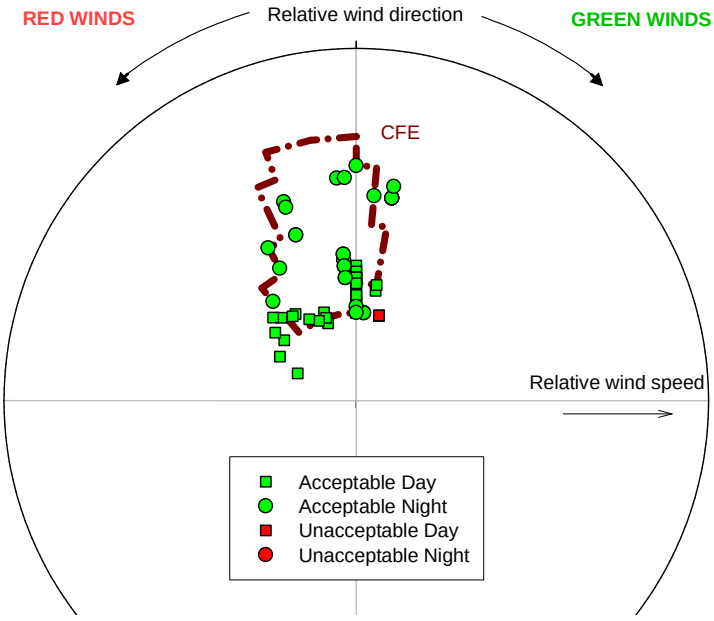

Figure 6-11; Subjective 11 600 kg referred weight - *Example 2*

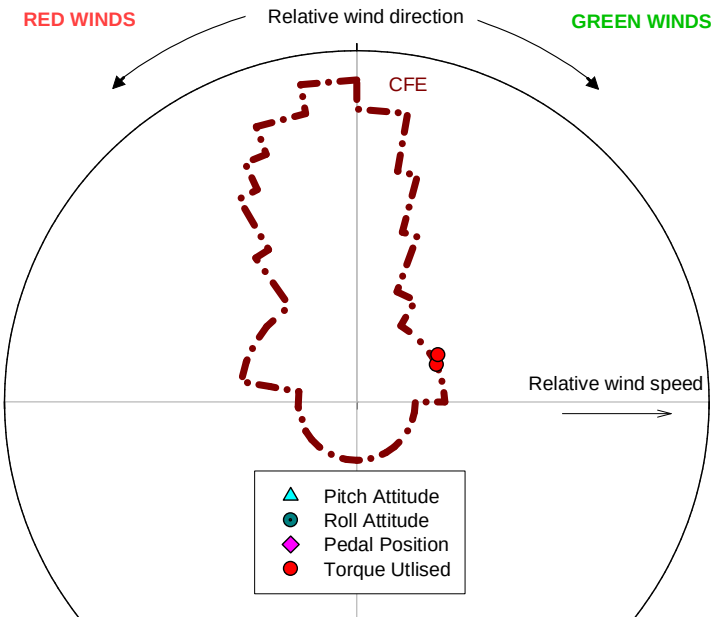

Figure 6-12; Objective 10 000 kg referred weight - *Example 1*

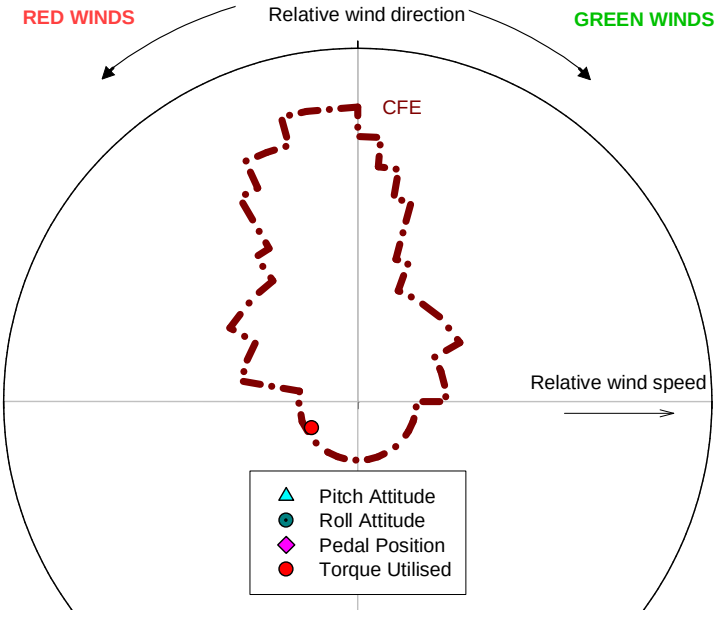

Figure 6-13; Objective 10 000 kg referred weight - *Example 2*

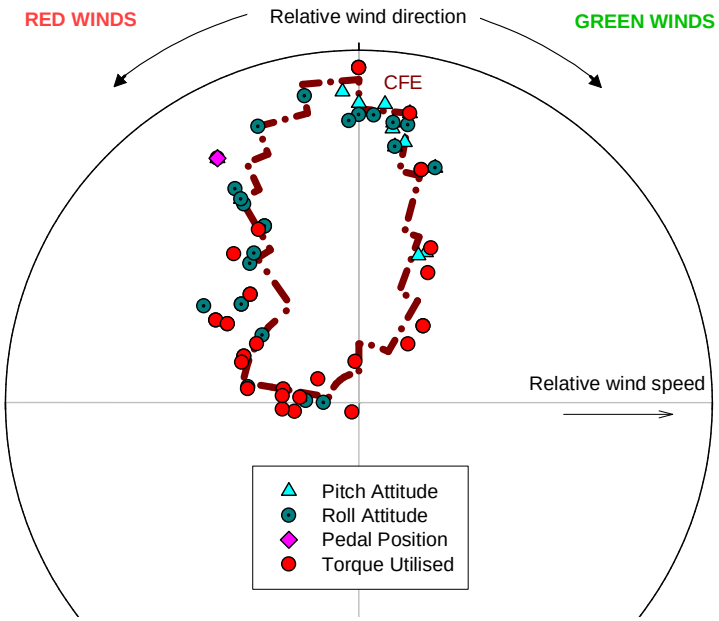

Figure 6-14; Objective 11 000 kg referred weight - *Example 1*

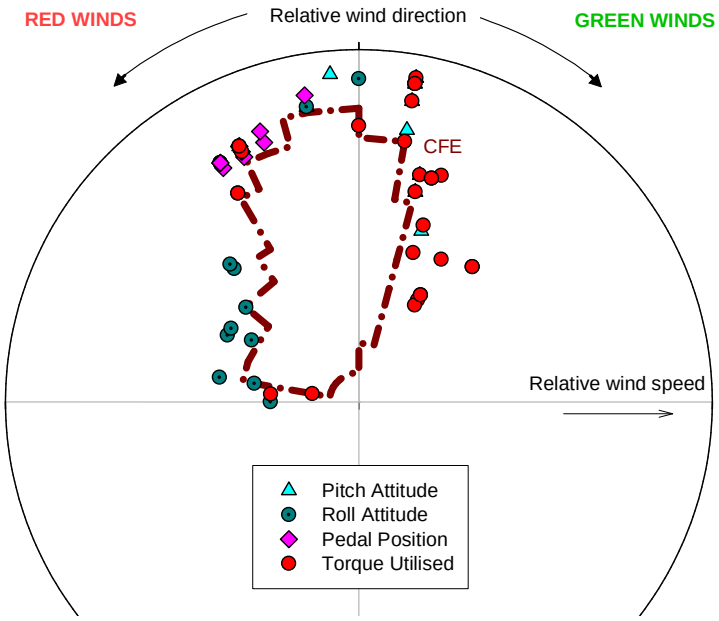

Figure 6-15; Objective 11 000 kg referred weight - *Example 2*

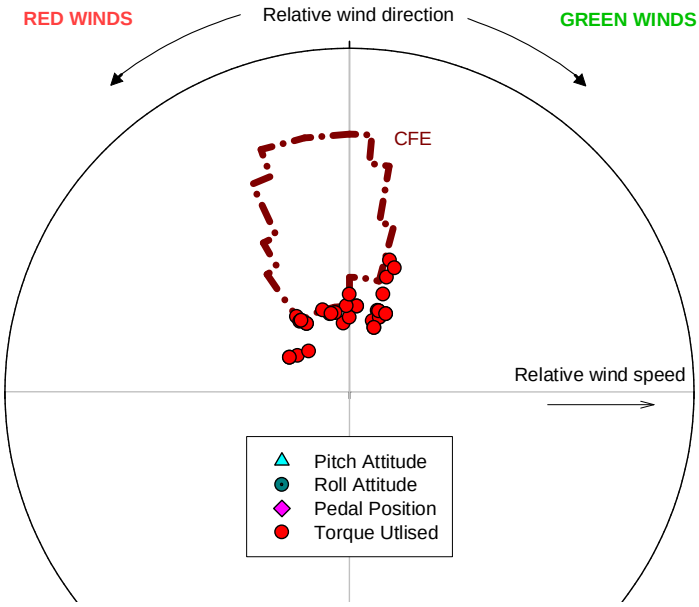

Figure 6-16; Objective 11 600 kg referred weight - *Example 1*

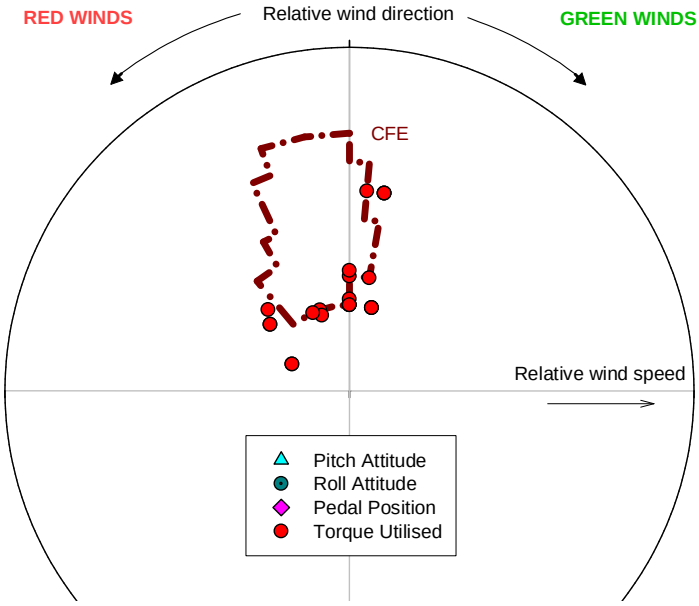

Figure 6-17; Objective 11 600 kg referred weight - *Example 2*

Fore-aft procedure at 11 000 kg referred weight	
Spot: Single	Condition: Day & Night (aided / unaided)
Ship: LCF	Aircraft: NH90 NFH

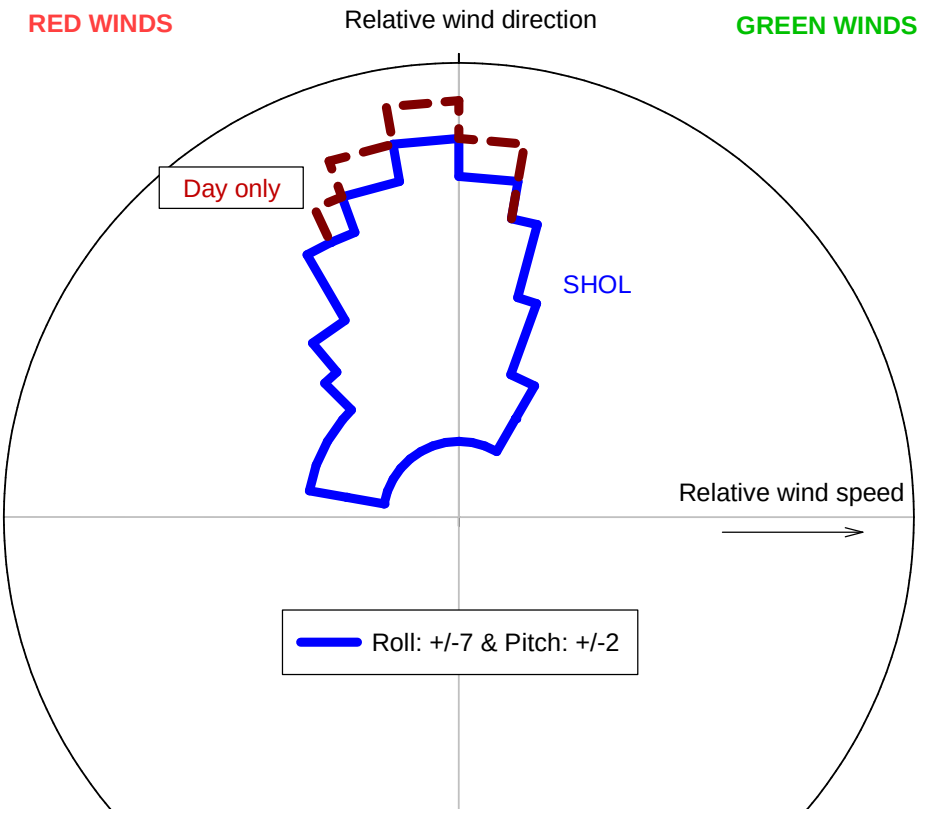

NOTES

- The Fore-aft procedure is valid for both port take-off and landings;
- The Fore-aft procedure is valid for starboard take-off into green wind conditions;
- The Fore-aft procedure is only valid for starboard landings into green wind conditions performed by a pilot in the left seat;
- The SHOL is only valid for 104 % Nr;
- The SHOL is developed for Wind Correction Algorithm (WCA) enabled and both ship anemometers correctly aligned at 0°;
- *"Strong rotor downwash expected deck personnel to be made aware"*.

Figure 6-18; Example SHOL 11 000 kg referred weight

6.4 Construction of the Ship Helicopter Operational Limitations

The construction of a SHOL envelope can now be achieved by two different options. The first and most common option is using dedicated sea trials in which the potential boundaries for the various take-off and landing procedures are validated. Preferably, during the sea trials the complete CFE is explored, such that all the evaluated parts can be released to service. By doing so, it also provides a validation of the predictive tool and gives the associated level of confidence for that particular helicopter-ship combination to be used as baseline for successive trials. The second option is the construction of the Hot & Heavy envelope by desk-top analysis alone. This option is novel and only feasible in case the structured test methodology is applied as described in this dissertation. In both cases, a SHOL released to service contains the following information as shown for example in Figure 6-18:

- The required flight procedures for take-off and landing;
- The maximum referred weight of the helicopter (i.e. helicopter weight divided by density ratio);
- The applicable landing spot, day or night condition, aided and/or unaided flight, the ship type and the helicopter type;
- The relative wind limitations based on the indicated wind as presented to the ship's crew. The data are presented as a diagram (i.e. polar plot) representing wind speed (in radial coordinates) and direction (in angular coordinates);
- The allowable ship motions for pitch and roll attitude;
- The establishment of additional rules and procedures if applicable. In addition any comments that deemed to be necessary to increase flight safety can be included.

6.4.1 After Sea Trials

The main objective of the sea trials is to confirm the CFE's, by collecting quantitative test data to validate the predictions. In addition, at least equally important, a confirmation is required based on qualitative elements to determine the effects on pilot workload from, for example, visual references, ship motion and turbulence. The merging of the quantitative and qualitative assessment is what defines the operational capacities for a particular helicopter-ship combination and is defined as the operational limitations in the SHOL's for take-off and landing. A thorough merging process between the quantitative and qualitative flight test data is achieved by a novel feature in "*SHOL-X*". This feature allows flight test data to be uploaded, and instantly organizes the flight test data such that it is presented in graphical format. It is now a matter of constructing the SHOL such that it excludes as many rejection criteria as possible. However, some test points with rejection criteria indicated may still be included, in case acceptable test points are flown around it. In general the following rules apply for the construction of the SHOLs after sea trials:

1. Test points rated as unacceptable by the pilot must be excluded (see for example Figure 6-8).

2. The rejection criteria inside the potential envelope must be verified. In case, multiple test points are flown, these test points may still be included based on engineering judgement after discussion within the test team (see for example Figure 6-14).
3. The limitations in ship motion for take-off and landing are determined as part of the flying routine during the sea trials as summarized in Figure 6-19. In case the targeted ship motion limits have not been achieved during the sea trials, flight test data and experience from other similar ship types may be used. Note that the deck handling limitations should preferably be larger to ensure the maximum operational capability for the helicopter-ship combination.

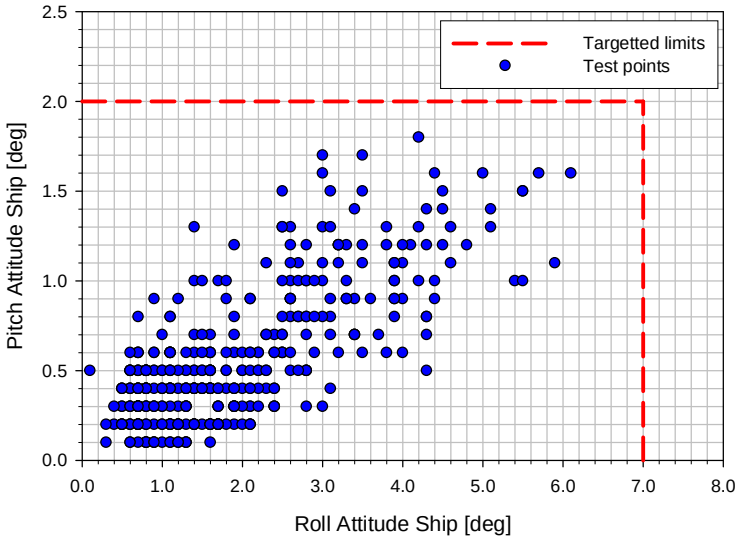

Figure 6-19; Example encountered ship motion conditions

4. Test points with a severe turbulence rating, if only flown during daytime, should be excluded from the nighttime envelope. This is required due to violent helicopter motion, in combination with the disadvantages of the NVG's such as, limitations in the pilot's field of view and a reduction in depth perception (see for example Figure 2-13 in Chapter 2).
5. The closure rate to the ship is more difficult to judge at night during the approach to the ship, which may result in a last-minute flare to arrest closure rates toward the ship. This is undesirable and for safety reasons no tail winds are allowed during night operations.
6. The operational limitations should include a consideration of the amount of risk the operator is willing to take for shipboard operations, and be a reflection of the training and experience level of the pilots.

6.4.2 Desk-top Analysis for Hot & Heavy Conditions

Unfortunately, the upper boundaries for Hot & Heavy conditions with 11 600 kg referred weight were not tested due to a lack of sufficient wind during the test

campaign and thus not validated with flight test data [9,10]. In case, the operational capabilities for a helicopter-ship combination would be solely based on acceptable test points achieved during dedicated sea trials as applied in any other present-day test methodology, this would have caused restrictions in the operational capability. In the contrary, there is a large amount of flight test data and experience gained during the sea trials for each ship type within the entire Dutch fleet in the North Sea with testing up to 11 000 kg referred weight [3,4,5,6,7,8]. In addition, flight test data is available from the shore-based hover trials up to 11 750 kg referred weight [11,12]. Therefore, in a joint session with the Subject Matter Experts (SME) within the maritime division of the flight test department of the Netherlands Ministry of Defence (NLMoD), it has been decided that based on these documents and the high level of confidence in the predictions made for the CFE's, enough expertise is available such that these upper boundaries are released to service.

More important, it has been decided that actual sea trials will not be required anymore in Hot & Heavy conditions for the remaining ship types within the Dutch fleet, as with the *"SHOL-X"* test methodology as described in this dissertation, the operational limitations can be developed by desk-top analyses alone [13,14]. This is a novel approach to the construction of SHOL envelopes, and can be seen as the most important achievement of this work. In general, the same rules apply as for the construction of an envelope after the sea trials. In addition, the following steps are applied for desk-top analysis for Hot & Heavy conditions:

1. It is assumed that subjective ratings (i.e. pilot workload and turbulence level) do not vary significantly between 11 000 kg and 11 600 kg referred weight, and as such the results for 11 000 kg referred weight can be used for the construction of the Hot & Heavy envelope as shown in Figure 6-20. However, areas with moderate turbulence levels above level 6 (i.e. medium bumps with occasional heavy ones) are to be excluded as shown in Figure 6-21. Note that in these figures the blue solid line is the SHOL envelope as derived for 11 000 kg referred weight by testing in the North Sea, and the brown dotted line is the CFE as predicted for 11 600 kg referred weight.
2. It is assumed that the following rejection criteria do not vary with referred weight: pedal position, longitudinal cyclic, lateral cyclic, pitch attitude and roll attitude of the helicopter (as demonstrated in Chapter 4).
3. The performance related rejection criteria vary with changes in atmospheric conditions, namely torque required, engine gas generator rotational speed N_g, engine power turbine inlet temperature T_{46} and tail rotor actuator position. Therefore, a correction needs to be applied towards the data gathered during the sea trials at 11 000 kg referred weight as shown in Figure 6-22. For safety reasons, the required torque increase between 11 000 kg referred weight (i.e. 15.0 ˚C) and 11 600 kg (i.e. 30.7 ˚C) is multiplied by two (note that torque required is still the limiting performance parameter at 30.7 ˚C for NH90 NFH).
4. Due to a somewhat more sluggish helicopter response, the Hot & Heavy envelope needs to be smaller than for 11 000 kg referred weight (unless tested in actual conditions).

5. Only the most restrictive outcome of the above mentioned considerations can be released to service by desk-top analyses.

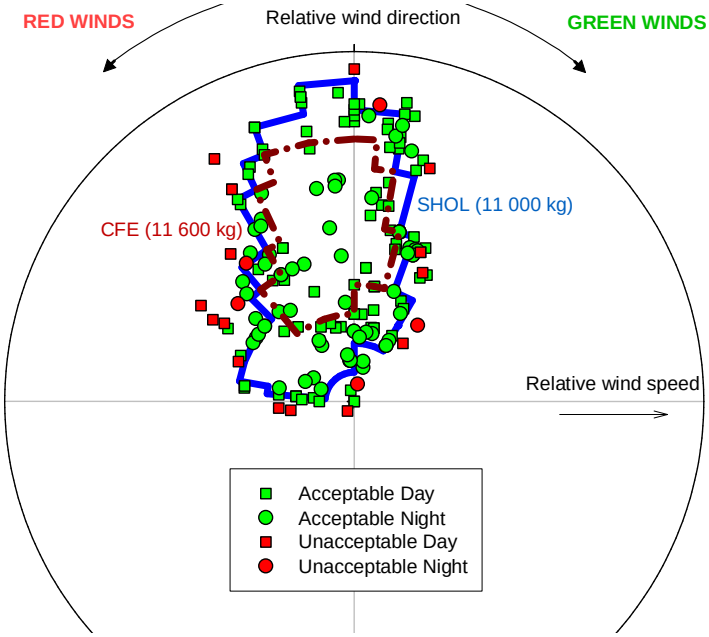

Figure 6-20; Example pilot workload prediction for Hot & Heavy

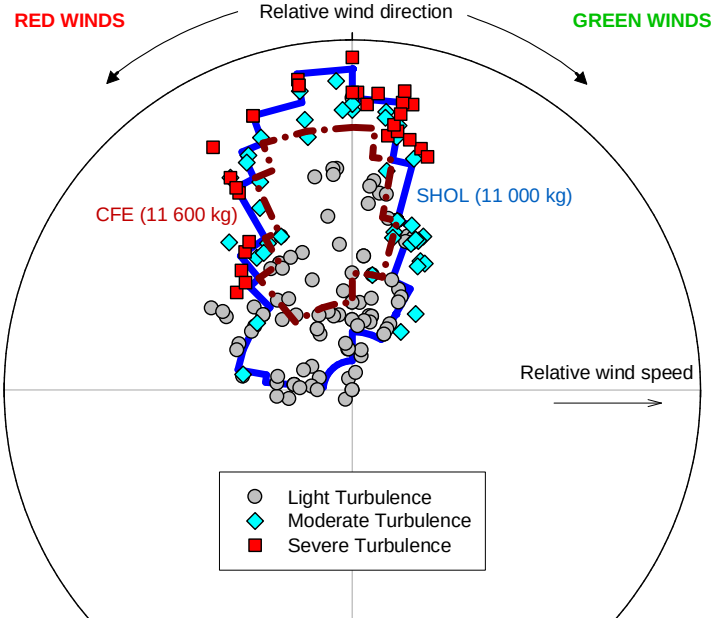

Figure 6-21; Example turbulence levels prediction for Hot & Heavy

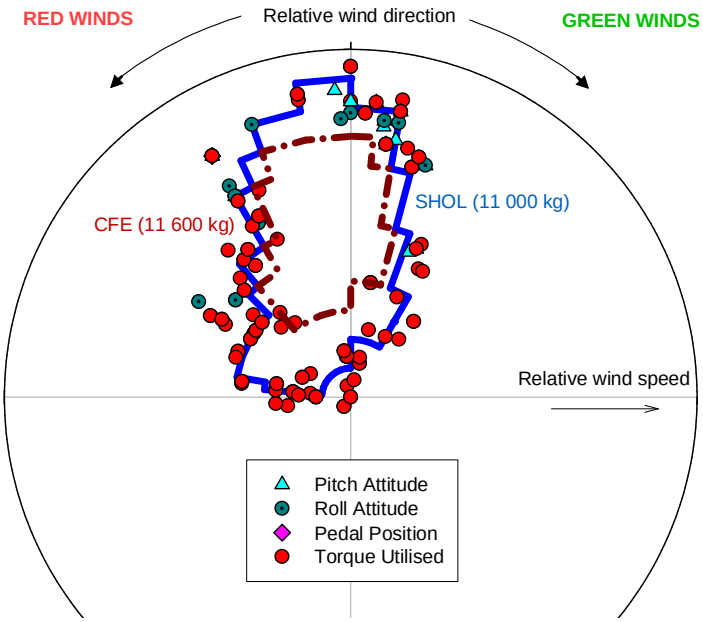

Figure 6-22; Example objective rejection criteria prediction for Hot & Heavy

6.4.3 Operational Application of Limitations

There are for each helicopter-ship combination various SHOLs developed e.g. fore-aft port, fore-aft starboard, oblique facing port, oblique facing starboard, cross-deck facing port and cross-deck facing starboard, for day and night conditions, at 10 000 kg, 11 000 kg and 11 600 kg referred weight. Depending on the atmospheric conditions and the All-Up Weight (AUW) of the helicopter, the corresponding envelope(s) should be used. It is at pilot discretion to determine the preferred take-off or landing procedure within these envelopes. The selected take-off or landing procedure is stated to the ship by the pilot. The corresponding limitations are then verified on board the ship by the navigation bridge, command centre and FDO. In case required, the ship has to alter course to be within the relative wind and ship motion limitations. Once verified that the ship is within the applicable limitations Command will provide a "*green*" deck for approval to take-off or land. Note that as both the aircrew and various involved position on board the ship are required to completely understand the SHOL, the presentation is of utmost importance to avoid unnecessary radio communication from either side.

6.5 Overlapping Results across Entire Dutch Fleet

The overlapping results of the SHOLs for a diversity of ship types within the entire Dutch fleet have a large similarity as shown by the blue line in Figure 6-23. This indicates that when the anemometer corrections are made correctly, and the operational envelopes are presented as undisturbed relative wind (e.g. Z_{ABL} = 1), the SHOL boundaries are mainly helicopter related and thus not ship related. The discrepancies in

the upper boundaries (pink dotted line in figure) of the envelope are caused by the differences in turbulence level for each ship type with increasing relative wind speed and the effect of the atmospheric boundary layer. The variations in turbulence levels are caused due to e.g. the height of the hangar and/or the distance between the landing spot and the hangar. The variations in atmospheric boundary layer coefficients are dependent on the vertical distance between the flight deck and anemometer locations, which are not compensated for by the Wind Correction Algorithm (WCA). In general, the higher the anemometers are above sea level, the larger the exponential increase in indicated wind speed, whilst the local wind speed at the height of the flight deck remains similar.

The discrepancies in the starboard boundaries (green dotted line in figure) are mainly caused by the strength of the downdraft on the leeward side of the ship (e.g. port-side departure for green winds) and related to the dimensions of the ship. The discrepancies on the port boundary (red dotted line in figure) are mainly caused by differences in the indicated wind direction between the various ship types, as not all ships were yet equipped with a WCA to compensate for disturbances at the anemometer locations. It is a fundamental prerequisite of efficient helicopter-ship qualification testing to understand that the operational limitations are mainly caused by the helicopter flight characteristics, and not the ship type, once the anemometer corrections are applied correctly towards the undisturbed relative wind. This allows for quick exploration of the potential boundaries for each ship type without wasting time to pursue the boundaries with a conservative incremental approach. In this way, potential losses are avoided of valuable time and/or useful environmental conditions which could not be compensated for at a later stage of the test campaign.

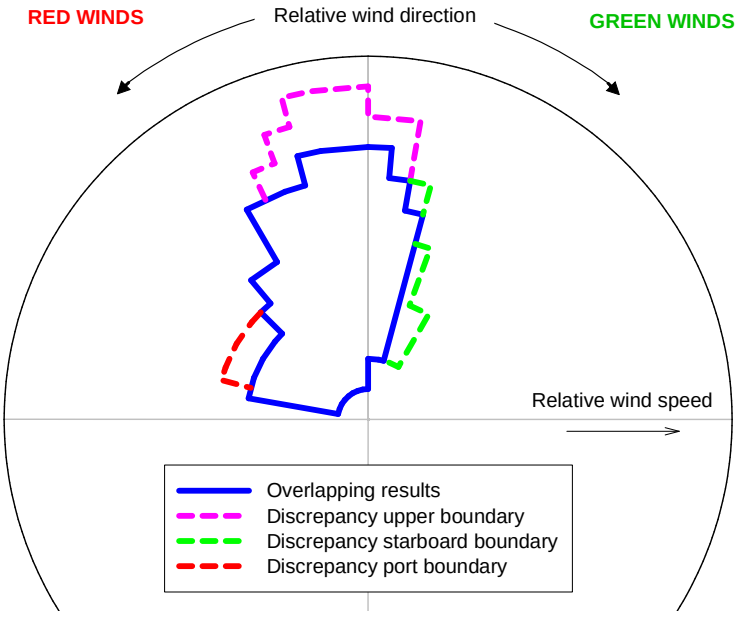

Figure 6-23; Overlapping results across entire Dutch fleet

6.6 Minimum Amount of Sea Trials Required

The "*SHOL-X*" test methodology has been used in practise to enable a much reduced flight test campaign on board the ship. However, regardless of what pre/post test data manipulation is performed, the fleet remains required for testing of some relative wind conditions and ship motion to assess the pilot workload and visual references acceptability (e.g. visual references, ship motion and turbulence). Therefore, with the novel test methodology applied, 10-15 flight hours are recommended as a bare minimum for sea trials in order to evaluate a particular helicopter-ship combination. The corresponding savings for the sea trials, compared with other current test methodologies, in time required and flight hours consumed for it are roughly 70% whilst at least the same operational capability can be achieved. This is equivalent to a reduction in time required for the sea trials from at least a three week period towards a seven day period, and a reduction from at least 45 flight hours towards a maximum of 15 flight hours required [15]. Consequently, the construction of the operational limitation for Hot & Heavy condition are based on the data gathered during the shore-based hover trials, and the flight test results for the other referred weights on board the same ship type. In case the structured test methodology is applied as described in this dissertation, the Hot & Heavy envelope can be developed by desk-top analysis alone.

6.7 Lessons Learned from the Sea Trials

The following lessons learned from the sea trials are observed:

1. A so-called "*wedding cake*" strategy should be used in which the results for the higher referred weight are also valid for the lower referred weights;
2. A test point should only be considered successful in case the pilot gives an acceptable workload rating, while at the same time objective data indicates sufficient safety margins;
3. There is always a minimum amount of sea trials required for each ship type to assess the effects on pilot workload, for example, visual references, ship motion and turbulence;
4. The objective test data is usually more consistent and restrictive in defining the boundaries of the operational envelope than the subjective ratings given by the pilot;
5. When the anemometer corrections are made correctly the SHOL boundaries are mainly helicopter related and thus not ship related.

6.8 Chapter Review

The "*SHOL-X*" approach seeks to replace some or much of the experimentation at sea with less expensive simulation results that are validated with experimental data. The rejection criteria are used to accurately define the boundaries of the operational limitations and to assess whether actual limits are approached or whether there is still room for expansion of the envelope. The construction of a SHOL envelope can now be

achieved by two different options. The first and most common option is using dedicated sea trials in which the potential boundaries for the various take-off and landing procedures are validated. Preferably, during the sea trials the complete CFE is explored, such that all the evaluated parts can be released to service. By doing so, it also provides a validation of the predictive tool and gives the associated level of confidence for that particular helicopter-ship combination to be used as baseline for successive trials. The second option is the construction of the Hot & Heavy envelope by desk-top analysis alone. This option is new and only feasible in case the structured test methodology is applied as described in this dissertation. The construction of the operational limitation for Hot & Heavy condition are based on the data gathered during the shore-based hover trials, and the flight test results for the other referred weights on board the same ship type. The construction of operational limitations by desk-top analysis alone is a novel approach, and can be seen as the most important achievement of this work.

In the SHOL's released to service within the entire Dutch fleet, the objective rejection criteria are generally more consistent and restrictive in defining the boundaries of the operational envelopes determined during the sea trials than the subjective ratings given by the test pilots involved. Although there is no straightforward explanation, this is an important conclusion as it supports the philosophy to use objective rejection criteria to accurately predict the likely outcome of the sea trials. It also enables to minimize the amount of test pilots involved in the sea trials whilst ensuring that the released envelopes may be safely operated by the "*average*" fleet pilot. Furthermore, the combined results of the SHOL's for each ship type within the entire Dutch fleet have a large similarity. This indicates that when the anemometer corrections are made correctly, the SHOL boundaries are mainly helicopter related and thus not ship related. It is a fundamental prerequisite of efficient helicopter-ship qualification testing to understand that the operational limitations are mainly caused by the helicopter flight characteristics, and not the ship type, once the anemometer corrections are applied correctly towards the undisturbed relative wind. This allows for quick exploration of the potential boundaries for each ship type without wasting time to pursue the boundaries with a conservative incremental approach. In this way, potential losses are avoided of valuable time and/or useful environmental conditions which could not be compensated for at a later stage of the test campaign.

The fleet remains required for testing of some relative wind conditions and ship motion to assess the pilot workload and visual references acceptability. Therefore, with the novel test methodology applied, 10-15 flight hours are recommended as a bare minimum for sea trials in order to evaluate a particular helicopter-ship combination. The corresponding savings for the sea trials, compared with other current test methodologies, in time required and flight hours consumed for it are roughly 70% whilst at least the same operational capability can be achieved. This is equivalent to a reduction in time required for the sea trials from at least a three week period towards a seven day period, and a reduction from at least 45 flight hours towards a maximum of 15 flight hours required.

Chapter 7 Conclusions, Recommendations and Alternative Use

7.1 General

The goal of this research project is to develop a novel test methodology which can be used for optimizing cost and time efficiency of helicopter-ship qualification testing without reducing safety. For this purpose, the so-called "*SHOL-X*" test methodology has been established, which includes the associated predictive software tool as developed in this dissertation. The test methodology comprises three distinctive phases. In *phase I* the ship-environment in which the helicopter will operate is determined by conducting wind tunnel measurements of the airflow in the take-off and landing paths of the ship. For the helicopter, a ground assessment and shore-based hover trials are carried out to verify precisely the helicopter limitations, including aspects such as e.g. pilot workload in cross-wind conditions, engine performance and control margins. This initial phase is necessary to rightfully use the predictive tool to assess the likely operational capability for take-off and landing of a particular helicopter-ship combination. Thereafter, in *phase II*, the potential operational limitations are derived by combining the behaviour of the isolated helicopter and the environmental conditions for a particular ship type. This so-called "*Candidate Flight Envelope*" is used as starting point for sea trials. Finally, in *phase III*, a (partial) flight test campaign on board the ship is conducted preferably in a range of weather conditions by day and by night. This is to determine for the particular helicopter-ship combination the effects on the pilot workload from, for example, visual references, ship motion and turbulence.

The main advantage of the new test methodology, aided by the presented predictive tool, is that the operator can perform early evaluation of safety limits for helicopters operating on ships in a wide range of in-service conditions. In this way, the qualification process is less dependent on the successful outcome of solely qualitative assessed test points during dedicated sea trials. As such, the test methodology can be used to allow a well-considered assessment of the gap between the Safe Flight Envelope (SFE), as determined by the helicopter manufacturer, and the user-defined Operational Flight Envelope (OFE) for a particular helicopter-ship combination. Additionally, the tool allows initial assessment of the impact of design changes to both helicopter and/or ship after the finally established Ship Helicopter Operational Limitations (SHOL) have been released to service with regard to flight performance and control capability.

In the first place this dissertation aims at answering the research questions as were posed in Chapter 1. These questions relate to the increase in knowledge of the behaviour of the helicopter in the shipboard environment required for the development, but also the verification, calibration and validation of the new predictive tool.

Subsequently, the innovative test methodology and validated predictive tool are to be used to improve trials efficiency of helicopter-ship qualification testing for various operational conditions at sea. Furthermore, the effects of environmental conditions on the performance of the helicopter by means of full-scale trials had to be evaluated. This is required to determine to which extent results from sea trials, performed in the North Sea, can be used to construct operational limitations for Hot & Heavy conditions by desk-top analysis alone, i.e., above approximately 25 °C outside air temperature (hot) with maximum weight of the helicopter (heavy).

7.2 Conclusions

In the following paragraph the main conclusions for the objectives and their related research questions are summarized:

1. *Create a predictive software tool that represents reality accurately enough to make it useful to evaluate the operational capability of any helicopter-ship combination. The questions to be answered are:*

    a. *What is the validity of this tool with respect to: helicopter performance, flight characteristics and other limitations?*

To enable a well-considered consideration of the various aspects that determine the limitations of a particular helicopter-ship combination, firstly there is a distinction made between "*rejection criteria"* for each helicopter type, and their "*dependencies*" in the ship environment as defined by the author (see paragraph 4.3):

- *Rejection criteria* are quantitative and qualitative helicopter parameters which, once exceeded, prevent safe execution of a flight phase;
- *Dependencies* are variables in a flight phase which directly influence their related rejection criteria.

The subdivision is made to be less dependent on the dedicated sea trials. Rejection criteria, and how they are influenced by dependencies, are determined for every new type of helicopter or are a consequence of significant changes to an old aircraft, which might affect low-speed performance and/or handling qualities. A distinction is made between rejection criteria for subjective, performance, control position, and aircraft attitude related issues. The model code of the predictive tool was initially verified and validated at sub-model level, after which the predictive tool has been calibrated as a whole. The calibration phase was used to improve agreement between the computational results and the experimental data that were obtained by actual sea trials. The only noteworthy calibration performed for the predictive tool is an increase in the minimum wind speed as determined during the wind-tunnel tests, and applied towards the helicopter flight characteristics. Otherwise, there would be too much torque required throughout the predicted envelope (i.e. the torque required decreases with increasing wind speed). Possible causes for the discrepancy between the predictive tool and the experimental data could be either: the absence in the model of ground effect or a spatially distributed flow field as seen for the various blade sections of the rotor in the ship airwake, too large safety margins, different piloting techniques in case

the helicopter is power limited, the application of minimum and maximum wind values throughout the whole approach and departure paths whilst certain phases thereof may be more relevant, or any combination of these items. In general, the validity of the individual aspects that together form the basis of the predictive tool is adequate to make predictions about helicopter performance, flight characteristics and other limitations for full-scale behaviour (see paragraph 5.7).

b. To what extent can this tool be used to evaluate the operational capabilities of a specific helicopter-ship combination objectively?

In the operational limitations as released to service within the entire Dutch fleet, the objective rejection criteria are generally more consistent and restrictive in defining the boundaries of the operational envelopes determined during the sea trials than the subjective ratings given by the test pilots involved. Although there is no straightforward explanation, this is an important conclusion as it supports the philosophy to use objective rejection criteria to accurately predict the likely outcome of the sea trials. In addition, the preliminary investigation in *Phase I* of the test methodology enables a systematic approach to the assembly of the database for the construction of the Candidate Flight Envelope (CFE), related to the concept of rejection criteria and their quantification. As a starting point of the sea trials, the CFE is used, which is a diagram giving the likely combinations of indicated wind speed (in radial coordinates) and direction (in angular coordinates) for safe take-offs and landings from a particular ship type. As such any issues can be properly investigated before being embarked on board the ship whilst under huge pressure to provide the widest operational capabilities within the least amount of time. Furthermore, the consistency in the objective rejection criteria enables to minimize the amount of test pilots involved in the sea trials whilst ensuring that the released envelopes may be safely operated by the "*average*" fleet pilot. The predictive tool has proved to give a good agreement between the experimental and computational data, and thus can be used to evaluate the operational capabilities of a specific helicopter-ship combination objectively (see paragraph 6.3).

2. Use the predictive software tool to develop a test methodology that aims at a bare minimum in flight hours and the lowest possible demand on sailing periods for ships without any concessions to flight safety. This requires the following questions to be answered:

a. How should the predictive software tool be used in order to have maximum benefit during the construction and exploration of a practically applicable operational flight envelope?

Once the innovative test methodology is applied, the construction of the operational limitations can be achieved by two different options. The first and most common option is using dedicated sea trials in which the potential boundaries for the various take-off and landing procedures are validated. The main objective of the sea trials is now the confirmation of the CFE's by collecting quantitative test data to validate the predictions to ensure that within the released operational envelopes no helicopter limitations are exceeded. In addition, at least equally important, a confirmation is required based on qualitative elements to determine the effects on pilot workload from,

for example, visual references, ship motion and turbulence. The merging of the quantitative and qualitative assessment is what defines the operational capacities for a particular helicopter-ship combination and is defined as the operational limitations in the SHOL's released to service for take-off and landing. The merging process between the quantitative and qualitative flight test data from the sea trials is achieved by an innovative feature in "*SHOL-X"*. This feature allows flight test data to be uploaded, and instantly organizes the flight test data such that it is presented in graphical format. It is then a matter of constructing the SHOL such that it excludes as many rejection criteria as possible. The novelty in this approach for the sea trials is an increased efficiency in the execution and thorough understanding in the boundaries of the operational capabilities. The second option is the construction of the operational limitations for Hot & Heavy conditions by desk-top analysis alone. The construction of the operational limitations for Hot & Heavy condition are based on the data gathered during the shore-based hover trials, and the flight test results for the other referred weights (i.e. helicopter weight as a function of air density) on board the same ship type. The construction of operational limitations by desk-top analysis alone is a novel approach, and can be seen as the most important achievement of this work (see paragraph 6.4).

b. How should a newly developed predictive software tool be tested in order to assess its accuracy in the predictions made?

The innovative test methodology, including the associated predictive tool, has already been successfully applied between 2012 and 2014 during the helicopter-ship qualification process of the NH90 NFH across the entire Dutch fleet. The academic research is mainly performed somewhere between technology readiness level 2 (i.e. technology concept and/or application formulated) and technology readiness level 4 (i.e. model and/or sub-models validation). However, the validation sea trials at full-scale enabled the high ambition of this research project to be achieved: technology readiness level 7 (i.e. model demonstration in an operational environment). This high aim might seem ambitious for an academic research; although the reader should fully understand that the aim of this research is to reduce the number of flight hours for helicopter-ship qualification testing without reducing safety. To draw rightful conclusions from this ambitious research objective, the test methodology and consequential software model, needs to be made available and validated to make meaningful conclusions for full-scale predictions. The validity of the predictive tool has been evaluated by comparing it to data sources not previously used from various independent experimental derived data sets from sea trials. The new test methodology and the implementation thereof in a predictive tool, used to perform early evaluation of safety limits for helicopters operating on ships, are considered original, and can be seen as the most important novelty of this work (see paragraph 6.3).

c. How much actual at-sea testing is required as a bare minimum for a specific helicopter-ship combination?

The "*SHOL-X"* test methodology has been used in practise to enable a much reduced flight test campaign on board the ship. However, regardless of what pre/post test data manipulation is performed, the fleet remains required for testing of some relative wind

conditions and ship motion to assess the pilot workload and visual references acceptability. Therefore, with the new test methodology applied, 10-15 flight hours are recommended as a bare minimum for sea trials in order to evaluate a particular helicopter-ship combination. The corresponding savings for the sea trials, compared with other current test methodologies, in time required and flight hours consumed for it are roughly 70% whilst at least the same operational capabilities can be achieved. This is equivalent to a reduction in time required for the sea trials from at least a three week period towards a seven day period, and a reduction from at least 45 flight hours towards a maximum of 15 flight hours required (see paragraph 6.6).

d. How should any regulations for helicopter-ship qualification testing be defined, in order to be applied as an international standard?

A comprehensive analysis of the current methodologies used for helicopter-ship qualification testing, also known as dynamic interface testing, reveals that the operational capabilities for shipboard operations are evaluated after the ship and helicopter are built independently from each other. The limitations and associated operational envelope that results from the combination of the independent designs is accepted. This process contrasts sharply with a typical procurement procedure in which a 'system' is designed and built to an agreed set of requirements. For some reason, the establishment of helicopter-ship operational limitations is still considered a national responsibility, and there are no internationally agreed regulations or standard procedures. Consequently, the kind of interpretation given to such limitations differs strongly between countries. Therefore, as it is assumed that each country or operator aims for maximum operational flexibility of a particular helicopter-ship combination, with minimal expenses and without any concessions to flight safety, this dissertation has the ambition to function as the starting point for international regulations or standard procedures to conduct helicopter-ship qualification testing (see paragraph 1.1).

3. Investigate the effects of variations in the atmospheric conditions on the performance of the helicopter during shipboard operations in a world-wide theatre. The questions to be answered are:

a. What are the effects of variations in the atmospheric conditions on the boundaries of the operational flight envelope?

The following effects are visible in variations in the atmospheric conditions on the performance of the helicopter that is applicable to shipboard operations in a world-wide theatre. An increase in referred weight results in an increase in torque required, engine gas generator speed N_g, engine power turbine inlet temperature T_{46} and tail rotor thrust. As a result, for higher referred weights, an associated minimum relative wind speed is required to perform flight operations. An increase in referred weight has negligible influence on the boundaries of the operational flight envelope with regard to pedal position, longitudinal cyclic, lateral cyclic, pitch attitude and roll attitude (see paragraph 4.3.5).

b. What are the most restricting aspects for the operational flight envelope?

The following aspects are relevant for the NH90 NFH, which is a twin engine medium weight transport helicopter with a fully articulated four-bladed counter-clockwise

turning main rotor, when seen from above, with a separate tail rotor. Roll attitude of the helicopter is the main limitation in red wind conditions (which may also result in more torque utilised to manoeuvre the helicopter). Note that a red and green terminology is used throughout this dissertation to refer to winds coming from either the port or starboard side of the ship, respectively. The torque utilised is the main limitation for take-offs towards the leeward side of the ship and the lower boundaries of the envelope. Torque utilised, instead of torque required is mentioned, as the pilot may have used temporarily more torque than what would be required. The upper boundaries are mainly defined by the large pitch and roll attitude deviations of the helicopter due to the turbulence resulting from the ship's superstructure, with a corresponding increase in pilot workload (see paragraph 6.3).

c. What is the impact of a particular ship type (due to for instance airwake disturbances or ship motion) on the operational flight envelope?

The combined results of the operational envelopes as released to service within the entire Dutch fleet have a large similarity. This indicates that when the anemometer corrections are made correctly, the operational limitations are mainly helicopter related and thus not ship related. It is a fundamental prerequisite of efficient helicopter-ship qualification testing to understand that the operational limitations are mainly caused by the helicopter flight characteristics, and not the ship type, once the anemometer corrections are applied correctly towards the undisturbed relative wind. This allows for quick exploration of the potential boundaries for each ship type without wasting time to pursue the boundaries with a conservative incremental approach. In this way, potential losses of valuable time and/or useful environmental conditions which could not be compensated for at a later stage of the test campaign are avoided (see paragraph 6.5).

7.3 Recommendations

In the following paragraph the recommendations for further research are summarized:

1. More sophisticated regression trend lines could be considered for future application of the predictive tool (e.g. sine functions). These trend lines should for example be able to prevent the discrepancy in downward versus upward trends for the same data points at -180˚ and 180˚ (see paragraph 3.4).
2. The Dynamic Interface Pilot Effort Scale (DIPES) used during the shore-based hover trials is originally developed for the helicopter-ship interface. The main reason to use the DIPES scale as well for the shore-based hover trials is to ensure that the same rating scale for pilot workload is used throughout. This avoids potential error introduced by converting pilot workload from one scale to another. However, it is recommended to verify whether a single pilot workload rating scale can be developed that is suitable to correlate the pilot workload ratings from both the shore-based hover trials and the sea trials, allowing a direct comparison for these dynamic multiple axis task without specific task tolerances being required (see paragraph 4.3.3).
3. The NH90 NFH helicopter showed good handling qualities throughout. However, for other helicopter types there may be more pronounced areas with

higher workload ratings which in that case should be further investigated. For this reason, it is recommended to keep up a database belonging to each specific helicopter type under evaluation, to determine if, and to which level of complexity a pilot model can and should be incorporated in the predictive tool at a later stage (see paragraph 5.5.1).

4. The current research shows that the prediction capabilities in the field of turbulence intensity are not mature yet. Therefore, to identify areas with increased turbulence intensity including the associated responses in helicopter flight characteristics, a specific (sub) model should be developed. As such the (upper) boundaries to the potential operational limitations for a specific helicopter-ship combination can be predicted with greater precision (see paragraph 5.7.2).
5. This dissertation demonstrates that the current research in modelling and prediction for helicopter-ship qualification testing has grown to such level that it can be used as a valuable support tool. This does however necessitate a structured test methodology and a clear understanding of the various phases during the development of the predictive tool. To improve the validity of the predictive tool even further it is recommended to incorporate a collection of high quality calibration and validation data as an on-going element in the execution of new helicopter-ship qualification test campaigns. This requires keeping up a validation-portfolio belonging to each specific helicopter-ship combination, showing the results from validation studies. This will ensure that new users have realistic expectation levels, thereby decreasing the risk or erroneous decision making, based on simulation model output (see paragraph 6.3).
6. So far, the novel test methodology, assisted by the predictive tool, has successfully been applied across the entire Dutch fleet by the author. However, this assumes that to understand the process, another test crew should have already gained maritime experience and consist at least of personnel graduated from an international recognized institution trained as test pilot and/or Flight Test Engineer (FTE), e.g. at the Empire Test Pilot School (ETPS), United States Naval Test Pilot School (USNTPS) or École du personnel navigant d'essais et de reception (EPNER). However, even once graduated from a test pilot school, it is unlikely that someone can readily function as a test lead in the field of helicopter-ship qualification testing. Furthermore, it cannot even be ensured that every graduate will be involved in any helicopter-ship qualification tests during their tour at the flight test department due to few occurrences, either for a new helicopter type (e.g. every 30 years) or a new ship type (e.g. every 10 years). The small amount of occurrences also makes it difficult for any (national) flight test institution to maintain proficiency once personnel rotate within their organization. Therefore, it is recommended to develop a helicopter-ship qualification testing course consisting at least of the material described in this dissertation. This includes, for example, dealing with uncertainty analysis, analyses of the data required to define the ship environment, and the test methodology to conduct the shore-based hover trials

and sea trials as efficiently and safely as possible. In addition, work-up training of the flight test crew in a full-motion simulator should be taken into account. Most likely, the ground school would take approximately 5 days, whilst the work-up training in the simulator would take approximately 3 days. The outcome of the course contents should be used to develop international regulations for the minimum training and currency requirement required for any test crew (and managers involved in flight trials) to conduct helicopter-ship qualification testing (see paragraph 6.3).

7.4 Alternative Use of the Predictive Tool

The novel test methodology, including the associated predictive tool, has already been successfully applied to optimize cost and time efficiency for helicopter-ship qualification testing across the entire Dutch fleet. However, the author believes that the current research demonstrates that the art of modelling and prediction in the field of helicopter-ship qualification testing has grown to such level that it has potential as a valuable supporting tool for alternative use. In this context, one should for example investigate the potential for unmanned aircraft operating from ships, and consider the test methodology for helicopter operations from elevated helicopter platforms on top of buildings and in the oil and gas industry. On one side, for the application of unmanned aircraft operating from ships a structured test methodology is necessary, as there are less qualitative elements to rely upon to define the operational limitations. On the other side, for helicopter operations from elevated helicopter platforms on top of buildings and in the oil and gas industry, the combination between helicopter and platform types are numerous requiring an efficient analysis tool to aim for the highest safety standards achievable nowadays.

Appendix A **Helicopter and Ships Description**

A.1 Helicopter Characteristics

The NH90 NFH was a twin engine medium weight transport helicopter with a four bladed counter-clockwise turning main rotor, when seen from above, and a bottom-forward rotating tail rotor as shown in Figure A-1. Its maximum take-off weight was 11 000 kg. The helicopter was fitted with a retractable tricycle type landing gear and a harpoon deck-lock system. The landing gear had a hydraulic castoring nose-wheel for rotating the helicopter in any direction, whilst remaining secured on the flight deck. The helicopter had Rolls-Royce RTM 322-01/9 engines, including Full Authority Digital Engine Controller (FADEC) software, variable main rotor rotational speed N_r (i.e. 100 % or 104 %) with automatic management, and a First Limit Indicator (FLI) presented the power margin between power required and power available on the primary flight display in the cockpit. Conventional cyclic, collective and yaw pedals were fitted, assisted by a fly-by-wire control system and a hydraulic system. The general helicopter characteristics are summarized in Table A-1.

Figure A-1; NH90 NFH helicopter

The Flight Control System (FCS) was an electrical quadruplex (dual digital, dual analogue) control system as shown in Figure A-2. The FCS interfaced with the core and mission systems for sensor data, guidance commands and displays. It was grouped into the following functional areas:

- The pilot/co-pilot interfaces which included:
    - Pilot/co-pilot flying controls (i.e. collective, cyclic and yaw pedals);

Main rotor	Units	Characteristics
Diameter	m	16.3
Speed at 100% Nr	RPM	256
Speed at 104% Nr	RPM	266
Rotating direction	-	Counter-clockwise
Tail rotor	**Units**	**Characteristics**
Type	-	Pusher
Rotating direction	-	Bottom forward
Engines	**Units**	**Characteristics**
Number	-	2
Type	-	RTM 322-01/9
Max continuous power	kW (at 100% Nr)	2 265

Table A-1; General helicopter characteristics

  - Pilot control units for Automatic FCS (AFCS) mode selection:
    - Two Flight Control Lateral Control Panels (FCLCP);
    - One Flight Control Central Control Panel (FCCCP).
  - An FCS Auxiliary Unit (FCSAU) to perform some FCS reconfiguration and select certain FCS modes;
  - A Winchman Trim Unit (WTU) installed in the cabin.
- Flight Control Processing (FCP), of which each Flight Control Computer (FCC) contained:
  - AFCS processing of outputs from the Automatic Flight Control Computer (AFCC) to control the upper modes for hands-off operation;
  - Flight control digital processing Primary Flight Control Digital Computer (PFCDC) 1a and 1b, which provided the basic modes for the enhanced functions;
  - Flight control analogue processing Primary Flight Control Analogue Computer (PFCAC) 1a and 1b, which provided the minimum functions necessary for safe flight.
- Servo Actuation System.

The servo actuation system controls the Actuator Control Computer (ACC) 1 and 2. A selector chooses one input among the four actuator command inputs received from the FCP in accordance with the priority logic which processes the validity of the different actuator commands. In nominal configuration (all redundancies available), the four ACC channels were active and drove the four actuators. Each ACC channel drove a single torque motor for each of the four actuators. All channels operated simultaneously and performed self monitoring. In case of a detected failure, the torque motor channel and the associated position transducers were inhibited. There were three identical Main Rotor Actuators (MRA) installed on the main gear box and evenly

spaced around the fixed swashplate. Their combined displacement controlled the collective and cyclic pitch of the main rotor blades. There was no physical mixer unit, as this function was controlled by the FCC. The Tail Rotor Actuator (TRA) displacement controlled the pitch applied to the tail rotor blades for yaw control.

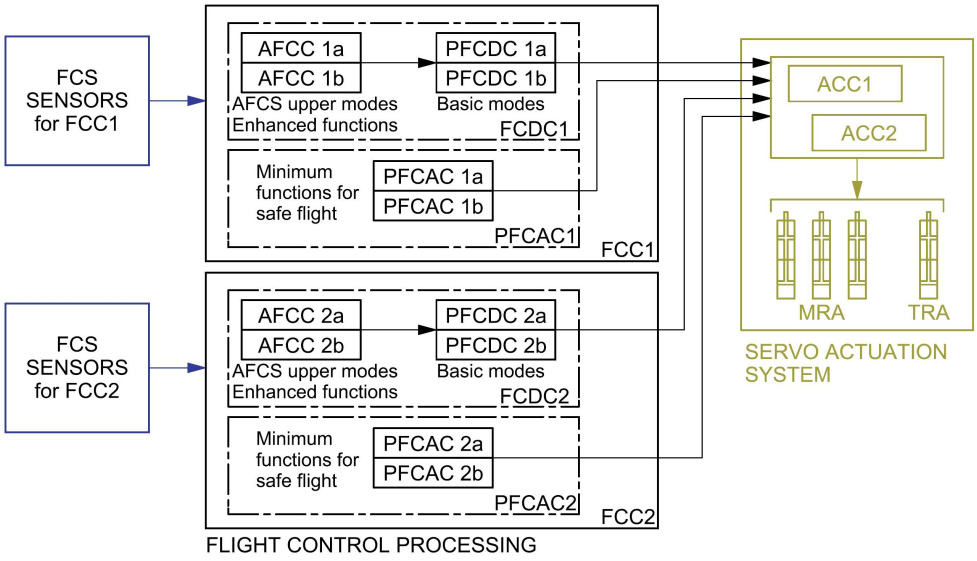

Figure A-2; Flight control system functional areas [1]

A.2 Ships Characteristics

A.2.1 AOR "Zr.Ms. Amsterdam"

Figure A-3; Auxiliary Oiler Replenishment (AOR) "Zr.Ms. Amsterdam" [2]

Figure A-4; AOR "Zr.Ms. Amsterdam"

Parameter	Units	Characteristics
Length overall	m	166.0
Displacement (max)	tons	17 040
Maximum speed	knots	21
Number of spots	-	1
Dimensions of flight deck	m	29.1 x 22.1
Height of spot above sea level	m	8.0
Hangar height above flight deck	m	8.0
Distance of grid centre to hangar	m	16.0

Table A-2; Relevant ship characteristics AOR

A.2.2 LCF "Zr.Ms. Zeven Provinciën" class

Figure A-5; Air defence and Command Frigate (LCF) "Zr.Ms. Zeven Provinciën" class [2]

Figure A-6; LCF "Zr.Ms. Zeven Provinciën"

Parameter	Units	Characteristics
Length overall	m	144.2
Displacement (max)	tons	6 280
Maximum speed	knots	26
Number of spots	-	1
Dimensions of flight deck	m	27.2 x 18.8
Height of spot above sea level	m	5.0
Hangar height above flight deck	m	8.9
Distance of grid centre to hangar	m	14.4

Table A-3; Relevant ship characteristics LCF

A.2.3 LPD1 “Zr.Ms. Rotterdam”

Figure A-7; Landing Platform Dock No.1 (LPD1) “Zr.Ms. Rotterdam” [2]

Figure A-8; LPD1 “Zr.Ms. Rotterdam”

Parameter	Units	Characteristics
Length overall	m	166.0
Displacement (max)	tons	12 750
Maximum speed	knots	20
Number of spots	-	2
Dimensions of flight deck	m	56.2 x 22.6
Height of forward spot above sea level	m	13.0
Height of rear spot above sea level	m	13.6
Slope angle flight deck(docking)	deg	1.2 stern-down
Slope angle flight deck (cruise)	deg	1.7 stern-up
Hangar height above flight deck	m	14.7
Distance of forward grid centre to hangar	m	22.8
Distance between both grids	m	29.4
Distance lateral for both spots from centre line	m	1.5 to port

Table A-4; Relevant ship characteristics LPD1

A.2.4 LPD2 “Zr.Ms. Johan de Witt”

Figure A-9; Landing Platform Dock No.2 (LPD2) “Zr.Ms. Johan de Witt” [2]

Figure A-10; LPD2 “Zr.Ms. Johan de Witt”

Parameter	Units	Characteristics
Length overall	m	176.3
Displacement (max)	tons	15 325
Maximum speed	knots	20
Number of spots	-	2
Dimensions of flight deck	m	57.6 x 24.4
Height of both spots above sea level	m	11.4
Slope angle flight deck (docking)	deg	2.5 stern-down
Slope angle flight deck (cruise)	deg	0.0
Hangar height above flight deck	m	17.4
Distance of forward grid centre to hangar door	m	28.8
Distance between both grids	m	30.0
Distance lateral for both spots from centre line	m	1.5 to port

Table A-5; Relevant ship characteristics LPD2

A.2.5 MFRI "Zr.Ms. van Speijk" class

Figure A-11; Multi-purpose frigate (MFRI) "Zr.Ms. van Speijk" class [2]

Figure A-12; MFRI "Zr.Ms. van Nes"

Parameter	Units	Characteristics
Length overall	m	122.3
Displacement (max)	tons	3 384
Maximum speed	knots	29
Number of spots	-	1
Dimensions of flight deck	m	24.6 x 14.9
Height of spot above sea level	m	5.1
Hangar height above flight deck	m	6.3
Distance of grid centre to hangar	m	13.9

Table A-6; Relevant ship characteristics MFRI

A.2.6 OPV "Zr.Ms. Holland" class

Figure A-13; Ocean Patrol Vessel (OPV) "Zr.Ms. Holland" class [2]

Figure A-14; OPV "Zr.Ms. Holland"

Parameter	Units	Characteristics
Length overall	m	108.4
Displacement (max)	tons	3 750
Maximum speed	knots	20
Number of spots	-	1
Dimensions of flight deck	m	28.5 x 15.5
Height of spot above sea level	m	5.6
Hangar height above flight deck	m	8.8
Distance of grid centre to hangar	m	15.3

Table A-7; Relevant ship characteristics OPV

Page intentionally left blank

Appendix B **Basic Knowledge Helicopter Performance**

B.1 Helicopter Performance

Most current helicopters are of the single four-bladed main rotor configuration with a separate tail rotor. For this reason only this type of helicopter will be focused on with specific emphasize on the NH90 NATO Frigate Helicopter (NFH) which is in service within the Netherlands Ministry of Defence (NLMoD) and many other countries worldwide. The basic theoretical knowledge required to understand the calculations of the helicopter performance for shipboard operations is summarized in this section. For this reason the helicopter performance is only described for hover, vertical climb and forward climbing flight conditions. Other flight conditions, such as for example descents, autorotation and vortex ring state have been omitted as these are not considered relevant for determination of the operational limitations of helicopter performance for shipboard operations.

B.1.1 Performance Calculations in Hover

The hover performance of the helicopter is described by two commonly used theories, namely (1) the actuator disc theory and (2) the blade element theory.

Actuator Disc Theory

In case the drag caused by the fuselage and other parts of the helicopter are neglected, equilibrium exists in hover between the thrust T (in this case delivered by the main rotors) and the weight W of the helicopter as shown in Figure B-1. This is expressed by the following equation:

$$T = W \qquad \textbf{(Eq. B-1)}$$

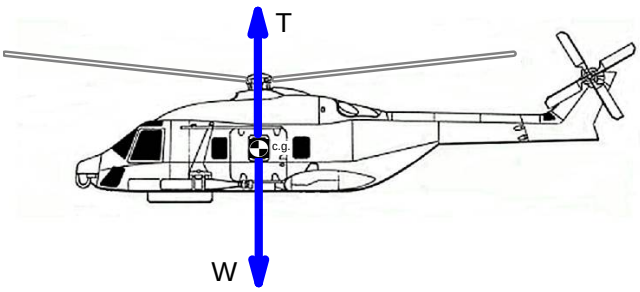

Figure B-1: Equilibrium in hovering flight

Acceleration of the amount of air that goes through the main rotors generates the thrust. The thrust is taken as being equal to the rate of change in momentum of the airflow

passing through the disc, alternatively as the mass flow rate through the disc multiplied by a change in velocity. An expression can be derived for the power required to deliver the thrust as demonstrated by Glauert [1]. The actuator disc theory states that the first part of the velocity change is realised in the region of contracting flow before the disc (i.e. main rotor). The second part of the velocity change is realised downstream the disc, where the airflow is contracting further. It is possible to show that this velocity is twice the induced velocity v_i just before the actuator disc. The velocity in the far wake w is:

$$w = 2v_i \qquad \textbf{(Eq. B-2)}$$

Thus, just above the disc, the induced velocity has a magnitude that is exactly half the magnitude of the velocity in the far-distant rotor wake as shown in Figure B-2. When a constant mass flow rate $\dot{m}$ is assumed and v_i is the induced velocity at the location of the rotor disc, the thrust is given by the following expression for the momentum equation:

$$T = \dot{m}w = 2\dot{m}v_i = 2\rho\pi R_r^2 v_i^2 \qquad \textbf{(Eq. B-3)}$$

In the last term the mass flow rate $\dot{m}$ through the disc is equated to the following equation for mass-balance, where ρ is the air density and R_r is the rotor radius:

$$\dot{m} = \rho\pi R_r^2 v_i \qquad \textbf{(Eq. B-4)}$$

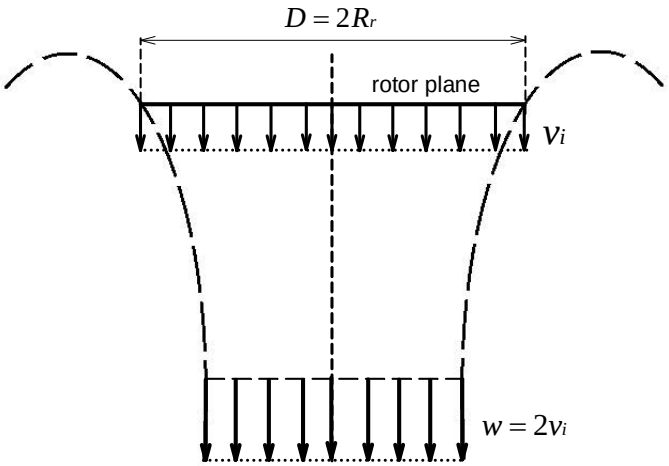

Figure B-2: Actuator disc theory in the hover

The ideal induced power to drive the main rotor in hover can then be calculated. This power is equal to the rate of increase in kinetic energy of the flow. This can be expressed with the use of the energy-balance in the following equation for ideal induced power P_{ideal}:

$$P_{ideal} = \frac{1}{2}\dot{m}(2v_i)^2 = Tv_i \qquad \textbf{(Eq. B-5)}$$

So that for the hover condition the induced velocity v_i can be written as follows:

$$v_i = \frac{w}{2} = \frac{P_{ideal}}{W} = \sqrt{\frac{W}{2\rho\pi R_r^2}} \qquad \textbf{(Eq. B-6)}$$

This expression shows that for a given air density the induced power loading W/P_{ideal} is only a function of the rotor disc loading $W/\pi R_r^2$, the latter being an important design parameter for a helicopter. Note that the downward airflow caused by the main rotor, known as the main rotor downwash, can cause spray if a helicopter is hovering close above water, snow, and or other loose surface material.

The actual power required for hovering P_{hov} is larger than the ideal induced power P_{ideal}. This is caused by a number of reasons of which some are given below [2,3]:

- The induced velocity is not uniformly distributed over the main rotor;
- The rotor blades are assumed to be rigid, but in reality a rotor blade twists and bends in complex varying modes as it rotates in azimuth;
- The flow in the wake is not free of rotation, and may interact with the tail rotor and fuselage to produce extra drag or a change in the angle of attack. Note that the increase in fuselage drag (and thus power requirements) in side winds has not been considered here;
- Power is needed to overcome the profile drag of the main rotor blades, changing with e.g. compressibility, stall, or reverse flow for varying flight conditions;
- There are lift losses at the main rotor tips;
- Aerodynamics interference exists with other components of the helicopter.

The performance of a main rotor in hover condition can be expressed by comparing the actual power required P_{hov} to produce a given thrust with the minimum possible power required to produce that thrust. The real performance in hover is often expressed in the so-called "*Figure of Merit*" (M) which is defined as the ratio of ideal induced power to actual hover power required:

$$M = \frac{P_{ideal}}{P_{hov}} \qquad \textbf{(Eq. B-7)}$$

The actual power required in hover P_{hov} is then given by the following expression:

$$P_{hov} = \frac{W}{M}\sqrt{\frac{W}{2\rho\pi R_r^2}} \qquad \textbf{(Eq. B-8)}$$

For a given rotor type, the value of M depends on the disc loading and the tip speed, among others. A well-designed rotor with good hover capabilities has $M \approx 0.75$ to 0.80, meaning that the before mentioned effects increase the power required in hover, which would result in an increase in power required of 20 % to 30 % [2].

The characteristics of the main rotor can be expressed in non-dimensional coefficients. These are usually based on the main rotor tip speed $V_{tip} = \Omega R_r$, where Ω is the main rotor rotational velocity, and on the rotor disc area πR_r^2. Two non-dimensional coefficients will now be introduced, namely the thrust coefficient C_T and the power coefficient C_P. For these two coefficients the following definitions apply:

$$C_T = \frac{T}{\rho(\Omega R_r)^2 \pi R_r^2} \quad \textbf{(Eq. B-9)}$$

$$C_P = \frac{P}{\rho(\Omega R_r)^3 \pi R_r^2} \quad \textbf{(Eq. B-10)}$$

where in this case P is a general representation of the power required. With the use of the equation above for the thrust coefficient C_T and assuming $T = W$, a characteristic main rotor parameter can be derived, namely the inflow ratio λ_i:

$$C_T = \frac{W/\pi R_r^2}{\rho V_{tip}^2} = 2\left(\frac{v_i}{V_{tip}}\right)^2 = 2\lambda_i^2 \quad \textbf{(Eq. B-11)}$$

Using Eq. B-8 the following relation between non-dimensional thrust coefficient C_T and non-dimensional power coefficient C_P can be derived:

$$C_P = \frac{C_T}{M}\sqrt{\frac{C_T}{2}} \quad \textbf{(Eq. B-12)}$$

Blade element theory

The results as derived from the actuator disc theory give useful information how the main rotor works - especially the change in the momentum flow and the kinetic energy of the flow through the main rotor. However, it does not examine how the thrust is exerted on the main rotor. Therefore, the flow on a blade section will be looked at more closely now. A blade element will be considered, this is why the accompanying theory is called the blade element method theory. The blade element theory calculates the aerodynamic forces on a number of blade elements and then integrates them along the rotor blade as demonstrated by Drzwiecki [4,5]. The blade element theory relies on the assumption that there is no flow in the radial direction (two-dimensional flow).

A blade element which is located at radius r from the main rotor centre is considered, as shown in Figure B-3, with the associated velocities and forces on this blade element applying at the aerodynamic centre. The aerodynamic centre is the point where the airfoil pitching moment coefficient does not vary with the lift coefficient, and is usually at a quarter chord of the airfoil. The blade has a pitch angle θ_p, which denotes the angle between the chord and the shaft plane. The inflow angle φ is measured between the resulting flow velocity and the main rotor plane so that $\tan \varphi = v_i / \Omega r$. The angle of attack α of the blade element equals the pitch angle θ_p minus the inflow

angle φ. With this angle of attack α, the lift force dL of the blade element can be determined.

A hover situation is considered with no forward airspeed. This means that there are only two velocity components involved. The first component is the induced velocity v_i in vertical direction. The second component is the velocity as caused by the rotation of the blade Ωr in horizontal direction. These two components form the resulting flow velocity of the blade V_{res}:

$$V_{res} = \sqrt{v_i^{\,2} + (\Omega r)^2} \qquad \textbf{(Eq. B-13)}$$

The blade element with chord c is located between the radius r and $r + dr$ and the air force dR acting on it is resolved according to different approaches. The lift force component dL on the blade element perpendicular to the flow, and the profile drag component dD_p in the direction of the flow are determined by the local conditions:

$$dL = c_l \frac{1}{2} \rho V_{res}^2 c\,dr \quad \text{and} \quad dD_p = c_{dp} \frac{1}{2} \rho V_{res}^2 c\,dr \qquad \textbf{(Eq. B-14)}$$

where c_l is the local blade section lift coefficient and c_{dp} is the local blade section profile drag coefficient. Alternatively, the air force dR is resolved into the thrust component dT in the direction of the main rotor shaft and the torque component dQ/r perpendicular to it:

$$dT = (dL\cos\varphi - dD_p \sin\varphi) \quad \text{and} \quad dQ/r = (dL\sin\varphi + dD_p \cos\varphi) \qquad \textbf{(Eq. B-15)}$$

Except for small values of r the inflow angle φ is considered small. This means that by applying the small angle approximation, the tangent of φ can also be approximated by the sine of the same angle. The cosine of φ can be approximated by one. This means that by neglecting stall and compressibility effects and assuming a constant lift curve slope $dD_p / dL << 1$, it is assumed that $dL \approx dT$.

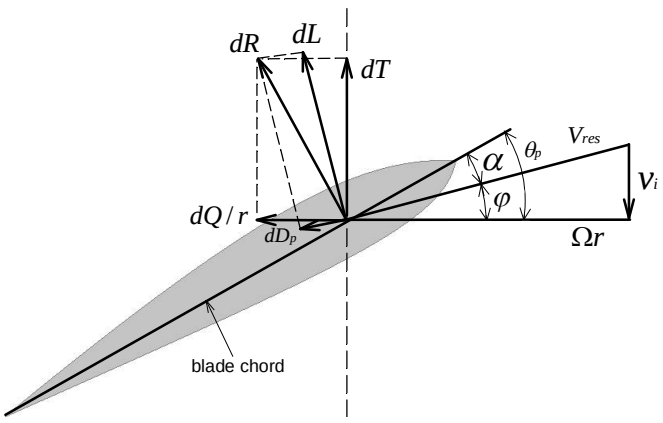

Figure B-3; Simplified view of forces on a blade element in hover

The thrust of one main rotor blade can be determined by integrating the contribution of all elements over the complete span. If it is assumed that the rotor has *N* blades then the thrust of the complete main rotor can be determined by the summation of the contribution of all *N* blades. This gives the following expression:

$$T = \int dL = N \int_0^{R_e} c_l \frac{1}{2} \rho (\Omega r)^2 c dr \qquad \textbf{(Eq. B-16)}$$

The integration is performed from the blade root ($r = 0$) to the effective rotor radius ($r = R_e$). The effective rotor radius is somewhat smaller than the actual radius because there will be losses in lift at the tip of the blade. A representative value for the effective rotor radius is $R_e = 0.97 \cdot R_r$ [3]. The integral can be evaluated analytically when a number of assumptions are made. It is assumed that the chord *c* is constant along the blade, and that there is a mean lift coefficient C_L along the blade to allow for variations along the blade:

$$T = NC_L \frac{1}{2} \rho \Omega^2 c \frac{R_e^3}{3} \qquad \textbf{(Eq. B-17)}$$

Combining this with the definition for the non-dimensional thrust coefficient C_T in Eq. B-9 leads to the following expression:

$$C_T = \frac{Nc}{\pi R_r} \frac{C_L}{6} \left(\frac{R_e}{R_r} \right)^3 \qquad \textbf{(Eq. B-18)}$$

The first term in the expression $Nc/\pi R_r$ is called the solidity σ of the main rotor. This value is normally presented as the ratio of the total blade area and the area of the main rotor disc itself. When the previously given value of $0.97 \cdot R_r$ for the ratio of the effective and the actual radius is used, the following result is obtained:

$$C_T \approx \frac{\sigma C_L}{6.6} \qquad \textbf{(Eq. B-19)}$$

The engine torque is applied to the main rotor shaft, which makes the main rotors turn with a certain Revolutions Per Minute (RPM). Equilibrium has to exist between what the main rotor blades require and what is transmitted to the shaft. Using the blade element theory it is possible to make an estimation of the power required by the main rotor. The power required by the main rotor blades is determined by taking the force on the blade element in the backward direction and by multiplying this with the distance to the main rotor axis. Subsequently, the general representation of power torque *Q* is multiplied with the angular velocity of the rotor. This leads to an expression for the general representation of power required *P*. For one blade element the following expression applies:

$$dP = \Omega dQ = \left(dL \sin \varphi + dD_p \cos \varphi \right) \Omega r \qquad \textbf{(Eq. B-20)}$$

It is possible to integrate the contribution of each element over the complete rotor radius and to sum the contributions of all blades. This gives the following result for the power required in hover P_{hov}, since $\Omega r \sin \varphi = v_i$:

$$P_{hov} = N \int_0^{R_e} v_i dT + N \int_0^{R_r} c_{dp} \frac{1}{2} \rho (\Omega r)^3 c dr \qquad \textbf{(Eq. B-21)}$$

The contribution of the lift dL is integrated over the radius from 0 to the effective radius R_e for reasons previously mentioned. The contribution of the profile drag D_p is integrated over the complete radius. When it is assumed that the chord c and the induced velocity v_i, are constant over the blade and when a mean value is assumed for the profile drag coefficient, C_{Dp}, then the integrals can be evaluated again whilst including the expression for solidity σ. Furthermore, the ideal induced power can be corrected for the effects of the non-uniform distribution of the inflow velocity v_i over the rotor disc and the small rotation in the wake. This is done with the induced drag power factor k. The induced power then becomes $P_i = kTV_i$. This leads to the following result:

$$P_{hov} = kTv_i + \frac{\sigma C_{D\,p}}{8} \rho (\Omega R_r)^3 \pi R_r^2 = P_i + P_p \qquad \textbf{(Eq. B-22)}$$

This expression shows that the power required in hover P_{hov} can be divided into two contributions. The first contribution comes from the induced power P_i. The second contribution comes from the profile drag power P_p. The induced power is caused by the backward tilt of the lift vector with respect to the main rotor axis, which is caused by the induced velocity v_i. The profile drag power is necessary to overcome the blade profile drag and the drag created by the asymmetric flow around the blades. This eventually gives for the power coefficient C_p in hover condition:

$$C_P = kC_T \sqrt{\frac{C_T}{2}} + \frac{\sigma C_{Dp}}{8} \qquad \text{with} \qquad v_i = \sqrt{\frac{W}{2\rho\pi R_r^2}} = \Omega R_r \sqrt{\frac{C_T}{2}} \qquad \textbf{(Eq. B-23)}$$

This is an important result since it suggests that for a hovering rotor the power coefficient is proportional to the thrust coefficient raised to the power 3/2 (as already demonstrated by the actuator disc theory in Eq. B-12) provided the drag coefficient remains unchanged. Likewise, if the helicopter weight is fixed and the profile drag coefficient is constant, thus C_p remains unchanged, then the power required to drive the rotor will vary with Ω^3.

B.1.2 Performance Calculations in Vertical Climb

The airflow conditions for a blade element in vertical climbing flight change in comparison to the hover condition. There are still only two velocity components involved, however, in vertical flight also the rate of climb C has to be added into the equation for the resultant flow velocity of the blade V_{res}. The first component is the induced velocity v_i, combined with the rate of climb C in vertical direction. The

second component is the velocity as caused by the rotation of the blade in horizontal direction Ωr. These two components now form the resulting flow velocity of the blade:

$$V_{res} = \sqrt{(v_i + C)^2 + (\Omega r)^2} \qquad \textbf{(Eq. B-24)}$$

Therefore from Eq. B-21 the power required in vertical climb for the main rotors P_{clb} becomes:

$$P_{clb} = N \int_0^{R_e} (v_i + C) dT + N \int_0^{R_r} c_{dp} \frac{1}{2} \rho (\Omega r)^3 c dr \qquad \textbf{(Eq. B-25)}$$

The integration leads to the following result:

$$P_{clb} = kTv_i + TC + \frac{\sigma C_{Dp}}{8} \rho (\Omega R_r)^3 \pi R_r^2 = P_i + P_c + P_p \qquad \textbf{(Eq. B-26)}$$

The power required for vertical climb is the sum of the induced power P_i, the climbing power P_c and the profile drag power P_p. The actuator disc theory gives an expression for the induced velocity using the expression for the momentum equation:

$$W = T = 2\dot{m}v_i = 2\rho\pi R_r^2 (C + v_i) v_i \qquad \textbf{(Eq. B-27)}$$

Because of the rate of climb, the mass flow through the rotor disc has become larger. This means that for the same weight the induced velocity will be smaller. Therefore, the induced power will be smaller as well. For the same weight, altitude and rotor RPM the profile drag power P_p is equal both in hovering and climbing flight.

Now introducing a non-dimensional rate of climb $\overline{C}$ and a non-dimensional induced velocity $\overline{v}_i$, where v_{ih} is the induced velocity in hover condition:

$$\overline{C} = C / v_{ih} \qquad \text{and} \qquad \overline{v}_i = v_i / v_{ih} \qquad \textbf{(Eq. B-28)}$$

Then Eq. B-27 can be manipulated to:

$$(\overline{C} + \overline{v}_i)\overline{v}_i = 1 \qquad \textbf{(Eq. B-29)}$$

Removing the brackets gives:

$$\overline{v}_i^2 + \overline{C}\overline{v}_i - 1 = 0 \qquad \textbf{(Eq. B-30)}$$

Only the positive root of the equation has any physical meaning in this case, so:

$$\overline{v}_i = -\frac{\overline{C}}{2} + \sqrt{\frac{\overline{C}^2}{4} + 1} \qquad \textbf{(Eq. B-31)}$$

In most cases the non-dimensional rate of climb $\overline{C}$ is much smaller than one. For example, for the NH90 NFH operating at 11 000 kg in ISA conditions and a Figure of

Merit *M* of 0.75, the rate of climb *C* should exceed approximately 3 650 ft/min for the non-dimensional rate of climb to become higher than one. That is the reason why the next approximations can be used:

$$\bar{v}_i = -\frac{\bar{C}}{2} + 1 \qquad \text{or} \qquad v_i = -\frac{C}{2} + v_{ih} \qquad \textbf{(Eq. B-32)}$$

When this result is substituted in the equation for power required in vertical climb in Eq. B-26, then this will lead to the following expression:

$$P_{clb} = T\left(-\frac{C}{2} + kv_{ih}\right) + TC + \frac{\sigma C_{Dp}}{8}\rho(\Omega R_r)^3 \pi R_r^2 = P_{hov} + T\frac{C}{2} \qquad \textbf{(Eq. B-33)}$$

If the tail rotor power and transmission losses are neglected thus the power delivered by the engine(s) P_{eng} is equal to the power required in climb P_{clb}, a simple expression can be found for the rate of climb *C*, and with $T = W$ applied gives:

$$C = 2 \cdot \frac{P_{eng} - P_{hov}}{W} \qquad \textbf{(Eq. B-34)}$$

In this simple expression the rate of climb *C* will be twice the value estimated from the excess power in hover.

B.1.3 Performance Calculations in Forward Climbing Flight

An important feature of the forward flight regime is the asymmetry of the flow around the main rotor disc. The flow velocity of the main rotor is different on the advancing and retreating side (the main rotor rotates counter-clockwise when seen from above) as shown in Figure B-4.

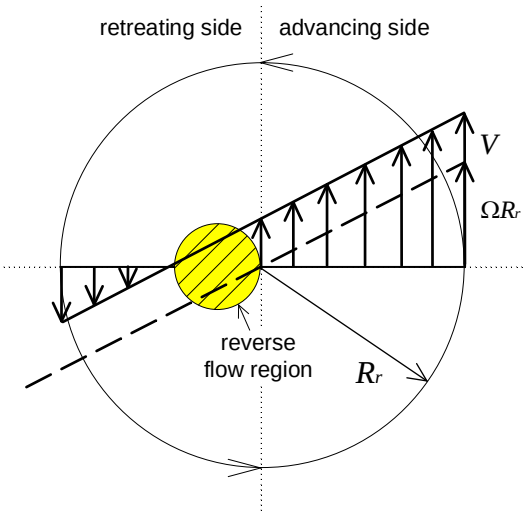

Figure B-4; Main rotor blade velocity distribution

This means that the relative velocity of the blade on the advancing side of the hub (right side) is increased with forward flight speed *V*. The blade on the retreating side of the hub (left side) has a velocity equal to the rotational velocity decreased with the forward flight speed *V*. In the circular area depicted in this figure (yellow circle in figure), the flow velocity is positive, meaning that there is a forward flow from the blade trailing edge, and this region is known as the "*reverse flow region*".

In forward flight not only the weight *W* of the entire helicopter including the main rotor must be supported, but also the air drag needs to be overcome. For this reason the main rotor plane is tilted forward. The weight and drag act on the helicopter's fuselage in a steady forward climbing flight as shown in Figure B-5. Note that the parasite drag D_{par} consists of the drag of the entire helicopter except the rotor. The H_i-force is caused by the difference in inclination of the lift force on the left and right side of the hub. The H_0-force is caused by the difference in profile-drag on the left and right side of the hub. The blade tips describe a conical plane relative to the rotor hub, and this plane described by the blade tips is known as the tip-path plane. Furthermore, the angle of attack of the rotor tip-path plane α_{tip} and the flight path angle γ are introduced.

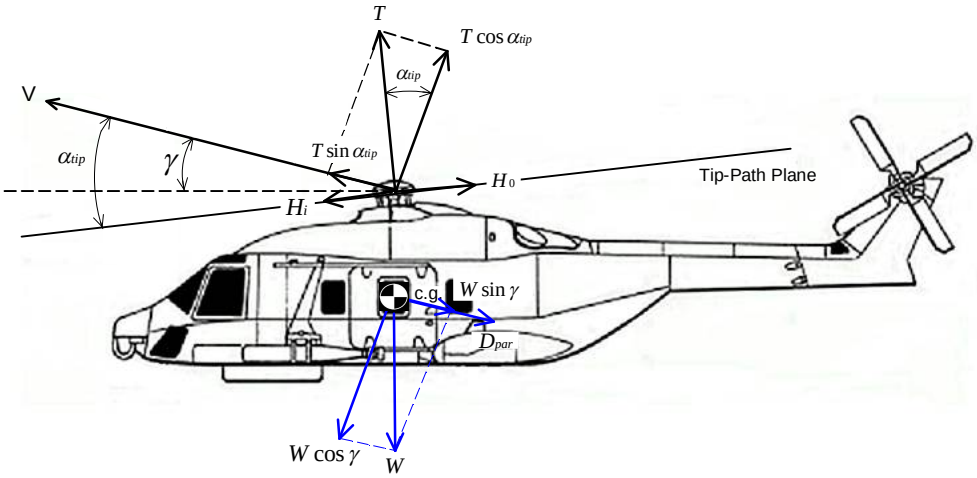

Figure B-5; Forces on a helicopter in forward climbing flight

The angle of attack of the tip-path plane α_{tip} is defined such that a forward tilt of the rotor disc results in a positive angle of attack. The equilibrium of forces on the helicopter gives along the flight path and perpendicular to the flight path the following expressions respectively:

$$T \sin \alpha_{tip} + H_i \cos \alpha_{tip} = D_{par} + H_0 \cos \alpha_{tip} + W \sin \gamma \qquad \textbf{(Eq. B-35)}$$

$$T \cos \alpha_{tip} - H_i \sin \alpha_{tip} + H_0 \sin \alpha_{tip} = W \cos \gamma \qquad \textbf{(Eq. B-36)}$$

In practice, the *H*-forces are usually small and opposite in direction. Calculating the work done by the rotor forces per unit of time and adding the profile-drag power P_p

determines the power required to drive the rotor in forward flight P_{fwd}. This leads to the following equation for power required to drive the main rotor in forward climbing flight along the flight path:

$$P_{fwd} = T\left(V \sin \alpha_{tip} + k v_i\right) + P_p + H_i V \cos \alpha_{tip} \qquad \textbf{(Eq. B-37)}$$

The velocity v_i is the induced velocity perpendicular to the tip-path plane. The above equation for the power required in forward climbing flight P_{fwd} can now be combined by substituting Eq. B-35 and Eq. B-36 into it, whilst knowing that the climb rate C is equal to $V \sin \gamma$:

$$P_{fwd} = kTv_i + D_{par} V + P_p + H_0 V \cos \alpha_{tip} + WC \qquad \textbf{(Eq. B-38)}$$

$$P_{fwd} = P_i + P_{par} + P_p + P_d + P_c \qquad \textbf{(Eq. B-39)}$$

This means that in forward flight the power required is built up from the induced power P_i, the parasite drag power P_{par}, the total profile drag power $P_p + P_d$, and the climbing power P_c. The profile drag power consists of two contributions. The first contribution P_p comes from the profile drag of the main rotor blades. The second contribution P_d comes from the H_0-force. In the following paragraphs the different contributions will be analysed separately.

Induced power in forward flight

According to Glauert [1] the momentum theory is applicable in forward flight assuming that the rotor mass flow is proportional to the combined result of the forward flight speed V and the induced velocity v_i:

$$\dot{m} = \rho \pi R_r^2 V_{res} \qquad \textbf{(Eq. B-40)}$$

In this equation V_{res} is the resulting flow velocity originating from a vector summation of the forward flight speed V and the induced velocity v_i as shown in Figure B-6.

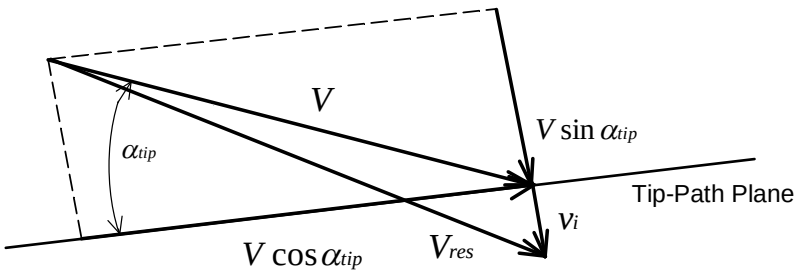

Figure B-6; Resulting flow velocity for the rotor disc

For high forward flight speeds $v_i << V$ and thus $V_{res} \approx V$, the thrust of the main rotors is given by the change of momentum per unit of time:

$$T = \dot{m} 2 v_i = 2 \rho \pi R_r^2 V_{res} v_i \qquad \textbf{(Eq. B-41)}$$

From Figure B-6 the following expression can be derived for the resultant flow velocity V_{res} which then combined with the equation above and assuming $T = W$ yields:

$$V_{res}^2 = (V \sin \alpha_{tip} + v_i)^2 + V^2 \cos^2 \alpha_{tip} = \left(\frac{W}{2\rho\pi R_r^2 v_i} \right)^2 = \left(\frac{v_{ih}}{v_i} \right)^2 \qquad \textbf{(Eq. B-42)}$$

This equation can be written in non-dimensional form. The non-dimensional velocities are obtained by dividing their dimensional values by the induced velocity in hover v_{ih}:

$$\frac{1}{\bar{v}_i^2} = \left(\bar{V} \sin \alpha_{tip} + \bar{v}_i \right)^2 + \bar{V}^2 \cos^2 \alpha_{tip} \qquad \textbf{(Eq. B-43)}$$

where $\bar{v}_i$ is the non-dimensional induced velocity and $\bar{V}$ is the non-dimensional forward flight speed.

In order to solve the non-dimensional induced velocity for a given non-dimensional flight speed, the angle of attack of the rotor disc α_{tip} is needed. This angle can be approximated from equilibrium of forces on the helicopter in forward climbing flight provided that the *H*-forces are neglected.

$$\sin \alpha_{tip} = \frac{D_{par}}{W} + \sin \gamma \qquad \text{or} \qquad V \sin \alpha_{tip} = \frac{P_{par}}{W} + C \qquad \textbf{(Eq. B-44)}$$

For a given flight condition in level or climbing flight the angle of attack can be derived, and the non-dimensional induced velocity determined. After that, the induced power can be calculated. For rough estimations in practice it is possible to use a number of simple approximations. In high-speed flight the induced velocity is small. This is a result of the large mass flow passing through the rotor. The resulting flow velocity is then nearly equal to the flight speed. In this case a simple expression follows:

$$v_i = \frac{T}{2\rho\pi R_r^2 V} \qquad \text{or} \qquad \bar{v}_i = \frac{1}{\bar{V}} \qquad \textbf{(Eq. B-45)}$$

The approximation can be applied for high-speed flight conditions both for level flight as well as for climbing flight, resulting in the following expression for induced power P_i:

$$P_i = kTv_i \qquad \textbf{(Eq. B-46)}$$

Parasite drag power in forward flight

The parasite drag D_{par} consists of the drag of the entire helicopter except for the main rotor. The parasite drag power P_{par} is the power required to overcome the helicopter drag. For performance calculations it can be assumed that this power is equal to the parasite drag multiplied by the forward speed. The parasite drag is simply approached by assuming an equivalent flat plate area of the geometry of the helicopter. It is

impossible to calculate the equivalent flat plate analytically. Therefore, experimental data are often used. There is some correlation between the dimensions (and therefore the weight) of the helicopter and its equivalent flat plate area, although there is a difference between the aerodynamically refined and less refined helicopters. The parasite drag is obtained by multiplying the equivalent flat plate areas by the dynamic pressure. For a given altitude, the power required to overcome the parasite drag is proportional to the airspeed to the third power and to the helicopter's parasite drag area $(C_D S)_{par}$, where C_D is the 3-dimensional drag coefficient and S the equivalent flat plate area:

$$P_{par} = D_{par} V = \sum (C_D S)_{par} \frac{1}{2} \rho V^3 \qquad \textbf{(Eq. B-47)}$$

Profile drag power in forward flight

The speed of the airflow over a blade element contains a term that varies with the blade azimuth ($V sin\psi$), where ψ is the azimuth angle, and consequently the drag force will vary as the blade element moves around the hub as shown in Figure B-7. By integrating the drag force acting normal to the blade element the relationship for the profile drag power is obtained.

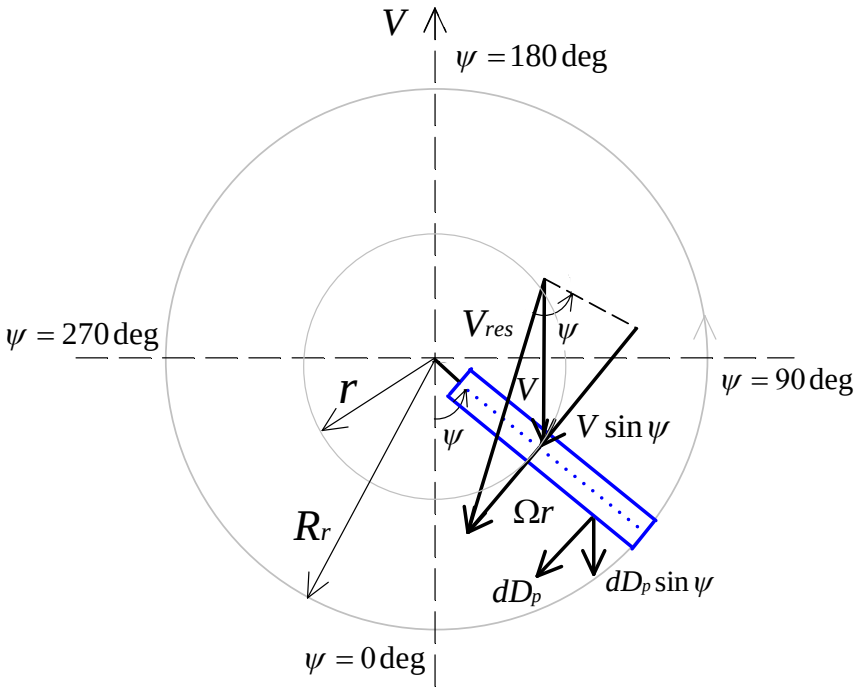

Figure B-7; Velocity diagram for a blade element

Unfortunately, this is not the complete picture. Although the power required to drive the main rotor around the hub has been found, for a forward flight speed V, it has not

been accounted for the power required to drive the main rotor system forward; the profile drag power as caused by the H_0-force. This additional power arises because there will be a hub force acting rearward which must be matched by a component of the main rotor thrust. The hub force appears because there is an asymmetry of drag acting on opposing blades. When a blade reaches the advancing side, it will see increased drag, a component of which will act rearwards. An opposing blade will see reduced drag as it enters the retreating side. Although a component of the drag on the retreating side acts forward, it will be less than on the advancing side and a net rearward hub force will result. The rotor parasite power P_p could be added to the parasite power arising from the fuselage P_{par}, however, it is more often incorporated into the estimate of profile drag power.

The profile drag power consists of two terms. The first term P_p originates from the profile drag of the rotor blades. The second contribution P_d originates from the resultant of the profile drag in the direction of the H_0-force. Both the H_0-force and the profile drag power P_p can be calculated by applying the blade element method. The profile drag power is necessary to overcome the blade profile drag and the drag created by the asymmetric flow around the blades. This power can be calculated by integrating the profile drag contribution along the blade span. For the H_0-force the following expression applies as shown in Figure B-7:

$$dP_d = VdD_p \sin\psi = Vc_{dp}\frac{1}{2}\rho(\Omega r + V\sin\psi)^2 cdr\sin\psi \qquad \textbf{(Eq. B-48)}$$

The profile drag power P_d can be obtained by multiplying dP_d by the number of blades N and integrating both along the radius and around the azimuth:

$$P_d = \frac{1}{2\pi}N\int_0^{2\pi}\int_0^{R_r} Vc_{dp}\frac{1}{2}\rho(\Omega r + V\sin\psi)^2\sin\psi cdrd\psi \qquad \textbf{(Eq. B-49)}$$

Note that the term ½ π is introduced because the average power is required around the azimuth. Now:

$$P_d = \frac{1}{2\pi}NVC_{Dp}\frac{1}{2}\rho c\int_0^{2\pi}\int_0^{R_r}(\Omega^2 r^2\sin\psi + 2V\Omega r\sin^2\psi + V^2\sin^3\psi)drd\psi \qquad \textbf{(Eq. B-50)}$$

Note that the section profile drag coefficient c_{dp} at each blade element has been replaced by the mean profile drag coefficient C_{Dp} along the blade. This is required as the profile drag coefficient is removed from the integration. Integration around the azimuth ψ now gives:

$$P_d = VC_{Dp}\frac{1}{2}\rho Nc\int_0^{R_r} V\Omega r dr \qquad \textbf{(Eq. B-51)}$$

Integration along the radius r and inserting solidity σ gives:

$$P_d = \frac{\sigma C_{Dp}}{4} \rho (\Omega R_r)^3 \pi R_r^2 \left(\frac{V^2}{\Omega^2 R_r^2} \right) \quad \textbf{(Eq. B-52)}$$

Now introducing the definition of advance ratio μ:

$$\mu = \frac{V \cos \alpha_{tip}}{\Omega R_r} \approx \frac{V}{\Omega R_r} \quad \textbf{(Eq. B-53)}$$

The definition for the profile drag power P_d caused by the H_0-force then becomes:

$$P_d = \frac{\sigma C_{Dp}}{4} \rho (\Omega R_r)^3 \pi R_r^2 \mu^2 \quad \textbf{(Eq. B-54)}$$

For the profile drag power P_p caused by the profile drag of the rotor blades, the following expression holds as shown in Figure B-7:

$$dP_p = \Omega dQ = \Omega r dD_p = \Omega r c_{dp} \frac{1}{2} \rho (\Omega r + V \sin \psi)^2 c dr \quad \textbf{(Eq. B-55)}$$

The profile drag power P_p can be obtained by multiplying dP_p by the number of blades N and integrating both along the radius and around the azimuth:

$$P_p = \frac{1}{2\pi} N \int_0^{2\pi} \int_0^{R_r} \Omega r c_{dp} \frac{1}{2} \rho (\Omega r + V \sin \psi)^2 c dr d\psi \quad \textbf{(Eq. B-56)}$$

Again, note that the term ½ π is introduced because the average power is required around the azimuth. Now:

$$P_p = \frac{1}{2\pi} N \Omega C_{Dp} \frac{1}{2} \rho c \int_0^{2\pi} \int_0^{R_r} r (\Omega^2 r^2 + 2V\Omega r \sin \psi + V^2 \sin^2 \psi) dr d\psi \quad \textbf{(Eq. B-57)}$$

The local blade section profile drag coefficient c_{dp} at each blade element has been replaced by the mean profile drag coefficient C_{Dp} along the blade. This is required as the profile drag coefficient is removed from the integration. Integration around the azimuth ψ now gives:

$$P_p = \frac{1}{2} N c \rho \Omega C_{Dp} \int_0^{R_r} \Omega^2 r^3 + \frac{1}{2} V^2 r dr \quad \textbf{(Eq. B-58)}$$

Integration along the radius r and inserting solidity σ gives:

$$P_p = \frac{\sigma C_{Dp}}{8} \rho (\Omega R_r)^3 \pi R_r^2 \left(1 + \frac{V^2}{\Omega^2 R_r^2} \right) \quad \textbf{(Eq. B-59)}$$

And with the advance ratio μ gives for the profile drag power P_p caused by the profile drag of the rotor blades:

$$P_p = \frac{\sigma C_{Dp}}{8} \rho \left(\Omega R_r\right)^3 \pi R_r^2 (1+\mu^2) \qquad \textbf{(Eq. B-60)}$$

The power equation for forward flight contains a term accounting for the total profile drag power as $P_p + P_d$. This leads to the following result:

$$P_p + P_d = \frac{\sigma C_{Dp}}{8} \rho \left(\Omega R_r\right)^3 \pi R_r^2 (1+3\mu^2) \qquad \textbf{(Eq. B-61)}$$

To calculate the profile drag, the component of the flight speed perpendicular to the blade axis is used. For small angles of attack the profile drag is to a large extent a friction drag. That is why it could be argued that the resulting flow velocity V_{res} through the rotor disc is better suited for the evaluation of the profile drag. Using this velocity leads to the following result:

$$P_p + P_d = \frac{\sigma C_{Dp}}{8} \rho \left(\Omega R_r\right)^3 \pi R_r^2 (1+n\mu^2) \qquad \textbf{(Eq. B-62)}$$

This equation shows that the profile drag power is larger for greater forward airspeeds. The value of the parameter n depends on the value of the tip speed ratio. In many cases the value 4.65 is used for the parameter n [2,3].

B.1.4 Miscellaneous Effects

In this section miscellaneous effects are described that have an impact on helicopter performance P_{misc}. The main effects are caused by the tail rotor and ground effect. Other miscellaneous effects are for example due to: losses in the gearing, transmission losses and powering requirements for the on-board systems.

Tail rotor

The engine(s) of a helicopter applies a certain torque to the main rotor. Because the helicopter is free to move when applying the torque generated by the engines Q_{eng}, the helicopter will rotate in the opposite direction due to the reaction torque Q_R. Thus for a helicopter with the main rotors turning in counter-clockwise direction when seen from above, the fuselage starts to rotate in clockwise direction (nose to the right). To prevent the rotation of the fuselage for a conventional helicopter, a tail rotor is required to deliver an anti-torque moment as shown in Figure B-8. The equilibrium about the yaw axis prescribes:

$$T_{tr} = \frac{Q_R}{l_{tr}} = \frac{P}{\Omega l_{tr}} \qquad \textbf{(Eq. B-63)}$$

where T_{tr} is the thrust delivered by the tail rotor and l_{tr} is the distance of the tail rotor from the main rotor hub. The tail rotor provides the anti-torque reaction in hover and forward flight, whilst it also serves as a yaw control device in manoeuvres. In this case, a left pedal input increases the collective pitch angle of the tail rotor which increases the tail rotor thrust force to the right. This means that the nose of the helicopter starts

rotating to the left. A right pedal input decreases the tail rotor thrust force and thus the nose of the helicopter rotates to the right.

The use of a vertical tail surface to produce a side force in forward flight can help to relieve the power required by the tail rotor, albeit at the expense of some increase in parasite and induced drag. The tail rotor power required is initially high in hover, but it quickly deceases as airspeed builds up once the main rotor torque requirements decrease. In high speed forward flight, tail rotor power required increases again as the main rotor torque increases to overcome parasite drag. However, this is usually offset to some extent by the aerodynamic side force produced on the vertical fin. The power required by the tail rotor typically varies between 5 % and 10 % of the main rotor power [1,3,6]. The interference between the main rotor and the tail rotor, and between the tail rotor and the vertical fin, is further neglected.

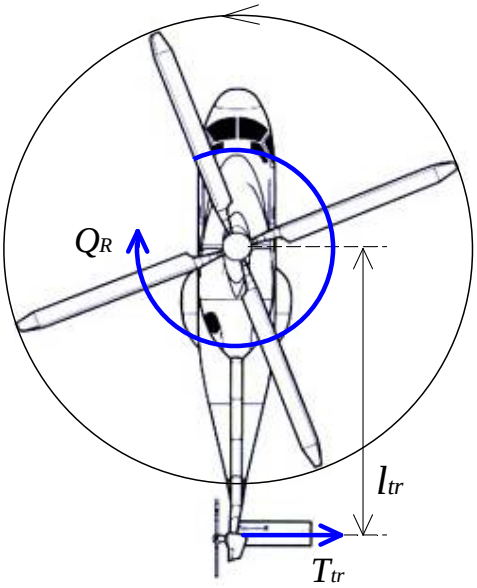

Figure B-8; Main rotor torque reaction on the fuselage, balanced by the tail rotor

Ground Effect

So far the helicopter is considered in hover without taking the ground effect into account. The presence of the ground has a positive influence on the lifting capacity of the rotor. This particularly applies for the rotor in the direct vicinity of the ground (height is smaller than one rotor radius). The effect that occurs here is a reduction of the induced velocity by the presence of the ground. This means that the required induced power is reduced, or that for a given power setting the thrust of the rotor is increased. This cushioning effect leads to the main rotor lifting more weight in the ground effect than in free flight given the engine power. However, ground effect becomes hardly noticeable if the helicopter is more than one rotor diameter above the ground. Maximum benefit from the ground effect is only accomplished when hovering

over smooth paved surfaces. Whilst hovering over tall grass, rough terrain or water the benefits of the ground effect may be seriously reduced. This phenomenon is due to the partial breakdown and cancellation of ground effect and the return of large vortex patterns with increased downwash angles. Although there may be some benefit from ground effect during shipboard operations, the effect will be further neglected in the dynamic ship environment [7].

B.2 The Atmospheric Model

The atmosphere is assumed to consist of a perfect gas with local pressure p, density ρ and temperature T related by the equation of state [2]. Furthermore, the atmosphere is assumed to be in static equilibrium with respect to the earth. The variation of pressure with height h is derived from the equilibrium condition for a small vertical cylinder of air with height dh and a cross section of a unit of area as shown in Figure B-9. The weight of the cylinder $\rho g dh$ is shown as a downward force, with g the acceleration due to gravity. A pressure p acts upwards on its bottom face, the downward pressure on the top face is slightly different and amounts to $p + dp$.

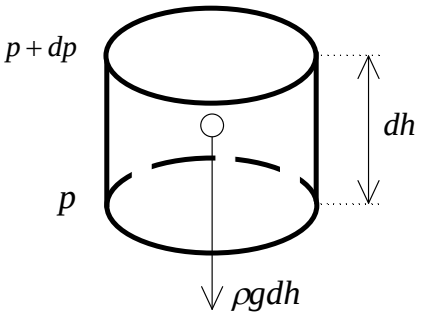

Figure B-9; Equilibrium of a cylinder element of stationary air

Since the cylinder is at rest, the pressure forces are in equilibrium with the weight. This is expressed in the following equations, showing that the decrease in pressure per unit of height is equal to the specific weight of air:

$$dp = -\rho g dh \qquad \text{or} \qquad \frac{dp}{dh} = -\rho g \qquad \textbf{(Eq. B-64)}$$

The air pressure at a certain altitude can be seen as the weight of an air column above a unit of surface area at that height. When considering the pressure distribution in the atmosphere it is convenient to use geopotential height H, which is based on a constant value for the acceleration due to gravity. The geopotential height is the geometric height in a uniform gravitational field that gives the same potential energy as exists at the point under consideration in the actual, variable gravity field. Now the work done in raising a body mass m from one geopotential surface to a higher surface is equal to the potential energy that the body has at the higher surface. If the surfaces are separated by a distance h then:

$$mg_{sl}H = m\int_0^h g\,dh \qquad \text{and} \qquad H = \frac{1}{g_{sl}}\int_0^h g\,dh \qquad \textbf{(Eq. B-65)}$$

This equation relates the geopotential height in a uniform gravitational field, in which the acceleration due to gravity is taken as equal to the sea-level value g_{sl}, and the actual variation of g with h. A relationship between standard geopotential height and pressure can be obtained by combining the above equations with the equation of state, and by assuming that the molecular composition of air is constant over the altitudes of interest. So, with R as the gas constant:

$$\frac{dp}{dh} = -g\frac{p}{RT} \qquad \textbf{(Eq. B-66)}$$

In atmospheric modelling of helicopter performance g is taken as the standard value g_0 (9.80665 m/s^2). This accepted value of g_0 corresponds to geographic latitude of 45.5425 º. Hence:

$$\frac{dp}{dH} = -g_0\frac{p}{RT} \qquad \textbf{(Eq. B-67)}$$

A particular atmospheric model is defined by substituting into the equation above a given variation of temperature with height and then deducing the corresponding variation of pressure with height. Standard atmospheres consist of layers in which the temperature is either constant or varies linearly with altitude such that:

$$T = T_b + \lambda(H - H_b) \qquad \textbf{(Eq. B-68)}$$

where T_b is the temperature at height H_b and λ is the temperature gradient, or lapse rate between different heights. Thus for the standard atmospheres under consideration, the lapse rate λ will either be zero or a constant. Consider the troposphere in which the temperature decreases linearly with altitude with a constant negative lapse rate ($dT/dH = \lambda$):

$$\int_{p_b}^{p}\frac{dp}{p} = -\frac{g_0}{\lambda R}\int_{T_b}^{T}\frac{dT}{T} \qquad \text{and} \qquad \ln\frac{p}{p_b} = -\frac{g_0}{\lambda R}\ln\frac{T}{T_b} \qquad \textbf{(Eq. B-69)}$$

where p_b is the pressure at height H_b. The equation can be simplified to:

$$\frac{p}{p_b} = \left(\frac{T}{T_b}\right)^{-g_0/\lambda R} \qquad \textbf{(Eq. B-70)}$$

In the troposphere, which extends up to 11 km, the temperature falls linearly with the lapse rate of -6.5 x 10^{-3} K/m (i.e. close to 2 ºC/1 000 ft) from sea-level value (T_0) of 288.15 K. With the sea-level ambient pressure (p_0) defined as 101.325 kN/m^2 (i.e. equivalent to 1013.25 hPa), it is possible to generate specific equations relating pressure to geopotential height.

Since only helicopters operations in the troposphere at sea level are considered, the following relation is derived:

$$\frac{p}{p_0} = \left(\frac{T}{T_0}\right)^{-g_0/\lambda R} \quad \text{and} \quad p = p_0\left(1+\frac{\lambda}{T_0}H\right)^{-g_0/\lambda R} \qquad \textbf{(Eq. B-71)}$$

Then substituting the defined constants for the International Standard Atmosphere (ISA) gives the following for height in feet:

$$p = 101.325 \cdot (1 - 6.8756 \times 10^{-6} \times H_p)^{5.2559} \qquad \textbf{(Eq. B-72)}$$

Note that H is replaced by H_p (the pressure height) as both the sea-level ISA constants and the lapse rate have been used for the formulation of the equations. This gives for the relative pressure δ:

$$\delta = (1 - 6.8756 \times 10^{-6} \times H_p)^{5.2559} \qquad \textbf{(Eq. B-73)}$$

Summary basic properties in ISA conditions

The relevant basic state variables at sea level and the acceleration due to gravity at 45.5425 º northern latitude are summarized in Table B-1.

Abbreviation	Meaning	SI
p	Pressure	1013.25 hPa
T	Temperature	15 ºC (288.15 K)
ρ	Density	1.225 kg/m^3
a	Speed of sound	340.29 m/s
g	Gravity acceleration	9.80665 m/s^2
R	Gas constant	287.05 J/kgK
γ	Ratio of specific heats	1.40
h_Δ	Vertical change in height for 1 hPa difference	27.0 ft

Table B-1; Basic properties in ISA conditions

B.3 Dimensional Analysis

Dimensional analysis is used, often unconsciously, by practically everyone who deals with physical problems. It provides a guide to experimental planning and to the correlation of data. Dimensional analysis is concerned with the nature of the relationship between various parameters which enter a physical problem. These parameters consist of groups of relevant dimensional quantities. However, before dimensional analysis can be applied it must be assured that only one relationship exists between a certain numbers of physical quantities, and that no pertinent quantities have been omitted, and no extraneous quantities included. Dimensional analysis is a step toward the goal of describing a physical entity or phenomenon in terms of relationships between groups of parameters. The ultimate goal can never be reached by dimensional analysis alone, and it is therefore not a substitute for complete analysis or for flight test. It is nevertheless a useful tool, especially for improving physical insight.

One of the most valuable uses of dimensional analysis is the derivation of the form for the equation relating the various variables involved in any particular problem. Limited knowledge of the physical side of the problem is required to perform the analysis, once the dependent and independent variables are determined. In general, application of dimensional analysis can be divided in five basic steps:

1. Analysis of basic physical quantities involved:
    a. Determine the dependent variables of the problem;
    b. Determine the independent variables of the problem.
2. Determine dimensionless groups;
3. Simplifications and analysis;
4. Converting into referred quantities;
5. Making useful conclusions.

Although an extremely useful concept, dimensional analysis does have its limitations. The main difficulty comes right at the beginning in deciding which variables are involved. If important variables have been left out of the initial list, then the results obtained from the mathematical analysis may be different from those obtained in practical tests. Dimensional analysis will not indicate whether all the variables have been included or not. There is another thing that dimensional analysis will not do; it will not predict numerical constants in any way. In fact it may not even indicate the exact numerical values of all powers of the variables, some of these may have to be left undetermined.

B.3.1 Basic Quantities

The basic quantities involved in the analysis can be expressed in terms of physical dimensions such as length (L), mass (M), time (T) and temperature (Θ) as summarized in Table B-2. For example, regardless of whether an area is expressed in units of feet, inches or meter, its physical dimension remains the same. However, when units are relevant it is required to be consistent in the units that are used in mathematical equations, i.e. they must all be from the same system.

Quantity	Physical dimensions	SI
Mass	M	kg
Length	L	m
Time	T	s
Temperature	Θ	K
Area	L^2	m^2
Volume	L^3	m^3
Angular velocity	T^{-1}	rad/s
Angular acceleration	T^{-2}	rad/s^2
Velocity	LT^{-1}	m/s
Acceleration	LT^{-2}	m/s^2
Mass flow	MT^{-1}	kg/s
Momentum	MLT^{-1}	$kg\,m/s$
Force, Weight	MLT^{-2}	kgm/s^2 (N)
Moment, Energy or Work	ML^2T^{-2}	Nm (J)
Power	ML^2T^{-3}	Nm/s (W)
Density	ML^{-3}	kg/m^3
Pressure	$ML^{-1}T^{-2}$	N/m^2 (P_a)
Viscosity	$ML^{-1}T^{-1}$	Ns/m^2
Heat value	L^2T^{-2}	J/kg
Gas constant	$L^2T^{-2}\Theta^{-1}$	J/kgK
Angle	$M^0L^0T^0$	$radian$
Adiabatic index	$M^0L^0T^0$	-
Relative humidity	$M^0L^0T^0$	-

Table B-2; Overview physical dimensions basic quantities

B.3.2 Engine Performance

In this section dimensional analysis is used to make useful conclusions of engine performance. The related variable sets with their physical dimensions are as demonstrated in the following.

Step 1; Analysis of basic physical quantities involved

a. Determine the dependent variables of the problem.

Set 1. Characteristics of the engine:

1. Diameter of the engine at a specified nominal point D_e [L]
2. Position of Inlet Guide Vanes Δ_{IGV} [$M^0L^0T^0$]
3. Position of Variable Stator Vanes Δ_{VSV} [$M^0L^0T^0$]

Set 2. Property of the medium:

4. Adiabatic index γ [$M^0L^0T^0$]
5. Gas constant R [$L^2T^{-2}\Theta^{-1}$]
6. Viscosity coefficient μ [$ML^{-1}T^{-1}$]
7. Relative humidity ϕ_{RH} [$M^0L^0T^0$]

Set 3. Characteristics of the flow through the engine:

8. Ambient pressure p_a [$ML^{-1}T^{-2}$]
9. Ambient temperature T_a [Θ]
10. Fuel mass flow through the engine $\dot{m}_f$ [MT^{-1}]
11. Lower heat value of fuel LHV [L^2T^{-2}]
12. Free power turbine rotational speed N_f [T^{-1}]
13. Forward airspeed V [LT^{-1}]
14. Relative wind direction ζ [$M^0L^0T^0$]

Note; The density can be established using the equation of state of the fluid, $p = \rho RT$ and therefore is not an independent variable.

b. Determine the independent variables of the problem.

Set 4. Properties of engine performance:

a. Power delivered by the engine P_{eng} [ML^2T^{-3}]
b. Engine gas generator rotational speed N_g [T^{-1}]
c. Engine power turbine inlet temperature T_{46} [Θ]

Step 2; Determine dimensionless groups

The three properties of the engine performance are functions of the fourteen physical variables:

$$P_{eng} = f_1(D_e, \Delta_{IGV}, \Delta_{VSV}, \gamma, R, \mu, \phi_{RH}, p_a, T_a, \dot{m}_f, LHV, N_f, V, \zeta)$$

$$N_g = f_2(D_e, \Delta_{IGV}, \Delta_{VSV}, \gamma, R, \mu, \phi_{RH}, p_a, T_a, \dot{m}_f, LHV, N_f, V, \zeta)$$

$$T_{46} = f_3(D_e, \Delta_{IGV}, \Delta_{VSV}, \gamma, R, \mu, \phi_{RH}, p_a, T_a, \dot{m}_f, LHV, N_f, V, \zeta)$$

So 3 dependent + 14 independent = 17 (n) variables appear, while 4 (k) basic dimensions play a role (M, L, T, Θ). Then according to the Π-theorem from Buckingham [8] there are $n - k$, in this case 17 – 4 = 13 independent dimensionless variables. Note that the choice of fundamental variables can be made arbitrarily. The fact that a physical variable is designated as a fundamental variable merely means that a unit of measurement can be assigned to it, independent of the units of measurement chosen for the other fundamental variables involved in the problem. In a given problem it is necessary that there be a sufficient number of fundamental variables so that each of the derived variables can be expressed in terms of products of these fundamental variables. In this case, D_e, R, p_a and T_a are used as the fundamental independent variables to make the other variables dimensionless by using their product, as for these variables a unit of measurement can be assigned to it from Table B-2.

$$\Pi_1 = D_e^{W_1} \cdot R^{X_1} \cdot p_a^{Y_1} \cdot T_a^{Z_1} \cdot P_{eng}$$

$$\Pi_2 = D_e^{W_2} \cdot R^{X_2} \cdot p_a^{Y_2} \cdot T_a^{Z_2} \cdot N_g$$

$$\Pi_3 = D_e^{W_3} \cdot R^{X_3} \cdot p_a^{Y_3} \cdot T_a^{Z_3} \cdot T_{46}$$

$$\Pi_4 = D_e^{W_4} \cdot R^{X_4} \cdot p_a^{Y_4} \cdot T_a^{Z_4} \cdot \Delta_{IGV}$$

$$\Pi_5 = D_e^{W_5} \cdot R^{X_5} \cdot p_a^{Y_5} \cdot T_a^{Z_5} \cdot \Delta_{VSV}$$

$$\Pi_6 = D_e^{W_6} \cdot R^{X_6} \cdot p_a^{Y_6} \cdot T_a^{Z_6} \cdot \gamma$$

$$\Pi_7 = D_e^{W_7} \cdot R^{X_7} \cdot p_a^{Y_7} \cdot T_a^{Z_7} \cdot \mu$$

$$\Pi_8 = D_e^{W_8} \cdot R^{X_8} \cdot p_a^{Y_8} \cdot T_a^{Z_8} \cdot \phi_{RH}$$

$$\Pi_9 = D_e^{W_9} \cdot R^{X_9} \cdot p_a^{Y_9} \cdot T_a^{Z_9} \cdot \dot{m}_f$$

$$\Pi_{10} = D_e^{W_{10}} \cdot R^{X_{10}} \cdot p_a^{Y_{10}} \cdot T_a^{Z_{10}} \cdot LHV$$

$$\Pi_{11} = D_e^{W_{11}} \cdot R^{X_{11}} \cdot p_a^{Y_{11}} \cdot T_a^{Z_{11}} \cdot N_f$$

$$\Pi_{12} = D_e^{W_{12}} \cdot R^{X_{12}} \cdot p_a^{Y_{12}} \cdot T_a^{Z_{12}} \cdot V$$

$$\Pi_{13} = {D_e}^{W_{13}} \cdot R^{X_{13}} \cdot {p_a}^{Y_{13}} \cdot {T_a}^{Z_{13}} \cdot \zeta$$

For finding the specific form of the corresponding dimensionless dependent variable Π, each quantity should be replaced by the known dimensional equivalent for it in terms of whatever set of *k* fundamental units (such as mass, length, time, temperature) which may happen to be convenient.

$$\Pi_1 = (L)^{W_1} \cdot \left(L^2T^{-2}\Theta^{-1}\right)^{X_1} \cdot \left(ML^{-1}T^{-2}\right)^{Y_1} \cdot (\Theta)^{Z_1} \cdot \left(ML^2T^{-3}\right)$$

$$\Pi_2 = (L)^{W_2} \cdot \left(L^2T^{-2}\Theta^{-1}\right)^{X_2} \cdot \left(ML^{-1}T^{-2}\right)^{Y_2} \cdot (\Theta)^{Z_2} \cdot \left(T^{-1}\right)$$

$$\Pi_3 = (L)^{W_3} \cdot \left(L^2T^{-2}\Theta^{-1}\right)^{X_3} \cdot \left(ML^{-1}T^{-2}\right)^{Y_3} \cdot (\Theta)^{Z_3} \cdot (\Theta)$$

$$\Pi_4 = (L)^{W_4} \cdot \left(L^2T^{-2}\Theta^{-1}\right)^{X_4} \cdot \left(ML^{-1}T^{-2}\right)^{Y_4} \cdot (\Theta)^{Z_4} \cdot \left(M^0L^0T^0\right)$$

$$\Pi_5 = (L)^{W_5} \cdot \left(L^2T^{-2}\Theta^{-1}\right)^{X_5} \cdot \left(ML^{-1}T^{-2}\right)^{Y_5} \cdot (\Theta)^{Z_5} \cdot \left(M^0L^0T^0\right)$$

$$\Pi_6 = (L)^{W_6} \cdot \left(L^2T^{-2}\Theta^{-1}\right)^{X_6} \cdot \left(ML^{-1}T^{-2}\right)^{Y_6} \cdot (\Theta)^{Z_6} \cdot \left(M^0L^0T^0\right)$$

$$\Pi_7 = (L)^{W_7} \cdot \left(L^2T^{-2}\Theta^{-1}\right)^{X_7} \cdot \left(ML^{-1}T^{-2}\right)^{Y_7} \cdot (\Theta)^{Z_7} \cdot \left(ML^{-1}T^{-1}\right)$$

$$\Pi_8 = (L)^{W_8} \cdot \left(L^2T^{-2}\Theta^{-1}\right)^{X_8} \cdot \left(ML^{-1}T^{-2}\right)^{Y_8} \cdot (\Theta)^{Z_8} \cdot \left(M^0L^0T^0\right)$$

$$\Pi_9 = (L)^{W_9} \cdot \left(L^2T^{-2}\Theta^{-1}\right)^{X_9} \cdot \left(ML^{-1}T^{-2}\right)^{Y_9} \cdot (\Theta)^{Z_9} \cdot \left(MT^{-1}\right)$$

$$\Pi_{10} = (L)^{W_{10}} \cdot \left(L^2T^{-2}\Theta^{-1}\right)^{X_{10}} \cdot \left(ML^{-1}T^{-2}\right)^{Y_{10}} \cdot (\Theta)^{Z_{10}} \cdot \left(L^2T^{-2}\right)$$

$$\Pi_{11} = (L)^{W_{11}} \cdot \left(L^2T^{-2}\Theta^{-1}\right)^{X_{11}} \cdot \left(ML^{-1}T^{-2}\right)^{Y_{11}} \cdot (\Theta)^{Z_{11}} \cdot \left(T^{-1}\right)$$

$$\Pi_{12} = (L)^{W_{12}} \cdot \left(L^2T^{-2}\Theta^{-1}\right)^{X_{12}} \cdot \left(ML^{-1}T^{-2}\right)^{Y_{12}} \cdot (\Theta)^{Z_{12}} \cdot \left(T^{-1}\right)$$

$$\Pi_{13} = (L)^{W_{13}} \cdot \left(L^2T^{-2}\Theta^{-1}\right)^{X_{13}} \cdot \left(ML^{-1}T^{-2}\right)^{Y_{13}} \cdot (\Theta)^{Z_{13}} \cdot \left(T^{-1}\right)$$

In order to make the Π quantities dimensionless, the summation of the powers for *M*, *L*, *T* and *Θ* need to be equal to zero.

So for the quantity Π_1:

$$\left.\begin{aligned} Y_1 + 1 &= 0 \\ W_1 + 2X_1 - Y_1 + 2 &= 0 \\ -2X_1 - 2Y_1 - 3 &= 0 \\ -X_1 + Z_1 &= 0 \end{aligned}\right\} \quad \text{gives} \quad \begin{aligned} W_1 &= -2 \\ X_1 &= -1/2 \\ Y_1 &= -1 \\ Z_1 &= -1/2 \end{aligned}$$

$$\Pi_1 = D_e^{-2} \cdot R^{-1/2} \cdot p_a^{-1} \cdot T_a^{-1/2} \cdot P_{eng} = \frac{P_{eng}}{D_e^{\,2} p_a \sqrt{RT_a}}$$

So for the quantity Π_2:

$$\left.\begin{aligned} Y_2 &= 0 \\ W_2 + 2X_2 - Y_2 &= 0 \\ -2X_2 - 2Y_2 - 1 &= 0 \\ -X_2 + Z_2 &= 0 \end{aligned}\right\} \quad \text{gives} \quad \begin{aligned} W_2 &= 1 \\ X_2 &= -1/2 \\ Y_2 &= 0 \\ Z_2 &= -1/2 \end{aligned}$$

$$\Pi_2 = D_e^{\,1} \cdot R^{-1/2} \cdot p_a^{\,0} \cdot T_a^{-1/2} \cdot N_g = \frac{N_g D_e}{\sqrt{RT_a}}$$

So for the quantity Π_3:

$$\left.\begin{aligned} Y_3 &= 0 \\ W_3 + 2X_3 - Y_3 &= 0 \\ -2X_3 - 2Y_3 &= 0 \\ -X_3 + Z_3 + 1 &= 0 \end{aligned}\right\} \quad \text{gives} \quad \begin{aligned} W_3 &= 0 \\ X_3 &= 0 \\ Y_3 &= 0 \\ Z_3 &= -1 \end{aligned}$$

$$\Pi_3 = D_e^{\,0} \cdot R^0 \cdot p_a^{\,0} \cdot T_a^{-1} \cdot T_{46} = \frac{T_{46}}{T_a}$$

So for the quantity Π_4:

$$\left.\begin{aligned} Y_4 &= 0 \\ W_4 + 2X_4 - Y_4 &= 0 \\ -2X_4 - 2Y_4 &= 0 \\ -X_4 + Z_4 &= 0 \end{aligned}\right\} \quad \text{gives} \quad \begin{aligned} W_4 &= 0 \\ X_4 &= 0 \\ Y_4 &= 0 \\ Z_4 &= 0 \end{aligned}$$

$$\Pi_4 = D_e^{\,0} \cdot R^0 \cdot p_a^{\,0} \cdot T_a^{\,0} \cdot \Delta_{IGV} = \Delta_{IGV}$$

So for the quantity Π_5:

$$\left.\begin{aligned} Y_5 &= 0 \\ W_5 + 2X_5 - Y_5 &= 0 \\ -2X_5 - 2Y_5 &= 0 \\ -X_5 + Z_5 &= 0 \end{aligned}\right\} \quad \text{gives} \quad \begin{aligned} W_5 &= 0 \\ X_5 &= 0 \\ Y_5 &= 0 \\ Z_5 &= 0 \end{aligned}$$

$$\Pi_5 = D_e^{\,0} \cdot R^0 \cdot p_a^{\,0} \cdot T_a^{\,0} \cdot \Delta_{VSV} = \Delta_{VSV}$$

So for the quantity Π_6:

$$\left.\begin{aligned} Y_6 &= 0 \\ W_6 + 2X_6 - Y_6 &= 0 \\ -2X_6 - 2Y_6 &= 0 \\ -X_6 + Z_6 &= 0 \end{aligned}\right\} \quad \text{gives} \quad \begin{aligned} W_6 &= 0 \\ X_6 &= 0 \\ Y_6 &= 0 \\ Z_6 &= 0 \end{aligned}$$

$$\Pi_6 = D_e^{\,0} \cdot R^0 \cdot p_a^0 \cdot T_a^{\,0} \cdot \gamma = \gamma$$

So for the quantity Π_7:

$$\left.\begin{aligned} Y_7 + 1 &= 0 \\ W_7 + 2X_7 - Y_7 - 1 &= 0 \\ -2X_7 - 2Y_7 - 1 &= 0 \\ -X_7 + Z_7 &= 0 \end{aligned}\right\} \quad \text{gives} \quad \begin{aligned} W_7 &= -1 \\ X_7 &= 1/2 \\ Y_7 &= -1 \\ Z_7 &= 1/2 \end{aligned}$$

$$\Pi_7 = D_e^{\,-1} \cdot R^{1/2} \cdot p_a^{-1} \cdot T_a^{\,1/2} \cdot \mu = \frac{\mu\sqrt{RT_a}}{D_e p_a}$$

So for the quantity Π_8:

$$\left.\begin{aligned} Y_8 &= 0 \\ W_8 + 2X_8 - Y_8 &= 0 \\ -2X_8 - 2Y_8 &= 0 \\ -X_8 + Z_8 &= 0 \end{aligned}\right\} \quad \text{gives} \quad \begin{aligned} W_8 &= 0 \\ X_8 &= 0 \\ Y_8 &= 0 \\ Z_8 &= 0 \end{aligned}$$

$$\Pi_8 = D_e^{\,0} \cdot R^0 \cdot p_a^0 \cdot T_a^{\,0} \cdot \phi_{RH} = \phi_{RH}$$

So for the quantity Π_9:

$$\left.\begin{aligned} Y_9 + 1 &= 0 \\ W_9 + 2X_9 - Y_9 &= 0 \\ -2X_9 - 2Y_9 - 1 &= 0 \\ -X_9 + Z_9 &= 0 \end{aligned}\right\} \quad \text{gives} \quad \begin{aligned} W_9 &= -2 \\ X_9 &= 1/2 \\ Y_9 &= -1 \\ Z_9 &= 1/2 \end{aligned}$$

$$\Pi_9 = D_e^{\,-2} \cdot R^{1/2} \cdot p_a^{-1} \cdot T_a^{\,1/2} \cdot \dot{m}_f = \frac{\dot{m}_f \sqrt{RT_a}}{D_e^{\,2} p_a}$$

So for the quantity Π_{10}:

$$\left.\begin{aligned} Y_{10} &= 0 \\ W_{10} + 2X_{10} - Y_{10} + 2 &= 0 \\ -2X_{10} - 2Y_{10} - 2 &= 0 \\ -X_{10} + Z_{10} &= 0 \end{aligned}\right\} \quad \text{gives} \quad \begin{aligned} W_{10} &= 0 \\ X_{10} &= -1 \\ Y_{10} &= 0 \\ Z_{10} &= -1 \end{aligned}$$

$$\Pi_{10} = D_e{}^0 \cdot R^{-1} \cdot p_a^0 \cdot T_a{}^{-1} \cdot LHV = \frac{LHV}{RT_a}$$

So for the quantity Π_{11}:

$$\left.\begin{aligned} Y_{11} &= 0 \\ W_{11} + 2X_{11} - Y_{11} &= 0 \\ -2X_{11} - 2Y_{11} - 1 &= 0 \\ -X_{11} + Z_{11} &= 0 \end{aligned}\right\} \quad \text{gives} \quad \begin{aligned} W_{11} &= 1 \\ X_{11} &= -1/2 \\ Y_{11} &= 0 \\ Z_{11} &= -1/2 \end{aligned}$$

$$\Pi_{11} = D_e{}^1 \cdot R^{-1/2} \cdot p_a^0 \cdot T_a{}^{-1/2} \cdot N_f = \frac{N_f D_e}{\sqrt{RT_a}}$$

So for the quantity Π_{12}:

$$\left.\begin{aligned} Y_{12} &= 0 \\ W_{12} + 2X_{12} - Y_{12} + 1 &= 0 \\ -2X_{12} - 2Y_{12} - 1 &= 0 \\ -X_{12} + Z_{12} &= 0 \end{aligned}\right\} \quad \text{gives} \quad \begin{aligned} W_{12} &= 0 \\ X_{12} &= -1/2 \\ Y_{12} &= 0 \\ Z_{12} &= -1/2 \end{aligned}$$

$$\Pi_{12} = D_e{}^0 \cdot R^{-1/2} \cdot p_a^0 \cdot T_a{}^{-1/2} \cdot V = \frac{V}{\sqrt{RT_a}}$$

So for the quantity Π_{13}:

$$\left.\begin{aligned} Y_{13} &= 0 \\ W_{13} + 2X_{13} - Y_{13} &= 0 \\ -2X_{13} - 2Y_{13} &= 0 \\ -X_{13} + Z_{13} &= 0 \end{aligned}\right\} \quad \text{gives} \quad \begin{aligned} W_{13} &= 0 \\ X_{13} &= 0 \\ Y_{13} &= 0 \\ Z_{13} &= 0 \end{aligned}$$

$$\Pi_{13} = D_e{}^0 \cdot R^0 \cdot p_a^0 \cdot T_a{}^0 \cdot \zeta = \zeta$$

Formally according to Buckingham the performance of the engine can be expressed as:

$$\Pi_1 = f_1(\Pi_4, \Pi_5, \Pi_6, \Pi_7, \Pi_8, \Pi_9, \Pi_{10}, \Pi_{11}, \Pi_{12}, \Pi_{13})$$
$$\Pi_2 = f_2(\Pi_4, \Pi_5, \Pi_6, \Pi_7, \Pi_8, \Pi_9, \Pi_{10}, \Pi_{11}, \Pi_{12}, \Pi_{13})$$
$$\Pi_3 = f_3(\Pi_4, \Pi_5, \Pi_6, \Pi_7, \Pi_8, \Pi_9, \Pi_{10}, \Pi_{11}, \Pi_{12}, \Pi_{13})$$

Step 3; Simplifications and analysis

The main structure is that three non-dimensional dependent engine performance variables are a function of ten independent variables. However, this can be simplified as follows:

1. For all practical purposes the adiabatic index γ can be considered a constant value in the atmosphere, and thus the non-dimensional group could be omitted.
2. For all practical purposes the viscosity coefficient μ can be considered a constant value as inertial effects dominate viscosity effects, and thus the non-dimensional group could be omitted.
3. For all practical purposes the relative humidity ϕ_{RH} can be considered to have negligible effect on the engine performance, and thus the non-dimensional group could be omitted.
4. Defining the heat flow of the fuel as $\phi_f = \dot{m}_f LHV$ it can be argued that Π_8 (fuel mass flow through the engine) and Π_9 (lower heat value of fuel) can be combined as a product as follows:

$$\Pi_{11} = \Pi_8 \cdot \Pi_9 = \frac{\dot{m}_f \sqrt{RT_a}}{D_e{}^2 p_a} \cdot \frac{LHV}{RT_a} = \frac{\dot{m}_f LHV}{D_e{}^2 p_a \sqrt{RT_a}} = \frac{\phi_f}{D_e{}^2 p_a \sqrt{RT_a}}$$

5. For all practical purposes the forward airspeed V can be considered to have negligible effect on the engine performance in the low speed region, and thus the non-dimensional group could be omitted. This implies that the differences between the turbine engine inlet temperature T_1 and the ambient temperature T_a are considered negligible in the low speed region.
6. For all practical purposes the relative wind direction ζ can be considered to have negligible effect on the engine performance in the low speed region, and thus the non-dimensional group could be omitted. Note that variation in engine performance occurs due to variation in main rotor torque required at different azimuth, although this is not further taken account at this stage as up to now the engine is considered in isolation.

Each time a pair of pertinent variables are substituted for an extraneous one (like for heat flow of the fuel), the extraneous variable in terms of itself becomes unity and the number of arguments of the unknown function is reduced by one. In this case the unknown functions should be further reduced by five due to omitted variables for adiabatic index γ, viscosity μ, relative humidity ϕ_{RH}, forward airspeed V and relative wind direction ζ. Now there are 10 – 1 (extraneous) – 5 (omitted) = 4 dimensionless

independent variables left. The formal structure with these simplifications made is now that the non-dimensional engine performance properties are a function of the following four independent variables:

Non-dimensional engine power function

$$\frac{P_{eng}}{D_e^{\,2} p_a \sqrt{RT_a}} = f_1\left(\Delta_{IGV}, \Delta_{VSV}, \frac{\phi_f}{D_e^{\,2} p_a \sqrt{RT_a}}, \frac{N_f D_e}{\sqrt{RT_a}}\right)$$

Non-dimensional gas generator rotational speed function

$$\frac{N_g D_e}{\sqrt{RT_a}} = f_2\left(\Delta_{IGV}, \Delta_{VSV}, \frac{\phi_f}{D_e^{\,2} p_a \sqrt{RT_a}}, \frac{N_f D_e}{\sqrt{RT_a}}\right)$$

Non-dimensional power turbine entry temperature function

$$\frac{T_{46}}{T_a} = f_3\left(\Delta_{IGV}, \Delta_{VSV}, \frac{\phi_f}{D_e^{\,2} p_a \sqrt{RT_a}}, \frac{N_f D_e}{\sqrt{RT_a}}\right)$$

Step 4; Converting into referred quantities

In practice (in particular in the helicopter industry) one does not use non-dimensional quantities but so-called "*referred quantities*". The idea is that one refers the quantity to certain ambient conditions, and corrects them to the value it would have had in standard atmospheric conditions, whilst assuming that the non-dimensional quantity remains unaltered. The significance of these referred parameters is that it can be used to produce information relevant to atmospheric conditions different from those actually tested. Consequently, with few exceptions, a relatively small number of tests at carefully chosen test sites can produce information relevant to much of the helicopter's flight envelope. So for the above mentioned non-dimensional quantities applied for the same type of engine, with the relative pressure $\delta = p_a / p_{ref}$ and the relative temperature $\theta = T_a / T_{ref}$, where p_{ref} is the referred pressure and T_{ref} the referred temperature, which gives:

Referred engine power

$$\frac{P_{eng,ref}}{D_e^{\,2} p_{ref} \sqrt{RT_{ref}}} = \frac{P_{eng}}{D_e^{\,2} p_a \sqrt{RT_a}} \quad \Rightarrow \quad P_{eng,ref} = \frac{p_{ref}}{p_a} \cdot \sqrt{\frac{T_{ref}}{T_a}} \cdot P_{eng} = \frac{P_{eng}}{\delta \sqrt{\theta}}$$

Referred gas generator rotational speed

$$\frac{N_{g,ref} D_e}{\sqrt{RT_{ref}}} = \frac{N_g D_e}{\sqrt{RT_a}} \quad \Rightarrow \quad N_{g,ref} = \sqrt{\frac{T_{ref}}{T_a}} \cdot N_g = \frac{N_g}{\sqrt{\theta}}$$

Referred engine power turbine inlet temperature

$$\frac{T_{46,ref}}{T_{ref}} = \frac{T_{46}}{T_a} \qquad \Rightarrow \qquad T_{46,ref} = \frac{T_{ref}}{T_a} \cdot T_{46} = \frac{T_{46}}{\theta}$$

Referred heat flow of the fuel

$$\frac{\phi_{f,ref}}{D_e{}^2 p_{ref} \sqrt{RT_{ref}}} = \frac{\phi_f}{D_e{}^2 p_a \sqrt{RT_a}} \qquad \Rightarrow \qquad \phi_{f,ref} = \frac{p_{ref}}{p_a} \cdot \sqrt{\frac{T_{ref}}{T_a}} \cdot \phi_f = \frac{\phi_f}{\delta\sqrt{\theta}}$$

Referred free turbine rotational speed

$$\frac{N_{f,ref} D_e}{\sqrt{RT_{ref}}} = \frac{N_f D_e}{\sqrt{RT_a}} \qquad \Rightarrow \qquad N_{f,ref} = \sqrt{\frac{T_{ref}}{T_a}} \cdot N_f = \frac{N_f}{\sqrt{\theta}}$$

Note that by using referred quantities the constants are eliminated from the equations. In other words if one looks at a particular engine operating in the troposphere the values of diameter of the engine D_e and gas constant R are fixed and disappear. Now for the referred engine performance property functions for an uncontrolled engine follows:

Referred engine power function (uncontrolled engine)

$$P_{eng,ref} = \frac{P_{eng}}{\delta\sqrt{\theta}} = f_1\left(\Delta_{IGV}, \Delta_{VSV}, \frac{\phi_f}{\delta\sqrt{\theta}}, \frac{N_f}{\sqrt{\theta}}\right)$$

Referred gas generator rotational speed function (uncontrolled engine)

$$N_{g,ref} = \frac{N_g}{\sqrt{\theta}} = f_2\left(\Delta_{IGV}, \Delta_{VSV}, \frac{\phi_f}{\delta\sqrt{\theta}}, \frac{N_f}{\sqrt{\theta}}\right)$$

Referred engine power turbine inlet temperature function (uncontrolled engine)

$$T_{46,ref} = \frac{T_{46}}{\theta} = f_3\left(\Delta_{IGV}, \Delta_{VSV}, \frac{\phi_f}{\delta\sqrt{\theta}}, \frac{N_f}{\sqrt{\theta}}\right)$$

Step 5; Making useful conclusions

The basic purpose of an Engine Electronic Control Unit (EECU) is to control fuel flow and air flow into the engine by means of a fuel metering unit, as well as Inlet Guide Vanes (IGV) and Variable Stator Vanes (VSV) position actuators. The EECU processes data from position sensors, including sensors at the collective, with the corrected gas generator speed, air inlet temperature and ambient air pressure. Thereby, the computed data allows the system to avoid the suspected surge area of the compressor. Therefore, the referred functions as mentioned above for an uncontrolled

engine should be re-written for a controlled engine with only two independent variables remaining:

Referred engine power function (controlled engine)

$$P_{eng,ref} = \frac{P_{eng}}{\delta\sqrt{\theta}} = f_1\left(\frac{\phi_f}{\delta\sqrt{\theta}}, \frac{N_f}{\sqrt{\theta}}\right)$$

Referred gas generator rotational speed function (controlled engine)

$$N_{g,ref} = \frac{N_g}{\sqrt{\theta}} = f_2\left(\frac{\phi_f}{\delta\sqrt{\theta}}, \frac{N_f}{\sqrt{\theta}}\right)$$

Referred engine power turbine inlet temperature function (controlled engine)

$$T_{46,ref} = \frac{T_{46}}{\theta} = f_3\left(\frac{\phi_f}{\delta\sqrt{\theta}}, \frac{N_f}{\sqrt{\theta}}\right)$$

Position Inlet Guide Vanes function (controlled engine)

$$\Delta_{IGV} = f_4\left(\frac{\phi_f}{\delta\sqrt{\theta}}, \frac{N_f}{\sqrt{\theta}}\right)$$

Position Variable Stator Vanes function (controlled engine)

$$\Delta_{VSV} = f_5\left(\frac{\phi_f}{\delta\sqrt{\theta}}, \frac{N_f}{\sqrt{\theta}}\right)$$

In normal operating mode the EECU controls the free power turbine rotational speed N_f in order to hold it as close as possible to the nominal demand throughout the flight envelope regardless of main rotor load variations. This is achieved by varying the gas generator rotational speed N_g by taking into account free turbine rotational speed N_f, collective pitch position and the load sharing between both engines. The gas generator rotational speed N_g is controlled by the collective pitch position input, such that it anticipates the rotor load variations to obtain a fast engine response. The gas generator rotational speed N_g is also corrected by the twin engine load sharing correction exchanged by a direct link between both EECUs. The free power turbine rotational speed N_f output is proportional to the gas generator rotational speed N_g. As a consequence all variables controlled by the EECU and impacting the gas generator rotational speed N_g are related to the same variables.

All gas turbines deteriorate in performance during operation, known as the Performance Power Index (PPI). The impact of performance deterioration results in loss in power output and increases fuel consumption. Loss in power output can have an impact on safety because power available can be reduced. Increase in fuel

consumption increases operating costs. Performance deterioration also results in higher firing temperatures, resulting in increased turbine creep life used for a given power demand. For this reason, it is required during flight tests to note the PPI values to ensure sufficient power margins are available even for the engine with the minimum PPI values allowed during operational scenarios.

B.3.3 Main Rotor Performance

In this section dimensional analysis is used to make useful conclusions of main rotor performance. The related variable sets with their physical dimensions are as demonstrated in the following.

Step 1; Analysis of basic physical quantities involved

a. Determine the dependent variables of the problem.

Set 1. Characteristics of the main rotor:

1. Diameter of the main rotor D_r [L]
2. Main rotor blade area A_b [L^2]
3. Main rotor chord c [L]

Set 2. Property of the medium:

4. Adiabatic index γ [$M^0L^0T^0$]
5. Gas constant R [$L^2T^{-2}\Theta^{-1}$]
6. Viscosity coefficient μ [$ML^{-1}T^{-1}$]
7. Relative humidity ϕ_{RH} [$M^0L^0T^0$]
8. Ambient pressure p_a [$ML^{-1}T^{-2}$]
9. Ambient temperature T_a [Θ]

Note; The density can be established using the equation of state of the fluid, $p = \rho RT$ and therefore is not an independent variable.

Set 3. Characteristics of the flight dynamics:

10. Acceleration due to gravity g [LT^{-2}]
11. Helicopter mass m [M]
12. Forward flight speed V [LT^{-1}]
13. Vertical speed V_c [LT^{-1}]
14. Height above ground Z [L]
15. Main rotor rotational velocity Ω [T^{-1}]
16. Main rotor blade pitch angle θ_p [$M^0L^0T^0$]
17. Relative wind direction ζ [$M^0L^0T^0$]

b. Determine the independent variables of the problem.

Set 4. Properties of main rotor performance:

a. Main rotor power required P_{req} [ML^2T^{-3}]

Step 2; Determine dimensionless groups

The properties of the main rotor performance are a function of the seventeen physical variables:

$$P_{req} = f(D_r, A_b, c, \gamma, R, \mu, \phi_{RH}, p_a, T_a, g, m, V, V_c, Z, \Omega, \theta_p, \zeta)$$

So 1 dependent + 17 independent = 18 (n) variables appear, while 4 (k) basic dimensions play a role (M, L, T, Θ). Then according to the Π-theorem from Buckingham [8] there are $n - k$, in this case 18 – 4 = 14 independent dimensionless variables. Note that the choice of fundamental variables can be made arbitrarily. The fact that a physical variable is designated as a fundamental variable merely means that a unit of measurement can be assigned to it, independent of the units of measurement chosen for the other fundamental variables involved in the problem. In a given problem it is necessary that there be a sufficient number of fundamental variables so that each of the derived variables can be expressed in terms of products of these fundamental variables. In this case, D_r, R, p_a and T_a are used as the fundamental independent variables to make the other variables dimensionless by using their product, as for these variables a unit of measurement can be assigned to it from Table B-2.

$$\Pi_1 = D_r^{W_1} \cdot R^{X_1} \cdot p_a^{Y_1} \cdot T_a^{Z_1} \cdot P_{req}$$

$$\Pi_2 = D_r^{W_2} \cdot R^{X_2} \cdot p_a^{Y_2} \cdot T_a^{Z_2} \cdot A_b$$

$$\Pi_3 = D_r^{W_3} \cdot R^{X_3} \cdot p_a^{Y_3} \cdot T_a^{Z_3} \cdot c$$

$$\Pi_4 = D_r^{W_4} \cdot R^{X_4} \cdot p_a^{Y_4} \cdot T_a^{Z_4} \cdot \gamma$$

$$\Pi_5 = D_r^{W_5} \cdot R^{X_5} \cdot p_a^{Y_5} \cdot T_a^{Z_5} \cdot \mu$$

$$\Pi_6 = D_r^{W_6} \cdot R^{X_6} \cdot p_a^{Y_6} \cdot T_a^{Z_6} \cdot \phi_{RH}$$

$$\Pi_7 = D_r^{W_7} \cdot R^{X_7} \cdot p_a^{Y_7} \cdot T_a^{Z_7} \cdot g$$

$$\Pi_8 = D_r^{W_8} \cdot R^{X_8} \cdot p_a^{Y_8} \cdot T_a^{Z_8} \cdot m$$

$$\Pi_9 = D_r^{W_9} \cdot R^{X_9} \cdot p_a^{Y_9} \cdot T_a^{Z_9} \cdot V$$

$$\Pi_{10} = D_r^{W_{10}} \cdot R^{X_{10}} \cdot p_a^{Y_{10}} \cdot T_a^{Z_{10}} \cdot V_c$$

$$\Pi_{11} = D_r^{W_{11}} \cdot R^{X_{11}} \cdot p_a^{Y_{11}} \cdot T_a^{Z_{11}} \cdot Z$$

$$\Pi_{12} = D_r^{W_{12}} \cdot R^{X_{12}} \cdot p_a^{Y_{12}} \cdot T_a^{Z_{12}} \cdot \Omega$$

$$\Pi_{13} = D_r^{W_{13}} \cdot R^{X_{13}} \cdot p_a^{Y_{13}} \cdot T_a^{Z_{13}} \cdot \theta_p$$

$$\Pi_{14} = D_r^{W_{14}} \cdot R^{X_{14}} \cdot p_a^{Y_{14}} \cdot T_a^{Z_{14}} \cdot \zeta$$

For finding the specific form of the corresponding dimensionless dependent variable Π, each quantity should be replaced by the known dimensional equivalent for it in terms of whatever set of *k* fundamental units (such as mass, length, time, temperature) which may happen to be convenient.

$$\Pi_1 = (L)^{W_1} \cdot \left(L^2T^{-2}\Theta^{-1}\right)^{X_1} \cdot \left(ML^{-1}T^{-2}\right)^{Y_1} \cdot (\Theta)^{Z_1} \cdot \left(ML^2T^{-3}\right)$$

$$\Pi_2 = (L)^{W_2} \cdot \left(L^2T^{-2}\Theta^{-1}\right)^{X_2} \cdot \left(ML^{-1}T^{-2}\right)^{Y_2} \cdot (\Theta)^{Z_2} \cdot \left(L^2\right)$$

$$\Pi_3 = (L)^{W_3} \cdot \left(L^2T^{-2}\Theta^{-1}\right)^{X_3} \cdot \left(ML^{-1}T^{-2}\right)^{Y_3} \cdot (\Theta)^{Z_3} \cdot (L)$$

$$\Pi_4 = (L)^{W_4} \cdot \left(L^2T^{-2}\Theta^{-1}\right)^{X_4} \cdot \left(ML^{-1}T^{-2}\right)^{Y_4} \cdot (\Theta)^{Z_4} \cdot \left(M^0L^0T^0\right)$$

$$\Pi_5 = (L)^{W_5} \cdot \left(L^2T^{-2}\Theta^{-1}\right)^{X_5} \cdot \left(ML^{-1}T^{-2}\right)^{Y_5} \cdot (\Theta)^{Z_5} \cdot \left(ML^{-1}T^{-1}\right)$$

$$\Pi_6 = (L)^{W_6} \cdot \left(L^2T^{-2}\Theta^{-1}\right)^{X_6} \cdot \left(ML^{-1}T^{-2}\right)^{Y_6} \cdot (\Theta)^{Z_6} \cdot \left(M^0L^0T^0\right)$$

$$\Pi_7 = (L)^{W_7} \cdot \left(L^2T^{-2}\Theta^{-1}\right)^{X_7} \cdot \left(ML^{-1}T^{-2}\right)^{Y_7} \cdot (\Theta)^{Z_7} \cdot \left(LT^{-2}\right)$$

$$\Pi_8 = (L)^{W_8} \cdot \left(L^2T^{-2}\Theta^{-1}\right)^{X_8} \cdot \left(ML^{-1}T^{-2}\right)^{Y_8} \cdot (\Theta)^{Z_8} \cdot (M)$$

$$\Pi_9 = (L)^{W_9} \cdot \left(L^2T^{-2}\Theta^{-1}\right)^{X_9} \cdot \left(ML^{-1}T^{-2}\right)^{Y_9} \cdot (\Theta)^{Z_9} \cdot \left(LT^{-1}\right)$$

$$\Pi_{10} = (L)^{W_{10}} \cdot \left(L^2T^{-2}\Theta^{-1}\right)^{X_{10}} \cdot \left(ML^{-1}T^{-2}\right)^{Y_{10}} \cdot (\Theta)^{Z_{10}} \cdot \left(LT^{-1}\right)$$

$$\Pi_{11} = (L)^{W_{11}} \cdot \left(L^2T^{-2}\Theta^{-1}\right)^{X_{11}} \cdot \left(ML^{-1}T^{-2}\right)^{Y_{11}} \cdot (\Theta)^{Z_{11}} \cdot (L)$$

$$\Pi_{12} = (L)^{W_{12}} \cdot \left(L^2T^{-2}\Theta^{-1}\right)^{X_{12}} \cdot \left(ML^{-1}T^{-2}\right)^{Y_{12}} \cdot (\Theta)^{Z_{12}} \cdot \left(T^{-1}\right)$$

$$\Pi_{13} = (L)^{W_{13}} \cdot \left(L^2T^{-2}\Theta^{-1}\right)^{X_{13}} \cdot \left(ML^{-1}T^{-2}\right)^{Y_{13}} \cdot (\Theta)^{Z_{13}} \cdot \left(M^0L^0T^0\right)$$

$$\Pi_{14} = (L)^{W_{43}} \cdot \left(L^2T^{-2}\Theta^{-1}\right)^{X_{14}} \cdot \left(ML^{-1}T^{-2}\right)^{Y_{14}} \cdot (\Theta)^{Z_{14}} \cdot \left(M^0L^0T^0\right)$$

In order to make the Π quantities dimensionless, the summation of the powers for *M*, *L*, *T* and *Θ* need to be equal to zero. So for the quantity Π_1:

$$\left.\begin{aligned} Y_1 + 1 &= 0 \\ W_1 + 2X_1 - Y_1 + 2 &= 0 \\ -2X_1 - 2Y_1 - 3 &= 0 \\ -X_1 + Z_1 &= 0 \end{aligned}\right\} \quad \text{gives} \quad \begin{aligned} W_1 &= -2 \\ X_1 &= -1/2 \\ Y_1 &= -1 \\ Z_1 &= -1/2 \end{aligned}$$

$$\Pi_1 = D_r^{-2} \cdot R^{-1/2} \cdot p_a^{-1} \cdot T_a^{-1/2} \cdot P_{req} = \frac{P_{req}}{D_r^2 p_a \sqrt{RT_a}}$$

So for the quantity Π_2:

$$\left.\begin{aligned} Y_2 &= 0 \\ W_2 + 2X_2 - Y_2 + 2 &= 0 \\ -2X_2 - 2Y_2 &= 0 \\ -X_2 + Z_2 &= 0 \end{aligned}\right\} \quad \text{gives} \quad \begin{aligned} W_2 &= -2 \\ X_2 &= 0 \\ Y_2 &= 0 \\ Z_2 &= 0 \end{aligned}$$

$$\Pi_2 = D_r^{-2} \cdot R^0 \cdot p_a^0 \cdot T_a^0 \cdot A_b = \frac{A_b}{D_r^2}$$

So for the quantity Π_3:

$$\left.\begin{aligned} Y_3 &= 0 \\ W_3 + 2X_3 - Y_3 + 1 &= 0 \\ -2X_3 - 2Y_3 &= 0 \\ -X_3 + Z_3 &= 0 \end{aligned}\right\} \quad \text{gives} \quad \begin{aligned} W_3 &= -1 \\ X_3 &= 0 \\ Y_3 &= 0 \\ Z_3 &= 0 \end{aligned}$$

$$\Pi_3 = D_r^{-1} \cdot R^0 \cdot p_a^0 \cdot T_a^0 \cdot c = \frac{c}{D_r}$$

So for the quantity Π_4:

$$\left.\begin{aligned} Y_4 &= 0 \\ W_4 + 2X_4 - Y_4 &= 0 \\ -2X_4 - 2Y_4 &= 0 \\ -X_4 + Z_4 &= 0 \end{aligned}\right\} \quad \text{gives} \quad \begin{aligned} W_4 &= 0 \\ X_4 &= 0 \\ Y_4 &= 0 \\ Z_4 &= 0 \end{aligned}$$

$$\Pi_4 = D_r^0 \cdot R^0 \cdot p_a^0 \cdot T_a^0 \cdot \gamma = \gamma$$

So for the quantity Π_5:

$$\left.\begin{aligned} Y_5 + 1 &= 0 \\ W_5 + 2X_5 - Y_5 - 1 &= 0 \\ -2X_5 - 2Y_5 - 1 &= 0 \\ -X_5 + Z_5 &= 0 \end{aligned}\right\} \quad \text{gives} \quad \begin{aligned} W_5 &= -1 \\ X_5 &= 1/2 \\ Y_5 &= -1 \\ Z_5 &= 1/2 \end{aligned}$$

$$\Pi_5 = D_r^{-1} \cdot R^{1/2} \cdot p_a^{-1} \cdot T_a^{1/2} \cdot \mu = \frac{\mu\sqrt{RT_a}}{D_r p_a}$$

So for the quantity Π_6:

$$\left.\begin{aligned} Y_6 &= 0 \\ W_6 + 2X_6 - Y_6 &= 0 \\ -2X_6 - 2Y_6 &= 0 \\ -X_6 + Z_6 &= 0 \end{aligned}\right\} \quad \text{gives} \quad \begin{aligned} W_6 &= 0 \\ X_6 &= 0 \\ Y_6 &= 0 \\ Z_6 &= 0 \end{aligned}$$

$$\Pi_6 = D_r^{0} \cdot R^{0} \cdot p_a^{0} \cdot T_a^{0} \cdot \phi_{RH} = \phi_{RH}$$

So for the quantity Π_7:

$$\left.\begin{aligned} Y_7 &= 0 \\ W_7 + 2X_7 - Y_7 + 1 &= 0 \\ -2X_7 - 2Y_7 - 2 &= 0 \\ -X_7 + Z_7 &= 0 \end{aligned}\right\} \quad \text{gives} \quad \begin{aligned} W_7 &= 1 \\ X_7 &= -1 \\ Y_7 &= 0 \\ Z_7 &= -1 \end{aligned}$$

$$\Pi_7 = D_r^{1} \cdot R^{-1} \cdot p_a^{0} \cdot T_a^{-1} \cdot g = \frac{gD_r}{RT_a}$$

So for the quantity Π_8:

$$\left.\begin{aligned} Y_8 + 1 &= 0 \\ W_8 + 2X_8 - Y_8 &= 0 \\ -2X_8 - 2Y_8 &= 0 \\ -X_8 + Z_8 &= 0 \end{aligned}\right\} \quad \text{gives} \quad \begin{aligned} W_8 &= -3 \\ X_8 &= 1 \\ Y_8 &= -1 \\ Z_8 &= 1 \end{aligned}$$

$$\Pi_8 = D_r^{-3} \cdot R^{1} \cdot p_a^{-1} \cdot T_a^{1} \cdot m = \frac{mRT_a}{D_r^{3} p_a}$$

So for the quantity Π_9:

$$\left.\begin{aligned} Y_9 &= 0 \\ W_9 + 2X_9 - Y_9 + 1 &= 0 \\ -2X_9 - 2Y_9 - 1 &= 0 \\ -X_9 + Z_9 &= 0 \end{aligned}\right\} \quad \text{gives} \quad \begin{aligned} W_9 &= 0 \\ X_9 &= -1/2 \\ Y_9 &= 0 \\ Z_9 &= -1/2 \end{aligned}$$

$$\Pi_9 = {D_r}^0 \cdot R^{-1/2} \cdot p_a^0 \cdot {T_a}^{-1/2} \cdot V = \frac{V}{\sqrt{RT_a}}$$

So for the quantity Π_{10}:

$$\left.\begin{aligned} Y_{10} &= 0 \\ W_{10} + 2X_{10} - Y_{10} + 1 &= 0 \\ -2X_{10} - 2Y_{10} - 1 &= 0 \\ -X_{10} + Z_{10} &= 0 \end{aligned}\right\} \quad \text{gives} \quad \begin{aligned} W_{10} &= 0 \\ X_{10} &= -1/2 \\ Y_{10} &= 0 \\ Z_{10} &= -1/2 \end{aligned}$$

$$\Pi_{10} = {D_r}^0 \cdot R^{-1/2} \cdot p_a^0 \cdot {T_a}^{-1/2} \cdot V_c = \frac{V_c}{\sqrt{RT_a}}$$

So for the quantity Π_{11}:

$$\left.\begin{aligned} Y_{11} &= 0 \\ W_{11} + 2X_{11} - Y_{11} + 1 &= 0 \\ -2X_{11} - 2Y_{11} &= 0 \\ -X_{11} + Z_{11} &= 0 \end{aligned}\right\} \quad \text{gives} \quad \begin{aligned} W_{11} &= -1 \\ X_{11} &= 0 \\ Y_{11} &= 0 \\ Z_{11} &= 0 \end{aligned}$$

$$\Pi_{11} = {D_r}^{-1} \cdot R^0 \cdot p_a^0 \cdot {T_a}^0 \cdot Z = \frac{Z}{D_r}$$

So for the quantity Π_{12}:

$$\left.\begin{aligned} Y_{12} &= 0 \\ W_{12} + 2X_{12} - Y_{12} &= 0 \\ -2X_{12} - 2Y_{12} - 1 &= 0 \\ -X_{12} + Z_{12} &= 0 \end{aligned}\right\} \quad \text{gives} \quad \begin{aligned} W_{12} &= 1 \\ X_{12} &= -1/2 \\ Y_{12} &= 0 \\ Z_{12} &= -1/2 \end{aligned}$$

$$\Pi_{12} = {D_r}^1 \cdot R^{-1/2} \cdot p_a^0 \cdot {T_a}^{-1/2} \cdot \Omega = \frac{\Omega D_r}{\sqrt{RT_a}}$$

So for the quantity Π_{13}:

$$\left.\begin{aligned} Y_{13} &= 0 \\ W_{13} + 2X_{13} - Y_{13} &= 0 \\ -2X_{13} - 2Y_{13} &= 0 \\ -X_{13} + Z_{13} &= 0 \end{aligned}\right\} \quad \text{gives} \quad \begin{aligned} W_{13} &= 0 \\ X_{13} &= 0 \\ Y_{13} &= 0 \\ Z_{13} &= 0 \end{aligned}$$

$$\Pi_{13} = {D_r}^0 \cdot R^0 \cdot {p_a}^0 \cdot {T_a}^0 \cdot \theta_p = \theta_p$$

So for the quantity Π_{14}:

$$\left.\begin{aligned} Y_{14} &= 0 \\ W_{14} + 2X_{14} - Y_{14} &= 0 \\ -2X_{14} - 2Y_{14} &= 0 \\ -X_{14} + Z_{14} &= 0 \end{aligned}\right\} \quad \text{gives} \quad \begin{aligned} W_{14} &= 0 \\ X_{14} &= 0 \\ Y_{14} &= 0 \\ Z_{14} &= 0 \end{aligned}$$

$$\Pi_{14} = {D_r}^0 \cdot R^0 \cdot {p_a}^0 \cdot {T_a}^0 \cdot \zeta = \zeta$$

Formally according to Buckingham the performance of the main rotor can be expressed as:

$$\Pi_1 = f\left(\Pi_2, \Pi_3, \Pi_4, \Pi_5, \Pi_6, \Pi_7, \Pi_8, \Pi_9, \Pi_{10}, \Pi_{11}, \Pi_{12}, \Pi_{13}, \Pi_{14}\right)$$

Step 3; Simplifications and analysis

The main structure is that one non-dimensional dependent main rotor performance variable is a function of thirteen independent variables. However, this can be simplified as follows:

1. For all practical purposes the adiabatic index γ can be considered a constant value in the atmosphere, and thus the non-dimensional group could be omitted.
2. For all practical purposes the viscosity coefficient μ can be considered a constant value as inertial effects dominate viscosity effects, and thus the non-dimensional group could be omitted.
3. For all practical purposes the relative humidity ϕ_{RH} can be considered to have negligible effect on the main rotor performance, and thus the non-dimensional group could be omitted.
4. Defining the weight as $W = mg$ it can be argued that Π_7 (acceleration due to gravity) and Π_8 (helicopter mass) can be combined as a product as follows:

$$\Pi_{14} = \Pi_7 \cdot \Pi_8 = \frac{gD_r}{RT_a} \cdot \frac{mRT_a}{{D_r}^3 p_a} = \frac{mg}{{D_r}^2 p_a} = \frac{W}{{D_r}^2 p_a}$$

Each time a pair of pertinent variables are substituted for an extraneous one (like for weight), the extraneous variable in terms of itself becomes unity and the number of arguments of the unknown function is reduced by one. In this case the unknown function should be further reduced by three due to omitted variables for adiabatic index γ, viscosity μ and relative humidity ϕ_{RH}. Now there are 13 – 1 (extraneous) – 3 (omitted) = 9 dimensionless independent variables left. The formal structure with these simplifications made is now that the non-dimensional main rotor performance property is a function of the following nine independent variables:

Non-dimensional main rotor power required function

$$\frac{P_{req}}{D_r{}^2 p_a \sqrt{RT_a}} = f\left(\frac{A_b}{D_r{}^2}, \frac{c}{D_r}, \frac{W}{D_r{}^2 p_a}, \frac{V}{\sqrt{RT_a}}, \frac{V_c}{\sqrt{RT_a}}, \frac{Z}{D_r}, \frac{\Omega D_r}{\sqrt{RT_a}}, \theta_p, \zeta\right)$$

For engine performance this relationship is generally used. However, the choice of a referred group to use for main rotor performance testing, will depend, to a degree, on whether main rotor rotational velocity Ω can be varied in flight. If the main rotor rotational velocity Ω cannot be varied in flight, tests should be made at the normal governed main rotor rotational velocity Ω. Therefore, an alternative grouping must be found to conduct flight testing for helicopters with a fixed main rotor rotational velocity Ω. Note that although the alternative grouping is further discussed, for engine performance the following derivations should also be performed, whilst now only the final result is given in step 5. The Π-theorem states that all variables may be multiplied with each other to form other non-dimensional groups, in this case using the equation of state $p_a = \rho_a R T_a$ giving $1/\rho_a = RT_a / p_a$, thus:

$$\Pi_1 \cdot \Pi_{10}{}^{-3} = \frac{P_{req}}{D_r{}^2 p_a \sqrt{RT_a}} \cdot \left(\frac{\Omega D_r}{\sqrt{RT_a}}\right)^{-3} = \frac{P_{req}\sqrt{RT_a}^3}{D_r{}^2 p_a \sqrt{RT_a}\Omega^3 D_r{}^3}$$

$$= \frac{RT_a}{p_a} \cdot \frac{P_{req}}{\Omega^3 D_r{}^5} = \frac{P_{req}}{\rho_a \Omega^3 D_r{}^5}$$

and

$$\Pi_{12} \cdot \Pi_{10}{}^{-2}$$

$$= \frac{W}{D_r{}^2 p_a} \cdot \left(\frac{\Omega D_r}{\sqrt{RT_a}}\right)^{-2} = \frac{WRT_a}{D_r{}^2 p_a \Omega^2 D_r{}^2} = \frac{RT_a}{p_a} \cdot \frac{W}{\Omega^2 D_r{}^4} = \frac{W}{\rho_a \Omega^2 D_r{}^4}$$

Furthermore, expressing the forward flight speed V and the vertical speed V_c as the more commonly known advance ratios:

$$\Pi_7 \cdot \Pi_{10}{}^{-1} = \frac{V}{\sqrt{RT_a}} \cdot \left(\frac{\Omega D_r}{\sqrt{RT_a}}\right)^{-1} = \frac{V}{\Omega D_r}$$

$$\Pi_8 \cdot \Pi_{10}{}^{-1} = \frac{V_c}{\sqrt{RT_a}} \cdot \left(\frac{\Omega D_r}{\sqrt{RT_a}}\right)^{-1} = \frac{V_c}{\Omega D_r}$$

The formal structure for the non-dimensional main rotor power required function, with the simplification made and converted into an alternative non-dimensional grouping which is applicable for helicopters with a fixed main rotor rotational velocity Ω in flight is now:

Non-dimensional main rotor power required function

$$\frac{P_{req}}{\rho_a \Omega^3 {D_r}^5} = f\left(\frac{A_b}{{D_r}^2}, \frac{c}{D_r}, \frac{W}{\rho_a \Omega^2 {D_r}^4}, \frac{V}{\Omega D_r}, \frac{V_c}{\Omega D_r}, \frac{Z}{D_r}, \frac{\Omega D_r}{\sqrt{RT_a}}, \theta_p, \zeta\right)$$

Note that a test method in which only density ρ is used affords a more compact presentation of results but does not permit the effects of changes in rotor Mach number ($\Omega D_r / \sqrt{RT_a}$) to be investigated. The effects of disregarding rotor Mach number varies and depends on the range of temperature in which tests, including hover, are carried out as well as the flight condition considered. Consequently, significant errors can arise if such test results are used to predict performance in temperatures markedly different from those in which the tests were conducted. As a consequence, if main rotor rotational velocity Ω cannot be varied, sorties should be flown at extremes of Outside Air Temperature (OAT) to establish the required spread of values of $1/\sqrt{\theta}$. As a large amount of current operational deployments are in areas with a high OAT, at least shore-based hover trials should be conducted in similar environmental conditions. If for whatever reason, tip effects are evident then it would be required to enlarge the range of referred rotor speeds by testing in colder atmospheres for high referred rotor speeds.

Step 4; Converting into referred quantities

In practice (in particular in the aircraft industry) one does not use non-dimensional quantities but so-called "*referred quantities*". The idea is that one refers the quantity to certain ambient conditions, and corrects them to the value it would have had in standard atmospheric conditions, whilst assuming that the non-dimensional quantity remains unaltered. The significance of these referred parameters is that it can be used to produce information relevant to atmospheric conditions different from those actually tested. Consequently, with few exceptions, a relatively small number of tests at carefully chosen test sites can produce information relevant to much of the helicopter's flight envelope. So for the above mentioned non-dimensional quantities applied for the same type of helicopter with the relative temperature $\theta = T_a / T_{ref}$, the relative density $\sigma = \rho_a / \rho_{ref}$ and the relative rotorspeed $\omega = \Omega / \Omega_{ref}$, where ρ_{ref} is the referred density and Ω_{ref} the referred rotor rotational velocity, which gives:

Referred main rotor power required

$$\frac{P_{req,ref}}{\rho_{ref} \Omega_{ref}^3 {D_r}^5} = \frac{P_{req}}{\rho_a \Omega^3 {D_r}^5} \quad \Rightarrow \quad P_{req,ref} = \frac{\rho_{ref}}{\rho_a} \cdot \left(\frac{\Omega_{ref}}{\Omega}\right)^3 \cdot P_{req} = \frac{P_{req}}{\sigma \omega^3}$$

Referred main rotor blade area

$$\frac{A_{b,ref}}{{D_r}^2} = \frac{A_b}{{D_r}^2} \quad \Rightarrow \quad A_{b,ref} = A_b$$

Referred main rotor chord

$$\frac{c_{ref}}{D_r} = \frac{c}{D_r} \qquad \Rightarrow \qquad c_{ref} = c$$

Referred weight

$$\frac{W_{ref}}{\rho_{ref}\Omega_{ref}^2 D_r^{\,4}} = \frac{W}{\rho_a \Omega^2 D_r^{\,4}} \qquad \Rightarrow \qquad W_{ref} = \frac{\rho_{ref}}{\rho_a} \cdot \left(\frac{\Omega_{ref}}{\Omega}\right)^2 \cdot W = \frac{W}{\sigma\omega^2}$$

Referred forward flight speed

$$\frac{V_{ref}}{\Omega_{ref} D_r} = \frac{V}{\Omega D_r} \qquad \Rightarrow \qquad V_{ref} = \frac{\Omega_{ref}}{\Omega} \cdot V = \frac{V}{\omega}$$

Referred vertical speed

$$\frac{V_{c,ref}}{\Omega_{ref} D_r} = \frac{V_c}{\Omega D_r} \qquad \Rightarrow \qquad V_{c,ref} = \frac{\Omega_{ref}}{\Omega} \cdot V_c = \frac{V_c}{\omega}$$

Referred height above ground

$$\frac{Z_{ref}}{D_r} = \frac{Z}{D_r} \qquad \Rightarrow \qquad Z_{ref} = Z$$

Referred main rotor rotational velocity

$$\frac{\Omega_{ref} D_r}{\sqrt{RT_{ref}}} = \frac{\Omega D_r}{\sqrt{RT_a}} \qquad \Rightarrow \qquad \Omega_{ref} = \sqrt{\frac{T_{ref}}{T_a}} \cdot \Omega = \frac{\omega\Omega_{ref}}{\sqrt{\theta}}$$

Note that by using referred quantities the constants could be eliminated from the equations. In other words, if one looks at a particular main rotor the values of main rotor blade area A_b, main rotor chord c and main rotor diameter D_r are fixed and could be removed from the equation. Now for the main rotor power required function:

Referred main rotor power required function

$$P_{req,ref} = \frac{P_{req}}{\sigma\omega^3} = f\left(\frac{W}{\sigma\omega^2}, \frac{V}{\omega}, \frac{V_c}{\omega}, Z, \frac{\omega}{\sqrt{\theta}}, \theta_p, \zeta\right)$$

Step 5; Making useful conclusions

It is common for helicopters that the main rotor blade pitch θ_p is directly coupled to the collective lever position set by the pilot to manoeuvre the helicopter. The main rotor blade pitch angle θ_p is thus related to the same variables as the main rotor power

required. Therefore, the referred main rotor power required function as mentioned above should be re-written for a controlled main rotor blade pitch with only six independent variables remaining:

Referred main rotor power required function (θ_p *controlled*)

$$P_{req,ref} = \frac{P_{req}}{\sigma\omega^3} = f_1\left(\frac{W}{\sigma\omega^2}, \frac{V}{\omega}, \frac{V_c}{\omega}, Z, \frac{\omega}{\sqrt{\theta}}, \zeta\right)$$

Main rotor blade pitch function (θ_p *controlled*)

$$\theta_p = f_2\left(\frac{W}{\sigma\omega^2}, \frac{V}{\omega}, \frac{V_c}{\omega}, Z, \frac{\omega}{\sqrt{\theta}}, \zeta\right)$$

Within the dynamic ship environment, the benefits of ground effect could be considered negligible [7]. Hence, only Out-of-Ground Effect (OGE), low speed, conditions are tested without any vertical speed once established on the test condition behind the pace-car. The relationship shows that the performance of the helicopter is mainly influenced by the referred weight, the relative wind velocity (airwake in the vicinity of the ship), rotorspeed setting and the relative wind direction (airwake in the vicinity of the ship):

Referred main rotor power required function (θ_p *controlled*)

$$P_{req,ref} = \frac{P_{req}}{\sigma\omega^3} = f_1\left(\frac{W}{\sigma\omega^2}, \frac{V}{\omega}, \frac{\omega}{\sqrt{\theta}}, \zeta\right)$$

Main rotor blade pitch function (θ_p *controlled*)

$$\theta_p = f_2\left(\frac{W}{\sigma\omega^2}, \frac{V}{\omega}, \frac{\omega}{\sqrt{\theta}}, \zeta\right)$$

The selection of specific values or ranges of non-dimensional parameter will depend on the test results required, the flying time available and the likely atmospheric conditions at the test site. Note that for a particular test point with a defined relative wind speed, relative wind direction and OAT, the referred main rotor power required is solely a function of the weight of the helicopter. This grouping cannot be used, if a test technique requires constant $\omega/\sqrt{\theta}$ as well as $W/\sigma\omega^2$ since by testing at different locations with other environmental conditions to vary $\omega/\sqrt{\theta}$ the referred weight will be altered. The requirement to obtain performance information at constant $\omega/\sqrt{\theta}$ and $W/\sigma\omega^2$ occurs, especially during the evaluation of tip effects. A tip effect causes an actual increase in power required arising from a change in rotor speed Ω. Therefore, an alternative to adjusting the main rotor rotational velocity must be introduced. The alternative grouping for power required as previously derived in step 3, although easier to use since it lacks air density, cannot be used for helicopters with fixed rotor speed but is given here for application to analysis of the engine performance:

Referred main rotor power required function (θ_p *controlled*)

$$P_{req,ref} = \frac{P_{req}}{\delta\sqrt{\theta}} = f_1\left(\frac{W}{\delta}, \frac{V}{\omega}, \frac{\omega}{\sqrt{\theta}}, \zeta\right)$$

Main rotor blade pitch function (θ_p *controlled*)

$$\theta_p = f_2\left(\frac{W}{\delta}, \frac{V}{\omega}, \frac{\omega}{\sqrt{\theta}}, \zeta\right)$$

The relationship between $P_{req}/\sigma\omega^3$ and $P_{req}/\delta\sqrt{\theta}$ confirms this alternative grouping as demonstrated below. Therefore, the flight test data gathered for power required $P_{req}/\sigma\omega^3$ can still be converted into the alternative grouping of power required $P_{req}/\delta\sqrt{\theta}$:

$$\frac{P_{req}}{\sigma\omega^3} \cdot \left(\frac{\omega}{\sqrt{\theta}}\right)^3 = \frac{P_{req}}{\sigma\theta\sqrt{\theta}} = \frac{P_{req}}{\delta\sqrt{\theta}}$$

Appendix C **Subjective Rating Scales**

Scale	Effort	Guidance
1	Slight to Moderate	Reasonable compensation required. Tracking and position accuracy is constantly maintained throughout the operation. Fleet pilots will have enough spare capacity to conduct ancillary tasks.
2	Considerable	Significant compensation required. Tracking and position accuracy occasionally degrades during peaks in ship motion, turbulence or sea state. Fleet pilots will have difficulty conducting ancillary tasks.
3	Highest tolerable	Highest tolerable compensation required. Tracking and positioning accuracy degrades regularly during peaks in ship motion, turbulence or sea state. Fleet pilots will be able to keep up with task requirements but no more. Degraded operations (ship or aircraft) will probably require an abort. Repeated safe operations are achievable.
	Acceptable	
	Unacceptable	
4	Excessive	Excessive compensation required. Accuracy is poor in one or more axes. Fleet pilots will be purely reacting to external influences rather than anticipating them. A safe abort may not be possible if an aircraft or ship system is lost during a critical phase of the evolution. Fleet pilots under operational conditions could not consistently repeat these evolutions safely.
5	Dangerous	Extreme compensation required. Repeated safe evolutions are not possible even under controlled test conditions with fully proficient pilot.

Table C-1; Deck Interface Pilot Effort Scale (DIPES); modified from [1]

Each DIPES rating may be given one or more suffixes to describe the cause(s) of the increased workload:

P: Pitch control	A: Aircraft attitude	D: Deck motion	H: Height control
R: Roll control	F: Fore/aft positioning	S: Spray	T: Turbulence
Y: Yaw control	L: Lateral positioning	V: Visual cues	Q: Tq/Eng control

Scale	Definition	Description
0	No vibration	No discernible vibration.
1	Slight	Not apparent to experienced aircrew fully occupied by their task, but noticeable if their attention is directed to it or if not otherwise occupied.
2		
3		
4	Moderate	Experienced aircrew is aware of the vibration but it does not affect their work, at least over a short period.
5		
6		
7	Severe	Vibration is immediately apparent to experienced aircrew even when fully occupied. Performance of primary task is affected or tasks can only be done with difficulty.
8		
9		
10	Intolerable	Sole preoccupation of aircrew is to reduce vibration level.

Table C-2; Vibration Assessment Rating (VAR) scale; modified from [1]

Scale	Definition	Description
1	-	Flat calm
2	Light	Fairly smooth, occasional gentle displacement
3		Small movements requiring correction if in manual control
4	Moderate	Continuous small bumps
5		Continuous medium bumps
6		Medium bumps with occasional heavy ones
7	Severe	Continuous heavy bumps
8		Occasional negative ‘g’
9	Extreme	Rotorcraft difficult to control
10		Rotorcraft lifted violently several hundreds of feet

Table C-3; Turbulence rating scale; modified from [1]

Appendix D **Basic Knowledge Uncertainty Analysis**

D.1 Basic Concepts and Definitions

Because it is important to have a proper understanding of the inaccuracies in any measurement and the way errors propagate through calculations, first the concepts and definitions are carefully defined. To use experimentally determined information in an analytical solution, it is required to consider how "*good*" the experimental information is. Similarly, comparing results of a mathematical model with experimental data (and perhaps with the results of other mathematical models) should consider the "*degree of goodness*" of the data based on the comparisons. The mathematics involved in uncertainty analysis which is relevant for helicopter-ship qualification testing are summarized here for convenience [1,2,3].

Errors in measurements

Consider a variable X in a process that is considered to be steady so that its true value X_{true} is constant. As an example, suppose that a measurement system is used to make a measurement of X and that the measurement is influenced by five significant error sources. In this case, the measurement is given by:

$$X = X_{true} + \delta_1 + \delta_2 + \delta_3 + \delta_4 + \delta_5 \qquad \textbf{(Eq. D-1)}$$

where δ_1 is the value of the error from the first source, δ_2 the value of the error from the second source, and so on. Each repeated measurement of X has a different value since errors from the sources vary during the period when the measurements are taken and so are different for each measurement while others do not vary and so are the same for each measurement. Using traditional nomenclature, the symbol β is assigned to designate an error that does not vary during the measurement period and the symbol ε to designate an error that does vary during the measurement period for a parent population. For this example, it is assumed that the errors from sources 1 and 2 do not vary and the errors from sources 3, 4 and 5 do vary, so:

$$X = X_{true} + \beta_1 + \beta_2 + \varepsilon_3 + \varepsilon_4 + \varepsilon_5 \qquad \textbf{(Eq. D-2)}$$

Just by looking at the measured values there is no distinction between β_1 and β_2 or between ε_3, ε_4 and ε_5. The next equation describes what actually has been measured:

$$X = X_{true} + \beta + \varepsilon \qquad \textbf{(Eq. D-3)}$$

Where now:

$$\beta = \beta_1 + \beta_2 \qquad \text{and} \qquad \varepsilon = \varepsilon_3 + \varepsilon_4 + \varepsilon_5 \qquad \textbf{(Eq. D-4)}$$

The first component, bias, is the constant or systematic error. The bias error is a systematic error that always occurs with the same magnitude in the same direction when measurements are repeated under identical circumstances. The bias cannot be determined unless the measurements are compared with the true value of the quantity measured. In most cases, the bias error is equally likely to be plus or minus about the measurement. That is, it is not known if the limit is positive or negative. The second component, random error, also known as scatter, is seen in repeated measurements. Measurements do not, and are not, expected to agree exactly. There are always numerous small effects which cause disagreements. The variation between repeated measurements is called precision error, also known as scatter.

The difference between the measured value X_i and the true value X_{true} is the total error δx_i, which is the sum of the systematic error β (the combination of all errors from the systematic elemental error sources) and the random error ε_i (the combination at the time X_i is measured of all the error sources that vary during the period that the N measurement are taken) as shown in Figure D-1. The mean μ offset from X_{true} by β, is the combination of all the systematic errors. If continued additional measurements are taken, this distribution of the sample population of N measurements tends to have a larger number of the measured values near the mean of the sample and a decreasing number of measured values away from the mean. In case the number of measurements approaches infinity, the parent distribution would likely appear to be Gaussian. Of course, there will never be an infinite number of measurements, but conceptually the idea of the parent population distribution is very useful. In reality, a sample distribution is used composed of a finite number of measurements taken from the parent population.

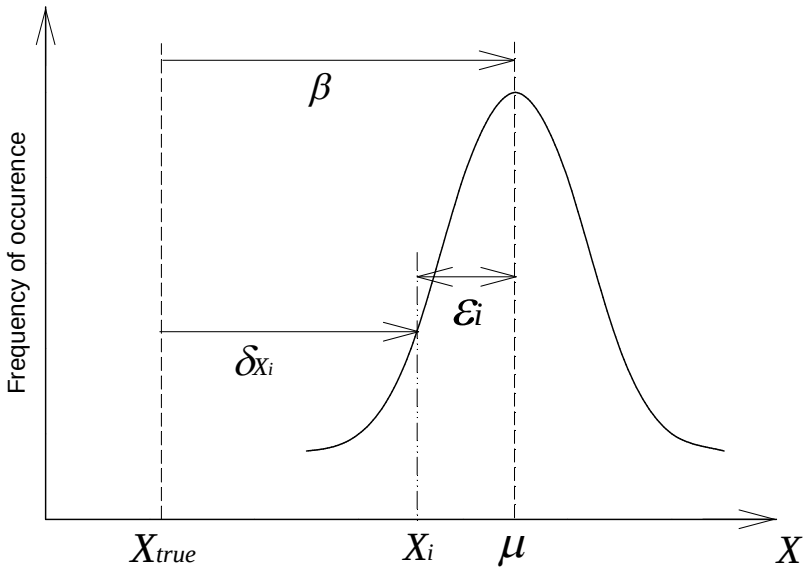

Figure D-1; Successive measurements of a variable X_i

Statistical parameters of sample function

A mean value $\overline{X}$ can be calculated, as can a standard deviation s_X, which is an indicator of the width of the distribution of the X values (the amount of "*scatter*" of the measurements caused by the errors from the elemental sources that varied during the measurement period). For N measurements of X, the standard deviation s_X of the sample function can be calculated as:

$$s_X = \left[\frac{1}{N-1} \sum_{i=1}^{N} (X_i - \overline{X})^2 \right]^{1/2} \qquad \textbf{(Eq. D-5)}$$

where the $N - 1$ occurs instead of N because the sample mean $\overline{X}$ is used instead of the mean μ. The mean value of X is calculated from:

$$\overline{X} = \frac{1}{N} \sum_{i=1}^{N} X_i \qquad \textbf{(Eq. D-6)}$$

The square of the standard deviation is known as the variance of the distribution. Note that as the value of s_x increases, the range of values of X expected also increases. Larger values of s_x therefore correspond to cases in which the scatter in the X measurements is large and thus the range of potential random errors is large. A key point in the determination of the standard deviation of a variable is how well the standard deviation s_x describes the possible random variations of the variable. All the factors that influence the random variation must be present when the N measurements of the variable are taken. The measurements will have to be taken over the appropriate time frame. Therefore, data sets for determining estimates of standard deviations of measured variables, or of experimental results should be acquired over a time period that is large relative to the time scales of the factors that have a significant influence on the data and that contribute to the random uncertainty.

Note that an alternative way to determine the standard deviation s_X from a time history of experimental flight test data is by taking the square root of the upper limit X_{up} minus the lower limit X_{low} squared divided by 12 [3]:

$$s_X = \sqrt{\frac{(X_{up} - X_{low})^2}{12}} \qquad \textbf{(Eq. D-7)}$$

Although the above equation is applicable for a uniform (rectangular) distribution it can still be useful, as a normal distribution will often be appropriate for a variable even if some of the error sources have distributions that are not-Gaussian (e.g. in this case rectangular), which is a power result of the central limit theorem.

Uncertainty in measurements

With a data sample, the information from the sample can be used to specify some range ($X_{best} \pm u_X$) within which X_{true} is likely to fall. Generally, X_{best} is taken to be equal to the average value of N measurements. The uncertainty u_X is an estimate of the interval

($\pm u_X$) that likely contains the magnitude of the combination of all the errors affecting the measured value X. To associate an uncertainty with a measured X value, elemental uncertainty estimates are needed for all the elemental error sources. That is, u_1 is an uncertainty that defines an interval ($\pm u_1$) within which the value of β_1 is assumed to fall, while u_3 is an uncertainty that defines an interval ($\pm u_3$) within which the value of ε_3 is assumed to fall, etc.. A standard uncertainty u is defined as an estimate of the standard deviation of the parent population from which a particular elemental error originates. It may be centred about the measurement unless there is a non-symmetrical bias limit expected. The uncertainty u_X is found from the combination of all the elemental uncertainties by so-called "*summation in quadrature*" as shown in Figure D-2. The summation in quadrature is allowed once it is unreasonable to assume that all of the individual errors are cumulative. There is very likely a cancelling effect because some are positive and some are negative, thus:

$$u_X = \sqrt{(u_1^2 + u_2^2 + u_3^2 + u_4^2 + u_5^2)} \qquad \textbf{(Eq. D-8)}$$

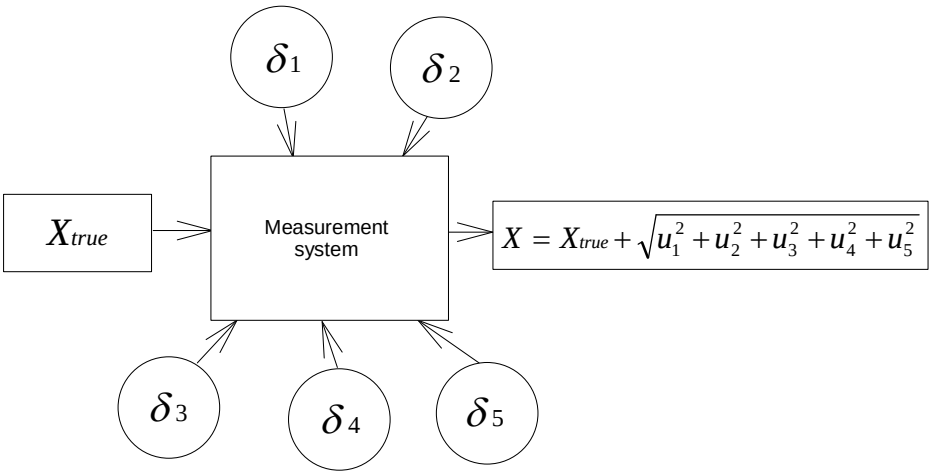

Figure D-2; Measurement of a variable influenced by five error sources

Confidence level of uncertainty

It is desirable to take the information from a data sample to specify some range ($X_{best} \pm u_X$) within which it is assumed that X_{true} lies. The problem with using the standard uncertainty is that no probability can be associated with it. An expanded uncertainty estimate, U_X, is needed such that with C percent confidence the true value of X lies within the interval:

$$X_{best} \pm U_X \qquad \textbf{(Eq. D-9)}$$

It is assumed that X_{best} is the mean value of the N measurements made, and U_X is the uncertainty in X that corresponds to the estimate with C percent confidence of the effects of the combination of the systematic and random errors. That is, $\pm U_X$ is the

range within which the estimate δ_X (the value of the total error) lies C percent of the time. If, for example, a 95% confidence estimate of U_X is made, it is expected that X_{true} would be in the interval $X_{best} \pm U_X$ about 95 times out of 100. This confidence specification is necessary because it is an estimate. It is always 100% confident that the true value of some quantity will lie between plus and minus infinity, but specifying U_X as infinite provides no useful information. Uncertainty is thus the maximum error which might reasonably be expected and is a measure of accuracy, i.e., the closeness of the measurement to the true value and may be centred about the measurement as shown in Figure D-3. Note that for experimental flight test data the value of the standard deviation for the parent population σ remains unknown – the standard deviation s_X of a finite sample of measurements is only an estimate of the value of σ.

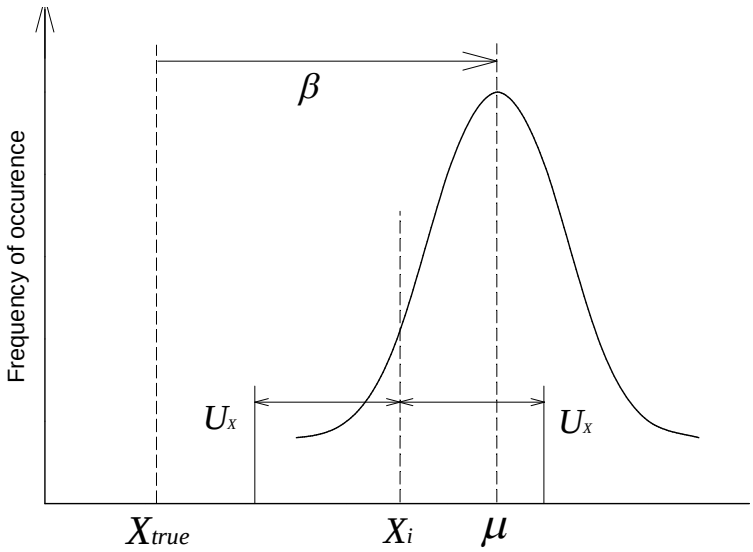

Figure D-3: The confidence interval about a single measurement

Uncertainty of a measured variable

The overall uncertainty of a measured variable X is the interval around the best value of X within which it is expected that the true value X_{true} lies with a given confidence level. To obtain the overall uncertainty, it is required to appropriately combine the random and systematic standard uncertainty estimates. The standard deviation estimate for the systematic uncertainty of the parent population for error source k is b_k. The combined standard uncertainty u_c for variable X is:

$$u_c^2 = s_X^2 + \sum_{k=1}^{M} b_k^2 \qquad \textbf{(Eq. D-10)}$$

where M is the number of significant elemental systematic error sources. In order to associate a level of confidence with the uncertainty for the variable, a coverage factor is applied such that:

$$U_c = t_{\%} u_c \quad \textbf{(Eq. D-11)}$$

where U_c is the overall or expanded uncertainty at a given percent level of confidence. The central limit theorem tells that the distribution for the total error δX for the variable will usually approach Gaussian, where the factor u_c is in a sense an estimate of the standard deviation of this total error distribution. For this reason, the *t* distribution can be used to obtain $t_{\%}$ as shown in Table D-1. The $\pm U_{\%}$ band around the variable *X*, or the mean value of *X*, will contain the true value of the variable with the given percent level of confidence.

A number of degrees of freedom is needed in order to select the *t* value for a given level of confidence. However, it has been demonstrated that the degrees of freedom will be generally large enough to consider the *t* value to be constant, known as the "*large-sample approximation*" [2]. This constant will be approximately equal to the Gaussian value for a given level of confidence (i.e. 1.96 for 95%) which is applicable for a parent population with an infinite number of measurements. For example, the resulting large-sample approximation for a 95% level of confidence using the *t* distribution ($t_{95} \approx 2$) is determined by:

$$U_{95} = 2 \cdot \left[s_X^2 + \sum_{k=1}^{M} b_k^2 \right]^{1/2} \quad \textbf{(Eq. D-12)}$$

The true value of the variable will then be within the limits of a 95% level of confidence:

$$X - U_{95} \le X_{true} \le X + U_{95} \quad \textbf{(Eq. D-13)}$$

Uncertainty in a result determined from multiple variables

In many experiments or flight test programs the experimental result is not directly measured but is determined by combining multiple measured variables in a data reduction equation. Examples are the dimensionless groups, such as referred torque required, referred engine gas generator rotational speed, and referred engine power turbine inlet temperature that are often used to present the results of a flight test. The Taylor Series Method (TSM) is applied for propagating the uncertainties of the variables into the determined result. In this dissertation, the TSM expression is an approximation that includes only the first-order terms from the Taylor series expansion. Also, the derivatives are evaluated at the measured values of, for example, *x* and *y* instead of at x_{true} and y_{true}, which would be required for a normal Taylor series expansion. For most engineering and scientific application, these approximations are reasonable, and the resulting combined standard uncertainty u_r is a good estimate of the standard deviation for the parent population for the result, *r* [2]. Consider a general case in which an experimental result *r* is a function of *J* measured variables X_i:

$$r = r(X_1, X_2, ..., X_J) \quad \textbf{(Eq. D-14)}$$

The combined standard uncertainty is given by:

$$u_r^2 = \sum_{i=1}^{J}\left(\frac{\partial r}{\partial X_i}\right)^2 b_{X_i}^2 + \sum_{i=1}^{J}\left(\frac{\partial r}{\partial X_i}\right)^2 s_{X_i}^2 \qquad \textbf{(Eq. D-15)}$$

where b_{Xi} and s_{Xi} values are the standard deviations for the measurement of each variable X_i. Using the defined systematic b_r and random s_r standard uncertainties of the result, the combined standard uncertainty becomes:

$$u_r = \left(b_r^2 + s_r^2\right)^{1/2} \qquad \textbf{(Eq. D-16)}$$

In order to associate a level of confidence with the uncertainties for the variables, a coverage factor is applied such that:

$$U_r = t_{\%} u_r \qquad \textbf{(Eq. D-17)}$$

where U_r is the overall or expanded uncertainty at a given percent level of confidence. The $\pm U_r$ band around the variable X, or the mean value of X, will contain the true value of the variable with the given percent level of confidence. In this case, the resulting large-sample approximation for a 95% level of confidence using the t distribution ($t_{95} \approx 2$) is determined by:

$$U_{95} = 2 \cdot \left[\sum_{i=1}^{J}\left(\frac{\partial r}{\partial X_i}\right)^2 \left(b_{X_i}^2 + s_{X_i}^2\right)\right]^{1/2} \qquad \textbf{(Eq. D-18)}$$

If reasonably assumed that there are no correlated systematic or random errors within the flight test data, then all of the b_{Xi} and s_{Xi} terms are independent. Taking the coverage factor inside the summation, results in:

$$U_{95} = \left[\sum_{i=1}^{J}\left(\frac{\partial r}{\partial X_i}\right)^2 U_i^2\right]^{1/2} \qquad \textbf{(Eq. D-19)}$$

where each U_i is the large-sample 95% expanded uncertainty for the variable X_i. This equation describes the propagation of the overall uncertainties in the measured variables into the overall uncertainty of the result. The application of this equation is termed general uncertainty analysis.

Correlation terms

Correlation terms for systematic and/or random errors maybe included in the equation for the general uncertainty analysis, as in some cases errors may not be independent [2]. If all systematic error sources are totally independent of each other, then the systematic error correlation effects term would be zero. But in some cases, for example x and y may share a common error source, as in a calibration standard error that is the same for both. For instance, x and y could be a temperature measurement made by separate thermocouples. If the two thermocouples were calibrated against the same standard, then the two temperature measurements would have a common, identical, systematic error resulting from the accuracy of the calibration standard.

	C				
υ	**0.900**	**0.950**	**0.990**	**0.995**	**0.999**
1	6.314	12.706	63.657	127.321	636.619
2	2.920	4.303	9.925	14.089	31.598
3	2.353	3.182	5.841	7.453	12.924
4	2.132	2.776	4.604	5.598	8.610
5	2.015	2.571	4.032	4.773	6.869
6	1.943	2.447	3.707	4.317	5.959
7	1.895	2.365	3.499	4.029	5.408
8	1.860	2.306	3.355	3.833	5.041
9	1.833	2.262	3.250	3.690	4.781
10	1.812	2.228	3.169	3.581	4.587
11	1.796	2.201	3.106	3.497	4.437
12	1.782	2.179	3.055	3.428	4.318
13	1.771	2.160	3.012	3.372	4.221
14	1.761	2.145	2.977	3.326	4.140
15	1.753	2.131	2.947	3.286	4.073
16	1.746	2.120	2.921	3.252	4.015
17	1.740	2.110	2.898	3.223	3.965
18	1.734	2.101	2.878	3.197	3.922
19	1.729	2.093	2.861	3.174	3.883
20	1.725	2.086	2.845	3.153	3.850
21	1.721	2.080	2.831	3.135	3.819
22	1.717	2.074	2.819	3.119	3.792
23	1.714	2.069	2.807	3.104	3.768
24	1.711	2.064	2.797	3.090	3.745
25	1.708	2.060	2.787	3.078	3.725
26	1.706	2.056	2.779	3.067	3.707
27	1.703	2.052	2.771	3.057	3.690
28	1.701	2.048	2.763	3.047	3.674
29	1.699	2.045	2.756	3.038	3.659
30	1.697	2.042	2.750	3.030	3.646
40	1.684	2.021	2.704	2.971	3.551
60	1.671	2.000	2.660	2.915	3.460
120	1.658	1.980	2.617	2.860	3.373
∞	1.645	1.960	2.576	2.807	3.291

Table D-1; The *t* distribution [a]

[a] Given are the values of *t* for a confidence level *C* and the number of degrees of freedom υ.

The systematic error correlation term allows for the correction of the combined standard uncertainty to take into account the effects of these correlated errors. In general, the random errors from time-varying error sources are normally considered to be uncorrelated and the random error correlation effects ignored. However, the data sets for determining estimates of standard deviations of measured variables of experimental results should be acquired over a time period that is large relative to the time scales of the factors that have a significant influence on the data and that contribute to the random uncertainty. For example, barometric pressure varies with a time scale on the order of hours, as does relative humidity. If these factors are uncontrolled but do influence a variable in the experiment, this should be recognized. If reasonably assumed that there are no correlated systematic or random errors within the flight test data, then all of the b_{Xi} and s_{Xi} terms are independent.

D.2 Example Calculations

Rarely are performance parameters measured directly; usually more basic quantities such as temperature, force, pressure, and fuel flow are measured, and the performance parameter is calculated as a function of the measurements. In this section examples are shown for the propagation of the overall uncertainties in the measured variables into the overall uncertainty of the result. The expressions for the propagation of uncertainties that arise are represented by the relative uncertainty. In each case, a calculation is performed to identify any dominant error source.

Common data

Field elevation, h_{field}	= 158.0 ft
Hover height above ground level, h_{AGL}	= 60.0 ft
Air pressure with reference to mean sea level, *QNH*	= 1 012.5 mbar
Vertical change in height for 1 mbar difference, h_{Δ}	= 27.0 ft/mbar
Outside Air Temperature (OAT)	= 16.0 ºC
Main rotor rotational speed, Ω	= 104.0 % (default value)

Calculation of pressure height

Pressure height: $$H_p = h_{field} + h_{AGL} + (QNH_{ISA} - QNH) \cdot h_{\Delta}$$

$$= 158.0 + 60.0 + (1013.25 - 1012.5) \cdot 27.0 = 231.5 \text{ ft}$$

It assumed that no Instrument Error Correction (IEC) and/or Pressure Error Correction (PEC) have to be applied. The uncertainties in the measured parameters are in accordance with the data presented in Chapter 3 (Table 3-1).

Calculation of relative quantities

Relative pressure: $$\delta = (1 - 6.8756 \times 10^{-6} \times H_p)^{5.2559}$$

$$= (1 - 6.8756 \times 10^{-6} \times 231.5)^{5.2559} = 0.99166$$

Relative temperature: $$\theta = \frac{273.15 + \mathrm{OAT}}{288.15} = \frac{273.15 + 16.0}{288.15} = 1.00347$$

Relative density: $$\sigma = \frac{\delta}{\theta} = \frac{0.99166}{1.00347} = 0.98823$$

Relative rotorspeed: $$\omega = \frac{\Omega}{\Omega_0} = \frac{104.0}{104.0} = 1.00000$$

Relative uncertainty in relative pressure δ

First determine the uncertainty in the relative pressure U_δ:

$$U_\delta = \frac{\partial \delta}{\partial H_p} \cdot U_{H_p} = 5.2559 \cdot (1 - 6.8756 \times 10^{-6} \times H_p)^{4.2559} \cdot (-6.8756 \times 10^{-6}) \cdot U_{H_p}$$

where the uncertainty in the pressure altitude U_{H_p} is:

$$U_{H_p} = \sqrt{(U_{QNH} \cdot 27)^2 + (U_{field})^2 + (U_{AGL})^2}$$

$$= \sqrt{(0.1 \cdot 27)^2 + (1.00)^2 + (3.16)^2} = 4.3\,\mathrm{ft}$$

So at the example pressure altitude the uncertainty in relative pressure U_δ is:

$$U_\delta = 5.2559 \cdot (1 - 6.8756 \times 10^{-6} \times 231.5)^{4.2559} \cdot (-6.8756 \times 10^{-6}) \cdot 4.3 = 0.00015$$

and the relative uncertainty for the relative pressure:

$$\frac{U_\delta}{\delta} = \frac{0.00015}{0.99166} = 0.00015$$

Relative uncertainty in relative temperature θ

First determine the uncertainty in the relative temperature U_θ:

$$U_\theta = \frac{\partial \theta}{\partial (OAT)} \cdot U_{OAT} = \frac{1}{288.15} \cdot U_{OAT}$$

where the uncertainty in the OAT U_{OAT} is 0.10 °C:

$$U_\theta = \frac{1}{288.15} \cdot 0.10 = 0.00035$$

and the relative uncertainty for the relative temperature:

$$\frac{U_\theta}{\theta} = \frac{0.00035}{1.00347} = 0.00035$$

Relative uncertainty in relative density σ

The relative uncertainty in the relative density is calculated as follows:

$$\frac{U_\sigma}{\sigma} = \sqrt{\left(\frac{U_\delta}{\delta}\right)^2 + \left(\frac{U_\theta}{\theta}\right)^2} = \sqrt{\left(\frac{0.00015}{0.99166}\right)^2 + \left(\frac{0.00035}{1.00347}\right)^2} = 0.00038$$

Relative uncertainty in relative rotorspeed ω

The relative uncertainty in the relative rotorspeed is calculated as follows:

$$\frac{U_\omega}{\omega} = \frac{U_\Omega}{\Omega} = \frac{0.14}{104.0} = 0.00136$$

D.2.1 Uncertainty in Referred Torque Required

Consider the function of the referred torque required $Q_{req,ref}$:

$$Q_{req,ref} = \frac{Q_{req}}{\sigma\omega^2}$$

where Q_{req} is the torque required. Using the general uncertainty analysis expression for the referred torque required, the uncertainty is determined as:

$$\frac{U_{Q_{req,ref}}}{Q_{req,ref}} = \sqrt{\left(\frac{U_{Q_{req}}}{Q_{req}}\right)^2 + \left(\frac{U_\sigma}{\sigma}\right)^2 + \left(2 \cdot \frac{U_\omega}{\omega}\right)^2}$$

Relative uncertainty in torque required Q_{req}

The relative uncertainty in torque required for a multi-engine helicopter, with similar engines, is a function of the bias errors and precision errors of the individual engines combined. Note that it is assumed there is no systematic dependence between the uncertainties of both engines for a particular test point, although the time-varying random uncertainties for the torque required measurement itself are considered identical. At the sample data point:

$Q_{1,req}$	= 86.8 %
$Q_{2,req}$	= 86.8 %
$U_{Q_{1,req}}$	= 5.2 %
$U_{Q_{2,req}}$	= 5.2 %

The relative uncertainty in torque required is calculated as follows:

$$\frac{U_{Q_{req}}}{Q_{req}} = \frac{U_{(Q_{1,req}+Q_{2,req})}}{Q_{1,req}+Q_{2,req}} = \frac{5.2+5.2}{86.8+86.8} = 0.05993$$

Relative uncertainty in relative density σ

The relative uncertainty in the relative density has already been calculated and is:

$$\frac{U_\sigma}{\sigma} = 0.00038$$

Relative uncertainty in relative rotorspeed ω

The relative uncertainty in the relative rotorspeed has already been calculated and is:

$$\frac{U_\omega}{\omega} = 0.00136$$

Relative uncertainty in referred torque required $Q_{req,ref}$

The relative uncertainty in the referred torque required is now calculated as follows:

$$\frac{U_{Q_{req,ref}}}{Q_{req,ref}} = \sqrt{\left(\frac{U_{Q_{req}}}{Q_{req}}\right)^2 + \left(\frac{U_\sigma}{\sigma}\right)^2 + \left(2 \cdot \frac{U_\omega}{\omega}\right)^2}$$

$$= \sqrt{(0.05993)^2 + (0.00038)^2 + (2 \cdot 0.00136)^2} = 0.05999$$

The dominant error in the referred torque required is from the error in the torque measurement itself, whilst the errors in relative density and relative rotorspeed being very small in comparison. So at the sample data point, the absolute uncertainty for a given level of confidence in referred torque required is:

$$U_{Q_{req,ref}} = \frac{Q_{req}}{\sigma\omega^2} \cdot 0.05999 = \frac{86.8}{0.98823 \cdot 1.00000^2} \cdot 0.05999 = 5.3\,\%$$

D.2.2 Uncertainty in Referred Engine Speed

Consider the function of the referred engine gas generator rotational speed $N_{g,ref}$:

$$N_{g,ref} = \frac{N_g}{\sqrt{\theta}}$$

where N_g is the engine gas generator rotational speed. Using the general uncertainty analysis expression for the referred engine gas generator rotational speed, the uncertainty is determined as:

$$\frac{U_{N_{g,ref}}}{N_{g,ref}} = \sqrt{\left(\frac{U_{N_g}}{N_g}\right)^2 + \left(0.5 \times \frac{U_\theta}{\theta}\right)^2}$$

Relative uncertainty in engine gas generator rotational speed N_g

The engine gas generator rotational speed is considered separately for each engine. At the sample data point:

N_g = 97.2 %

U_{N_g} = 0.5 %

The relative uncertainty in engine gas generator rotational speed is calculated as follows:

$$\frac{U_{N_g}}{N_g} = \frac{0.5}{97.2} = 0.00525$$

Relative uncertainty in relative temperature θ

The relative uncertainty in the relative temperature has already been calculated and is:

$$\frac{U_\theta}{\theta} = 0.00035$$

Relative uncertainty in referred engine gas generator rotational speed $N_{g,ref}$

$$\frac{U_{N_{g,ref}}}{N_{g,ref}} = \sqrt{\left(\frac{U_{N_g}}{N_g}\right)^2 + \left(0.5 \times \frac{U_\theta}{\theta}\right)^2}$$

$$= \sqrt{(0.00525)^2 + (0.5 \cdot 0.00035)^2} = 0.00525$$

The dominant error in the referred engine gas generator rotational speed is from the error in the N_g measurement itself, whilst the error in relative temperature being very small in comparison. So at the sample data point, the absolute uncertainty for a given level of confidence in referred engine gas generator rotational speed is:

$$U_{N_{g,ref}} = \frac{N_g}{\sqrt{\theta}} \cdot 0.00525 = \frac{97.2}{\sqrt{1.00347}} \cdot 0.00525 = 0.51\%$$

D.2.3 Uncertainty in Referred Engine Temperature

Consider the function of the referred engine power turbine inlet temperature $T_{46,ref}$:

$$T_{46,ref} = \frac{T_{46}}{\theta}$$

where T_{46} is the engine power turbine inlet temperature. Using the general uncertainty analysis expression for the referred engine power turbine inlet temperature, the uncertainty is determined as:

$$\frac{U_{T_{46,ref}}}{T_{46,ref}} = \sqrt{\left(\frac{U_{T_{46}}}{T_{46}}\right)^2 + \left(\frac{U_\theta}{\theta}\right)^2}$$

Relative uncertainty in engine power turbine inlet temperature T_{46}

The engine power turbine inlet temperature is considered separately for each engine. At the sample data point:

T_{46} = 731.2 °C

$U_{T_{46}}$ = 9.8 °C

The relative uncertainty in engine power turbine inlet temperature is calculated as follows:

$$\frac{U_{T_{46}}}{T_{46}} = \frac{9.8}{731.2} = 0.01340$$

Relative uncertainty in relative temperature θ

The relative uncertainty in the relative temperature has already been calculated and is:

$$\frac{U_\theta}{\theta} = 0.00035$$

Relative uncertainty in referred engine power turbine inlet temperature $T_{46,ref}$

$$\frac{U_{T_{46,ref}}}{T_{46,ref}} = \sqrt{\left(\frac{U_{T_{46}}}{T_{46}}\right)^2 + \left(\frac{U_\theta}{\theta}\right)^2}$$

$$= \sqrt{(0.01340)^2 + (0.00035)^2} = 0.01341$$

The dominant error in the referred engine power turbine inlet temperature is from the error in the T_{46} measurement itself, whilst the error in relative temperature being very small in comparison. So at the sample data point, the absolute uncertainty for a given level of confidence in referred engine power turbine inlet temperature is:

$$U_{T_{46,ref}} = \frac{T_{46}}{\theta} \cdot 0.01341 = \frac{731.2}{1.00347} \cdot 0.01341 = 9.8\ ^\circ\text{C}$$

D.2.4 Uncertainty in Referred Weight

Consider the function of the referred weight W_{ref}:

$$W_{ref} = \frac{W}{\sigma\omega^2}$$

where W is the weight of the helicopter. Using the general uncertainty analysis expression for the referred weight, the uncertainty is determined as:

$$\frac{U_{W_{ref}}}{W_{ref}} = \sqrt{\left(\frac{U_W}{W}\right)^2 + \left(\frac{U_\sigma}{\sigma}\right)^2 + \left(2 \cdot \frac{U_\omega}{\omega}\right)^2}$$

Relative uncertainty in helicopter weight W

At the sample data point:

W = 10 050.0 kg

U_W = 20.0 kg

The relative uncertainty in helicopter weight is calculated as follows:

$$\frac{U_W}{W} = \frac{20.0}{10\,050.0} = 0.00199$$

Relative uncertainty in relative density σ

The relative uncertainty in the relative density has already been calculated and is:

$$\frac{U_\sigma}{\sigma} = 0.00038$$

Relative uncertainty in relative rotorspeed ω

The relative uncertainty in the relative rotorspeed has already been calculated and is:

$$\frac{U_\omega}{\omega} = 0.00136$$

Relative uncertainty in referred helicopter weight W_{ref}

$$\frac{U_{W_{ref}}}{W_{ref}} = \sqrt{\left(\frac{U_W}{W}\right)^2 + \left(\frac{U_\sigma}{\sigma}\right)^2 + \left(2 \cdot \frac{U_\omega}{\omega}\right)^2}$$

$$= \sqrt{(0.00199)^2 + (0.00038)^2 + (2 \cdot 0.00136)^2} = 0.00339$$

The dominant error in the referred helicopter weight is from the error in the weight calculation itself, whilst the error in relative rotorspeed is quite similar and the errors in relative density being very small in comparison. So at the sample data point, the absolute uncertainty for a given level of confidence in referred helicopter weight is:

$$U_{W_{ref}} = \frac{W}{\sigma\omega^2} \cdot 0.00339 = \frac{10\,050.0}{0.98823 \cdot 1.00000^2} \cdot 0.00339 = 34.5 \text{ kg}$$

D.2.5 Uncertainty in Maximum Power Vertical Climb Factor

Consider the function of the maximum power vertical climb factor C_{MPV}:

$$C_{MPV} = \frac{C}{Q_{uti} - Q_{req}}$$

where C is the vertical climb speed and Q_{uti} is the maximum torque utilised in the climb. Using the general uncertainty analysis expression for the maximum power vertical climb factor, the uncertainty is determined as:

$$\frac{U_{C_{MPV}}}{C_{MPV}} = \sqrt{\left(\frac{U_C}{C}\right)^2 + \left(\frac{U_{Q_{uti}}}{Q_{uti}}\right)^2 + \left(\frac{U_{Q_{req}}}{Q_{req}}\right)^2}$$

Relative uncertainty in vertical climb speed C

At the sample data point:

C = 1 371.8 ft/min

U_C = 100.5 ft/min

The relative uncertainty in vertical climb speed is calculated as follows:

$$\frac{U_C}{C} = \frac{100.5}{1371.8} = 0.07326$$

Relative uncertainty in torque utilised in the climb Q_{uti}

The relative uncertainty in torque utilised for a multi-engine helicopter, with similar engines, is a function of the bias errors and precision errors of the individual engines combined. Note that it is assumed there is no systematic dependence between the uncertainties of both engines for a particular test point, although the time-varying random uncertainties for the torque required measurement itself are considered identical. As the First Limit Indicator (FLI) is used to set the maximum power in vertical climb, the pilot is much more aware of the power requirements and as such the random uncertainties are assumed to be half that for torque required. At the sample data point:

$Q_{1,uti}$ = 103.6 %

$Q_{2,uti}$ = 103.6 %

$U_{Q_{1,uti}}$ = 2.6 %

$U_{Q_{2,uti}}$ = 2.6 %

The relative uncertainty in torque required is calculated as follows:

$$\frac{U_{Q_{uti}}}{Q_{uti}} = \frac{U_{(Q_{1,uti}+Q_{2,uti})}}{Q_{1,uti}+Q_{2,uti}} = \frac{2.6+2.6}{103.6+103.6} = 0.02510$$

Relative uncertainty in torque required Q_{req}

The relative uncertainty in torque required for a multi-engine helicopter, with similar engines, is a function of the bias errors and precision errors of the individual engines combined. Note that it is assumed there is no systematic dependence between the uncertainties of both engines for a particular test point, although the time-varying random uncertainties for the torque required measurement itself are considered identical. At the sample data point:

$Q_{1,req}$ = 85.0 %

$Q_{2,req}$ = 85.0 %

$U_{Q_{1,req}}$ = 5.2 %

$U_{Q_{2,req}}$ = 5.2 %

The relative uncertainty in torque required is calculated as follows:

$$\frac{U_{Q_{req}}}{Q_{req}} = \frac{U_{(Q_{1,req}+Q_{2,req})}}{Q_{1,req}+Q_{2,req}} = \frac{5.2+5.2}{85.0+85.0} = 0.06119$$

Relative uncertainty in maximum power vertical climb factor C_{MPV}

$$\frac{U_{C_{MPV}}}{C_{MPV}} = \sqrt{\left(\frac{U_C}{C}\right)^2 + \left(\frac{U_{Q_{uti}}}{Q_{uti}}\right)^2 + \left(\frac{U_{Q_{req}}}{Q_{req}}\right)^2}$$

$$= \sqrt{(0.07326)^2 + (0.02510)^2 + (0.06119)^2} = 0.09869$$

The dominant error in the maximum power vertical climb factor is from the error in the vertical climb itself, whilst the errors in torque utilised in the climb and torque required for the test condition are quite similar in comparison. So at the sample data point, the absolute uncertainty for a given level of confidence in maximum power vertical climb factor is:

$$U_{C_{MPV}} = \frac{C}{Q_{uti}-Q_{req}} \cdot 0.09869 = \frac{1371.8}{103.6-85.0} \cdot 0.09869 = 7.3\,\text{ft/min/\%}$$

Page intentionally left blank

Appendix E Flight Test Philosophy and Test Techniques

E.1 General

The helicopter flight limitations are usually determined in a land-based environment by the helicopter manufacturer and/or by the procuring activity. However, these land-based limitations are not necessarily appropriate in the shipboard environment, for example, due to ship airwake / turbulence, ship motion, confined landing areas, visual cue limitations and due to any combined effects of these factors. In any case, operators and force commanders desire the maximum helicopter-ship operational capability that can be accomplished in any atmospheric condition. The purpose of this appendix is to briefly outline the helicopter-ship qualification test procedures including the preparation, execution and test philosophy that should be employed, combined with best safety practices to obtain the maximum operational capability. Attention is focused on helicopter take-off and landing, which constitutes the main part of the test program. The following relevant topics are described in this dissertation:

- The factors influencing helicopter-ship operations (see Chapter 2);
- The measurement uncertainties are quantified and possible sources of the errors that contribute to it are described (see Chapter 3);
- How these factors influence helicopter-ship operations are determined in various phases of the test campaign (see Chapter 4);
- How the data obtained in a preliminary investigation is used, such that it contributes to a bare minimum number of flying hours onboard any ship without affecting the quality of the results. Subsequently, how these data are used to set-up a flight test program onboard a ship (see Chapter 5);
- How the sea trials on board a ship, within the constraints of safety and efficiency, are carried out and result in the maximum operational capability for each particular helicopter-ship combination (see Chapter 6).

The execution of a helicopter-ship qualification test campaign, as described in this dissertation, may seem to be rather elaborate at first instant. However, the advantages that are gained in the long run are enormous. Once a ship and a helicopter have been qualified for shipboard operations, updating the Ship Helicopter Operational Limitations (SHOL) after modifications on the helicopter, or on the ship, is relatively easy as only the relevant parts of the qualification programme may have to be updated and/or repeated. The same holds for successive test campaigns with the same helicopter for other ship types, or the same ship with other helicopter types. This is accomplished by the establishment of a data base to be used for future flight test activities. In general, the scope of a helicopter-ship qualification programme is defined by the following elements:

- Operator's requirements;
- Operator's standard operating procedures for helicopter and ship;
- Proficiency and training standards of the aircrew;
- Operational environment (i.e. geographic region);
- Helicopter flight characteristics and capabilities;
- Knowledge of the ship environment;
- Efficiency of the test methodology;
- Safety standards applied.

E.2 Ship Environment Aspects

In this dissertation, a novel approach is demonstrated how wind tunnel measurements are used for an objective assessment of the ship-environment prior to conducting sea trials. The wind tunnel measurements were not performed as part of the data gathering campaign required for this dissertation. The data sets used were readily available within the Netherlands Ministry of Defence (NLMoD), of which the author had access, due to previous contract requirements [1,2,3,4,5,6]. With the information obtained, an unambiguous relation between the anemometer readings, the air flow conditions above the flight deck, in the helicopter approach and departure paths with the undisturbed relative wind condition is determined. In addition, a verification of the ship's anemometers is performed during the sea trial to ensure that the anemometers are correctly aligned with the ship's heading and to spot-check the ship environment simulation by the predictive tool used to construct the Candidate Flight Envelope (CFE). If required, dedicated full-scale measurements at sea can be conducted to validate the wind tunnel measurements although this is not further discussed in this dissertation. Note that the effects of ship motion on pilot workload for take-off and landing are determined as part of the flying routine during the sea trials, and for that reason are discussed not discussed here.

For the verification of the ship's anemometers during the sea trials, a reference anemometer is required. The location of the reference anemometer should be as much as feasible outside ship influences to provide most accurate correlation with the undisturbed relative wind. For an optimal location of the reference anemometer, the top of the jack staff at the bow of the ship is usually chosen as shown for example in Figure E-1. The position at the bow of the ship is used as the air flow deviations due to the presence of the ship's superstructure are minimal over a wide range of azimuth angles, and the correction factors to be applied are known from the wind tunnel measurements. In order to compare the measurements of the reference anemometer and the ship's anemometers the following steps are applied:

1. Calculate the atmospheric boundary layer coefficient Z_{ABL};
2. Determine any misalignment of the ship's anemometer systems;
3. Verify the ship's anemometers.

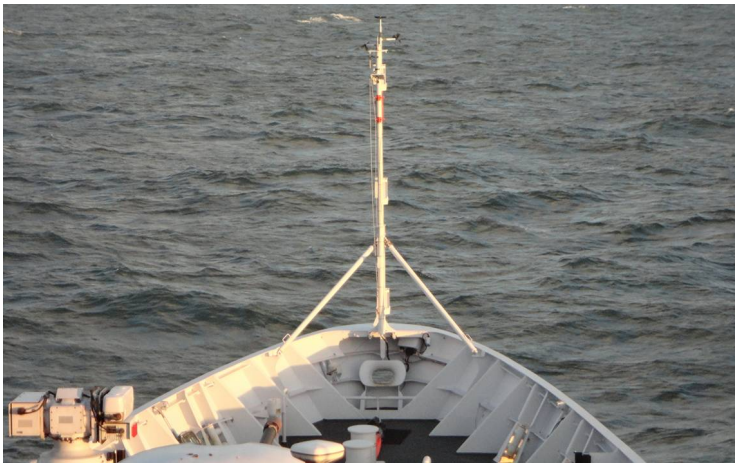

Figure E-1; Example reference anemometer at jack staff

Step 1: Calculate the atmospheric boundary layer coefficient

In the wind tunnel airflow measurements are carried out in a uniform airflow condition, i.e. the wind does not vary with height. In reality, the wind speed increases with height due to the effects of the atmospheric boundary layer. To correlate the local wind speeds of the reference anemometer with the indicated wind speeds measured at the anemometer locations, the airflow velocities should be increased by an amount dependent on the vertical distance between the flight deck and reference anemometer locations as explained in Chapter 5.

Step 2: Determine the misalignment of the ship's anemometer systems

For undisturbed relative winds from dead-ahead, the horizontal wind direction at the anemometer location β_{an} has a deviation from it as determined in the windtunnel and shown for example in Figure E-2. The local horizontal flow deviation with respect to port anemometer χ-*P* is determined as +5° and the local horizontal flow deviation with respect to starboard anemometer χ-*S* is determined as -4°. In case there is a discrepancy between these values and the actual measurements during the sea trials, the likely cause is a misalignment of the respective anemometer. Note that, although it seems straightforward, the mounting assembly of the ship's anemometers should be fitted with a device to ensure unambiguous alignment of the anemometer after removal and refitting for maintenance to avoid repeating the verification process each time. To check the alignment of the ship's anemometers, the following test programme is executed:

- Establish the wind dead-ahead by using the starboard anemometer;
- The ships' course and speed should be kept constant at approximately 5 knots for a time interval of five minutes;
- The ships' speed should be increased to approximately 10 knots, whilst maintaining the course determined previously for a time interval of five minutes;

- The ships' speed should be increased to approximately 15 knots, whilst maintaining the course determined previously for a time interval of five minutes;
- Establish the wind dead ahead by using the port anemometer;
- The ships' speed should be maintained at approximately 15 knots, whilst selecting a new course, which then should be maintained for a time interval of five minutes;
- The ships' speed should be decreased to approximately 10 knots, whilst maintaining the course determined previously for a time interval of five minutes;
- The ships' speed should be decreased to approximately 5 knots, whilst maintaining the course determined previously for a time interval of five minutes.

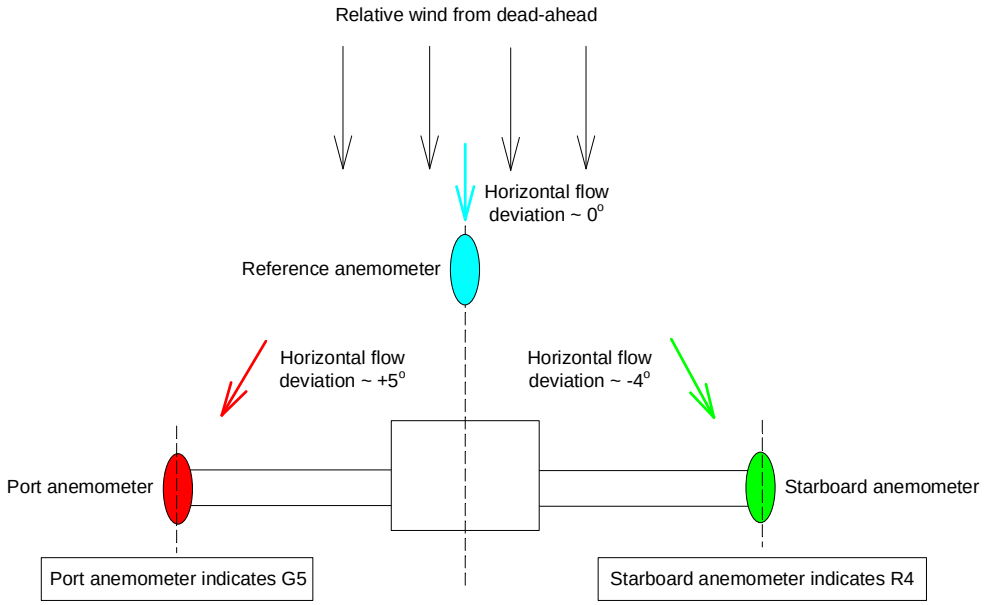

Figure E-2; Example horizontal flow deviations; modified from [6]

Step 3: Verify the ship's anemometers

A comparison should now be made between the indicated wind as measured during the sea trials by the ship's anemometers, and the wind tunnel measurements at the anemometer locations. After applying the atmospheric boundary layer coefficient to the wind tunnel data, the average of the measurements by the ship's anemometer should be within the tolerances set (i.e. 5° azimuth and 3 knots). If required, also other wind azimuths may be verified during post-flight analysis as these data are readily available due to the continuous recording during the sea trials of the ship's parameters.

E.3 Helicopter Aspects – Ground Assessment

The ground assessment of the helicopter aspects includes at least a test to determine the Flight Control Mechanical Characteristics (FCMC). The FCMC for the collective, cyclic and pedal control envelopes are required to express the control positions in a percentage of full travel in order to assess remaining control authority. In addition, a variety of helicopter specifics must be considered during the ground assessment to determine the operational capabilities for embarked operations from a ship at sea. The outcome of the ground assessment is the starting point from the flight test campaign and bounds the likely outcome of the operational envelope which is to be verified during dedicated sea trials. Not all items necessarily have to be tested, unless of course in-flight observations dictate so.

1. *Handling qualities.* A sub-division is made for the term flying qualities in accordance with Padfield – handling qualities, reflecting the helicopter's behaviour in response to pilot controls, and ride qualities, reflecting the response to external disturbances [7]. The handling qualities investigation of a helicopter is conducted to determine if the pilot-helicopter combination can safely and precisely perform the role for which it is intended (in this case shipboard operations). If a helicopter exhibits poor handling qualities, for any reason, then the low speed manoeuvre envelope may have to be restricted. The causes for poor handling qualities could be, stability and control characteristics, or cross-coupling issues:

- *FCMC.* Poor FCMC will affect the ability of the pilot to use the controls to achieve the desired flight condition and is often the cause of poor handling qualities. Tasks such as precise hovering will be made considerably more difficult with high breakout forces, excessively weak or strong force gradients and total system freeplay or trim system deficiencies. Control harmonization (both in terms of breakout force and force gradient) is particularly important in low speed flight where continual and simultaneous use of all controls is often required.
- *Stability and control.* The stability and control characteristics of a helicopter at low speed will be a major influence on the handling qualities and will often be the dominant factor. Ideally a helicopter should exhibit sufficient static and dynamic stability to ensure that control movements are made progressively, in the natural sense, and that the pilot is not required to continually intervene to prevent the helicopter departing from the trimmed flight condition. The helicopter must be sufficiently agile to perform take-offs to and landings from a ship, whilst the response to control inputs must be predictable and at a rate which is suitable.
- *Cross-coupling.* All helicopters suffer in some way from cross-coupling, which increases the difficulty in controlling the helicopter for the pilot. This is particularly relevant during manoeuvres requiring large power changes such as take-off and landings. The degree of additional workload required of the pilot to suppress these undesirable effects will determine if they constitute a deficiency.

2. *Ride qualities*. The helicopter's response to external disturbances like, for example, gusts and turbulence should be convergent and well-damped to minimize workload in the final phases of the approach and landing. Since this characteristic is normally at variance with agility, a good auto stabilization system is necessary. Poor gust response can also result in increased control activity, and as a consequence increased performance demands.

3. *Control margins*. During any manoeuvring there should be a margin of control authority remaining to counter any rates of movement caused by the manoeuvre itself or by other factors such as turbulence or changes in the Centre of Gravity (CG). For ease of understanding an international agreed value of 10% control margin is used.

4. *Centre of Gravity (CG)*. The position of the longitudinal and lateral CG may limit the low speed operations of a helicopter. For example, an extreme lateral CG position may result in there being insufficient lateral control authority to control an across slope landing, or to control flight at the maximum permitted sideways flight limit. In addition, considerations should be given to any tendency towards dynamic rollover. Dynamic rollover is a phenomenon where beyond a certain roll attitude when in contact with the ground the helicopter develops a rolling moment that exceeds the corrective moment that the pilot is able to generate with the cyclic and the collective.

5. *Degraded modes*. The majority of testing should take place with all helicopter normal flight systems engaged, however some testing may be required with systems such as, for example, the Automatic Flight Control System (AFCS) or hydraulic system disengaged. The amount of testing will depend on the probability of failure, the degree of system redundancy and the required mission profile following a failure.

6. *Engine and engine control system*. Poor engine acceleration and deceleration characteristics will limit the rate at which large collective lever movements can be made by the pilot for manoeuvres such as bob-ups or transitions. Furthermore, when moving rearwards or with quartering relative winds engines may re-ingest exhaust gases or may surge due to the changed airflow and pressure at the intake or exhaust. In rare circumstances, the exhaust gases of the ship may even increase the entry temperature of the engines, resulting in an increase of engine power turbine inlet temperature.

7. *Performance*. Poor vertical performance frequently restricts the low speed manoeuvring capability of a helicopter and may limit the size and rate of control inputs which can be made. Lack of available power may also define the control margin for the so-called "*power pedal*", as further application of pedal would result in the exceedance of an engine or transmission limitation (i.e. the left pedal is the power pedal in case of a helicopter with a counter-clockwise turning main rotor when seen from above).

8. *Main rotor system*. The design of the main rotor system may limit the degree of slope that a helicopter can operate on due to mast bending moments on semi-rigid

systems or droop stop bounding on articulated designs. These limitations are imposed by the manufacturer. Furthermore, main rotor coupling and de-coupling envelopes are usually defined by the helicopter manufacturer, along with the recommended techniques, and based on parameters such as blade sailing characteristics and rotor head stresses. It is highly recommended to ensure that the helicopter is fitted with a rotor brake system to minimize the risk for blade sailing in the turbulent airwake behind the superstructure of the ship. In addition, the main rotor blades and the tail pylon for a naval helicopter are usually fitted with folding systems such that the helicopter fits into the hangar.

9. *Vibration*. Most helicopters are affected by vibrations during low speed flight. Although it may not limit the manoeuvre envelope, it will affect the crew and may prevent the use of sighting systems or other items of equipment.

10. *Stress limitations*. The maximum rate of yaw in the hover and the maximum lateral velocity may be determined by fuselage / tail-cone stress limitations. From a test viewpoint these are straightforward forms of envelope limitation imposed by the manufacturer, although the way in which such limitations are defined and the accuracy and ease of flying within them should be considered.

11. *Undercarriage*. The design of the undercarriage may limit the rate of impact for all types of landings. The undercarriage should have good energy absorbing characteristics to enable the helicopter to land at high rates of descent with drift. There should be no tendency to ground resonance. The coefficient of friction between the tyres and the flight deck must be sufficient to prevent sliding, but low enough to prevent undercarriage damage.

12. *Field of View (FOV)*. The FOV from the cockpit should be such that the pilot can operate the helicopter with adequate visual references with the ship and the Flight Deck Officer (FDO) throughout the take-off and landing phases. In case required a FOV diagram of the cockpit can be made.

13. *Windscreen wipers*. Efficient windscreen wipers and washers are vital to remove sea spray during the final stages of the approach and landing to ensure adequate visual reference with the ship in case of sea spray and/or rain.

14. *Floatation gear*. The presence of a suitable floatation gear for the helicopter should be verified. If for whatever reason no floatation gear is installed, the requirements to install it should be documented.

15. *Corrosion prevention*. The suitability of the helicopter to operate in a salty environment should be verified. The shipboard environment is very salty and preventive actions should be taken to ensure that the helicopter can be operated for prolonged periods on board the ship without excessive maintenance penalties. For example, operations in a salt environment, particularly when spray is ingested into the engines, can cause rapid degradation of engine performance.

16. *Anthropometrical considerations*. An important aspect to ensure is that the aircrew can escape from the cockpit whilst wearing full flying gear with a life raft attached to the pilot. The arrangements for flying clothing and survival equipment are usually the operator's responsibility and are to be verified during the flight test campaign.

17. *Electro Magnetic Interference and Electro Magnetic Compatibility (EMI/EMC)*. The helicopter specifications with regard to EMI/EMC should be verified with the specifications of the communication and radar systems installed on board the ship to ensure that the helicopter can be operated safely in the shipboard electromagnetic environment. In case of any doubt, the respective communication and/or radar should not be operated during take-off and landing from the ship, or a dedicated qualification program should be conducted which is not further discussed in this dissertation.

18. *Night lighting assessment*. The night lighting assessment is normally conducted as part of the normal flying routine, both for aided flight operations with Night Vision Goggles (NVG) and unaided flight operations. The effectiveness and control of external lights installed on the helicopter and required for the role should also be evaluated during the night lighting assessment. The external lights of the helicopter should assist the aircrew in the take-off and landing tasks, and thus enable adequate outside visual references. For ships, the main aspects of a night assessment concern the adequacy of the flight deck markings, horizonbar and Glide Path Indicator (GPI) both for aided and unaided flight.

19. *Visual pilot aids*. Consider the suitability of any ship-based, cockpit and/or helmet displays to guide the pilot during the deck landing task. In addition, verify the sufficiency of visual cues for the pilot during lateral transition, station keeping and landing.

20. *Helicopter securing system*. A dedicated helicopter harpoon securing system is used for most naval helicopters to ensure the maximum operational capabilities with regard to ship motion for any helicopter-ship combination. In addition to the harpoon, and solely for non-maritime helicopter, lashings are applied to increase the ship motion even further. The helicopter securing systems must be evaluated to avoid contact with fuselage, or impact standard operating procedures in any way. In any case, the associated limitations should be known or established prior to or during the sea trials.

21. *Helicopter traversing system*. A dedicated helicopter traversing system may be used for most naval helicopters to ensure the maximum operational capabilities with regard to ship motion for any helicopter-ship combination. However, other options may be used, such as aircraft handlers also used on shore. In any case, the associated limitations should be known or established prior to or during the sea trials.

22. *Refuelling options*. The capacity of the ship and helicopter should be investigated to perform standard refuelling and Rotors Running Refuelling (RRR) at each relevant landing spot. Of course, the connectors of the ship should be compatible with the helicopter, and vice versa, but also the length of the fuel hose should be sufficient to

reach the helicopter at each landing spot. Preferably, there should be an unobstructed sight between the operator of the ship's fuel pump installation and the operator connecting the hose to the helicopter such that hand signals can be given.

23. *Helicopter-ship interface considerations*. Several other ship-related factors should be considered:

- Size – how big are the landing spots and the hangar in comparison to the dimensions of the helicopter?
- Are there any obstructions near the landing spot, approach, or take-off corridors that might impact flight operations?
- How high is the flight deck above the water?
- How high are the ship anemometers above the flight deck and where are they positioned?
- What are the ship motion characteristics?
- Flight Deck – adequate markings and lighting for pilot visual cues?
- Deck Handling - most flight deck handling issues can be evaluated through a paper analysis, with scale drawings and information on helicopter turning radius.
- If a missile is mounted on a helicopter, clearance issues, ordnance upload / download and helicopter re-spotting become important. Procedures must be developed to safely download ordnance from the helicopter to the magazine aboard the ship.
- Ship Interface – ability to connect test equipment and get access to required data during the sea trials?

E.3.1 Flight Control Mechanical Characteristics

The FCMC assessment can be divided into quantitative aspects which normally take place on the ground and qualitative aspects which are conducted in flight. As quantitative testing is concerned with the measurement of forces and displacements it can be conducted more easily and safely on the ground. The control envelopes can only be measured fully with rotors stopped. If required, tests should be made with hydraulic systems pressurized to in-flight values by using a ground hydraulic rig. The electrical system may well interact with the flying controls, especially trim systems, and therefore suitable ground power should be connected. In this dissertation, the FCMC assessment is limited to construction of the flight control envelopes. In case in-flight observations dictate so, a more pronounced FCMC assessment can be made. The control envelope is the area described by the maximum achievable control displacement in all directions (measured at the control reference point) from the pilot's normal seated position. Hand held tape measurements are used from fixed cockpit positions. The measured envelopes are then referenced to the data recorded via test instrumentation, allowing instrumentation output to be quantified as a distance margin and a percentage. Determining if the control envelope is satisfactory is not as simple as it may seem at first. If items within the cockpit restrict the range of control

movement it is not necessarily a deficiency; it is only significant if the restriction is encountered during role-related flight manoeuvres. When assessing and documenting flight control characteristics it is important to use a standard and accepted reference system for presenting results and sign conventions as explained in the following.

Control reference point

The Control Reference (CR) point is the position where all control displacements are measured from, and at which all control forces should be measured. A definition of the CR point is required, as the distances through which controls move and the forces needed to move them can vary depending on where the measurement is made. For the cyclic, it is common to use the position of the pilot's middle finger on the forward face of the cyclic grip with controls and trim neutral as shown for example in Figure E-3. For the collective, the location at which the operator's middle finger is in contact with the downward face of the control grip is used as shown for example in Figure E-4. For the pedals, a CR point is normally taken as the centre of the pilot's right pedal under the pilot's right foot as shown for example in Figure E-5.

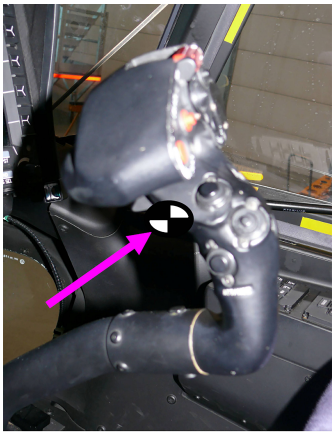

Figure E-3; Example control reference point - *cyclic*

Figure E-4; Example control reference point - *collective*

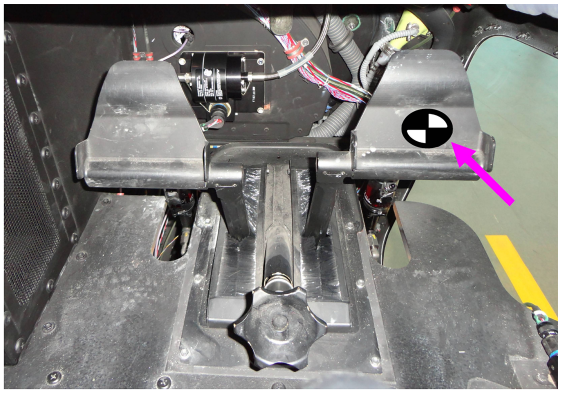

Figure E-5; Example control reference point - *pedals*

Control reference position

It is necessary to define a position in space to provide a datum for measuring control envelopes from. The CR position can be defined anywhere along the control throw although it is usual to set the position at the mid-point for the cyclic axes and the yaw pedals. The convention for the collective is to use the minimum pitch position. In order to define the cyclic position, a minimum of three measurements are made from the CR position to fixed points on the cockpit structure. For the NH90 NFH for example, the lateral range was measured from the second lower right hand line select key of the right Digital Keyboard Unit (DKU) as shown in Figure E-6. Due to their single axis of movement the collective and yaw pedals require only one measurement. For example, to measure the collective envelope, a tangent reference point to the collective movement was selected to be a fastener on the foot well floor at the beginning of the downward slope as shown in Figure E-7. The pedal control envelope was measured, while the pedals were adjusted towards the mid-trim position, using the lower right bolt just below the cyclic adjustment ring as shown in Figure E-8.

Figure E-6; Example control reference position - *cyclic*

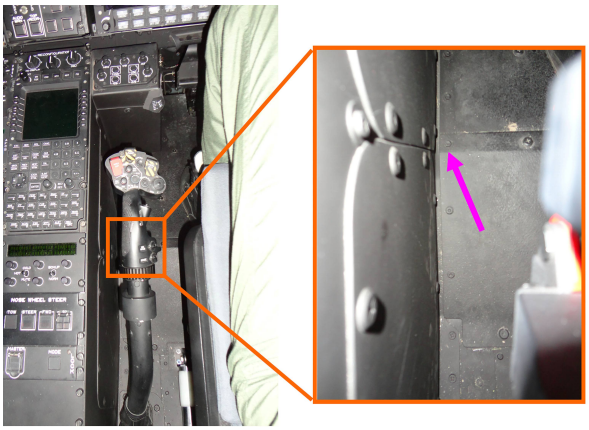

Figure E-7; Example control reference position - *collective*

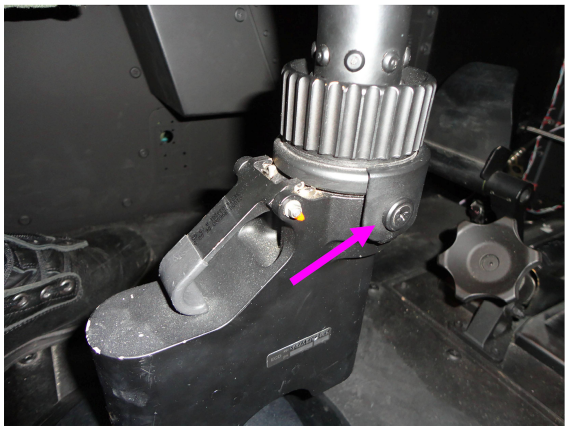

Figure E-8; Example control reference position - *pedals*

Control envelope

The cyclic control envelope may be affected by the operation of mechanical interlinks (if fitted) and should be measured with the collective and yaw pedals at both ends of their displacement range. The position of the pilot's seat may affect the amount of the envelope that could be used and should be placed in the most restrictive position – fully forward and normally fully up. For the NH90 NFH, at the full range of movement the longitudinal cyclic range was approximately 20.4 cm and the lateral range was approximately 19.6 cm. The cyclic envelope is presented as longitudinal cyclic vs. lateral cyclic in Figure E-9. The collective is restricted to move in only one plane and therefore the collective control envelope is usually straightforward, however, many collectives have interlinks with cyclic and yaw pedals and may have variable stops which makes it somewhat more complex. The collective travel from fully down to fully up was approximately 16.5 cm as shown in Figure E-10. The yaw pedals also move about one axis. Note that if the CR position is established with both pedals level, the displacement from this position may not be identical for each pedal in one direction,

however, the total range of movement for each pedal will be the same. Again any effect of interlinks should be taken into account and documented. The travel of both pedals was similar with approximately 11.6 cm travel range. The pedals had an offset, such that the left (power) pedal was set approximately 0.5 cm forward of the right pedal at the centre position as shown in Figure E-11.

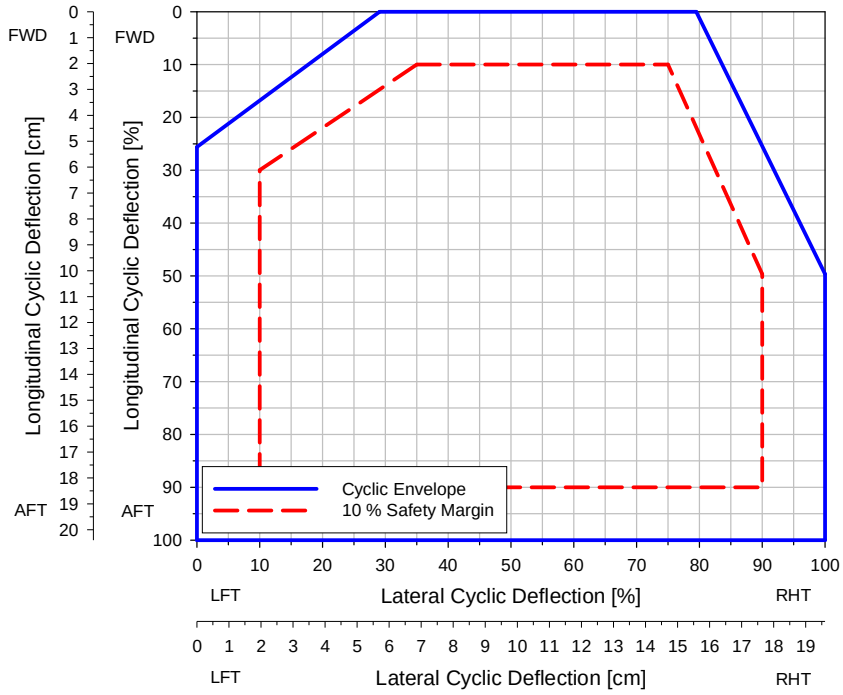

Figure E-9; Example control envelope - *Cyclic*

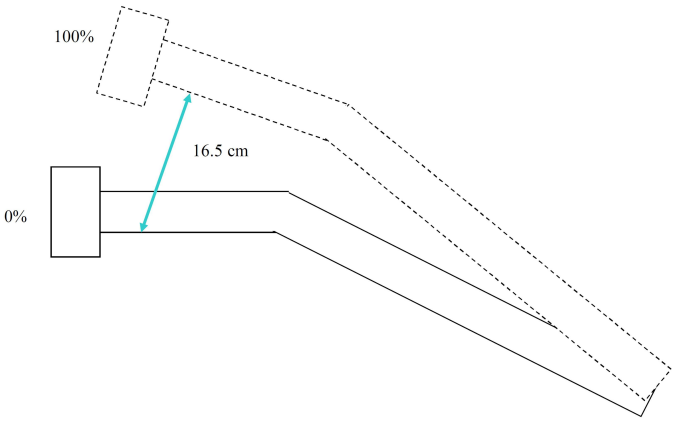

Figure E-10; Example control envelope - *Collective*

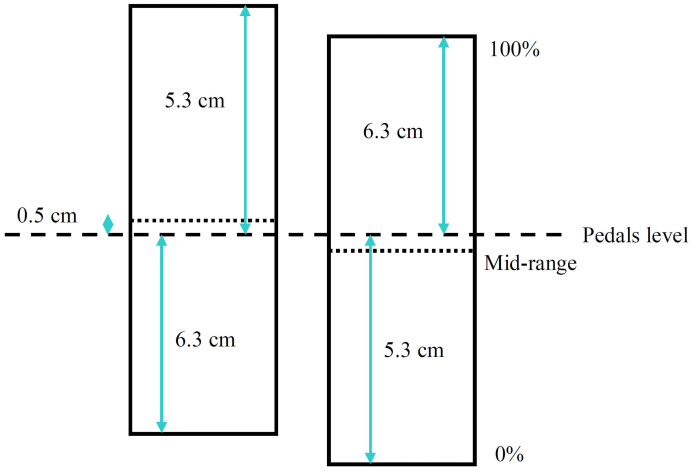

Figure E-11; Example control envelope - *Pedals*

E.3.2 Field of View

The FOV is fixed for a given helicopter model. It is based on the relation of the Design Eye Point (DEP) of the pilot with respect to the edges of the cockpit windows, door windows, or chin bubbles or anything inside the cockpit that may obstruct the pilots view outside the cockpit such as the glare shield. Field of regard is what the pilot sees based on the helicopter's FOV and attitude. The FOV is an area of great importance to the pilot. When designing the FOV the manufacturer is forced to arrive at a compromise between several different factors including the need to provide structural strength, protection for the crew and adequate presentation of information. If insufficient importance is placed on the FOV in the initial stages of a design it is unlikely that it could subsequently be improved to a satisfactory standard as this would probably involve expensive modifications to the cockpit structure. The FOV requirements of a helicopter depend on the role of the helicopter. For instance, an attack helicopter that operates at high speed close to the ground will require a much better all-round FOV than an anti-submarine naval helicopter. However, a naval helicopter will still require a good FOV in certain arcs to allow the pilot to judge its position and relative motion to the flight deck when landing on a ship. Problems with the FOV often arise when a helicopter has not been designed for the specific role in which it is used. In some cases, the FOV may be the factor which limits the aggression and speed with which a particular task can be completed.

In case in-flight observations reveal issues with the FOV, measuring it on the ground provides quantitative data to support the pilot's qualitative opinion of the FOV during role manoeuvres; it is this latter part of the assessment process that is the more important of the two. There are several methods of measuring the FOV of a helicopter. The easiest and most accurate method is to use a camera with a special lens which takes a wide angle photograph with azimuth and vertical angle lines superimposed. The traditional method of measuring the FOV is by use of a clinometers and protractor. Obstructions to the FOV are shown and annotated to tell the reader what is causing the

obstruction as shown for example in Figure E-12. Note that the red line in the figure represents the minimum unobstructed view according the United Kingdom Defence Standards (DEF STAN) [8]. It must be ensured that any items of cockpit equipment that affect the FOV are placed in their normal flight position i.e. rotor brake off and stowed. Where additional crewmembers affect the FOV available to the pilot, consideration should be given to including this information.

In case the traditional method is used for measuring the FOV the following equipment is required: clinometer, protractor, length of string with a weight attached, graph paper and a chinograph pen. The first step is to fix the string to the canopy, so that the weighted end coincides with the Reference Eye Position (REP) as determined by the test crew, in case the DEP is not known, or of course the DEP itself if provided by the manufacturer; this will be the point from which all FOV measurements are made. The REP is determined for the pilot in his normal seating position. It is required to document how the seat was adjusted. In a report the location of the REP should be presented with measurements from defined and fixed points of the cockpit structure. Once the REP is defined, the protractor should be held at the REP and turned so that 0º aligns with the longitudinal axis of the helicopter; this zero degree point should then be marked on the canopy/windscreen. The clinometer is then aligned with the 0º azimuth point and pointed at the upper surface of the obstruction which limits the downward FOV. By pressing and then releasing the trigger the angle of the point from the horizontal can be read-off the scale and then marked on the graph paper. The clinometer is then angled upwards to align with the lower edge of the next item which obscures the FOV and again the reading is taken and recorded. This process is repeated for different azimuth angles until the entire cockpit is mapped. With helicopters that have linear obstructions to the FOV such as door frames or windscreen supports it is easier to define the end points, take intermediate measurements and then join the points with a line.

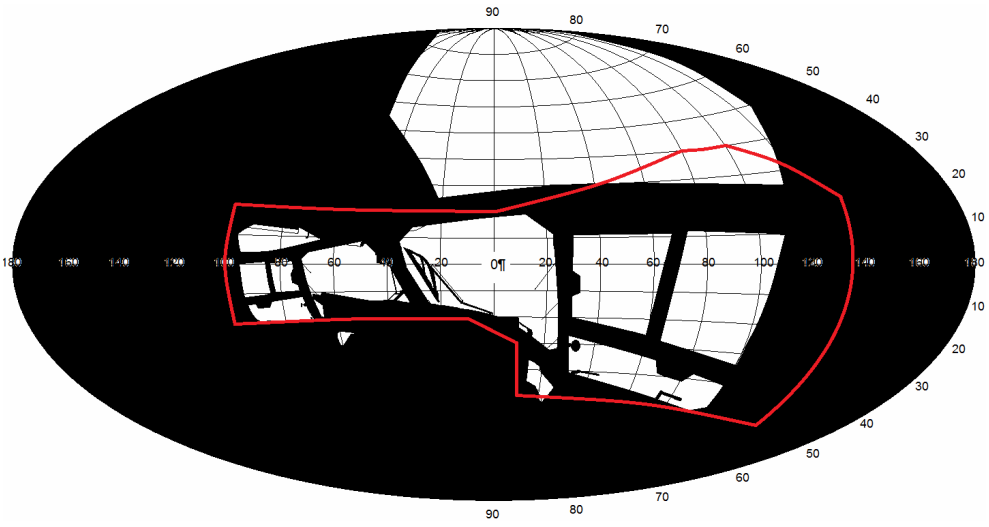

Figure E-12; Example FOV diagram with DEF STAN requirements (red line) [9]

E.4 Helicopter Aspects – Flight Test Philosophy

Flight test is a branch of aeronautical engineering that develops and gathers data during flight of an aircraft and then analyses the data to evaluate the flight characteristics. Thorough planning is vital for all flight trials to ensure that they are conducted safely, efficiently and that the trials objectives are met. To define the test objectives the exact requirements for the trial have to be understood clearly. Generally, the flight test process can be divided into three major areas:

1. Flight test planning;
2. Conducting the flight test;
3. Post-flight actions.

E.4.1 Flight Test Planning

The approach to the trial and the scope of the work, both depend on the requirement to collect evidence, and to identify where that evidence is located. The evidence itself does not necessarily need to come from a flight conducted as part of the trials; indeed because flight testing is such an expensive activity other sources of evidence are invariably considered first. These sources may be the helicopter manufacturer who may have conducted similar tests, earlier test results held at the flight test establishment, read across from other similar helicopter types, another test organization, or possibly an operator who already has experience of the test article. Modelling and simulation are also used where possible. In each case the evidence and the source should be considered carefully to determine to what extent it can be relied upon. If the existing evidence is determined to be reliable then it may be used without further testing or, more likely, a limited number of tests would be planned to 'spot check' the evidence to increase confidence in its validity. Once the existing evidence has been established then the difference between this and the evidence required is that which the flight trials must address, this defines the scope of the test. It is then decided how much testing is required to gather the missing evidence to allow the test objectives to be met. From this is defined the detailed work breakdown structure including for example: test techniques, required environmental conditions, trials location, the order of tests, test instrumentation requirements, and the test crew training standards. Part of the planning process is the technical documentation and reporting requirement. These include in the planning phase amongst others the test directive, test plan, risk assessment and test cards.

1. *Test directive*. The test directive is the initial output from the planning phase and is the document used to summarize the trial responsibilities and test objectives. One of the most important planning stage actions, particularly for large, multi-discipline tests, is to nominate a single person to be in overall charge of the test.

2a. *Test plan*. The test plan is the main output from the planning phase and is the document used to authorize and control the trial. Thus the document needs to define the test methods, test procedures, and test conditions that will be used. The test conditions always require careful thoughts as they vary with the trials being made. It is

not simply a case of defining the target conditions for the trial but rather a range of permissible values of variables is defined so that the trial can proceed even if the exact desired conditions are not present. The test plan also details the trials program including such aspects as the size of increments in control parameters between successive tests and the criteria for progressing to the next test or phase. The individual test points should be organized such that successive points can be achieved quickly. Included in the test plan will be the flight safety points, priorities, limitations, go/no go criteria, possible alternate tests, criteria for stopping the tests, and responsibilities of individual participants. A key element of the test plan is the safety section. This safety section comes mainly from the risk assessment which is also included in the document so that the authorizing authority can ensure that the process to reduce the risks has been conducted correctly. The test plan is reviewed by test team members and by approval officials representing the many disciplines addressed by the test program. No testing can take place until all planning has been completed and the test plan has been signed.

2b. *Risk assessment*. Test flying by its nature involves a degree of risk above that which is routinely accepted during normal operations. To ensure that tests are conducted as safely as possible a process of identifying and reducing risk is employed. The aim of this process is to determine what the risks are, decide on the best way to reduce them and then to decide if the residual risk is acceptable. The procedure relies to a large extent on the experience of the flight test crew. However, a thorough and logical assessment of each phase of flight should lead to the identification of individual risks. It is normal to involve a number of people by calling a review meeting where the group examines each aspect of the flight. Any databases are also examined to ensure that the lessons learned on pervious trials of a similar type are incorporated. On completion of this process a list of identified risk elements can be produced for each section of the program or flight. Having identified the risks, the next stage is to decide how they might be mitigated as much as possible, also known as Risk Reduction Measures (RRM). Possible solutions are for example: training of the test team, supervision of the test program, application of logical procedures, imposing limitations and accurate monitoring of the trials progress. Once the trials risks have been identified and the RRMs have been employed there will still be a certain amount of residual risk which is then quantified. This will lead to the trial being categorized as e.g. high, medium or low risk. The main reason for allocating a category is to indicate those trials which may require particularly careful supervision.

3. *Test cards*. A set of test cards is normally produced for each test flight. These cards serve two purposes: firstly they act as an aide-memoir of the tests to be conducted and limitations that apply, and secondly they provide a means of recording manual data to back-up flight test instrumentation data (if fitted).

E.4.2 Conducting the Flight Test

The scope of any flight test campaign will depend on the amount of flight time allocated for the complete assessment. A common approach is to arrange for the carriage of a role-representative mission load and for the helicopter to be operated in a

role-relatable manner onboard the ship during a representative embarkation period in appropriate environmental conditions. This approach seems to be the easiest, but in practice is the most difficult to realize. Each helicopter-ship combination is based on so many independent variables that the full operational potential is almost impossible to achieve within the small window allowed for sea trials. Even despite all the preliminary efforts, the resulting Ship Helicopter Operational Limitation (SHOL) would be solely based on acceptable test points achieved during dedicated sea trials. However, it occasionally happens that either due to prevailing weather conditions, ship availability or helicopter availability the limits of the helicopter can not be fully explored in some areas or at some masses, thereby restricting the operational capability. Nonetheless this approach should be considered if a very brief overall evaluation of the helicopter is being conducted.

The advantage of a more academic methodology including shore-based hover trials is that a comprehensive set of test data is generated to "*spot-check*" the flight manual, but more important to gain sufficient knowledge of the helicopter limitations within an omni-directional azimuth to complement the flight manual where necessary. This comprehensive data set is used to generate accurate predictions of any limitations due to the helicopter flight characteristics in the shipboard environment. In this way, although initially somewhat more effort is required, the test campaigns to determine operational limitations on board ships are reduced and less dependent on the results from dedicated sea trials in different environmental conditions.

E.4.3 Post-Flight Actions

Each report has an introductory section that contains all the information relating to how the trials were conducted. This includes who performed the trials, when it was performed, the state of the helicopter or equipment tested, the instrumentation used and the tests that were performed. The next section documents the results of the trials, including the conclusions of the test team and any recommendations made. There is a tendency to believe that a trial is complete once the report has been delivered and accepted by the customer. However, it is important to have a trials closure procedure which ensures that all the data gathered is retained. For example, this data may be required to provide baseline information for comparison purposes when the helicopter and/or ship are modified in the future.

E.5 Helicopter Aspects – Shore-Based Hover Trials

The purpose of the shore-based hover trials is to establish helicopter flight characteristics for e.g. power required, Trimmed Flight Control Positions (TFCP), helicopter attitude, controllability limits and pilot workload in an omni-directional relative wind envelope. This is done in order to complement the flight manual information. A dedicated pace-car is used to set up the required relative wind conditions in addition to the actual wind conditions encountered. Each test condition should be maintained for a period of approximately 90 seconds. This is required to ensure that all trends of the factors that have a significant influence on the data and

contribute to the random uncertainty are captured within a single sample record. The flight test data obtained indicates - within the low speed hover envelope - which regions exist where safety margins between available and required helicopter rejection criteria are marginal or even exceeded. This is required for safety reasons, as in these regions, limitations are likely to be exceeded by the operational aircrew during ship-board operations. Furthermore, there are Maximum Power Vertical (MPV) tests performed at different speeds to express the deltas (i.e. the differences) in torque required, between hover and maximum climb condition, associated to the achieved Rate of Climb (ROC). The climb performance data is used to ensure adequate power margins are maintained within the ship's airwake.

E.5.1 Low Speed Flight Characteristics

The quickest method to gather low speed flight characteristics is to conduct a hover turn within the natural wind conditions encountered. The test is performed at a height Out-of-Ground Effect (OGE), yawing the helicopter relative to the ambient wind in 15° increments starting at the nose of the helicopter and working around the complete 360° azimuth. When a stable hover condition is reached relevant parameters are recorded in addition to the ambient conditions. More important, the low speed flight characteristics are determined by stabilizing the helicopter in trimmed flight at the required airspeed with different azimuths behind the pace-car. This way, the required test conditions can be generated rapidly and are less dependent on the weather conditions, so significant time and cost savings can be achieved. The operations are conducted along a runway as this provides a good surface for the pace-car and an obstacle free environment for the helicopter.

The pace-car tests are performed at a sufficient height to remain OGE, whilst maintaining adequate visual references with the pace-car (e.g. 60 ft). The pace-car should be allowed to establish the test condition before the helicopter formats. Once the pace-car has achieved the groundspeed which gives the required test airspeed; the operator calls "*on-condition*". The pilot then positions the helicopter behind the vehicle and lines-up with the roof-mounted wind vane in the required heading; the roof-mounted wind vane gives the zero azimuth relative wind direction. Note that assessing the required helicopter heading in relation to the wind vane can be difficult and is usually not very accurate. In addition, promptly making the calculation of the helicopter heading needed to achieve a particular azimuth can be difficult. Therefore, to ease this process software functionality has been developed within "*SHOL-X*", calculating the heading to be maintained by the pilot for each test condition. At each test point the pilot ensures that the helicopter is keeping a good formation position with the vehicle whilst the data is taken. Once the data has been collected the helicopter is turned to achieve the next required wind azimuth, repositioning as necessary to keep the vehicle in sight. The procedure for execution of the pace-car trials is summarized as follows:

- The helicopter calls for example: "*Next run will be red 90˚ with 20 knots*";
- The pilot positions the helicopter in a location providing a good view to the pace-car (preferably downwind of the pace-car);

- Pace-car calls *"Ready for next run"*;
- Helicopter calls to the pace-car *"go, left/mid/right side runway"*;
- Pace-car accelerates to required relative wind speed, and when steady calls *"Pace-car on condition, your heading will be … "*;
- Helicopter follows the pace-car and pilot sets up test condition for the run corresponding to the given heading by the pace-car, and verified by the roof-mounted wind vane, and when steady calls *"Heli on condition"*;
- Flight Test Engineer (FTE), if feasible positioned in the jump-seat, starts recording and increases record number of the flight test data;
- The pace-car starts the timing, and drives along the runway with a constant groundspeed. Variation in the relative wind caused by variation in true wind are not compensated by the speed of the pace-car;
- In case during the measurements the helicopter wanders off condition, the pilot or FTE calls *"Off condition"*;
- Data recording stops after approximately 90 sec or when reaching the end of the runway. The FTE calls *"Stop recording, next test point will be … "*, or the pace-car calls *"At end marker"*;
- FTE stops recording;
- The next test run will preferably be flown in the opposite direction of the runway. Note: In case sufficient runway length is available to perform the next run, this will be performed in the same direction of the runway (e.g. low pace-car speeds);
- Pace-car sets-up for next run and calls *"Ready for next run"*.

Pace-car operations are relatively straightforward but there are a number of safety considerations that should be addressed to ensure that all risks are reduced as far as possible. The operations start with a face-to-face brief between the helicopter crew and the pace-car crew. At this brief the area of operations is defined, including the limits of the area in the form of end markers. As the helicopter may not be pointing in the direction of its ground track it can be difficult for the pilot to know when the end of the area is reached. When the helicopter or the pace-car reaches an end marker the pace-car crew makes the calls, '*approaching end marker*' or '*at end marker*' the latter indicating that the test should be halted. As the helicopter needs to move to different positions around the pace-car when conducting testing it might be necessary to position the vehicle to different sides of the runway to ensure that the helicopter remains over a clear area (i.e. left / mid / right side runway). The instructions that will be used to achieve this are briefed. The final call to be stipulated at the brief is the "*break-off*" call which the pace-car crew will use if for any reason they require the test to be stopped and the helicopter to move away. Also at the brief the minimum spacing between the vehicle and the helicopter is stipulated. This is usually a minimum distance of two rotor diameters for safety reasons. In practice the actual spacing used is often greater than this to prevent the helicopter downwash from affecting the pace-car anemometer. The 'golden rule' for safety in these operations is for the pilot to keep

the vehicle in clear sight at all times to prevent a collision. This means that the helicopter will not only have to turn to place the relative airflow at the required azimuth but also will have to move to a new position in relation to the pace-car to ensure that it can be seen clearly. At speeds at or close to the lateral or rearwards limits of the helicopter, care is needed not to exceed these limits when repositioning. The technique used is to turn the helicopter into the relative airflow, reposition as necessary, and then turn carefully to achieve the required wind azimuth. When each test run is complete the helicopter moves well away from the operating area to allow the pace-car to reposition safely.

E.5.2 Vertical Climb Performance

The helicopter's maximum achievable vertical climb performance is assessed for different speeds, using a technique known as MPV. The general principle is simple; the time is taken to climb through a given altitude band for various amounts of excess power over and above that required to hover in the nominal conditions at the centre of the band. The two main objectives of vertical climb performance for shipboard operations are:

1. To show how vertical rate of climb varies with Outside Air Temperature (OAT) and weight at a specified engine rating for different airspeeds;
2. To establish the effects of wind speed on the vertical climb performance.

From a practical viewpoint the difficulty with vertical performance testing is that of establishing and holding a steady airspeed flight condition in which accurate measurements can be made. In order to establish such a condition in free flight it is necessary to use some other means than the airspeed indicator in the cockpit to indicate a true hover or to rely on a fixed ground reference. For the NH90 NFH, vertical flight was established using ground references in combination with Doppler information presented on the flight navigation display with the hover page selected. The flight test started with the helicopter established in an OGE hover. Power was increased up to Maximum Continuous Power (MCP), and once steady on condition the maximum vertical rate of climb was measured. The helicopter was timed through an altitude band of 300 ft or for 20 seconds whichever was longer. Note that during the climb it is necessary to adjust the collective position to maintain MCP as altitude increases.

E.6 Helicopter Aspects – Sea Trials

The sea trials consist of take-off and landings, at least two per test condition at the potential boundaries of the envelope, for different procedures, spots, referred weights and ship motion. Once enough confidence and routine is established for shipboard operations at the lower referred weight around a number of test points, a higher referred weight is selected. For this higher referred weight the boundaries of the SHOL envelope are established first, and once determined, the original lower referred weight is re-selected and if feasible these boundaries are expanded further outwards. This method results in a so-called "*wedding cake*" strategy in which the results for the higher referred weight are also valid for the lower referred weight and the latter do not

have to be tested again. A test condition is only considered successful when the pilot gives an acceptable workload rating, while at the same time the objective data during post-flight analysis indicates sufficient safety margins. Note that finding the desired atmospheric conditions and wind strength during the short window allocated for the sea trials is a challenge by itself. Therefore, a dedicated person should be allocated to the test team, trained and specialised in forecasting the weather conditions such that the ship can be directed towards the most suitable geographical location. Furthermore, the timings of the test sorties should be reconsidered on a daily basis to ensure the most optimal period of the day is used for SHOL testing.

E.6.1 Defining Ship Helicopter Operational Limitations

Based on the analysis and simulation results, a dedicated flight test plan is developed to determine the full-mission capability and to define the limiting conditions for shipboard operations. Some work-up training during day time is taken into account, before flight testing at night should be performed. Once ready, emphasis is on boundaries that are critical from the standpoint of pilot workload and safety, but the sea trials also demonstrate performance at important nominal mission conditions. Generally, flight test time is expensive and therefore flight profiles are designed to produce the maximum amount of qualitative data. The key to successful helicopter-ship qualification testing is thorough planning and pre-flight briefing. Additionally, test cards must be used as the basis for the testing, and the entire flight must be reviewed as soon as possible after completion of the testing. The flight tests should preferably be performed in a range of weather conditions, by day and by night, in order to determine for the particular helicopter-ship combination the effects on the pilot workload from, for example, visual references, ship motion and turbulence. Parameters of concern for each event include a variety of qualitative and quantitative factors, including but not limited to usable cues, pilot workload, flight control activity, flight control margins, helicopter attitude, helicopter power requirements, landing dispersion, ship airwake turbulence intensity, ship motion and helicopter landing loads. A large amount of flexibility is required in the test program due to unforeseen elements like helicopter serviceability, ship serviceability, ship agenda and encountered weather conditions.

In optimising for test efficiency, all feasible take-off and landing procedures (e.g. fore-aft, oblique and cross-deck) should be applied once the ship is steady on a particular course and speed whilst for that period the ships maintains a "*green deck*" for take-off and landing. This is required as changing course and speed of the ship can be a time-consuming activity. In addition, maintaining a "*green deck*" simplifies the process for the ship by omitting the approval process by Command for each evolution. Furthermore, if feasible within the predicted envelope, for green winds at least a port-side approach from, and departure to, the leeward side of the ship should be conducted to maximize the helicopter's exposure to turbulence, or vice versa for red winds. For ships with a dual landing spot configuration, a read-across method may be adopted between spots by testing the predicted worse case to conservatively bracket the other case for the same relative wind conditions. Thus, in forward relative wind a condition, landing is initially conducted using the forward landing spot, as turbulence is usually

stronger closer to the ship's superstructure. By doing so, the aft spot is not necessarily to be tested again for each relative wind condition as it would not be worse than the forward spot. For aft wind cases, at least the aft landing spot should be tested as this spot experiences more wind roll-up from the stern of the ship.

For each relative wind condition, at least one landing is performed by the pilot from the right seat. The safety pilot on the left seat, preferably an instructor pilot, assesses whether an instructor is able to intervene or whether the second pilot is able to take-over the controls while performing a landing or take-off, indicated as cross-cockpit operation. Generally, cross-cockpit operations are more demanding for the pilot due to less visual reference, resulting in higher workload ratings. The test points will be scheduled such that an incremental approach will be used towards the boundaries of the CFE, whilst taking into account the required time for the ship to set-up for the next test point. When reaching boundaries of the envelope at least two approaches and landings will be made for the same relative wind condition in order to allow comparison and to set the boundaries correctly. However, to ensure maximum operational flexibility as the trials progresses (i.e. due to oil rigs and/or shipping), and to prevent the pilots from having a prejudiced opinion of the potential boundaries, the ship and pilots should not be thoroughly briefed by the test lead about the order of test points to be flown during a particular sortie. The order of test points is at the discretion of the flight test lead (i.e. FTE), and should be reconsidered constantly as the trial progresses to ensure maximum efficiency of the allocated flight hours. Generally, the following order of events is used:

1. Test crew determine target test point based on previously cleared points;
2. Officer of the watch coordinates ship;
3. Test point conduct:
    a. Pilot Flying (PF) flies test point;
    b. Pilot Non Flying (PNF) and FTE, if feasible positioned in the jump-seat, monitor safety (e.g. RADALT, engine parameters, clearances);
    c. Officer of the watch monitors ship motion, and wind speed and direction.
4. Test point debrief:
    a. PF debriefs workload, assigns DIPES, turbulence and visual cue ratings as required;
    b. FTE debriefs control margins, power margins, ship motion, and ship wind speed and direction;
    c. Test crew determines test point acceptability.
5. Repeat process, the heading and/or speed of the ship is changed. In the regions where safety margins are approached or encountered, the heading and speed of the ship will be changed in smaller steps;
6. The helicopter mass is kept within a 2% margin of the target referred weight by RRR and/or other ballast options. Therefore, during the flight trials qualified personnel should be stand-by. A call will be given 5 minutes prior refuelling such that the ship can prepare for it.

E.6.2 Operational Considerations

Ship alongside

When operating with a ship along side (windward or leeward side), the SHOLs are not applicable, and due to the enormous possibilities impossible to test. The airflow over and around the ship will change significantly due to the presence of the other ship. These airflow disturbances, caused by the ship along side, are dependent on the size and shape as it could range from a fishing boat to a helicopter carrier. When caution is practised and the other ship is on the leeward side, then only the windward parts of the fore-aft envelopes may be feasible. For all other scenarios, caution should be practised and it is at pilot discretion to choose the most suitable take-off and/or landing procedure, from the released SHOLs, without reducing safety.

Amphibious ships

Amphibious ships are able to lower their stern such that small boats can sail in and out of them. In general, there are no test requirements for the ships in dock condition, although the SHOLs are valid for both cruise and dock position, for the following reasons:

- The airflow characteristics around the ship are not significantly different whether the ship is in cruise or in dock condition;
- Tail boom clearance of the helicopter during hover and landing is more critical when the ship is in cruise condition, due to the more upward slope angle of the flight deck;
- High flexibility in manoeuvring the ship. In cruise condition, the maximum speed is usually approximately 20 knots, and sailing in any direction is possible. In dock condition, the maximum ship speed is approximately 6 knots, and sailing with the stern into the wave direction has to be avoided;
- Higher ship motions are attainable in cruise condition than in dock condition.

Dual spot operations

In order to allow the presented SHOL envelopes to be used for dual spot operations, unless dedicated tests are performed, the following restrictions do apply:

- During starting and stopping of the rotors, it should be prohibited for the other helicopter to take-off or land from the ship deck;
- To avoid hindrance of the downwash during dual spot operations an allowable time interval of at least 10 sec between two take-offs or two landings is recommended.

Appendix F Test Instrumentation and Data Reduction

F.1 Test Instrumentation

The use of flight test instrumentation, amongst other reasons, lessens the data recording working pressure on aircrew, enables engineers to monitor control authority and it results in more accurate performance data. In general, the advantages of test instrumentation for complex flight tests, overrule the disadvantages in costs. For helicopter-ship qualification test campaigns, test instrumentation is used for the pace-car, helicopter and the various ships. These recordings are synchronized in time to enable efficient post-flight analysis.

F.1.1 Pace-car Instrumentation

The pace-car was equipped with a calibrated speed measurement system, a display on top of the dashboard to present the driving speed instruction and relative wind to the driver, and a wind vane to provide the pilot with visual reference of the relative wind direction as shown in Figure F-1. The anemometer on the pace-car was calibrated at full scale in the German Dutch Wind Tunnels Large Low-speed Facility (DNW-LLF) to determine the disturbing effect of the pace-car on the anemometer readings. The calibration data was incorporated in the software providing the driving speed instructions to the driver.

Figure F-1; Pace-car

In order to function as a dedicated pace-car, the following equipment was installed:

- A detachable mast on which a Gill-Young anemometer was mounted at 4.6 m above the ground;

- An instrumentation system based on PC/104 standard components combined with a back-up data storage system using Flash Memory cards;
- A display on top of the dashboard to present the driving speed instruction and the relative wind to the driver;
- A wind vane to provide the pilot with visual reference of the relative wind direction;
- A Very High Frequency (VHF) radio set to communicate with the helicopter and Air Traffic Control (ATC).

F.1.2 Helicopter Instrumentation

The measurement system for helicopter parameters consisted of a variety of sensors part of the helicopter, and a flight test instrumentation suite to continuously record these data as shown in Figure F-2. The recorded helicopter parameters were either transmitted via the common MIL-STD 1553 databus (i.e. sending information to all users connected to it), or via direct ARINC-429 lines (i.e. sending information from point A to point B only). The measurements were transmitted via the databus by either the engines (ENG), Plant Management Computer (PMC) or the Inertial Reference System (IRS). The data-streams were fed, via test connectors in the rear left side of the cabin and test connectors behind the pilot and co-pilot seats, to the flight test instrumentation suite, and transferred into engineering units according to the Interface Control Document (ICD) [1,2]. An overview of the relevant helicopter parameters is summarized in Table F-1.

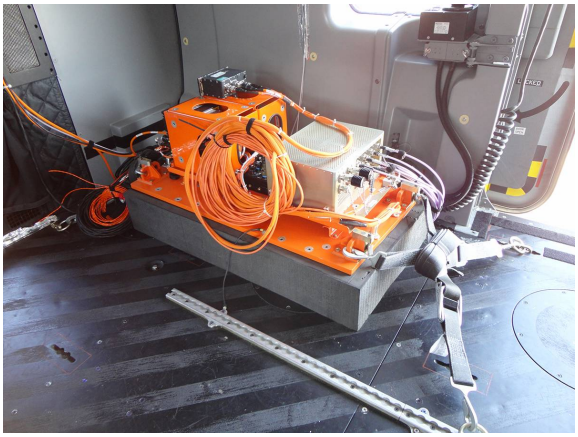

Figure F-2; Flight test instrumentation suite

Measurement system - helicopter performance

The helicopter performance measurement system is shown in Figure F-3. The free power turbine rotational speed N_f and torque measurements provided signals of the output shaft speed and torque for engine control and indications in the cockpit. For these measurements, two probes were fitted into each side of the air intake casing. Each probe contained two sensors. The front sensors measured the voltage frequency,

supplied to the Engine Electronic Control Unit (EECU) to be used for fuel flow control and indication of N_f in the cockpit. The rear sensors were used to measure the distance between the teeth of the output shaft and the teeth of the reference shaft to be used by the EECU for torque calculations and cockpit indications. In addition, a dedicated sensor was installed for N_f overspeed protection. The engine gas generator rotational speed N_g sensor was located in the right hand side of the accessory gearbox. The N_g sensor had four probes and send signals to the EECU. The N_g signals were used for cockpit indication, fuel flow control and overspeed protection. Seven thermocouples and two harnesses were installed around the power turbine casing to provide a cockpit indication of the engine power turbine inlet temperature T_{46}. The thermocouples and the harnesses were connected with the EECU to be used for fuel control.

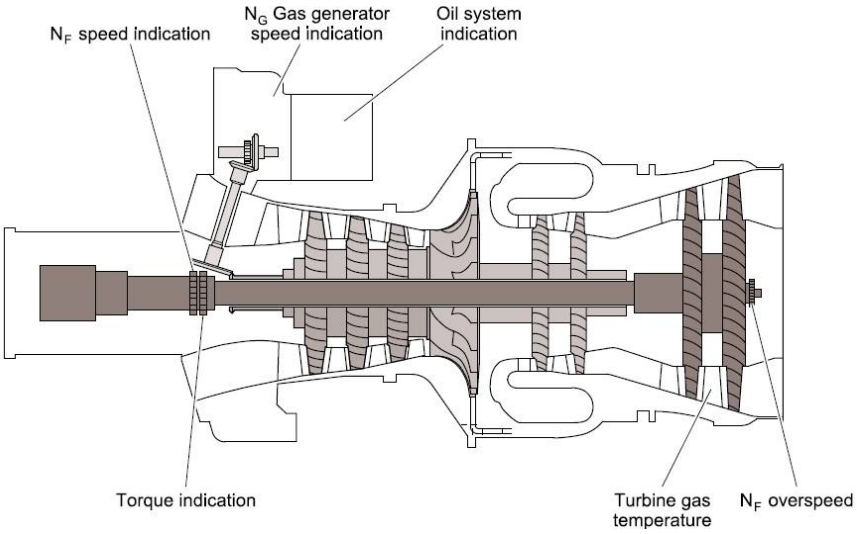

Figure F-3; Helicopter performance measurement system [3]

Measurement system - helicopter control position

A duplex Inceptor Transducer Unit (ITU) sensed the cyclic stick, collective lever and yaw pedal positions across the full deflection range. The purpose of the ITU was to measure the absolute pilot/co-pilot inceptor position in order to electrically feed the Flight Control Computer (FCC). Each ITU, packaged into two separate units (i.e. half ITU), was mechanically linked to the inceptors by two rods through a mechanical fuse to prevent an internal jamming. The eight ITU's were located on the inceptor's kinematics under the cockpit floor.

Measurement system - helicopter attitude

The helicopter attitude measurement system consisted of two laser-gyro IRS's, each including a Global Positioning System (GPS) receiver module. The critical data were computed by using the internal sensors (the three accelerometers and three ring laser gyros) and one Air Data Computer (ADC). The ADC permitted the adjustment of the physical parameters detected by the inertial sensors depending on the altitude.

Measurement system – miscellaneous

The Outside Air Temperature (OAT) sensor used a temperature probe located on the bottom of the helicopter. Note that other atmospheric conditions like ambient pressure, relative wind speed and direction were recorded from sensors that were not part of the helicopter.

Item	Measurement	Unit	Source
1	Engine Torque #1	Nm	CORE bus A or B (ENG)
2	Engine Torque #2	Nm	CORE bus A or B (ENG)
3	Engine speed, N_g #1	%	CORE bus A or B (PMC)
4	Engine speed, N_g #2	%	CORE bus A or B (PMC)
5	Engine temp, T_{46} #1	ºC	CORE bus A or B (PMC)
6	Engine temp, T_{46} #2	ºC	CORE bus A or B (PMC)
7	Free turbine speed, N_f #1	%	CORE bus A or B (PMC)
8	Free turbine speed, N_f #2	%	CORE bus A or B (PMC)
9	Tail rotor actuator position	mm	ARINC 203 Label 104
10	Pedal position	%	ARINC 192
11	Cyclic position longitudinal	%	ARINC 192
12	Cyclic position lateral	%	ARINC 192
13	Collective position	%	ARINC 192
14	Pitch attitude	deg	CORE bus A or B (IRS)
15	Roll attitude	deg	CORE bus A or B (IRS)
16	Vertical speed	ft/min	CORE bus A or B (IRS)
17	Rotor speed (N_r)	%	CORE bus A or B (PMC)
18	Radar altitude	ft	CORE bus A or B (IRS)
19	Heading	deg	CORE bus A or B (IRS)
20	Outside Air Temperature	ºC	CORE bus A or B (IRS)

Table F-1; Overview relevant helicopter parameters [1,2]

F.1.3 Ships Instrumentation

The signals from the ship's measurement systems were fed into a Data Acquisition Unit (DAU). The output of the DAU followed the RS-422 protocol. The acquired data was stored in engineering units in binary data files on magnetic media (hard disc and floppy disks), and were available for post-flight processing. The relevant parameters for the ship are summarized in Table F-2. The relative wind direction and speed were recorded both by the port anemometer (PT) and starboard (SB) anemometer system. A manual selection was made on the bridge, in order to use the windward anemometer system. In addition, for some ships a reference anemometer was installed at the bow of the ship during the sea trials.

Recorded ship parameters	
Attitude pitch	Ship wind direction (PT)
Attitude roll	Ship wind direction (SB)
Ship course	Ship wind speed (PT)
Ship speed	Ship wind speed (SB)
Reference anemometer	Selection PT/SB anemometer

Table F-2; Overview relevant ship parameters

F.2 Data Reduction

F.2.1 Data Qualification Sea Trials

An important consideration for the data qualification, are the take-off and landing techniques applied by the pilot during the sea trials, as these have a considerable impact on the maximum and minimum values. For example, torque required during the shore-based hover trials is for a steady-state condition to allow the helicopter to maintain level flight. In case the pilot performs a take-off from the ship he or she may utilise much more torque than required for the climb away from the ship, i.e. pull the collective towards the maximum allowed power setting as indicated on the First Limit Indicator (FLI). The FLI is in modern helicopter types a common representation of the power margin, and as such a useful tool. However, the torque utilised may not be representative for that particular test conditions. Another example is for the roll attitude of the helicopter. A pilot may use much more roll attitude during the take-off than during the landing. During the landing the pilot is worried about the visual references with the ship, assessing the ship motion and considering the impact with the flight deck during landing. However, during the departure the pilot only has to manoeuvre the helicopter away from the ship. Some general guidelines for the data qualification of the parameters potentially causing operational restrictions are summarized in Table F-3. There is a distinction made for the applicability or the respective parameters between the approach and the departure (i.e. take-off and landing). The highest value of both will be representative for the whole procedure.

Parameter	Applicability for approach	Applicability for departure
Pilot workload	Yes	Yes
Turbulence	Yes	Yes
Torque utilised	Yes	Comparison required with torque utilised for the approach and/or other test points, to assess whether maximum value is representative
Engine gas generator rotational speed N_g	Yes	See torque
Engine power turbine inlet temperature T_{46}	Yes	See torque
Tail rotor actuator position	Yes	See torque
Pedal position	Yes	Yes
Longitudinal Cyclic	Yes	Yes
Lateral Cyclic	Yes	Yes
Pitch attitude	Only above the flight deck	Only above the flight deck and in the initial transition phase away from the ship
Roll attitude	Only above the flight deck	Only above the flight deck, comparison required with roll attitude for the approach and/or other test points, to assess whether maximum value is representative
Ship motion	Yes	Yes

Table F-3; General guidelines data qualification

F.2.2 Data Analysis

The data analysis was conducted by using Excel (Microsoft office XP) on a commonly used personal computer. Curve plotting was accomplished by using standard trend line options in Excel.

F.2.3 Sign Conventions

The sign conventions as summarized in Table F-4 were used throughout the dissertation.

Parameter	Negative sign	Positive sign	Control displacement
Helicopter pitch attitude	Nose-down	Nose-up	-
Helicopter roll attitude	Bank to left	Bank to right	-
Vertical speed	Descent	Climb	-
Forward speed	Decreases	Increases	-
Relative wind direction	From port (red winds)	From starboard (green winds)	-
Tail rotor actuator position	-	-	Min thrust – 0% Max thrust – 100%
Pedal deflection	-	-	Full left – 0% Full right – 100%
Cyclic longitudinal	-	-	Full forward – 0% Full aft – 100%
Cyclic lateral	-	-	Full left – 0% Full right – 100%
Collective	-	-	Full down – 0% Full up – 100%

Table F-4; Sign conventions

Page intentionally left blank

References

Chapter 1

1. Mandal, U.K., Ghosh, S., and Mukherjee, P.C., (2007). D.I. Testing Challenge: Development of Ship / Rotorcraft Airwake Model by Simulation Method. In *Proceedings of the International Conference of Mechanical Engineering*, number ICME07-FL-03, Dhaka, Bangladesh.
2. Lumsden, R.B., Wilkinson, C.H., and Padfield, G.D., (1998). Challenges at the Helicopter-Ship Dynamic Interface. In *Proceedings of the 24th European Rotorcraft Forum*, Marseilles, France.
3. Hodge, S.J., Forrest, J.S., Padfield, G.D., and White, M.D. (2008). Determining Fidelity Standards for Maritime Rotorcraft Simulation. In *Proceedings of the RAeS*, London, United Kingdom.
4. Wilkinson, C.H., Roscoe, M.F., and VanderVliet, G.M., (2001). Determining Fidelity Standards for the Shipboard Launch and Recovery Task. In *Proceedings of the AIAA Modelling and Simulation Technologies Conference and Exhibit*, number A01-37292, Montreal, Canada.
5. Advani, S.K., and Wilkinson, C.H., (2001). Dynamic Interface Modelling and Simulation – A Unique Challenge. In *Proceedings of the RAeS Conference of Helicopter Flight Simulation*, London, United Kingdom.
6. Lee, D., and He, C., (2009). Development of a Unified Simulation and Control Tool to Enhance Shipboard Operation. In *Proceedings of the AHS 65th Annual Forum*, Grapevine, Texas.
7. Min, Z., et. al., (2004). Analytical Approach to Helicopter-Ship Certification. In *Proceedings of the AHS 60th Annual Forum*, Baltimore, Maryland.
8. Wilkinson, C.H., VanderVliet, G.M., and Roscoe, M.F., (2000). Modelling and Simulation of the Ship-Helicopter Environment. In *Proceedings of the AIAA Modelling and Simulation Technologies Conference*, number A00-37317, Denver, Colorado.
9. Roscoe, M.F., and Wilkinson, C.H., (2002). DIMSS – JSHIP's Modelling and Simulation Process for Ship / Helicopter Testing & Training. In *Proceedings of the AIAA Modelling and Simulation Technologies Conference and Exhibit*, number AIAA 2002-4597, Monterey, California.
10. Roper, D.M., Owen, I., and Padfield, G.D., (2006). Integrating CFD and Piloted Simulation to Quantify Ship-Helicopter Operating Limits. In *The Aeronautical Journal*, Paper No. 3051, pp. 419-428.
11. Hommel, G.C.S., and van der Vorst, J., (2006). Helicopter Ship Dynamic Interface Simulation (ROSDIS). In *Proceedings of the European Rotorcraft Forum 32nd*, Maastricht, The Netherlands.
12. Helicopter/Ship Qualification Testing (2003). Number RTO-AG-3000, Vol. 22, AC/323(SCI-038)TP/53.

13. Willemsen, E., (2008). Wind Tunnel Investigation on the Wind Loads on the Joint Support Ship. In *Project number 2710.8649 by German-Dutch Wind Tunnels*, number LST-2008-23.
14. Polsky, S.A., and Bruner, C.W.S., (2001). A Computational Study of Unsteady Ship Airwake. In *Proceedings of the RTO AVT Symposium on Advanced Flow Management*, Loen, Norway.
15. Forrest, J.S., and Owen, I., (2010). An Investigation of Ship Airwakes using Detached-Eddy Simulation. In *Elsevier Computers & Fluids*, No. 39, pp. 656-673.
16. Fang, R., and Booij, P.J.A., (2006). Helicopter-Ship Qualification Testing: The Dutch Clearance Process. In *Proceedings of the AHS 62nd Annual Forum*, Phoenix, Arizona.
17. Helicopter Operations from other Than Aircraft Carriers (HOSTAC), (2001). Number APP 2(F)/MPP 2(F), Volume I, Change 9.
18. Valerdi, R., and Kohl, R.J., (2004). An Approach to Technology Risk Management. In *Proceedings of the Engineering Systems Division Symposium*, Cambridge, Massachusetts.
19. United Stated of America Department of Defence, (2011). Technology Readiness Assessment (TRA) Guidance.
20. Blanchette, S., Jr., Albert, C., and Garcia-Miller, S., (2010). Beyond Technology Readiness Levels for Software: U.S. Army Workshop Report. Technical report, No. CMU/SEI-2010-TR-044 or ESC-TR-2010-109.

Chapter 2

1. Padfield, G.D., (2007). Helicopter Flight Dynamics. Blackwell Publishing, second edition, ISBN 978-1-4051-1817-0.
2. Integrated Electronic Technical Publication NH90 NFH, NAHEMA IETP V3.3.
3. Email RTM322 01/9 – NG laws, SAFRAN Turbomeca.
4. Padfield, G.D., (2015). So You Want To Be An Engineer? Publisher Gareth D. Padfield, second edition, ISBN 978-0-9929017-2-1.
5. International Organization for Standardization, (1975). Standard Atmosphere (Identical with the ICAO and WMO Standard Atmosphere from -2 to 32 km). ISO-2553-1975(E).
6. Forrest, J.S., and Owen, I., (2010). An Investigation of Ship Airwakes using Detached-Eddy Simulation. In Elsevier Computers & Fluids, No. 39, pp. 656-673.
7. Hakkaart, J.F., Hegen, G.H., and Fang, R., (1999). Wind tunnel investigation of the wind climate on a model of the LPD "Hr.Ms. Rotterdam". Number NLR-CR-99091.
8. Helicopter/Ship Qualification Testing (2003). Number RTO-AG-3000, Vol. 22, AC/323(SCI-038)TP/53.
9. Aeronautical Design Standard Performance Specification Handling Qualities Requirements for Military Rotorcraft, (2000). Number ADS-33E-PRF.
10. Helicopter Operations from other Than Aircraft Carriers (HOSTAC), (2001). Number APP 2(F)/MPP 2(F), Volume I, Change 9.
11. Cooke, A., and Fitzpatrick, E., (2002). Helicopter Test & Evaluation. Blackwell publishing, ISBN –632-05247-3.

12. Hoencamp, A., van Holten, Th., and Prasad, J.V.R., (2008). Relevant Aspects of Helicopter-Ship Operations. In *Proceedings of the 34th European Rotorcraft Forum*, Liverpool, United Kingdom.

Chapter 3

1. Isukapalli, S.S., (1999). Uncertainty analysis of transport-transformation models. PhD thesis, Graduate School - New Brunswick. Rutgers, The State University of New Jersey.
2. Coleman, H.W., and Steele, W.G., (2009). Experimentation, Validation, and Uncertainty for Engineers. Wiley Series, ISBN 978-0-470-16888-2, Third Edition.
3. Bendat, J.S., and Piersol, A.G., (2010). Random Data, Analysis and Measurement Procedures. Wiley Series in Probability and Statistics, ISBN 978-0-470-24877-5, Fourth Edition.
4. ESDU, (1997). Statistical Methods Applicable to Analysis of Aircraft Performance Data. Data item No. 91017.
5. Schulten, P.J.M., (2005). The interaction between diesel engines, ship and propellers during manoeuvring. PhD Thesis at Delft University of Technology, ISBN 90-407-2579-9.
6. Hoencamp, A., van Holten, Th., and Prasad, J.V.R., (2008). Relevant Aspects of Helicopter-Ship Operations. In *Proceedings of the 34th European Rotorcraft Forum*, Liverpool, United Kingdom.
7. Fang, R., and Booij, P.J.A., (1995). Wind-Tunnel investigation of the wind climate on a model of “Hr.Ms. Amsterdam”. NLR contract report CR 95403.
8. Hakkaart, J.F., Hegen, G.H., and Fang, R., (1999). Wind tunnel investigation of the wind climate on a model of the LPD “Hr.Ms. Rotterdam”. NLR contract report CR-99081.
9. Fang, R., Booij, P.J.A., and Hommel, G.C.S., (2003). Test Report Airflow measurements on a model (scale 1:75) of the Royal Netherlands Navy Air Defence and Command Frigate. NLR contract report CR-2003-415.
10. Booij, P.J.A., (2008). Airflow measurements on a model (scale 1:100) of the Royal Netherlands Navy second Landing Platform Dock. NLR contract report CR-2008-388.
11. Booij, P.J.A., Gooden, J.H.M., and Willemsen, E., (2008). Airflow measurements on a 1:70 scale model on the modified Multipurpose Frigate of the Royal Netherlands Navy and the Belgian Navy. NLR contract report CR-2008-708.
12. Booij, P.J.A., (2011). Airflow measurements on a 1:70 scale model of the Royal Netherlands Navy Patrol Vessel, NLR contract report CR-2011-588.
13. Fang, R., and Booij, P.J.A., (1996). Full scale wind climate and ship motion measurements on board the AOR oiler replenishment ship “Hr.Ms. Amsterdam” of the Royal Netherlands Navy, NLR contract report CR 96300 C.
14. Fang, R., and Booij, P.J.A., (2000). Full-scale wind climate and ship motion measurements on board the Royal Netherlands Navy Landing Platform Dock (LPD) “Hr. Ms. Rotterdam”. NLR contract report CR-2000- 609.

15. Fang, R., Booij, P.J.A., and Gooden, J.H.M., (2005). Full scale wind climate and ship motion measurements on board the Royal Netherlands Navy Air Defence Command Frigate (LCF) "Hr. Ms. De Ruyter", NLR contract report CR-2005-145.
16. Booij, P.J.A., and Smit, E.J., (2009). Validation wind correction algorithm wind measuring system LPD2. Interim report.
17. Booij, P.J.A., Hordijk, M.A., (2012). Validation wind measuring system on board RNLN modified Multipurpose Frigate "Hr.Ms. van Speijk", NLR contract report CR-2012-338.
18. Booij, P.J.A., and Hordijk, M.A., (2012). Validation wind measuring system on board RNLN Patrol Ship "Hr.Ms. Holland", NLR contract report CR-2012-340.
19. Willemsen, E., (2008). Wind Tunnel Investigation on the Wind Loads on the Joint Support Ship. Number LST-2008-23.
20. Polsky, S.A., and Bruner, C.W.S., (2001). A Computational Study of Unsteady Ship Airwake. In *Proceedings of the symposium on "Advanced Flow Management*, Loen, Norway.
21. Forrest, J.S., and Owen, I., (2010). An Investigation of Ship Airwakes using Detached-Eddy Simulation. In Elsevier Computers & Fluids, No. 39, pp. 656-673.
22. Booij, P.A., and Hordijk, M.A., (2012). Validation Wind Measuring System on Board RNLN Patrol Vessel "Hr.Ms. Holland", NLR contract report CR-2013-340.
23. Benschop, H., (1996). Windsnelheidmetingen op zeestations en kuststations: herleiding waarden windsnelheid naar 10-meter niveau. Technisch rapport TR-188, KNMI.
24. Email RTM322 01/9 – NG laws, SAFRAN Turbomeca.
25. Integrated Electronic Technical Publication NH90 NFH, NAHEMA IETP V3.3.

Chapter 4

1. Fang, R., and Booij, P.J.A., (1995). Wind-Tunnel investigation of the wind climate on a model of "Hr.Ms. Amsterdam". NLR contract report CR 95403.
2. Hakkaart, J.F., Hegen, G.H., and Fang, R., (1999). Wind tunnel investigation of the wind climate on a model of the LPD "Hr.Ms. Rotterdam". NLR contract report CR-99081.
3. Fang, R., Booij, P.J.A., and Hommel, G.C.S., (2003). Test Report Airflow measurements on a model (scale 1:75) of the Royal Netherlands Navy Air Defence and Command Frigate. NLR contract report CR-2003-415.
4. Booij, P.J.A., (2008). Airflow measurements on a model (scale 1:100) of the Royal Netherlands Navy second Landing Platform Dock. NLR contract report CR-2008-388.
5. Booij, P.J.A., Gooden, J.H.M., and Willemsen, E., (2008). Airflow measurements on a 1:70 scale model on the modified Multipurpose Frigate of the Royal Netherlands Navy and the Belgian Navy. NLR contract report CR-2008-708.
6. Booij, P.J.A., (2011). Airflow measurements on a 1:70 scale model of the Royal Netherlands Navy Patrol Vessel, NLR contract report CR-2011-588.

7. Willemsen, E., (2008). Wind Tunnel Investigation on the Wind Loads on the Joint Support Ship. Number LST-2008-23.
8. Polsky, S.A., and Bruner, C.W.S., (2001). A Computational Study of Unsteady Ship Airwake. In *Proceedings of the symposium on "Advanced Flow Management*, Loen, Norway.
9. Forrest, J.S., and Owen, I., (2010). An Investigation of Ship Airwakes using Detached-Eddy Simulation. In Elsevier Computers & Fluids, No. 39, pp. 656-673.
10. Hoencamp, A. and Pavel, M.D., (2012). Concept of a Predictive Tool for Ship-Helicopter Operational Limitations of Various In-Service Conditions. *Journal of the American Helicopter Society*, Volume 57, Number 3, page 032008-1 to 032008-9.
11. Dreier, M.E., (2007). Introduction to Helicopter and Tiltrotor Flight Simulation. AIAA Education Series, ISBN 978-1-56347-873-4.
12. Hoencamp, A., Blok, G., and van Kralingen, R.A., (2012). Report CLSK Directive 11-32, Part 1; NH90 NFH Shore-Based Hover Trials.
13. Hoencamp, A., (2012). Report CLSK Directive 11-32, Part 6; NH90 NFH Shore-Based Hover Trials Hot & Heavy.
14. Helicopter/Ship Qualification Testing (2003). Number RTO-AG-3000, Vol. 22, AC/323(SCI-038)TP/53.
15. Roscoe, M.F., and Wilkinson, C.H., (2002). DIMSS – JSHIP's Modelling and Simulation Process for Ship / Helicopter Testing & Training. In Proceedings of the AIAA Modelling and Simulation Technologies Conference and Exhibit, number AIAA 2002-4597, Monterey, California.
16. Email RTM322 01/9 – NG laws, SAFRAN Turbomeca.
17. Integrated Electronic Technical Publication NH90 NFH, NAHEMA IETP V3.3.

Chapter 5

1. Hoencamp, A. and Pavel, M.D., (2012). Concept of a Predictive Tool for Ship-Helicopter Operational Limitations of Various In-Service Conditions. Journal of the American Helicopter Society, Volume 57, Number 3, page 032008-1 to 032008-9.
2. Refsgaard, J.S., and Hernriksen, H.J., (2004). Modelling guidelines – terminology and guiding principles. Elsevier, Advances in Water Resources 27, page 71 to 82.
3. Schwer, L.E., (2006). Guide for Verification and Validation in Computational Solid Mechanics. American Society of Mechanical Engineers.
4. Beven, K., (2002). Towards a coherent philosophy for modelling the environment. Proceedings of the Royal Society A, Vol. 458, Number 2026, pages 2465 to 2484.
5. Oberkampf, W.L., Trucano, T.G., and Hirsch, C., (2003). Verification, Validation, and Predictive Capability in Computational Engineering and Physics. Sand Report, number SAND200-3769.
6. Easterling, R.G. and Berger, J.O., (2002). Statistical foundations for the validation of computer models. In *Proceedings of the Workshop on Foundations for V&V in the 21st Century*. Society for Modelling and Simulation International.
7. Booij, P.A., and Hordijk, M.A., (2012). Validation Wind Measuring System on Board RNLN Patrol Vessel "Hr.Ms. Holland". NLR contract report CR-2013-340.

8. Watkins, S., (2012). Turbulence Characteristics of the Atmospheric Boundary Layer and Possibilities of Replication for Aircraft. In *Proceedings of the Third Symposium "Simulation of Wing and Nacelle Stall"*, Braunschweig, Germany.
9. Aanwijzing CZSK Algemeen 010, (2014). Opereren met helicopters aan boord van CZSK-eenheden. Number A-CZSK ALG 010.
10. Benschop, H., (1996). Windsnelheidmetingen op zeestations en kuststations: herleiding warden windsnelheid naar 10-meter niveau. KNMI, Technical report TR-188.
11. Helicopter/Ship Qualification Testing (2003). Number RTO-AG-3000, Vol. 22, AC/323(SCI-038)TP/53.
12. Hoencamp, A., van Holten, Th., and Prasad, J.V.R., (2008). Relevant Aspects of Helicopter-Ship Operations. In *Proceedings of the 34th European Rotorcraft Forum*, Liverpool, United Kingdom.
13. Integrated Electronic Technical Publication NH90 NFH, NAHEMA IETP V3.3.
14. Hoencamp, A., Blok, G., and van Kralingen, R.A., (2012). Report CLSK Directive 11-32, Part 1; NH90 NFH Shore-Based Hover Trials.
15. Hoencamp, A., (2012). Report CLSK Directive 11-32, Part 6; NH90 NFH Shore-Based Hover Trials Hot & Heavy.
16. Email RTM322 01/9 – NG laws, SAFRAN Turbomeca.
17. Cooke, A., and Fitzpatrick, E., (2002). Helicopter Test & Evaluation. Blackwell publishing, ISBN –632-05247-3.

Chapter 6

1. Hoencamp, A., Lee, D., Pavel, M.D., and Stapersma, D., (2014). Lessons Learned from NH90 NFH Helicopter-Ship Qualification Testing across the Entire Dutch Fleet. In *Proceedings of the AHS 70th Annual Forum*, Montreal, Canada.
2. Roscoe, M.F., and Wilkinson, C.H., (2002). DIMSS – JSHIP's Modelling and Simulation Process for Ship / Helicopter Testing & Training. In Proceedings of the AIAA Modelling and Simulation Technologies Conference and Exhibit, number AIAA 2002-4597, Monterey, California.
3. Hoencamp, A., Sicking, J.P., and van Kralingen, R.A., (2012). Report CLSK Directive 11-32, Part 2; NH90 NFH sea trials LPD1 "Hr.Ms. Rotterdam".
4. Hoencamp, A., Sicking, J.P., and van Kralingen, R.A., (2012). Report CLSK Directive 11-32, Part 4; NH90 NFH sea trials LCF "Hr.Ms. De Ruyter".
5. Hoencamp, A., Sicking, J.P., and van Kralingen, R.A., (2012). Report CLSK Directive 11-32, Part 7; NH90 NFH sea trials OPV "Hr.Ms. Holland".
6. Hoencamp, A., Sicking, J.P., and van Kralingen, R.A., (2013). Report CLSK Directive 11-32, Part 8; NH90 NFH sea trials M-Frigate "Hr.Ms. van Speijk".
7. Hoencamp, A., Sicking, J.P., and van Kralingen, R.A., (2013). Report CLSK Directive 11-32, Part 10; NH90 NFH sea trials AOR "Zr.Ms. Amsterdam".
8. Hoencamp, A., and van Kralingen, R.A., (2014). Report CLSK Directive 11-32, Part 12; NH90 NFH sea trials LPD2 "Zr.Ms. Johan de Witt".
9. Hoencamp, A., Sicking, J.P., and van Kralingen, R.A., (2013). Report CLSK Directive 11-32, Part 9; NH90 NFH sea trials Hot & Heavy LCF "Hr.Ms. De Ruyter".

10. Hoencamp, A., and Sicking, J.P., (2013). Report CLSK Directive 11-32, Part 11; NH90 NFH sea trials Hot & Heavy AOR "Zr.Ms. Amsterdam".
11. Hoencamp, A., Blok, G., and van Kralingen, R.A., (2012). Report CLSK Directive 11-32, Part 1; NH90 NFH Shore-Based Hover Trials.
12. Hoencamp, A., (2012). Report CLSK Directive 11-32, Part 6; NH90 NFH Shore-Based Hover Trials Hot & Heavy.
13. Hoencamp, A., Sicking, J.P., and van Kralingen, R.A., (2014). Report CLSK Directive 11-32, Part 13; NH90 NFH Hot & Heavy M-frigate.
14. Hoencamp, A., Sicking, J.P., and van Kralingen, R.A., (2015). Report CLSK Directive 11-32, Part 14; NH90 NFH Hot & Heavy LPD1, LPD2 and OPV.
15. Hoencamp, A., Lee, D., Pavel, M.D., and Stapersma, D., (2014). Innovative Test Methodology Optimizing for Cost and Time Efficiency: NH90 NFH Helicopter-Ship Qualification across the Complete Dutch Fleet. In *Proceedings of the 8th Australian Pacific Vertiflite Conference on Helicopter Technology*, Melbourne, Australia.

Appendix A

1. Interactive Electronic Technical Publication NH90 NFH, NAHEMA IETP V3.3.
2. Aanwijzing CZSK Algemeen 010, (2014). Opereren met helicopters aan boord van CZSK-eenheden. Number A-CZSK ALG 010.

Appendix B

1. Glauert, H., (1948). The Elements of Aerofoil and Airscrew Theory. Cambridge University Press, Cambridge, United Kingdom.
2. Torenbeek, E., and Wittenberg, H., (2009). Flight Physics, Basics of Aeronautical Disciplines and Technology, with Historical Notes. Springer, ISBN 978-1-4020-8663-2;
3. van Holten, Th., and Melkert, J.A., (2002). Helicopter Performance, Stability and Control, number ae4-213.
4. Drzwiecki, S., (1892). Bulletin de l'Association Technique Maritime.
5. Drzwiecki, S., (1909). Theorie Generale de l'Helice, Paris.
6. Leishman, J.G., (2002). Principles of Helicopter Aerodynamics. Cambridge Aerospace Series, ISBN 0-521-52396-6.
7. Hoencamp, A., van Holten, Th., and Prasad, J.V.R., (2008). Relevant Aspects of Helicopter-Ship Operations. In *Proceedings of the 34th European Rotorcraft Forum*, Liverpool, United Kingdom.
8. Buckingham, E., (1914). On physically similar systems; illustrations of the use of dimensional equations. Physic Review, Vol. IV, No. 4, pp 345 – 376.

Appendix C

1. Helicopter/Ship Qualification Testing (2003). Number RTO-AG-3000, Vol. 22, AC/323(SCI-038)TP/53.

Appendix D

1. Bendat, J.S., and Piersol, A.G., (2010). Random Data, Analysis and Measurement Procedures. Wiley Series in Probability and Statistics, ISBN 978-0-470-24877-5, Fourth Edition.
2. Coleman, H.W., and Steele, W.G., (2009). Experimentation, Validation, and Uncertainty for Engineers. Wiley Series, ISBN 978-0-470-16888-2, Third Edition.
3. Abertethy, R.B., and Thopson, J.W., (1973). Handbook Uncertainty in Gas Turbine Measurement. Number AEDC-TR-73-5.

Appendix E

1. Fang, R., and Booij, P.J.A., (1995). Wind-Tunnel investigation of the wind climate on a model of "Hr.Ms. Amsterdam". NLR contract report CR 95403.
2. Hakkaart, J.F., Hegen, G.H., and Fang, R., (1999). Wind tunnel investigation of the wind climate on a model of the LPD "Hr.Ms. Rotterdam". NLR contract report CR-99081.
3. Fang, R., Booij, P.J.A., and Hommel, G.C.S., (2003). Test Report Airflow measurements on a model (scale 1:75) of the Royal Netherlands Navy Air Defence and Command Frigate. NLR contract report CR-2003-415.
4. Booij, P.J.A., (2008). Airflow measurements on a model (scale 1:100) of the Royal Netherlands Navy second Landing Platform Dock. NLR contract report CR-2008-388.
5. Booij, P.J.A., Gooden, J.H.M., and Willemsen, E., (2008). Airflow measurements on a 1:70 scale model on the modified Multipurpose Frigate of the Royal Netherlands Navy and the Belgian Navy. NLR contract report CR-2008-708.
6. Booij, P.J.A., (2011). Airflow measurements on a 1:70 scale model of the Royal Netherlands Navy Patrol Vessel, NLR contract report CR-2011-588.
7. Padfield, G.D., (2007). Helicopter Flight Dynamics. Blackwell Publishing, second edition, ISBN 978-1-4051-1817-0.
8. UK Ministry of Defence, (2010). Defence Standard 00-970 Part 7 – Design and Airworthiness Requirements for Service Aircraft, Issue 3.
9. van Kralingen, R.A., and Hoencamp, A., (2014). Report CLSK Directive 14-16, Evaluation of the 1st generation NH90 NFH cockpit door.

Appendix F

1. NHI Industries, (2010). Input data for NNLN step A production flight test instrumentation. Technical note S024A0503E01, Issue A.
2. NHI Industries, (2011). Complimentary flight test instrumentation NNLN step A.
3. Integrated Electronic Technical Publication NH90 NFH, NAHEMA IETP V3.3.

Samenvatting (Dutch Summary)

Op dit moment levert de helikopterindustrie een helikopter die een uitgebreide testcampagne heeft uitgevoerd om aan te tonen dat een veilige vlucht mogelijk is binnen de verwachte operationele omstandigheden voor landoperaties. Echter, de vaststelling van de operationele capaciteit en de bijbehorende beperkingen voor veilige operaties aan boord van schepen, wordt nog steeds beschouwd als een verantwoordelijkheid van de exploitant. Traditioneel, wordt elke specifieke combinatie van helikopter-schip uitvoerig op zee geëvalueerd tijdens verschillende omstandigheden zoals, windsnelheden, windrichtingen, staat van de zee en tijd van de dag. Hoewel dit vanzelfsprekend lijkt, is er een sterke afhankelijkheid van heersende weersomstandigheden tijdens de test en zijn er aanzienlijke kosten verbonden aan de beschikbaarheid van zowel de helikopter als schip, meestal voor een periode van weken. Aangezien men bovendien probeert om de beperkingen voor een specifieke helikopter-schip combinatie te bepalen, kunnen er veiligheidskwesties van invloed zijn op dergelijke experimenten. Zelfs ondanks alle voorafgaande inspanningen voor het uitvoeren van proeven op zee in (sommige) huidige testmethodologieën, is de resulterende helikopter-schip operationele potentie nog steeds uitsluitend gebaseerd op kwalitatief geëvalueerde testpunten bereikt door een testpiloot tijdens proefvaarten. Echter, als gevolg van de heersende weersomstandigheden, de beschikbaarheid van schip of helikopter gebeurt het regelmatig dat de grenzen van de helikopter-schip combinatie niet volledig onderzocht kunnen worden, waardoor de operationele capaciteit beperkt blijft. Bovendien is het aantal landen met grote kostenbesparingen groeiende, wat betekent dat defensieorganisaties moeten worden voorbereid op mogelijke concessies in operationele capaciteit en/of verlaging van de veiligheidsnormen voor evaluatie van de potentiële grenzen voor veilige vliegoperaties aan boord van schepen.

Het doel van dit onderzoeksproject is een innovatieve testmethode te ontwikkelen die kan worden gebruikt voor het optimaliseren van kosten en tijd voor helikopter-schip kwalificaties zonder verlaging van de veiligheid. Voor dit doel is de zogenaamde "*SHOL-X*" testmethodologie ontwikkeld, inclusief het in dit proefschrift ontwikkelde computermodel. De testmethodologie bestaat uit drie onderscheidende fasen. In *fase I* wordt de schip-omgeving waarin de helikopter zal opereren bepaald door het uitvoeren van windtunnelmetingen van de luchtstroom in de opstijg- en landingspaden vanaf het schip. Voor de helikopter worden boven land proeven uitgevoerd om beperkingen in helikoptereigenschappen te bepalen, waaronder aspecten als vliegeigenschappen in zijwind en prestaties van de motoren. Daarna, in *fase II*, worden de potentiële operationele beperkingen bepaald door het combineren van het gedrag van de geïsoleerde helikopter en de daadwerkelijke omstandigheden voor een bepaald type schip. Het resultaat wordt als uitgangspunt gebruikt voor proeven op zee. Ten slotte, in *fase III*, wordt een (beperkte) testvliegcampagne aan boord van het schip uitgevoerd bij voorkeur in een scala aan weersomstandigheden bij dag en bij nacht. Dit is om de effecten te bepalen voor een specifieke combinatie van helikopter-schip op de werklast

van de piloot, bijvoorbeeld door aanwezigheid van visuele referenties, scheepsbeweging en turbulentie.

Het belangrijkste voordeel van de innovatieve testmethodologie, geholpen door het ontwikkelde computermodel, is dat de exploitant vroegtijdg een evaluatie kan uitvoeren van veilige grenzen voor helikopters op willekeurige schepen. Op deze manier is het kwalificatieproces minder afhankelijk van uitsluitend kwalitatief beoordeelde testpunten tijdens speciale proefvaarten. De testmethodologie kan worden gebruikt voor een weloverwogen beoordeling van het verschil tussen de 'veilige vluchtenvelop', zoals bepaald door de fabrikant van de helikopter, en de door de gebruiker gedefinieerde 'operationele vluchtenvelop' voor een bepaalde helikopter-schip combinatie. Bovendien kan het model een eerste beoordeling geven over het effect van wijzigingen in het ontwerp van zowel helikopter en/of schip nadat de definitief vastgestelde operationele beperkingen zijn vrijgegeven voor gebruik. Het nieuw ontwikkelde software model in dit proefschrift wordt beschouwd als origineel en kan worden gezien als de meest belangrijke vernieuwing van dit werk.

De innovatieve testmethodologie, met inbegrip van het bijbehorende software model, is tussen 2012 en 2014 al met succes toegepast tijdens de helikopter-schip kwalificatie van de NH90 NFH over de gehele Nederlandse vloot. Deze proefvaarten hebben het hoge ambitieniveau van dit onderzoek bewerkstelligd, namelijk dat het model gevalideerd is door middel van experimenten op daadwerkelijke schaal. Het lijkt misschien een ambitieus doel voor een academisch onderzoek, maar hou dan het doel van dit proefschrift voor ogen: vermindering van het aantal vlieguren voor helikopter-schip kwalificatietesten zonder verlaging van de veiligheid. Het bepalen van de operationele limieten kan nu worden bereikt door twee verschillende opties. De eerste en meest voorkomende optie is tijdens proefvaarten waarin de potentiële grenzen voor de verschillende opstijg- en landingprocedures worden gevalideerd. De tweede optie is het bepalen van de operationele beperkingen voor warm weer omstandigheden met een zware helikopter door desk-top analyse alleen. Het bepalen van de operationele limieten is dan gebaseerd op de gegevens verzameld met vliegproeven boven land in warm weer omstandigheden, en de testresultaten van vliegproeven aan boord van hetzelfde type schip met een lager gewicht van de helikopter. Dit laatste is een nieuwe benadering van het vaststellen van operationele limieten en kan worden gezien als de belangrijkste verdienste van dit werk.

Het vastleggen van operationele limieten voor een helikopter-schip combinatie wordt nog steeds beschouwd als een nationale verantwoordelijkheid; er zijn helaas geen internationaal overeengekomen regels of standaardprocedures. Vandaar een sterk verschil in de interpretatie van dergelijke testmethodes tussen landen. Ervan uitgaande dat elk land of elke exploitant naar maximale operationele flexibiliteit van een bepaalde helikopter-schip combinatie streeft, met minimale kosten en zonder verlaging van de vliegveiligheid, heeft dit proefschrift de ambitie om te functioneren als het startpunt voor internationale regelgeving of standaardprocedures voor de uitvoering van helikopter-schip kwalificerende testen.

List of Helicopter-Ship Qualification Tests

As an observer

SH-14D *Lynx* evaluated at the Landing Platform Dock No.2 (LPD2) "Hr.Ms. Johan de Witt", (2007). In the North Sea.

NH90 MRH operated by the Australian Navy and evaluated at the Australian Landing Platform Amphibious (LPA) “HMAS Manoora”, (2009). In the Tasman Sea.

As flight test lead

NH90 NFH evaluated at the Landing Platform Dock No.1 (LPD1) “Hr.Ms. Rotterdam”, (2011). In the North Sea, 504 deck landings, 35.6 flight test hours, 10 days.

NH90 NFH evaluated at the Air Defence and Command Frigate (LCF) “Hr.Ms. De Ruyter”, (2012). In the North Sea, 27 deck landings, 5.2 flight test hours, 1 day.

NH90 NFH evaluated at the LCF “Hr.Ms. De Ruyter”, (2012). In the North Sea, 256 deck landings, 21.0 flight test hours, 8 days.

NH90 NFH evaluated at the Ocean Patrol Vessel (OPV) “Hr.Ms. Holland”, (2012). In the North Sea, 179 deck landings, 12.8 flight test hours, 9 days.

Aloutte III operated by the Belgium Navy and evaluated at the OPV “Hr.Ms. Friesland”, (2012). In the North Sea, 19 deck landings, 3.0 flight test hours, 1 day.

NH90 NFH evaluated at the Multi-purpose frigate (MFRI) “Hr.Ms. van Speijk”, (2012). In the North Sea, 66 deck landings, 7.8 flight test hours, 8 days.

AS-532 U2 *Cougar* evaluated at the LPD2 “Hr.Ms. Johan de Witt”, (2012). In the North Sea, 197 deck landings, 18.1 flight test hours, 8 days.

NH90 NFH evaluated at the LCF “Hr.Ms. De Ruyter”, (2013). In the Indian Ocean (Hot & Heavy), 96 deck landings, 8.1 flight test hours, 2 days.

NH90 NFH evaluated at the Auxiliary Oiler Replenishment (AOR) “Zr.Ms. Amsterdam”, (2013). In the North Sea, 210 deck landings, 16.6 flight test hours, 4 days.

UH-1N *Iroquois* operated by the United Stated Marine Corps (USMC) evaluated at the LPD1 “Zr.Ms. Rotterdam”, (2013). In the Atlantic Ocean, 46 deck landings, 5.1 flight test hours, 1 day.

NH90 NFH evaluated at the AOR "Zr.Ms. Amsterdam", (2013). In the Caribbean Sea (Hot & Heavy), 110 deck landings, 9.3 flight test hours, 3 days.

MH-65 *Dolphin* operated by the United Stated Coast Guard (USCG) evaluated at the OPV "Zr.Ms. Zeeland", (2014). In the Florida Straits, 22 deck landings, 2.1 flight test hours, 1 day.

NH90 NFH evaluated at the LPD2 "Zr.Ms. Johan de Witt", (2014). In the North Sea, 157 deck landings, 10.2 flight test hours, 9 days.

HKP15B operated by the Swedish Air Force and evaluated at the LPD2 "Zr.Ms. Johan de Witt", (2015). In the Atlantic Ocean, 72 deck landings, 7.9 flight test hours, 3 days.

Constructed by desk-top analyses

NH90 NFH at the LPD1 "Zr.Ms. Rotterdam" for Hot & Heavy conditions, (2014).

NH90 NFH at the LPD2 "Zr.Ms. Johan de Witt" for Hot & Heavy conditions, (2015).

NH90 NFH at the MFRI class for Hot & Heavy conditions, (2015).

NH90 NFH at the OPV class for Hot & Heavy conditions, (2015).

As flight test lead for unmanned aircraft

ScanEagle with Electro Optic and Long Wave Infra Red (EO/LWIR) evaluated at the LPD1 "Hr.Ms. Rotterdam", (2012). In the North Sea, 16 (dummy) recoveries, 8.0 flight hours, 1 day.

ScanEagle with Medium Wave Infra Red (MWIR) configuration evaluated at the LPD1 "Hr.Ms. Rotterdam", (2012). In the Indian Ocean, 8 (dummy) recoveries, 2.0 flight hours, 1 day.

ScanEagle with EO and MWIR evaluated at the LPD2 "Zr.Ms. Johan de Witt", (2013). In the North Sea, 9 (dummy) recoveries, 3.6 flight hours, 1 day.

List of Publications

Hoencamp, A., van Holten, Th., and Prasad, J.V.R., (2008). Relevant Aspects of Helicopter-Ship Operations. In *Proceedings of the 34th European Rotorcraft Forum*, Liverpool, United Kingdom.

Hoencamp, A., (2009). An Overview of SHOL Testing within the Royal Netherlands Navy. In *Proceedings of the 35th European Rotorcraft Forum*, Hamburg, Germany.

Hoencamp, A., (2009). An Overview of SHOL Testing within the Royal Netherlands Navy. In *Proceedings of the 2nd American Helicopter Society Specialist Meeting for Test & Evaluation*, Patuxent River, Maryland, United States.

Hoencamp, A., (2010). Prediction of Rejection Criteria for Ship Helicopter Operational Limitation Qualifications. In *Proceedings of the 36th European Rotorcraft Forum*, Paris, France.

Hoencamp, A., (2010). Prediction of Rejection Criteria for Ship Helicopter Operational Limitation Qualifications. In *Proceedings Heli Japan 2010*, Saitama, Japan.

Hoencamp, A., (2011). Concept of a Predictive Analysis Tool for Ship Helicopter Operational Limitations of Various In-Service Conditions. In *Proceedings of the 67th American Helicopter Society Annual Forum*, Virginia Beach, Virginia, United States[1].

Hoencamp, A., (2011). Concept of a Predictive Ship Helicopter Operational Limitations Analysis Tool. In *Proceedings of the AIAA Atmospheric Flight Mechanics Conference*, Portland, Oregon, United States.

Hoencamp, A., White, M.D., and Perfect, P., (2011). Proof of Concept for a Predictive Ship Helicopter Operational Limitation Analysis Tool. In *Proceedings of the 37th European Rotorcraft Forum*, Gallarate, Italy.

Hoencamp, A., (2012). Initial Flight Test Results NH90 NFH Helicopter-Ship Qualification Process. In *Proceedings of the 1st Asian-Australian Rotorcraft Forum*, Busan, Korea.

Hoencamp, A., and Pavel, M.D., (2012). Flight Test Results NH90 NFH Helicopter-Ship Qualification Process. In *Proceedings of the 68th American Helicopter Society Annual Forum*, Forth Worth, Texas, United States.

[1] Winner Best Technical Paper Award of the Operations Sessions

Hoencamp, A. and Pavel, M.D., (2012). Concept of a Predictive Tool for Ship-Helicopter Operational Limitations of Various In-Service Conditions. *Journal of the American Helicopter Society*, Volume 57, Number 3, page 032008-1 to 032008-9.

Hoencamp, A., and Pavel, M.D., (2012). Helicopter-Ship Qualification Testing for the NH90 NFH Helicopter. In *Proceedings of the 38th European Rotorcraft Forum*, Amsterdam, the Netherlands.

Hoencamp, A., Pavel, M.D., and Stapersma, D., (2013). The Key Facts of Helicopter-Ship Qualification Testing. In *Proceedings of the 69th American Helicopter Society Annual Forum*, Phoenix, Arizona, United States[2].

Hoencamp, A., Pavel, M.D., and Stapersma, D., (2013). The Key Facts of Ship Helicopter Operational Limitation Development. In *Proceedings of the 39th European Rotorcraft Forum*, Moscow, Russia.

Hoencamp, A., Pavel, M.D., and Stapersma, D., (2013). The Key Facts of Establishing NH90 NFH Shipboard Operational Limitations. In *Proceedings of the 2nd Asian-Australian Rotorcraft Forum*, Tianjin, China.

Hoencamp, A., Lee, D., Pavel, M.D., and Stapersma, D., (2014). Lessons Learned from NH90 NFH Helicopter-Ship Qualification Testing across the Entire Dutch Fleet. In *Proceedings of the 70th American Helicopter Society Annual Forum*, Montreal, Canada.

Hoencamp, A., Lee, D., Pavel, M.D., and Stapersma, D., (2014). Lessons Learned from NH90 NFH Helicopter-Ship Interface: Testing across the Complete Dutch Fleet. In *Proceedings of the 40th European Rotorcraft Forum*, Southampton, United Kingdom.

Hoencamp, A., Lee, D., Pavel, M.D., and Stapersma, D., (2014). Innovative Test Methodology Optimizing for Cost and Time Efficiency: NH90 NFH Helicopter-Ship Qualification across the Complete Dutch Fleet. In *Proceedings of the 8th Australian Pacific Vertiflite Conference on Helicopter Technology*, Melbourne, Australia.

[2] Winner Best Technical Paper Award of the Operations Sessions

About the Author

Alrik Hoencamp was born in Willemstad, Curaçao, on 24 October 1978. In 1997, he joined the Royal Netherlands Navy as midshipman of the operational discipline at the Royal Netherlands Naval College in Den Helder. After an initial deployment as officer of the watch aboard the guided missile frigate "Hr.Ms. de Ruyter" in 2000 on a trip throughout Asia, he broadened in Aerospace Engineering and completed his studies at Delft University of Technology. The study in Delft included a six month internship at the Boeing Company in Mesa, Arizona. In 2003 he received his Master of Science degree in Aerospace Engineering from Delft University, after which he served as officer of the watch aboard the multi-purpose frigate "Hr.Ms. Willem van der Zaan". This tour included counter-drugs operations in the Caribbean, for which he was also trained to operate as a Flight Deck Officer (FDO). Thereafter, various tours followed as senior officer of the watch aboard the auxiliary ship "Hr.Ms. Zuiderkruis" and multi-purpose frigate "Hr.Ms. Tjerk Hiddes".

In 2008 he started the Empire Test Pilots' School (ETPS) as a Flight Test Engineer (FTE) for rotary wing aircraft in Boscombe Down in the United Kingdom. After the one-year long course he graduated winning the Dunlop Trophy for best of class, after which he joined the flight test department of the Royal Netherlands Air Force and started as a research engineer. His research project on helicopter-ship qualification testing was part of a collaborative research effort of the Royal Netherlands Navy, Royal Netherlands Air Force, Netherlands Defence Academy and Delft University of Technology, whilst aiming to reduce time required and costs associated with the flight test campaigns on board the ships across the entire Dutch fleet. At present, Alrik works for the maritime division of the flight test department for the Royal Netherlands Air Force and holds a type rating for the NH90 NFH and AS-532 U2 *Cougar* helicopter. He has a Commercial Pilot License (CPL) and instrument rating for fixed wing aircraft, with a grand total amongst helicopter and fixed wing aircraft types of over 1 000 flight hours in more than 50 types.